Modulating factors of intracellular calcium dynamics in vascular smooth muscle cell

A numerical study

Jaijus Pallippadan Johny

Department of Mechanical Engineering
University of Canterbury

This dissertation is submitted for the degree of
Doctor of Philosophy

May 2016

Dedicated to

My Wife, ***Sowmia Paramban***
My son, ***Johan Jaijus***
My parents, ***Johny Pallippadan*** **and Chinnamma Johny**

Declaration

I hereby declare that except where specific reference is made to the work of others, the contents of this dissertation are original and have not been submitted in whole or in part for consideration for any other degree or qualification in this, or any other university. This dissertation is my own work and contains nothing which is the outcome of work done in collaboration with others, except as specified in the text and acknowledgements. This dissertation contains 221 pages including appendices, references, 5 tables and 76 figures.

Jaijus Pallippadan Johny
May 2016

Acknowledgements

Achievements are always accompanied by a whole lot of emotions and experiences. On looking back my three years of PhD journey, I am not holding these feelings in. To be frank, it was not at all an easy decision for me to come to Christchurch for doing PhD. When I got the admission to University of Canterbury, my wife was carrying our first baby. I was simultaneously happy and sad. Sad because, I had to leave our little bundle of joy, thousands of miles away and to come here in order to start all in time. But now, I feel like all those experiences have strengthened my inner soul and I am indebted to each and everyone who had been there, near and far. And without your encouragement and enduring support, I would not have materialized my dream.

First and foremost, I would like to express my sincere gratitude to my supervisors, Prof. Tim David and Dr. Michael Plank. Thank you for your exceptional guidance and advice throughout these years. I want to say thank you for allowing me to work in flexible hours. That really helped me to manage my family life and part-time jobs along with the PhD.

I need to thank my collegues especially Ealasukanthan Thavanayagam, Katharina Dormanns, Chirstine French, Mario Brando, Stewart Dowding, Allanah Kenny, Dr. Constantine Zakkaroff, Dr. Mohsin Shaikh, Michelle Goodman, Grace Strijbis, Tim Van Ginkel, Elshin Mathias for their wonderful company which gave me a pleasant space for work. Special thanks to Elshin for being such a charming friend of our family, especially for bringing so much affection to my son, Johan. I need to mention Tim Van Ginkel for proofreading my thesis and Grace Strijbis and Prof. Pierre Gremaud for performing the sensitivity analysis of our model. I extend my thanks to all the staff members of Bluefern supercomputing unit.

I would like to say many thanks to all the staff in Disability resource service, where I had a part time job during my PhD, especially Samuel Maddimadugula and Cam Scott for your tremendous support in this journey.

I extend my heartfelt thanks to all my friends who are around the globe for being so encouraging and supportive to me all these years. Since it is not possible to write all names here. I should atleast mentions some of you. Thanks Ciby & Alwin Teena for those cherishing late-night dinners and chats, thanks to Vini & Phillip for free babysitting my son and thanks to Anish & Nisha, Binu, Vishnu, Renjith, Rahul, George, Bibin for your great friendships.

I want to express my gratitude to the University of Canterbury for granting me a UC Doctoral Scholarship for last three years.

It won't be fair if I forget to say thanks to my family in India, though, you all are not here at the moment, I always behold the great memories of our old days. Without you I won't be able to reach wherever I am, thank you appachan (Johny), ammachi (Chinnamma), Jaimy, Shoy, Jainet, Jaimol, Amitha, Ameya, Eva and Jaina.

Above all I would like to thank my wife Sowmia for her immense love, encouragement and constant support, and for sharing my responsibilities to balance my "PhD life". Thank you for being my best friend, editor, proofreader, and many more. My son, Johan, you were always a breath of fresh air for me. I know, you have missed a lot of Daddy time. I promise, I will compensate for all the lost fun. I love you both.

Abstract

The prevalence of diabetes, a metabolic disorder characterized by hyperglycemia, is increasing rapidly worldwide. According to the world health organization (WHO), almost 422 million people in the world have diabetes. Vascular dysfunction, that is distinctively observed in diabetic patients, also leads to the high chance of cardiovascular diseases. The cellular mechanisms of vascular dysfunction in diabetes are not completely elucidated because of the high-level complexity involved. There are some recent studies in literature about the vascular smooth muscle cell (VSMC) dysfunction associated with diabetes. These studies imply that the dysfunction of diabetic VSMC is related to the alterations of functions of gap junctional intercellular communication (GJIC) and calcium handling proteins such as sarcoplasmic reticulum calcium ATPase (SERCA), inositol trisphosphate receptor (IP_3R), and ryanodine receptor (RyR). The main purpose of the thesis is to explore the importance of SERCA, IP_3R, RyR and GJIC as modulating factors of intracellular calcium $\left(\left[Ca^{2+}\right]_{cyt}\right)$ dynamics in VSMCs and investigate the related consequences in the perspective of diabetes.

As a powerful tool to investigate extremely complex biological systems, we have developed a mathematical model of VSMC to accomplish our research aims. The sarcoplasmic reticulum (SR) was modelled as a single luminally continuous store with homogeneous luminal calcium. None of the VSMC mathematical models has used sequential binding of calcium and IP_3 for the activation of IP_3R. As calcium is the central attention of the study, we have incorporated a simplified 4-state sequential-binding IP_3R model.

The change of SERCA, IP_3R or RyR level shifted the oscillatory state of intracellular calcium to steady and vice versa at a constant agonist concentration. Especially, increasing SERCA level move the oscillatory region to high agonist concentrations whereas increasing IP_3R or RyR level shift the oscillatory region to lower agonist concentrations. The shift of oscillatory region was significant at low SERCA levels and at low IP_3 levels. The model results indicate that using the same agonist concentration for studying the existence of intracellular concentrations in the absence of IP_3R or RyR may lead to contradictory findings because of the shift of oscillatory region.

The model results showed that Vm-mediated signalling mechanism plays dominant role in the propagation of calcium rise whereas the activation of IP_3R acts as a limiting step to

make the IP_3-mediated calcium propagation ineffective. It seems that the penetration depth and the wave velocity of intracellular calcium oscillations in coupled VSMCs are strongly related to the GJIC if the regenerative propagation was not extended to all the non-stimulated cells. The downregulation of IP_3R and RyR reduced the penetration of intracellular calcium propagation in VSMCs. The SERCA regulation of the frequency of intracellular calcium oscillations and penetration of regenerative propagation are biphasic.

Based on the model results, our hypothesis is that if an external environment influences the agonist-induced calcium transients, the VSMC may alter the levels of SERCA, IP_3R and/or RyR expressed in the SR to restore intracellular calcium transients matched with the functional need.

The reduced SERCA level is a possible mechanism for the “smoothed" calcium transients in diabetic VSMCs. The SERCA level tends to be the regulating factor of intracellular calcium in both the activation and relaxation phases of oscillations. Also, the model results indicate that the functional changes due to altered level of IP_3R in diabetic VSMCs might be regulated by altering the level of the RyR protein and vice versa. However, the impaired intracellular calcium dynamics due to reduced SERCA levels can not be restored by changing IP_3R or RyR levels because of the reduced intra-SR calcium load. These findings lead to the fact that reduced SERCA level is probably the primary factor responsible for the reduced intracellular calcium transients and the reduced contractility in diabetic VSMCs even though all the three proteins, SERCA, IP_3R and RyR, are varied.

Table of contents

List of figures

List of tables

Abbreviations

ACh acetylcholine.

ADP adenosine diphosphate.

AII angiotensin II.

ATP adenosine triphosphate.

Bcl B-cell lymphoma.

BK_{Ca} large conductance calcium-activated potassium channel.

Ca-CaM calcium-calmodulin complex.

CACC calcium activated chloride channel.

CAD coronary artery diseases.

cAMP cyclic adenosine monophosphate.

CCD charge-coupled device.

cGMP cyclic guanosine monophosphate.

CICR calcium induced calcium release.

CVD cardiovascular diseases.

DAG diacylglycerol.

E1 endothelin-1.

GHK Goldman–Hodgkin–Katz.

GJIC gap junctional intercellular communication.

IICR IP_3 induced calcium release.

IP_3 inositol trisphosphate.

IP_3R inositol trisphosphate receptor.

K_{Ca} calcium-activated potassium channel.

MLC myosin light chain.

MLCK myosin light chain kinase.

NaK sodium/potassium pump.

NCX sodium/calcium exchanger.

NE norepinephrine.

NSC non-selective cation channel.

ODE ordinary differential equation.

PAD peripheral arterial diseases.

PE phenylephrine.

PIP_2 phosphatidylinositol 4,5-bisphosphate.

PKC protein kinase C.

PLC phospholipase C.

PMCA plasma membrane calcium ATPase.

ROC receptor-operated cation.

RyR ryanodine receptor.

SERCA sarcoplasmic reticulum calcium ATPase.

SOC store-operated cation.

SR sarcoplasmic reticulum.

SR_{leak} SR leak channel.

STOC spontaneous transient outward current.

TDMA tridiagonal matrix algorithm.

TGF transforming growth factor.

TRPC transient receptor potential cation.

VOCC voltage-operated calcium channel.

VSMC vascular smooth muscle cell.

Nomenclature

Ca^{2+} calcium ion.

Cl^{-} chloride ion.

Cx connexin.

cyt cytosol.

F Faraday's constant.

G whole cell conductance.

I current.

K^{+} potassium ion.

L agonist.

Na^{+} sodium ion.

Chapter 1

Agonist-induced calcium signalling in VSMCs

1.1 Introduction

The human vascular system supplies oxygen and nutrients to all the tissues of the body, (refer to Figure 1.1), carries carbon dioxide to the lungs and other products of metabolism to the kidneys, distributes hormones and other agents that regulate cell function and have function in the regulation of body temperature. The blood, the carrier of these substances, is pumped through a closed system of blood vessels. The average volume of blood in a human body is approximately 5 litres.

Oxygenated blood is pumped from the left ventricle of the heart to the aorta, reaches major arteries and from there travels to the arterioles and capillaries, where blood exchanges substances and gases with the interstitial fluid. From the capillaries, blood drains through venules into the veins and reaches the right atrium of the heart. From there, deoxygenated blood enters the right ventricle, is pumped to the pulmonary arteries and reaches the lungs where the blood gets oxygenated. This blood returns to the left atrium and from there to the left ventricle.

The proper working of the vascular system is essential for maintaining the functions of every organ of the body. Adequate blood flow should reach the retinal blood vessels for the vision provided by the eyes, the renal arteries for the excretion of waste products from the body, the cerebral and vertebral arteries to maintain neuronal functions and so on. Any abnormality in the vascular system will severely affect the tissues and lead to the malfunctioning. For example, organ damage occurs in diabetic patients because of vascular

dysfunction and affect almost every part of the body, especially the brain, heart, kidneys, skin, and eyes.

The circulation of blood is controlled by various regulatory systems which maintain adequate capillary blood flow to all organs of the body. The most important component of the regulation is the pumping of the heart. Others include diastolic recoil of the walls of the arteries, compression of veins by the skeletal muscles and the negative pressure in the thorax during inspiration. The blood flow to each tissue is regulated by local chemical, general neural and hormonal mechanisms which dilate or constrict the blood vessels.

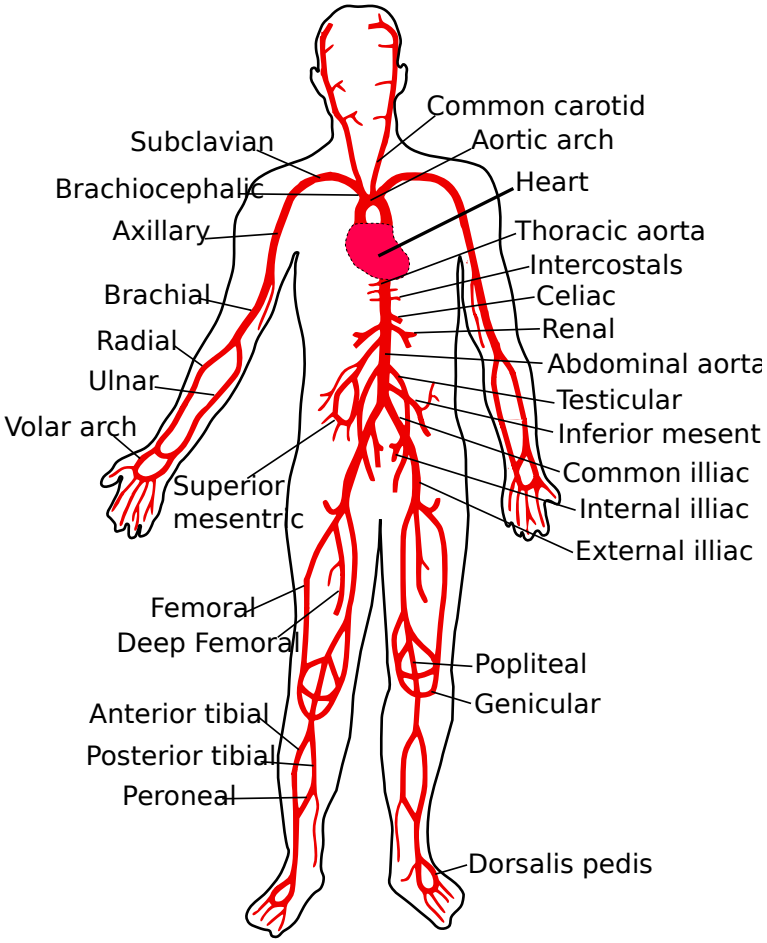

Fig. 1.1 Human vascular system

The circulatory system consists of both arterial and venous systems. It includes different blood vessels such as aorta, arteries, arterioles, capillaries, venules, veins, and vena cava. The arteries conduct blood away from the heart and the veins towards the heart. The arteries have a thick vascular wall which is capable of stretching to accommodate blood pulses when the heart pumps. When the heart is in systole, arteries are stretched and store energy. During

the diastolic phase of the heart, arteries release the stored energy and maintain the blood pressure. This cycle is repeated in each cardiac cycle and helps to achieve continuous blood flow between heartbeats.

The major arteries branch progressively into smaller arteries to reach deeper parts of the organs. The smaller arteries then branch into arterioles, (refer to Figure 1.2). Arterioles have an average diameter of 30 μm. Arterioles are capable of controlling the blood flow in responds to the needs of the tissues by changing their diameter. Arterioles lead to capillary bed. The capillary is a microscopic channel with thin a wall and has plenty of capillary pores in the wall. Exchange of oxygen, nutrients and other substances between the blood and surrounding cells and tissue fluid occurs in the capillaries. The diameter of the capillaries ranges from 5 μm to 10 μm.

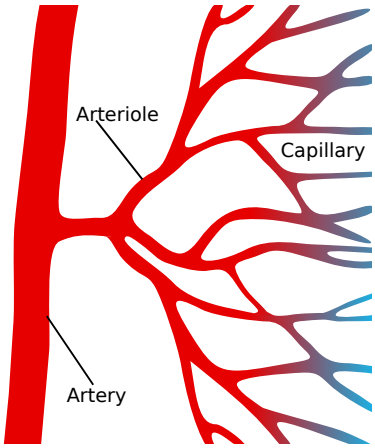

Fig. 1.2 Schemtic representation of arterial tree

An artery/arteriole is made up of three tissue layers, tunica intima, tunica media and tunica adventitia, (see Figure 1.3). Tunica intima is the inner layer of an artery and is made up of a single layer of endothelial cells (ECs) and an internal elastic lamina. Tunica media is the middle layer and is rich in vascular smooth muscle cells (VSMCs). The number of smooth muscle layers varies in arteries and arterioles. Large arteries contain up to 20 VSMC layers while the smallest arterioles may have only one or two layers of VSMCs. The outer layer, tunica adventitia, consists of connective tissue proteins and an external elastic lamina which is the inner boundary of the layer.

1.2 Vascular smooth muscle cell (VSMC)

VSMCs are essential for the structural integrity and functioning of arteries and arterioles. The primary characteristic of a VMSC is its ability to change the diameter of the blood vessel by

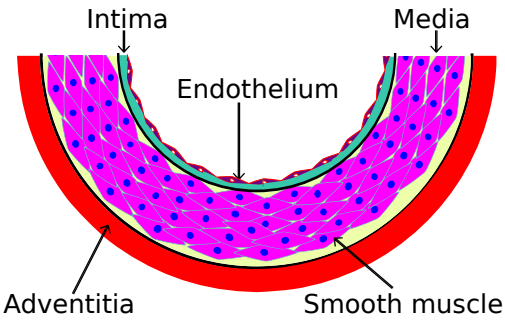

Fig. 1.3 Schematic representation of an artery

contraction and relaxation. The contractile property of VSMCs plays a significant functional role in the vasculature, as it allows dynamic regulation of the blood pressure. This property, in turn, controls blood flow and the distribution of nutrients and oxygen to a particular tissue.

1.2.1 Mechanism of VSMC contraction

The contractile property of a VSMC is obtained by the interaction between myosin and actin filaments. Myosin and actin occupy a major volume of the VSMC. VSMCs contain a large number of actin filaments which are connected to dense bodies. These bodies are either dispersed inside the cell or attached to the cell membrane. Myosin filaments are thicker and have a diameter more than twice that of actin filaments. Myosin filaments contain a globular head region and a long tail. Myosin filaments are interspersed with actin filaments and in between the dense bodies. The actin filaments extend from the dense bodies, and the myosin filament overlaps the ends of actin filaments. A VMSC contains approximately ten times as many actin filaments than myosin filaments.

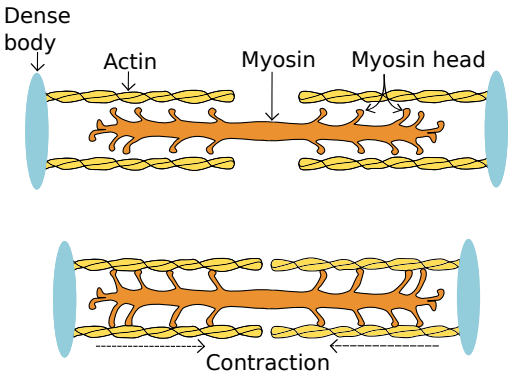

Fig. 1.4 VSMC contraction: Actin-myosin filaments slide over each other.

During a contraction, the globular heads of myosin filaments get bound to actin and form a cross-bridge. This binding allows the myosin to act as a motor driving the actin filaments to slide, (see Figure 1.4). The motor activity of myosin moves its globular heads over the actin filament and the head binds to actin at a specific position. After binding firmly to actin, the myosin head bends in the neck. This bend slides/"pulls" the actin filament over the myosin filament towards the centre of the contractile unit, causing contraction.

1.2.2 Role of intracellular calcium in the regulation of VSMC contraction

The contractility of VSMC is mainly regulated by the changes in intracellular calcium $\left(\left[Ca^{2+}\right]_{cyt}\right)$. An intracellular calcium rise initiates binding of myosin to actin. The intracellular calcium in the VSMC binds to the calmodulin protein forming calcium-calmodulin complex (Ca-CaM) complex. This complex activates myosin light chain kinase (MLCK), an enzyme which is capable of phosphorylating the chain of each myosin head in the presence of adenosine triphosphate (ATP). With myosin light chain (MLC) phosphorylation, the myosin head binds to an actin filament and forms the cross-bridge between myosin and actin filaments. If the MLC is not phosphorylated, the binding of a myosin head to an actin filament does not occur, which leads to relaxation. A schematic representation of the whole process is given in Figure 1.5.

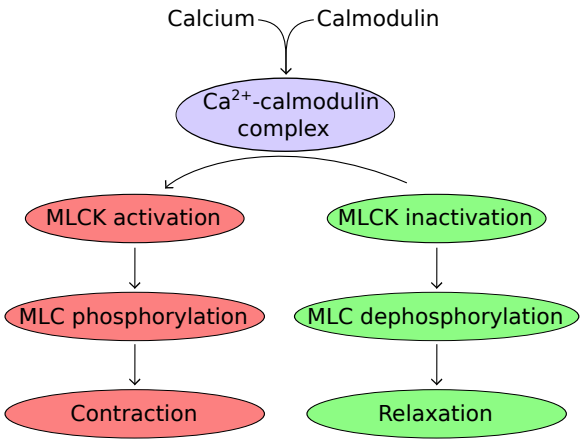

Fig. 1.5 Increase of intracellular calcium initiates myosin binding to actin.

Intracellular calcium in VSMCs is also known as a secondary messenger for many other cellular functions, such as proliferation, migration, and apoptosis, which is increasingly important in vessel remodelling by changing the number of cells and the connective tissue composition. A rise in intracellular calcium may lead to an increase in intranuclear calcium

by passive diffusion through the nuclear pores. The simultaneous increase of intracellular and nuclear calcium with the Ca-CaM complex promotes cell proliferation [96]. Spontaneous calcium transients are likely to be essential for the migration of VSMCs [151]. Alteration in the cellular calcium homeostasis is one of the causes of apoptosis or cell death in smooth muscle cells [165]. Therefore, a tight control over intracellular calcium is necessary for the proper functioning of VSMCs.

1.3 Agonist-induced calcium signalling mechanisms in VSMCs

The activation of contractility in VSMCs occurs as a subsequent event after an increase of intracellular calcium. There are various components which modulate intracellular calcium in VSMC; vasocative agonist is one of them. The vasocative agonists mediate several signalling pathways to induce intracellular calcium rise in VSMCs. The agonist-induced signalling pathways depend on the type of G-protein coupled to the receptor on which the agonist ligand binds. Gq, Gs and Gi are three types of G-protein which are commonly found in VSMCs. The activation of Gs-protein enhance the production of cyclic adenosine monophosphate (cAMP) whereas the activation of Gi-protein suppresses the production of cAMP. The Gq-protein activation leads to the production of inositol trisphosphate (IP_3) and diacylglycerol (DAG) molecules.

A G-protein is coupled to different types of receptors present in the cell membrane of VSMCs. An agonist binds only to a respective receptor on which it has affinity. The most common vasoactive agonists which activate on G-protein-coupled receptors in VSMC membrane are phenylephrine (PE), norepinephrine (NE), acetylcholine (ACh), vasopressin, endothelin-1 and angiotensin II (AII). To activate Gq-protein, NE and PE bind to α_1-adrenoceptors, AII binds to the AT_1 receptor, endothelin-1 binds to the ET_A receptors, vasopressin binds to the V_1 receptor and ACh binds to the M_3 receptor.

In experiments, agonists are applied by microinjection near the cell membrane or by circulating them in the superfusion liquid. For microinjection, micropipettes are filled with the agonist solution, which is then applied perpendicular to the cell membrane [157, 60]. In the latter method, the agonist solution is added to the superfusion liquid, which is circulated through the VSMC strip under investigation [95].

G-protein mediated agonist stimulation of VSMCs leads to a series of molecular levels events and generates secondary messengers such as IP_3 and DAG. Many mathematical models have been developed to describe the entire process of agonist binding on the receptor to the hydrolysis of phosphatidylinositol 4,5-bisphosphate (PIP_2) [101, 100, 141, 27]. According to these models, binding of an agonist ligand to the G-protein coupled receptor is the first step

of the agonist stimulation. The binding of an agonist is a part of several receptor activities such as phosphorylation of the receptors, sequestration or internalization of the receptors, coupling, and uncoupling of receptors from the G-protein, dephosphorylation and recycling of receptors.

The figure 1.6 shows a schematic representation of the molecular events from agonist binding to DAG and IP_3 production. First of all, an agonist ligand binds to the receptor. The ligand bound receptor is subjected to phosphorylation. The phosphorylated receptors are internalized and then dephosphorylated back as recycled receptors to the membrane. The unphosphorylated ligand-bound receptors strongly activate G-protein. The activated G-protein activates the phospholipase C (PLC). The full activation of PLC depends on the intracellular calcium concentration. The activated PLC hydrolyzes PIP_2 to form IP_3 and DAG molecules. These molecules mediate the initiation of calcium signalling mechanisms in the VSMC.

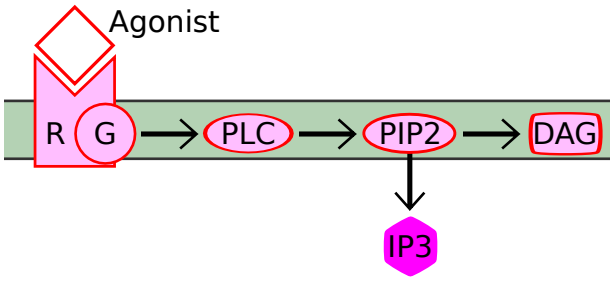

Fig. 1.6 Agonist stimulation of VSMC

1.3.1 Measurement of calcium in VSMCs

Enormous efforts have been made by previous researchers to understand the agonist-induced calcium signalling mechanisms in VSMCs. The improvement in experimental techniques to measure and visualize intracellular calcium in the VSMC advanced the understanding of calcium signalling mechanisms. A good example is the development of experiments using calcium sensitive fluorescent dyes [21, 175]. The fluorescent properties of calcium sensitive dyes change when a calcium ion is bound to the dye. Most commonly, these dyes shift the excitation wavelength or increase the fluorescent quantum intensity when binding to a calcium ion. The change in the fluorescent property of the dye is measured and quantified. Based on the ratio of calcium bound and unbound dyes, the intracellular calcium concentration is calculated. Along with the quantification of intracellular calcium, laser-scanning confocal microscopes are used to image the fluorescent dye. The development

of charge-coupled device (CCD) cameras along with improved calcium sensitive dyes makes it possible to provide the spatial detailing of calcium signalling with high temporal resolution on a subcellular and multicellular level [60].

1.3.2 Role of sarcoplasmic reticulum (SR)

The sarcoplasmic reticulum (SR) is a major calcium releasable store in VSMCs. The SR is a membranous tubular system and its parts are close to the cell membrane as well as the deep within the cell. The SR is referred as peripheral SR when it is close to the cell membrane or central when it is away from the cell membrane.

In general, the possible sources of calcium for intracellular calcium rise in a VSMC are, 1) calcium influx from extracellular space 2) calcium release from the SR. The main calcium handling proteins in the SR are sarcoplasmic reticulum calcium ATPase (SERCA), inositol trisphosphate receptor (IP3R), and ryanodine receptor (RyR). The voltage-operated calcium channel (VOCC) is the main calcium channel present in cell membrane that transport extracellular calcium to the cytosol.

Agonist-induced calcium increase in VSMCs, from the mesenteric artery and the pulmonary artery, is unaffected by the removal of extracellular calcium or by the application of blockers of calcium channel in the cell membrane[67, 10, 55]. In the Hamada et al. [61] study on VSMCs from a canine pulmonary artery, intracellular calcium oscillations gradually disappeared in the absence of extracellular calcium, but were unchanged in the presence of calcium channel blockers such as nifedipine, and verapamil. Similar to this, Bolton et al. [20] reported that the entry of calcium from the intracellular store, not from the voltage-sensitive calcium channels, is the leading cause of agonist-induced contraction. Recent experiments of Shmigol et al. [163] show that the agonist-induced calcium rise is associated with a simultaneous decrease in intra-SR calcium. Leijten et al. [99] showed that the intracellular calcium increase during agonist stimulation is coming from the intracellular store, the SR. These experiments suggest that the majority of calcium rise in the cytosol during agonist stimulation is due to the calcium release from the SR.

1.3.3 CICR and IICR mechanisms

The calcium-induced calcium release (CICR) and IP_3-induced calcium release (IICR) are two well-known calcium release mechanisms in the VSMCs. The IP_3 is identified as a secondary messenger involved in the calcium release mechanisms in VSMC. In experiments, the addition of IP_3 raised intracellular calcium in VSMCs. The amount of calcium released by the addition of IP_3 to the cell was enough to produce contractions in the VSMCs [167, 168].

In the early years of research, the IICR mechanism was assumed to be only dependent on the concentration of IP_3. The later studies provided more insights to the regulation of IICR and showed that IICR depends not only on IP_3, but also on intracellular calcium. The calcium regulation of IICR is identified as biphasic. The IICR mechanism is activated with the increase of calcium up to ≈300 nM and inhibited when calcium is increased above 300 nM. The biphasic nature of calcium regulation provide positive and negative feedback controls of IICR mechanism [69, 132].

The CICR mechanism is described as the release of calcium from the SR triggered by calcium rise. The CICR was recognized in the experiments as a calcium "flash". The calcium "flash" was observed as a response of the cell to caffeine. In some cases, the caffeine-induced calcium release from SR was enough to produce contractions in VSMCs [73]. Unlike IICR, CICR mechanism was activated at high calcium concentrations, above 1 μM [43].

The caffeine-induced calcium release from SR were blocked by an akaloid called ryanodine [64, 73]. The ryanodine showed high affinity to a protein in SR membrane. Experiments show that SR is sensitive to calcium [102]. Later on, the ryanodine binding protein was identified as a calcium ion channel, called RyR channel, with high conductance. The application of ryanodine locks the RyR channel leads to a low conductance of calcium and suppresses CICR.

In general, it is assumed that the RyR channel is responsible for CICR and IP_3R channel is responsible for IICR. Since both IP_3R and RyR are present in the SR, calcium release from the IP_3R channel may influence the RyR channel because of its calcium sensitivity. There is evidence for cross-talk between IP_3R and RyR in portal vein myocytes and retinal arteriolar myocytes [53, 177].

1.3.4 Intracellular calcium oscillations: Role of IP_3R and RyR

The IP_3R and RyR tend to be involved in the agonist-induced calcium release as the SR is the main component responsible for the intracellular calcium rise in the VSMC. The cyclic behaviour of calcium needs to be generated in the VSMCs for intracellular calcium oscillations. If only IP_3R is present in the SR, cyclic opening and closing of IP_3R may contribute to the existence of calcium oscillations. The calcium regulation of the IP_3R channel is complex and biphasic as reported in the studies of Bezprozvanny et al. [18] and Iino [68]. The bell-shaped curve of IP_3R open probability for dependence on calcium gives the maximum probability of opening at an intracellular concentration of ≈250 nM. Out of the three subtypes of IP_3R, type 1 IP_3R is predominantly found in VSMCs [180, 184]. The presence of 80% type 1 IP_3R is found in the aorta and A7r5 VSMCs. The functional importance of type 1 IP_3R in agonist stimulation is that the calcium regulation of type 1 IP_3R

is biphasic. This strongly suggests that type 1 IP_3R might be the main subtype involved in the agonist-induced calcium oscillations.

Similar to IP_3R, the calcium-dependent open probability of RyR is biphasic. The open probability of RyR reaches a maximum in micromolar concentrations of intracellular calcium and the calcium deactivation of RyR happens at a higher intracellular concentration of $\approx$100 μM [18]. Within the physiological range of intracellular calcium, IP_3R experiences both positive feedback and negative feedback for calcium release while RyR acts as a calcium-induced calcium channel.

The agonist-induced calcium oscillations disappear when IP_3R inhibitors, such as D-myo-Inositol 1,4,5-tris-phosphate trisodium salt and heparin, are used [19, 184, 110, 196]. This indicates the possibility of an IP_3 mediated pathway in agonist-induced calcium oscillations. When PLC blockers, U73122 or neomycin, are used in the experiments, agonist-induced calcium oscillations disappear [200, 61, 67, 55]. Activation of PLC is essential for the production of IP_3. The need for PLC activation confirms the existence of an IP_3 mediated calcium signalling pathway in agonist stimulation.

The agonist-induced calcium oscillations are unaffected by the inhibition of RyR in VSMCs from pulmonary arteries [61]. McCarron et al. [115] showed that RyR was not required for IP_3 induced calcium oscillations in the SMC and IP_3R alone was sufficient. In contrast to this, agonist-induced calcium oscillations were not completely blocked by RyR inhibitors, though the calcium rise reduced to some extent [19, 53]. In the study of Bai et al. [8] on airway smooth muscle cells, application of the RyR antagonist ryanodine had no effect on the agonist-induced calcium oscillations but with another RyR antagonist, tetracaine, agonist-induced calcium oscillations were inhibited in a concentration-dependent manner. Similar to that, Tumelty et al. [177] study on retinal arteriolar smooth muscle cells showed that RyR inhibitor, tetracaine, blocks agonist-induced calcium oscillations. Since the experimental evidence is not entirely consistent, the role of RyR on the agonist-induced calcium oscillations is still debatable.

1.3.5 Intracellular calcium oscillations: Role of SERCA

The termination of the calcium release from the SR happens when IP_3R and RyR are inactivated. The raised calcium in the cytosol is either extruded to the extracellular space or reloaded to the SR. Shmigol et al. [163] showed that intra-SR calcium would recover to the baseline even if the VSMC is continuously exposed to the agonist. Also, they showed that the increase of intra-SR calcium is analogous to intracellular calcium decrease, it indicates that calcium in the cytosol is taken for partial filling of the SR.

The calcium transporter of SR responsible for the sequestration of calcium is the SERCA pump. ATP hydrolysis and enzyme phosphorylation of SERCA causes conformational changes to SERCA and result in translocation of calcium ions from the cytosol to a high-affinity site of SERCA. The translocated ions, most commonly two calcium ions, are then released to the SR [195]. Three genes of SERCA proteins are identified, SERCA 1, SERCA 2 and SERCA 3. SERCA 2a and SERCA 2b are expressed in VSMCs [180, 41]. However, SERCA 2b is the most common and abundantly present in VSMCs [108]. Wu et al. [195] reported that SR of VSMCs from thoracic aorta contained 90% SERCA 2b proteins.

In most of the experiments, agonist-induced calcium oscillations disappear when the SERCA pump is inhibited [61, 67, 163, 200]. As the major calcium rise for agonist-induced calcium oscillations comes from the SR, refilling of intra-SR calcium is necessary for the onset of calcium oscillations. The SERCA pump would therefore be an essential calcium handling protein in the SR for the occurrence of agonist-induced calcium oscillations. Also, SERCA function plays a vital role in maintaining low intracellular calcium needed for the relaxation of the VSMC.

1.3.6 Calcium extrusion to extracellular space

Besides calcium translocation by the SR, calcium in the cytosol is extruded into the extracellular space during agonist stimulation by sodium/calcium exchanger (NCX) and plasma membrane calcium ATPase (PMCA) calcium transporters. NCX is an electrogenic antiporter and can transport calcium ions into or out of the cytosol [50]. At normal concentrations of sodium in the extracellular space, calcium is extruded to the extracellular space. It is reported that one calcium ion is exchanged for three sodium ions [143]. Meaning to say that, the exchange process of NCX is electrogenic causing the membrane potential to be more positive. Moreover, alteration of the membrane potential of the VSMC would change the calcium extrusion rate by the PMCA, leading to a change in intracellular calcium [50].

The PMCA pump belongs to the family of P-type ATPase. There are 4 genes of PMCA. PMCA-1 and PMCA-4 are commonly expressed in VSMCs. PMCA pumps calcium ions by consuming one ATP molecule. Since PMCA pumping is coupled with a proton uptake, it may lead to pH changes in the VSMC [6]. The molecular ratio, Ca^{2+}:H^{+}, of 1:1 is commonly accepted. This ratio makes PMCA an electrogenic pump which affects the membrane potential of the VSMC. However, the stoichiometry ratio of Ca^{2+}:H^{+} is still controversial.

The specific use of NCX and PMCA to extrude calcium to the extracellular space may vary in VSMC. In general, NCX is a low calcium affinity channel with a high capacity of calcium extrusion, while PMCA is a high-affinity channel with a low capacity calcium transport. PMCA is likely to be responsible for keeping intracellular calcium at resting

conditions. On the other hand, the main function of NCX seems to be to maintain the intracellular calcium level within the physiological range during cell stimulation. PMCA tends to be active in a concentration range at which NCX is apparently inactive. The extrusion of intracellular calcium is significantly reduced in the absence of extracellular sodium, which in turn reduces the calcium exchange of NCX. The primary calcium extrusion in arterial smooth muscle is happening through NCX as compared to PMCA [5].

1.3.7 Calcium influx from extracellular space

The VOCC is identified as the primary calcium channel present in the VSMC. L-type ($Ca_V1.2$), P/Q -type ($Ca_V2.1$) and T-type ($Ca_V3.1$ and $Ca_V3.2$) voltage-operated calcium channels are expressed in VSMCs. Among these, the L-type ($Ca_V1.2$) calcium channel plays the dominant role in agonist-induced calcium dynamics [124]. Depolarization of the cell triggers the VOCC and leads to calcium entry to the cytosol.

The extrusion of calcium to extracellular space may cause a dynamic loss of calcium released to the cytosol from the SR. To compensate the loss of intracellular store calcium, calcium influx from the extracellular space is needed. It is observed that the recovery of the SR is not blocked by the removal of extracellular calcium, but the recovery was less than 75% [163]. However, the rate of refilling of the SR is sped up when extracellular calcium is restored. This indicates the need of the VOCC for the complete recovery of intra-SR calcium.

The activation of non-selective cation channels (NSC) like the transient receptor potential cation (TRPC) channels and ligand-gated cation channels also enhance intracellular calcium. TRPC3, TRPC6, and TRPC7 are the most common NSC channels found in the VSMC. TRPC channels are activated either by depletion of intra-SR calcium or after a receptor occupancy. The former one is commonly called a store-operated cation (SOC), and the later one is known as a receptor-operated cation (ROC) channel.

The cell membrane and its components are under the influence of membrane potential. The membrane potential is determined by the ionic concentration gradient between the cytosol and the extracellular space, permeability of ions through their particular ion channel and the activity of electrogenic pumps and exchangers. The most common membrane potential regulated ion channels in VSMCs are potassium channels like the voltage-dependent potassium (K_V) channel and the calcium-activated potassium channel (K_{Ca}), the calcium activated chloride channel (CACC), the VOCC and the non-selective cation channel (NSC). The membrane potential also regulates the electrogenic pumps and exchangers such as the sodium/potassium pump (NaK), PMCA pump, and NCX exchanger.

1.3.8 Features of agonist-induced intracellular calcium oscillations

In general, the agonist-induced contraction of the VSMC is associated with a series of cyclic rises of intracellular calcium, called intracellular calcium oscillations. Upon agonist application, first calcium increase is obtained in a short time, mostly less than 10 seconds, followed by a series of regular oscillations of intracellular calcium [55, 61]. The peak value of agonist-induced intracellular oscillation is less than 1 μM. The frequency varies from 5 to 30 oscillations per minute. The frequency of oscillation depends on the agonist concentration and the type of tissue used for the experiment. In the Hamada et al. [61] study, 0.1 to 10 μM of PE produced intracellular calcium oscillations of 0.5 to 1.36 cycles/min in VSMCs from the pulmonary artery. In the study of Ruehlmann et al. [147], 0.1 to 10 μM of PE produced high-frequency calcium oscillations of 1.2 to 30 cycles/min in VSMCs from the inferior vena cava. Though the range of frequency of oscillations varies in different tissue beds used, it is consistent that concentration of agonist strongly modulates the frequency of calcium oscillations.

1.4 Propagation of intracellular calcium in VSMCs

The application of a vasoactive agonist induces contraction not only at the point of application in the artery, but also at the region far from the stimulation point. The local contraction propagates to downstream or upstream. The propagation of vasomotor response was reported in arteries of different tissues. Dietrich [39] observed conduction of NE-induced constriction in arterioles of rat mesentery at a distance of 400 μm. ACh and NE-induced vasomotor responses were observed in the arterioles of hamster cheek pouch [155]. The spread of ACh triggered vasodilation was found in feed arteries and arterioles of hamster skeletal muscle [156]. These experiments were conducted in endothelium-intact blood vessels. There might be the contribution of myoendothelial and EC coupling along with VSMC coupling in the conducted vasomotor responses.

Welsh and Segal [188] showed that agonist-induced depolarization and constriction were initiated and conducted along VSMCs, and these responses were independent of the endothelium. The NE and PE vasoactive agonists were used in their study to stimulate arterioles supplying blood to the hamster cheek pouch. Seppey et al. [158] conducted a detailed study to understand the role of the endothelium, in particular on arterial vasomotion. They have demonstrated that ECs are not needed for the occurrence of vasomotion. Contractions were generated on the endothelium-denuded artery at lower agonist concentrations than on the endothelium-intact artery. Endothelium showed only a modulating role in their study. Later, Seppey et al. [157] showed the propagation of intracellular calcium waves in the mesenteric

artery after a local stimulation with PE. This calcium propagation was unchanged in the presence and absence of endothelium. Bartlett and Segal [12] demonstrated that PE-induced agonist vasoconstriction was initiated and propagated within the VSMC layer alone. Conversely, ACh-induced vasodilation was initiated in endothelial cells (ECs) and propagation of the vasodilation signal was carried along VSMCs as well as ECs.

As discussed above, intercellular signalling between VSMCs is sufficient for the propagation of contraction and rhythmic oscillations of contraction-relaxation. The intracellular calcium in the layer of VSMCs regulates the contractile property of an artery. The intracellular calcium is the main regulator of many other cellular activities in VSMCs. The signalling mechanisms of propagation of intracellular calcium might be similar in all the cellular activities of VSMCs. Therefore, understanding the propagation of intracellular calcium dynamics in VSMCs would help us to explain the intercellular signalling mechanisms of propagation of vasomotor response on the endothelium-denuded artery and the other cellular activities.

The propagation of intracellular calcium between the cells seems to be different to passive diffusion of calcium from the stimulated cell to the non-stimulated cells. The peak amplitude is expected to reduce in passive propagation. In most of the experiments, the peak amplitude of calcium oscillations was not different from the stimulated cell [200, 157]. The regenerative nature of intracellular calcium propagation in VSMCs was reported in colonic SMCs by Young et al. [200]. In their study, the propagation was extended to all the cells of the system under consideration. In the study of Seppey et al. [157] using VSMCs, the propagation was not entirely regenerative; the propagation stopped after a distance of 385 μm. Halidi et al. [60] also observed the same level of calcium rise in the non-stimulated cells.

The propagation velocity of intracellular calcium oscillations between the cells by a local stimulation was unchanged for all the cells irrespective of their position relative to the stimulated cells [200, 157]. The calcium propagation velocity in cultured colonic SMCs was approximately 20 μm/s in the Young et al. [200] study. In cultured VSMCs, the calcium propagation velocity was not different from colonic SMCs [60]. Seppey et al. [157] reported a higher propagation velocity of 100 ± 21 μm/s in a strip of VSMCs .

Seppey et al. [157] demonstrated that calcium propagation is not possible in the absence of extracellular calcium. The use of nifedipine, a VOCC inhibitor, also abolished calcium propagation in their study. According to them, the propagation of depolarization might be necessary for the propagation of intracellular calcium as the opening of VOCC depends on membrane potential.

Young et al. [200] and Halidi et al. [60] showed that propagation does not fully depend on influx from the extracellular space. The calcium propagation was obtained in the absence of extracellular calcium, though the peak amplitude and propagation velocity reduced. The peak

calcium level in the non-stimulated cell was decreased by 25% in the absence of extracellular calcium. When a VOCC inhibitor was used in Halidi et al. [60], the calcium propagation was similar to that in the absence of extracellular calcium.

The inhibition of IP_3R significantly suppressed calcium propagation in the study of Halidi et al. [60]. The average calcium increase was reduced by 72%. However, inhibition of the RyR receptor had no effect on either the calcium peak or the propagation velocity of calcium oscillations, similar to Young et al. [200] study. When inhibitors of PLC were used, the propagation of calcium wave was totally abolished. The blocking of PLC affects the formation of IP_3. This indicates that IP_3 is a possible intercellular messenger for calcium propagation.

1.4.1 Gap junctional intercellular communication (GJIC)

Propagation of intracellular calcium from a stimulated cell to distant cells requires communication between cells. Intercellular communication is possible by chemical and electrical communications. Paracrine signalling and gap junctional intercellular communication (GJIC) are two main pathways responsible for intercellular communication. In the process of paracrine signalling, a cell releases a signalling molecule to the extracellular space. The signalling molecule diffuses through the extracellular space and binds to the membrane receptors of the neighbouring cell. GJIC is the result of transport of cytosolic ions and molecules through the gap junction which connects the cytosols of the two cells. GJIC is necessary to spread and synchronize the vascular tone along the vessel wall [36, 29, 40]. Paracrine signalling in VSMCs may be avoided because the propagation of intracellular calcium vanishes when the gap junctions are blocked [157, 200, 60]. Therefore, GJIC is considered as the key pathway that enables the propagation of intracellular calcium in VSMCs.

The gap junctions are made of two connexons, each containing six connexin (Cx) proteins, of the same or different types. Four different connexins are commonly found in the vascular bed; Cx37, Cx40, Cx43, and Cx45. The connexins Cx40 and Cx37 are found predominantly in ECs and Cx43 is expressed widely in SMCs. Cx45 is also found in SMCs. The expression of these connexin proteins at the gap junction vary between different types of vascular beds and between the same vascular beds of different species. The connexin expression at the gap junction is dynamically controlled in healthy vessels and in vessels during a disease progression [159, 94, 26, 47]

The permeability of a gap junction is defined as its ability to allow passage of certain molecules or ions through it. The gap junctions are larger in diameter than the ion channels, and they permit the passage of cytoplasmic ions and molecules with molecular weight slightly smaller than 1000 kDa. The gap junctions are permeable to many cytoplasmic molecules

and ions such as calcium (Ca^{2+}), potassium (K^{+}), sodium (Na^{+}), chloride (Cl^{-}), IP_3, cyclic guanosine monophosphate (cGMP), cAMP, adenosine diphosphate (ADP), and ATP. There is a scarcity of experimental data for getting a conclusive opinion about the selective permeability of a gap junction. Therefore, one can assume little selective permeability as gap junctions have a large pore. However, rapid diffusivity of cAMP is seen through Cx43 compared to Cx45 and Cx40 [81, 14].

The conductance is defined as the rate of passage of permeable molecules or ions through the gap junction. The conductance of different gap junction channels varies based on the pore topography. Homotypic or heterotypic channels are the two types of gap junctions based on the assembly of their connexins. A homotypic gap junction contains two identical connexons. A heterotypic gap junction consists of two distinct connexons and each connexon contains identical connexins. For the most common homotypic channels in the EC and SMC, the unitary conductance is in the order, Cx37 (300pS)>Cx40 (140pS)>Cx43 (60pS)> Cx45 (30pS). Commonly found heterotypic channels in the vascular bed are Cx37-Cx40, Cx43-45, Cx37-Cx43, Cx40-Cx45 and Cx40-Cx43. Prediction of unitary conductance of heterotypic channels from homotypic channels is extremely difficult since some heterotypic channels (Cx37-Cx43) have configuration-dependent conductance. However, Cx43-Cx40 (100-150pS) and Cx43-Cx45 (52pS) channels have conductance in agreement with homotypic channel conductances in series.

Gap junction channels are sensitive to membrane potential, V_m, and transjunctional voltage difference, V_{gj}. The gating mechanism of Cx45 is a good example [11]. The conductance of Cx45 increases upon depolarization of the cell. V_m gating of a Cx45 hemichannel depends on the V_m of the cell to which it is connected. This observation suggests that a Cx45 channel contains two V_m dependent gates in series, one in each hemichannel. On the other side, the conductance of Cx45 decreases when V_{gj} is varied from zero to positive or negative values. V_m and V_{gj} gating mechanisms are different and independent. Similarly, pH sensitive gating mechanisms exist in some connexin channels [54].

1.5 Research motivation: Vascular dysfunction in diabetes

Diabetes is a metabolic disorder characterized by hyperglycaemia as a result of defects in insulin action, insulin secretion or both. The prevalence of diabetes is increasing rapidly worldwide. According to the world health organization (WHO), almost 422 million people in the world have diabetes. The main reason for the death of more than 1.5 million people

worldwide is diabetes [131]. In Australia, almost 1.2 million people are affected by diabetes [7], whereas in New Zealand almost 210,000 people have diabetes [48].

The long-term dysfunction and damage of various organs of the body like blood vessels, nerves, heart, eyes and kidneys, occur at the chronic stage of hyperglycaemia of diabetes, that leads to renal failure, potential loss of vision, foot ulcers, cardiovascular diseases and sexual dysfunction. Vascular dysfunction that is distinctively observed in diabetic patients leads to the high prevalence of cardiovascular diseases (CVD) including stroke, coronary artery diseases (CAD), cerebral vascular disease and peripheral arterial diseases (PAD). The cardiovascular disease was the cause of death of 70% of diabetes in Australia [7]. In New Zealand, almost 50% of diabetics have died because of cardiovascular diseases [48]. Diabetic patients have a high risk for atherosclerosis as well, in particular for patients with type 2 diabetes mellitus. Almost 90% of diabetic patients have type 2 diabetes mellitus [32].

The vascular dysfunction in diabetes causes vast complications in the circulatory system, which includes regulation of blood flow to the tissues. The cellular mechanisms behind vascular dysfunction in diabetes are not completely elucidated because of the increased complexity like the involvement of multiple cell types, like VSMCs and ECs, and extended effects of the clotting factors, local production and function of vasoactive agents [74, 119]. The EC dysfunction associated with diabetes has been extensively studied in the literature [171]. VSMC dysfunction is exhibited in the microcirculation as well as in macrocirculation [123]. There are some experimental evidence to support the VSMC dysfunction in diabetic condition. However, the different factors that cause VSMC dysfunction in diabetes and its implications are not well addressed in the literature. This needs more investigation to understand the vascular dysfunction associated with diabetes.

Sharma et al. [161] reported that transforming growth factor (TGF)-β plays an essential role in VSMC dysfunction by modulating intracellular calcium dynamics. TGF-β inhibits intracellular calcium transients by reducing IP_3 sensitivity in VSMCs [201]. The IP_3 sensitivity is related to the TGF-β -induced downregulation of IP_3R [162]. TGF-β downregulation of IP_3R expression is found in diabetic VSMCs of aorta by Sharma et al. [161], (refer to Figure 1.7). In their study, the impaired intracellular calcium transients were restored by anti-TGF-β antibodies. Based on this, they have suggested that suppression of IP_3R expression might be the reason for the vascular dysfunction in diabetics.

Searls et al. [154] also reported downregulation of IP_3R expression in diabetic VSMCs of the aorta and femoral arteries. Expression of all three types of IP_3R protein, (refer to Figure 1.8) and IP_3-mediated calcium transients were reduced in diabetic-affected VSMCs. The impaired calcium transients and the change in IP_3R level in diabetic VSMCs matched closely with the same kind of experiments with VSMCs in a high-glucose medium. These

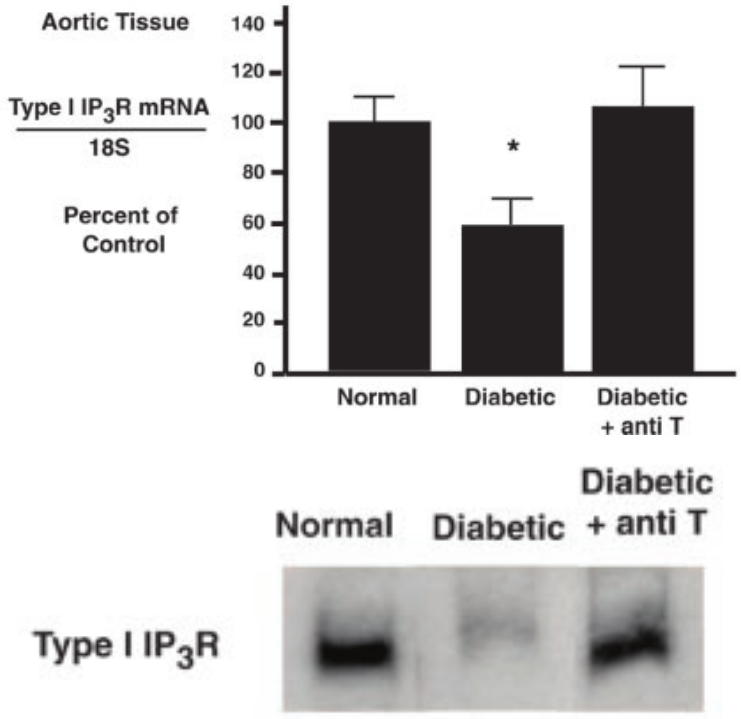

Fig. 1.7 Downregulation of IP_3R in diabetic VSMCs from aorta. The comparison of type 1 IP_3R in normal VSMC, diabetic VSMC and diabetic VSMC with anti-TGF-β antibodies is given. Reproduced from Sharma et al. [161] paper.

observations lead to the hypothesis that hyperglycemia could be the reason behind the downregulated IP_3R in diabetes causing impaired intracellular calcium transients.

Ma et al. [109] reported that a significant reduction of α_1-adrenoceptor agonist-induced contraction (PE used) in the diabetic aorta is related to the downregulation of IP_3R. According to them, the IP_3-induced calcium release (IICR) pathway plays a crucial role in the vascular dysfunction in diabetes.

The B-cell lymphoma (Bcl)-2 and Bcl-x_L proteins are upregulated in the VSMCs of diabetic patients and exposed to a high-glucose medium [148, 149, 105]. The IP_3-dependent activation of IP_3R was found directly related to the Bcl-2 and the Bcl-x_L protein levels [104, 182]. Velmurugan and White [182] observed Bcl-2-dependent increases in the IP_3R excitability and in the IP_3R-dependent calcium release in diabetic VSMCs. The Bcl-2 and the Bcl-x_L-induced IP_3R excitability might involve in the dysregulation of intracellular calcium in diabetic VSMCs.

In the study of Searls et al. [154], downregulation of SERCA 2 and SERCA 3 isoforms were found in diabetic VSMCs. The distribution of SERCA proteins was also altered. The alteration of SERCA expression in diabetic VSMCs was similar in VSMCs of high glucose

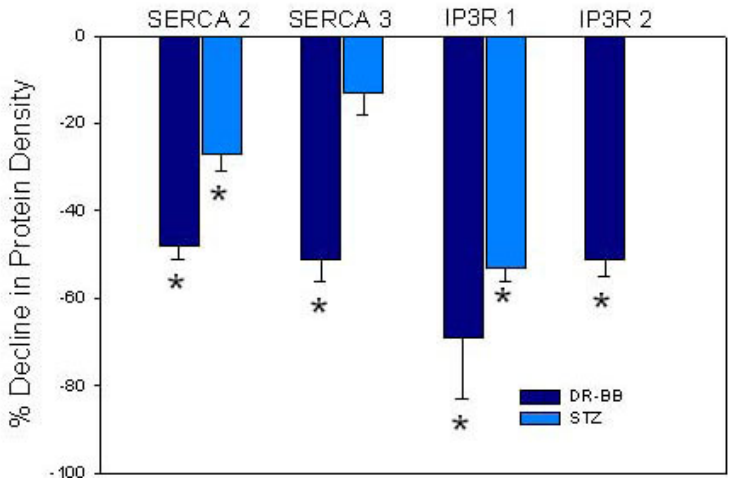

Fig. 1.8 Downregulation of SERCA and IP_3R proteins in diabetic VSMCs from aorta. Reproduced from Searls et al. [154] paper (open-access article).

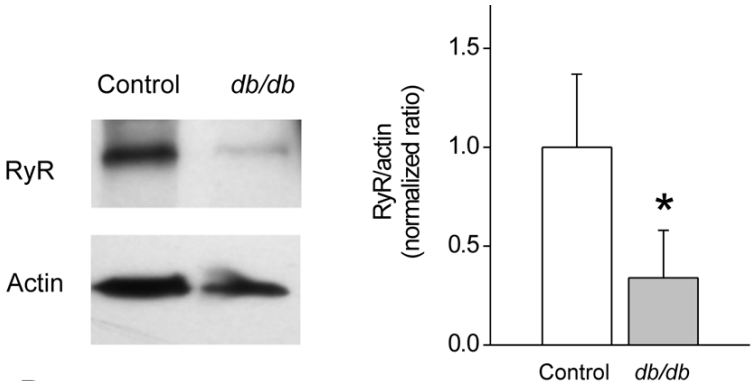

Fig. 1.9 Downregulation of RyR in VSMCs from cerebral arteries of type 2 diabetic mice. Reproduced from Rueda et al. [146] paper (open-access article).

fed rat models, suggesting hyperglycemia could be the reason for the altered levels of SERCA in diabetic VSMCs. Downregulation of SERCA is also reported in cardiac cells with diabetes. In the study of Kim et al. [88], the maximal calcium uptake of the SR was reduced due to the reduced level of SERCA in the diabetic cardiac cell.

Regardless of the type of diabetes, expression of RyR was found reduced in aortic and cerebral VSMCs [146, 109]. In these experiments, agonist-induced intracellular calcium rise was significantly reduced with the reduction of RyR expression. Rueda et al. [146]'s study on cerebral VSMCs of obese type 2 diabetic mice shows reduced spatiotemporal dynamics of intracellular calcium. The average calcium peak, full duration at half maximum, full width at half maximum and mean rising rate were decreased. The expression of downregulated RyR in the diabetic mouse was reported as the reason for the reduced calcium dynamics,

(refer to Figure 1.9). In contrast to this, increased expression of RyR is shown in Searls et al. [154]'s study on VSMCs of the aorta and femoral artery from diabetic Wistar rats. A similar change in the RyR level was obtained in A7r5 cells grown in hyperglycemic condition.

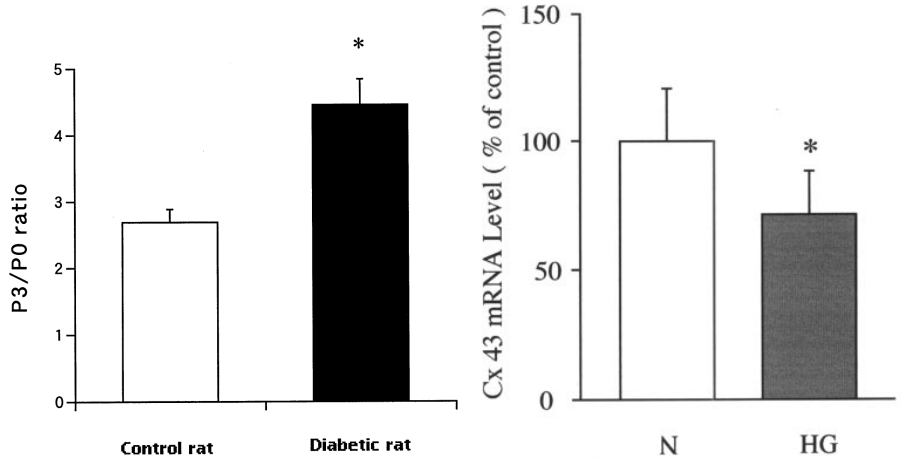

Fig. 1.10 (left) Increased phosphorylation of Cx43 in VSMCs from a bovine thoracic aorta under high glucose medium. Reproduced from Kuroki et al. [92] paper (permission granted from American diabetes association to reuse in the thesis, license number: 3852141143899). (right) Downregulation of Cx43 in retinal pericytes under high glucose medium. HG stands for high glucose. Reproduced from Li et al. [103] paper (permission granted from Association for Research in Vision and Ophthalmology (ARVO) by email contact)

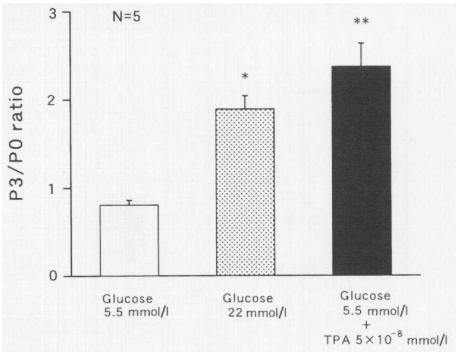

Fig. 1.11 Increased phosphorylation of Cx43 in the cardiac cell from a diabetic rat. Reproduced from Inoguchi et al. [71] paper (permission granted from Springer to reuse in the thesis and the license number is 3851261318462).

Vascular dysfunction in diabetes is also related to the alteration in connexins of gap junctions between VSMCs [92, 25, 71]). Kuroki et al. [92] showed increased protein kinase C (PKC) activity and reduced GJIC in VSMCs exposed to the high-glucose medium. The addition of calphostin C, an inhibitor of PKC, restored the GJIC in diabetic VSMCs. This

relation showed PKC-mediated inhibition of GJIC in the diabetic. The Cx43 is a phosphoprotein which exists in multi-phosphorylated forms in VSMCs such as P1, P2, and P3 along with nonphosphorylated form P0. The high-glucose content enhanced phosphorylation of Cx43, especially the P3 form, leads to the inhibition of GJIC, (refer to Figure 1.10). One possible mechanism for the inhibition of Cx43 function was the PKC-mediated phosphorylation of Cx43. When PKC activator, 12-O-Tetradecanoylphorbol-13-acetate (TPA), was used, phosphorylation of Cx43 was significantly increased, (refer to Figure 1.10). Based on these results, they have suggested that PKC-mediated inhibition of Cx43 might be the reason for the reduced GJIC between VSMCs in diabetics. Similar findings were reported by Inoguchi et al. [71] in the cardiac cells of diabetic rats, (refer to Figure 1.10). PKC β isoform was found to be the main isoform that causes the phosphorylation of Cx43. The reduction in ventricular conduction was related to the increased phosphorylation of Cx43. The high glucose level also reduces the expression of Cx43 in aortic ECs [92], microvascular ECs, and retinal pericytes [103]. Altogether, these studies indicate that inhibition of Cx43 function might be the reason for reduced GJIC in VSMCs.

Diabetes increases PKC activity [70], TGF-β production [161] and expression of Bcl-2 and Bcl-x_L [182] in VSMCs. In diabetic VSMCs, the PKC-mediated phosphorylation of Cx43 inhibited GJIC, the TGF-β induced downregulation of IP_3R and Bcl-2 and Bcl-x_L promote IP_3R activation. The expressions of SERCA, IP_3R and RyR are also altered in VSMCs under diabetic and high-glucose conditions. Interestingly, these modification in diabetes related to the intracellular calcium dynamics by affecting the calcium release from the SR and GJIC.

The experimental studies imply that impaired intracellular calcium dynamics in diabetic VSMCs is related to the alteration of the expression of calcium handling proteins such as SERCA, IP_3R, and RyR and the altered expression of Cx43 stands for the impaired GJIC in VSMCs. As intracellular calcium is a key component that defines the functioning of the VSMC, the impaired intracellular calcium dynamics might be the reason for the VSMC dysfunction in diabetes. This arises the need of research to understand how altered levels of SERCA, IP_3R, RyR and GJIC influence the intracellular calcium dynamics of VSMC. This study would help us to better understand the VSMC dysfunction in diabetes.

1.6 Research Aims

- Many experimental studies in the past aimed to understand the reason behind the impaired calcium dynamics in diabetic VSMCs. Some of these studies suggested that altered expression of calcium handling proteins in the SR such as SERCA, IP_3R

and RyR is related to the impaired calcium dynamics in diabetic VSMCs. However, the individual role of these proteins on the impaired calcium dynamics in diabetes is not clearly understood. This might be because of the difficulty in doing experiments to control the expression of each protein and to pinpoint the functional role of each protein. Therefore, it is important to study the implications of altered levels of each proteins, SERCA, IP_3R and RyR, on the intracellular calcium dynamics. Mathematical modelling can help us to do a systematic study and to unveil the knowledge gap that experiments may not able to explore in diabetic VSMCs.

- The experiments provided an indication of reduced GJIC due to the phosphorylation of Cx43 or downregulation of Cx43 expression in diabetic VSMCs. The GJIC controls the propagation of intracellular calcium which in turn affects the propagation of vasoactive agonist response. The experiments provided an indication of GJIC in diabetic VSMCs but failed to give a qualitative or quantitative relationship between the altered levels of GJIC and the propagation of intracellular calcium. To fully understand the VSMC dysfunction in diabetes, we have to figure out the cellular mechanisms of propagation of intracellular calcium in VSMCs and the implications of altered GJIC.

- None of the studies have reported the influence of altered levels of SERCA, IP_3R and RyR on the propagation of intracellular calcium. Since SERCA, IP_3R and RyR are altered in diabetic VSMCs, it is necessary to know whether the altered levels of these proteins have any role in the propagation of intracellular calcium.

Chapter 2

Mathematical models of VSMCs: A Review

Mathematical modelling is a powerful tool to investigate extremely complex biological systems such as connected cells and tissues. The computational models help researchers to advance the understanding of cellular processes, molecular interactions, and signalling pathways. New understanding would help us to develop cellular level reasoning of pathological conditions. Mathematical modelling is also capable of making a systematic approach to develop a hypothesis which may provide new directions for novel therapeutic strategies.

Though *in-vivo* and *in-vitro* experiments are regularly providing new understanding about intracellular calcium $\left(\left[Ca^{2+}\right]_{cyt}\right)$ dynamics in VSMCs, the need of mathematical models was recognised by early researchers. The main focus of the mathematical modelling was to describe intracellular calcium handling and the associated nature of membrane potential. However, not much progress has been made in the mathematical modelling of VSMCs. Especially, only a few VSMC mathematical models investigating agonist-induced calcium dynamics are available in the literature. Tsoukias [176] reported a detailed review on mathematical modelling of VSMCs. We have made a review of the existing mathematical models that describe agonist-induced calcium dynamics in VSMCs.

2.1 Single VSMC mathematical models

Meyer and Stryer [120] developed a molecular model for periodic calcium spiking induced by a constant stimulus. The intracellular calcium oscillations were assumed to be the result of cross coupling between intracellular calcium and IP_3. The calcium dependency on the production of IP_3 was modelled by including calcium activation of PLC. In this model, the

balance between IP_3 induced calcium release from the SR and intra-SR calcium reloading by SERCA defines the concentration of intracellular calcium. The intra-SR calcium was assumed as constant in this study. Later, Goldbeter et al. [52] developed a minimal model for agonist-induced calcium oscillations, (refer to Figure 2.1). This model included oscillator of intra-SR calcium $\left(\left[Ca^{2+}\right]_{SR}\right)$ but eliminated IP_3 oscillations. Calcium influx and efflux through the cell membrane were added to the intracellular calcium dynamics. The SR was assumed as a combination of two physically separate stores of which one was IP_3-sensitive and the other one was IP_3-insensitive. The calcium oscillations were regulated by the cycling of calcium between the IP_3-insensitive store and the cytosol. Calcium release from the IP_3-sensitive pool regulated the cyclic calcium release from the IP_3-insensitive pool by CICR. The model accounted for the effect of IP_3 by including the IP_3 sensitive calcium store. Moreover, the Goldbeter et al. [52] model shows that continuous agonist-induced calcium oscillations are possible in the absence of IP_3 oscillations.

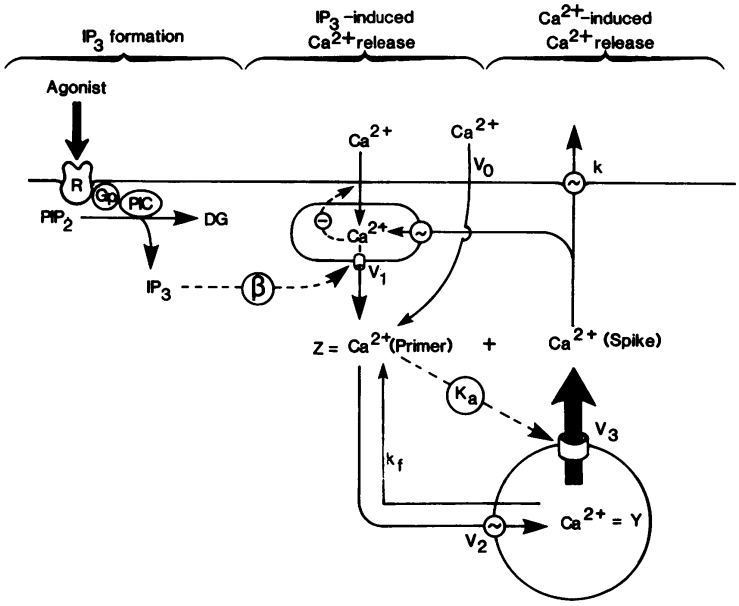

Fig. 2.1 Schematic representation of Goldbeter et al. [52] model. IP_3-sensitive and IP_3-insensitive calcium pools are used to model the calcium release from the intracellular calcium store. Reproduced from Goldbeter et al. [52] paper (permission is not needed to resuse in a thesis/dissertation for educational use).

Wong and Klassen [192] proposed a model to describe both electrical activity and intracellular calcium regulation induced by a PE agonist in the VSMC. The transmembrane calcium influx through an L-type calcium channel, the VOCC, was included in the model to account for membrane potential. Similar to the Goldbeter et al. [52] model, the intracellular store was divided into two calcium pools, IP_3-insensitive and IP_3-sensitive stores. However,

the two calcium pools were not physically separate. The IP_3-sensitive store was filled by calcium from the IP_3-insensitive store and ca-uptake pump while IP_3-insensitive store was refilled by taking calcium directly from the extracellular space. This model was extended by Wong and Klassen [193] to study both intracellular calcium dynamics and electrical activity induced by the endothelin-1 (E1) agonist. In this model, the ionic currents of an L-type calcium channel, a calcium-activated potassium channel (K_{Ca}), a voltage-dependent potassium channel and a NSC determine the membrane potential state of the cell. The NSC was modelled as an agonist-receptor complex and intracellular calcium dependent channel.

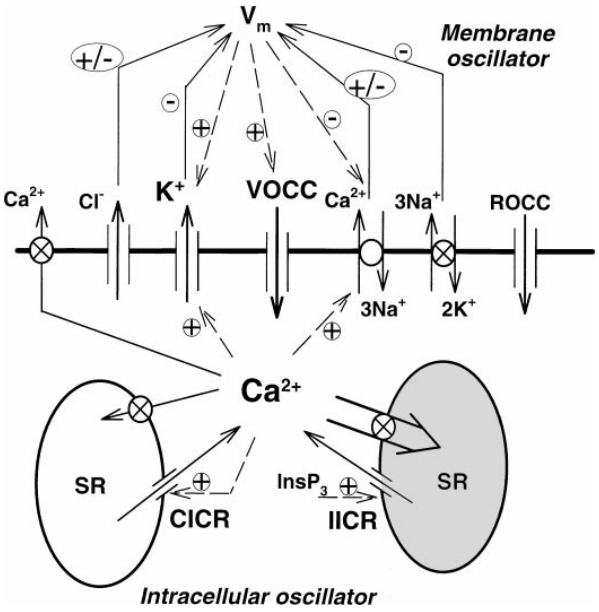

Fig. 2.2 Schematic representation of minimal model of Parthimos et al. [135]. Transmembrane components of the model along with the direction of ionic flow are given. The role of each component on the regulation of membrane potential is indicated. This model assumes intracellular store as being two physically distinctive calcium pools, where one is IP_3-sensitive and the other one is ryanodine-sensitive. The CICR mechanism is incorporated in the ryanodine-sensitive calcium pool while the IICR is used in the IP_3-sensitive calcium pool. Reproduced from Parthimos et al. [135] paper (permission is not needed to resuse in a thesis/dissertation).

Parthimos et al. [135] developed a minimal model to analyse arterial chaos by coupling membrane and calcium oscillators, (refer to Figure 2.2). Two physically distinct stores, ryanodine-sensitive and IP_3-sensitive, were used in the model to represent calcium induced calcium release (CICR) and IP_3 induced calcium release (IICR) respectively, similar to the Goldbeter et al. [52] model. In addition to the VOCC and the K_{Ca}, transmembrane currents through a chloride channel, NCX and Na/K pump were included in the model. Kinetics of the K_{Ca} channel activation and inactivation were used to study the temporal variation of

K_{Ca} open probability. They have used this model to explain complex non-linear calcium dynamics observed in different experimental conditions. Koenigsberger et al. [89] extended this model by adding IP_3 dynamics based on Höfer et al. [66]'s study.

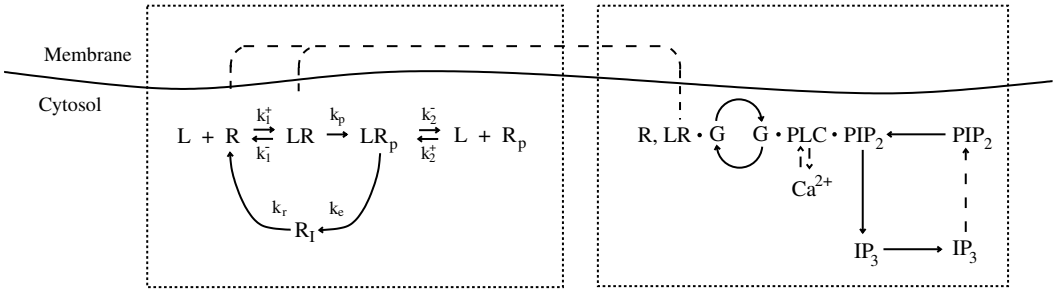

Fig. 2.3 Schematic representation of interaction between receptors (R) and ligands (L), receptor endocytosis, receptor recycling, G-protein interaction (G), PLC activation, PIP_2 hydrolysis and IP_3 & DAG formation from the Lemon et al. [101] model. Reproduced from Lemon et al. [101] paper (permission granted from Elsevier to reuse in the thesis, license number: 3856741143867).

An electrochemical model of the VSMC with material balance equations of Na^+, K^+ and Ca^{2+} was later developed by Yang et al. [197]. Voltage-clamp experimental data of isolated cells, mostly from cerebrovascular arteries, was used to validate the behaviour of model components. Additional transmembrane components used in this model were the stretch-activated channel and inward-rectifier potassium channel. Goldman–Hodgkin–Katz (GHK) model ionic current equations were used to model the stretch-activated current. A four-state kinetic model was used to find the open probability of the RyR channel. A second order gating of RyR was applied to calculate the ionic current as two activation sites were assumed in each RyR. In the following publication by the same group, an nitric oxide (NO)/cGMP signalling pathway was added to their VSMC model [198]. The NO/cGMP signalling pathway contains soluble guanylyl cyclase (sGC) activation, sGC-catalyzed production of cGMP, cGMP regulation of the K_{Ca} channel, and cGMP-mediated MLC phosphorylation. The NO regulation of the K_{Ca} channel was also included.

Later, Jacobsen et al. [76] formulated cGMP regulation of the CACC and studied the role of cGMP in converting calcium waves to whole-cell calcium oscillations in VSMCs. Model equations for cGMP-sensitive CACCs were validated against experimental data from the mesenteric artery. Their studies [76, 75] indicated that the essential role was played by the cGMP-sensitive CACC which allowed the membrane potential to move into an oscillatory state and induce vasomotion. However, their model was based on a single calcium efflux channel to simulate CICR. Importantly, Sanders [150] showed that both IP_3R and RyR channels were needed for VSMC oscillatory behaviour.

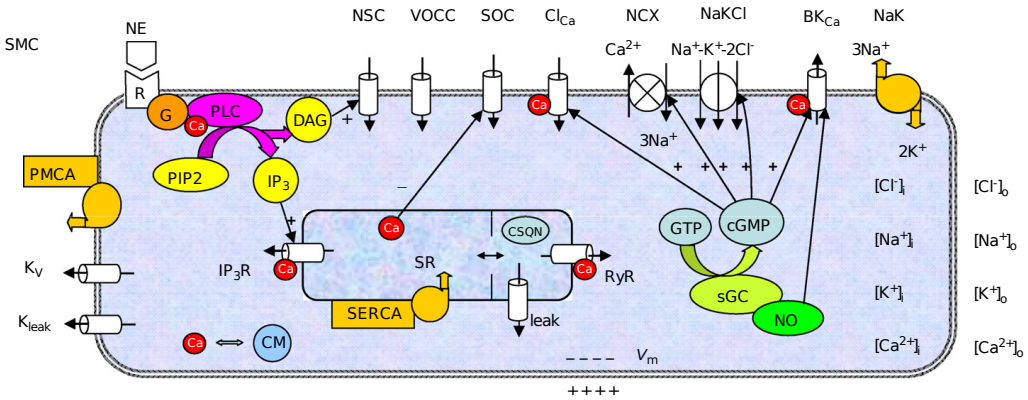

Fig. 2.4 Schematic representation of theVSMC model developed by Kapela et al. [83]. This model contains three compartments, cytosol, cell membrane, and the SR. The SR is compartmentalised into uptake and release compartments. An arrow is used to show the direction of the flow of ions or molecules through each SR and transmemrbane components of the model. The IP_3, DAG, calcium and NO/cGMP -mediated signalling mechanisms are shown. Reproduced from Kapela et al. [83] paper (permission granted from Elsevier to reuse in the thesis, license number: 3850771065526)

Lemon et al. [101] developed a mathematical model to account for the production of IP_3 following the application of an agonist to G-protein coupled receptors and subsequent intracellular calcium dynamics. A schematic representation of this model is given in Figure 2.3. The main components of the model were receptor activity, G-protein cascade, and calcium dynamics. Modelling of receptor activity is accomplished by connecting activities, such as binding to ligand agonist, phosphorylation, sequestration, dephosphorylation, coupling and uncoupling with the G-protein and recycling back to the cell membrane. The main elements of the G-protein cascade part of the model were G-protein activation, PLC activation, and hydrolysis of PIP_2. The G-protein dynamics were modelled by using the direct relationship of G-protein activation to ligand bound receptors and inactive G-proteins. The equation for the production of IP_3 was formed by linking calcium activation of PLC, replenishment of PIP_2 and degradation of IP_3. The net release of calcium from the SR was used to model the temporal variation of intracellular calcium. The net calcium from the SR was modelled by balancing the calcium release through the IP_3 sensitive store, the SR calcium leak and calcium uptake of the SR pump.

This model was later extended to study spontaneous transient outward current (STOC) in VSMCs [100]. The SR was represented as two physically separate compartments, a central SR and a peripheral SR. The main calcium release channels in the central SR and peripheral SR were IP_3R and RyR, respectively. Both compartments contain SR calcium pumps and leak channels. A kinetic scheme was used to model the RyR open probability. The STOC was

calculated as the ionic current through the BK_{Ca} channel as a response to the calcium release from the peripheral SR. The model equation for IP_3 production was simplified compared to the Lemon et al. [101] model by assuming no depletion of PIP_2 and no calcium activation of PLC. Based on that, the differential equation for the rate of change of PIP_2 was eliminated. Bennett et al. [15] further extended this model to study the contraction of blood vessels following NE stimulation.

Kapela et al. [83] developed a detailed VSMC model to study agonist-induced calcium dynamics by integrating most of the identified transmembrane channels, pumps, and exchangers along with new descriptions for sub-cellular processes (refer to Figure 2.4). Electrophysiological data from VSMCs of a mesenteric artery were used to model the majority of components of the model. Ionic current equations of the VOCC, BK_{Ca} and NSC were modelled using the GHK equation. The relaxation effect of NO was modelled by including a dependency of the BK_{Ca} channel opening on NO and cGMP. The regulatory effects of cGMP on CACC, NCX, and sodium-potassium-chloride cotransport (NaKCl) were also incorporated. The role of DAG, produced along with IP_3, on the depolarization of the cell was modelled by including a DAG-induced NSC channel. This model was capable of providing opposing effects of NE-induced intracellular calcium rise and NO-induced reduction of intracellular calcium. The main attractive feature of this model is that it can be used as a building block for studying the cellular behaviour of a specific interest by eliminating unwanted components or by including a new description of components and new signalling mechanisms.

2.2 Coupled VSMCs mathematical models

Koenigsberger et al. [89] studied calcium dynamics in a population of VSMCs by coupling the membrane potential, IP_3 and calcium between the adjacent cells. Gap junctional electrical coupling was modelled like an ohmic resistance by multiplying gap junctional conductance with the membrane potential gradient between adjacent cells. Similarly, a linear approximation of the molar flux across a gap junction directly proportional to the concentration gradient, was used to formulate coupling equations for calcium and IP_3. They have used the coupled cells model to analyse synchronisation of calcium oscillations in coupled smooth muscle cells. The study was conducted on a two-dimensional brick meshing of rectangular cells. Each cell communicates with six neighbouring cells. According to them, rather than IP_3 coupling, weak calcium coupling was crucial for synchronisation of calcium oscillations. The electrical coupling alone could produce propagation of calcium oscillations even if the number of coupled cells were increased.

The same group [90] has shown that propagation of intracellular calcium in VSMCs might result from the electrical coupling. This opinion was based on matching the simulation results, regarding propagation velocity, with the experimental studies of Seppey et al. [157] [90]. The influence of electrical coupling, VOCC conductance, CICR amplitude and chloride channel amplitude on propagation velocity were investigated. The time needed for generating a calcium 'flash' was the reason for the lowered propagation velocity of calcium oscillations compared to the electrical signal. The calcium 'flash' is defined as the rapid elevation of intracellular calcium in the cell. According to their study, CICR is essential for generating calcium 'flash' while the VOCC initiates calcium entry after depolarization.

Jacobsen et al. [75] used an additive electrodiffusion equation, similar to the Nernst-Plank equation for electrodiffusion, to model ionic currents through a gap junction,

$$I_{GJ,ion} = P_{ion}\sigma AF\left[\Delta[ion] + \frac{z_{ion}F\overline{[\Delta ion]}}{RT}\Delta V_m\right] \tag{2.1}$$

Where F - Faraday's constant, z - ion valency, R - universal gas constant, T - temperature, P - permeability of an ion, 'σA' represents the area of contact between the cells, $\Delta[ion]$ is the concentration difference between two the cells and $\overline{[\Delta ion]}$ is the average ion concentration between two cells. In contrast to Koenigsberger et al. [89] model, they integrated the influence of the calcium concentration gradient and the voltage gradient into a single ionic equation. This implies that gap junctional current by the passage of an ion is generated as a result of the concentration gradient of that ion and the electrical potential gradient across the gap junction.

Kapela et al. [84] used the GHK model equation to formulate the ionic fluxes across the gap junctions,

$$I_{GJ,ion} = P_{ion}\frac{z_{ion}^2F^2}{RT}\Delta V_j\frac{[ion]^i - [ion]^m Exp\left(-\frac{z_{ion}F\Delta V_m}{RT}\right)}{1 - Exp\left(-\frac{z_{ion}F\Delta V_m}{RT}\right)} \tag{2.2}$$

Where gap junctional current flows from cell n to cell m. All the four ions (Ca^{2+}, K^+, Na^+ and Cl^-) were coupled between the cells in this way. The permeability was assumed to be the same for all four ions. Permeability was calculated from the whole-cell resistance of the gap junction whose values for some vascular beds are available in the literature. For IP_3 coupling, molar flux was assumed to be directly proportional to the concentration gradient between two adjacent cells; this was similar to the Koenigsberger et al. [89] model. They have coupled VSMCs and ECs to study the effect of myoendothelial communication on vascular reactivity.

Most of the single cell mathematical model studies focused on the calcium signalling mechanisms in the VSMC and the role of different cellular components in the signalling [192, 120, 52, 76]. First, tissue-specific mathematical modelling in the VSMC was done by Yang et al. [197]. Their study aimed to investigate VSMC calcium dynamics and contraction in the cerebrovascular artery. The Lemon et al. [100] have used their model to study STOC generation in vascular A7r5 smooth muscle cells. The Kapela et al. [83]'s study aimed at mesenteric artery VSMCs. Coming to coupled VSMC models, propagation and synchronisation of intracellular calcium oscillations were mainly investigated [90, 75]. None of the modelling efforts aimed to understand the intracellular calcium dynamics of VSMCs in a pathological condition such as diabetes.

2.3 Thesis Objectives

1. **Development of a VSMC model to analyse agonist-induced intracellular calcium dynamics**
   Using Kapela et al. [83]'s VSMC model as a building block, we develop a new mathematical model by adding new or modified descriptions to the NCX exchanger, IP_3R channel, NSC channel, agonist-induced IP_3 production, SR structure, and functioning. The model takes only the most relevant channels, pumps and exchangers needed for the agonist-induced calcium dynamics from Kapela et al. [83] for the kind of study we do. The essential features of the model results will be validated against experimental results. We develop a numerical method, an integration of the Back-Euler method and fixed-point iteration, to solve the model equations. The numerical solver is programmed in 'C' code using Eclipse software, version: Juno service release 2 from http://eclipse.org/, installed on a local machine.

2. **Analysis of the effects of altered levels of SERCA, IP_3R and RyR on intracellular calcium dynamics of a single VSMC**.
   We conduct a detailed systematic investigation on the intracellular calcium dynamics in the presence of altered activation levels of SERCA, IP_3R, and RyR. In our knowledge, the cellular mechanism that alters the expression of SERCA, IP_3R, and RyR in diabetic VSMCs are not fully known. In the absence of such a mechanism, we change the level of a protein or a combination of two proteins, and the resulting dynamics of VSMCs are studied. This approach helps us to study the effects of different combinations of SERCA, IP_3R and RyR on the intracellular calcium dynamics in VSMCs. This method is reasonable as the aim of the research is to document the altered calcium dynamics

due to the altered expression of these proteins. We validate the results against available experimental results.

3. **Analysis of altered levels of SERCA, IP_3R, RyR and gap junctional coupling on the propagation of intracellular calcium in coupled VSMCs**
   We investigate the effects of altered levels of GJIC between VSMCs on the propagation of intracellular calcium. We alter the level of GJIC by changing the number of gap junctions. In addition to that, we alter the level of SERCA, IP_3R and RyR in the coupled cells and the resulting propagation of intracellular calcium will be analysed. We extend the numerical method used for single VSMC to coupled VSMCs by incorporating tridiagonal matrix algorithm (TDMA).

2.4 Thesis Overview

The overview of the thesis is illustrated in Figure 2.5. Chapter 1 provides a detailed discussion of the agonist-induced calcium dynamics in VSMCs. The chapter starts with an introduction to the human vascular system, then gives a brief explanation of the VSMC contraction mechanism and the role of calcium in the contraction. Sections 1.3 and 1.4 cover the calcium signalling mechanisms in VSMCs, the role of the SR, calcium release from the SR, CICR and IICR mechanisms, calcium translocation by the SR, calcium extrusion mechanisms, calcium influx mechanisms, the common features of agonist-induced calcium oscillations, intercellular signalling mechanisms, and GJIC. The research motivation and aims are states at the last sections of this chapter.

Chapter 2 describes the existing mathematical models of VSMCs, especially studying agonist-induced calcium dynamics. Both single cell and coupled cells models are reviewed. Thesis objectives and the overview of the thesis are given at the end of the chapter 2.

The methodologies of mathematical modelling in cell physiology are given in Appendix A, which will help to understand the model equations given in chapter 3. The development of a new VSMC model, the important changes made compared to previous model attempts, model equations and the comparison of model results against experimental studies are given in the chapter 3. The numerical method used to solve the model equations is also explained. Backward-Euler and fixed point iteration methods used to develop the numerical algorithm are given in Appendix B. The discretization of model equations, initial values of model variables and model parameters are supplied in Appendices C, D, and E respectively.

The VSMC model developed in the chapter 3 is used to study the effects of altered levels of SERCA, IP_3R and RyR on the intracellular calcium dynamics of VSMC, which is detailed in chapter 4. The combination of different parameters needed for the occurrence of calcium

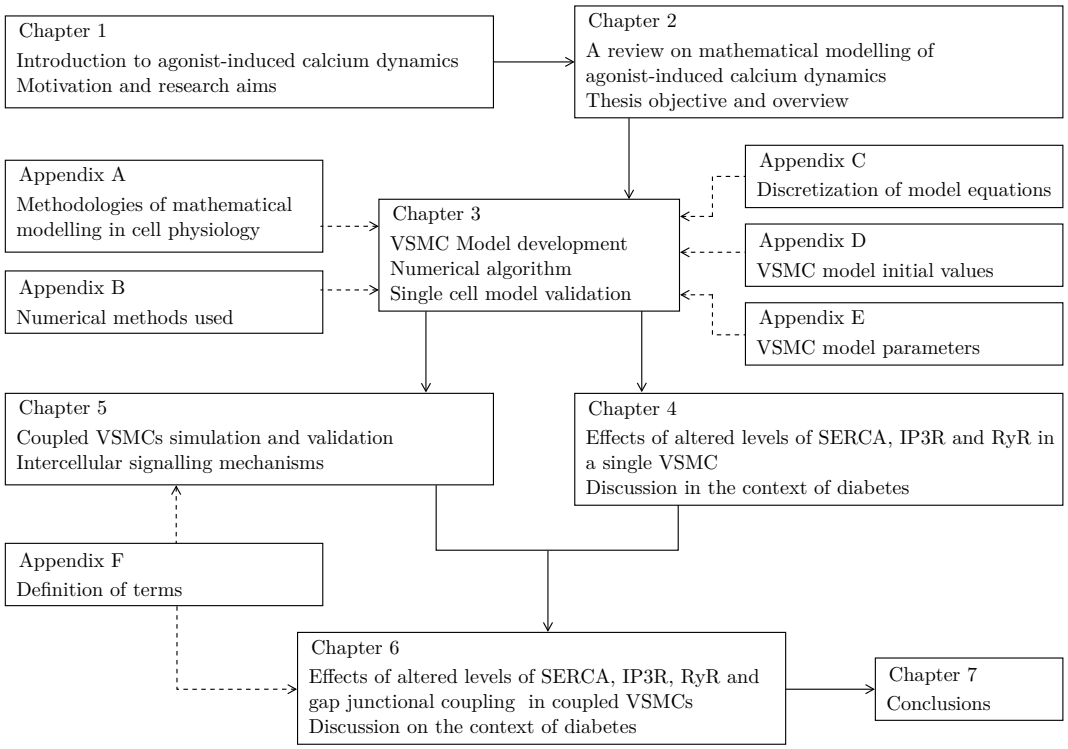

Fig. 2.5 Thesis roadmap

oscillations in the VSMC is investigated on the basis of bifurcation points of the system. The model results are discussed in the context of diabetes at the end of chapter 4.

Chapter 5 describes the propagation of intracellular calcium dynamics using the model developed in chapter 3. The coupled cells model equations are solved using a TDMA along with the numerical algorithm developed in chapter 3. The TDMA is detailed in Appendix B. A study was conducted on an in-silico VSMC strip of 100 serially coupled VSMCs in which first 51 cells were stimulated. The intracellular calcium propagation mechanisms in the model results are discussed and the dominant components are synthesised. The results are compared with the available experimental results. Appendix F gives definitions of some of the terms used in chapters 5 and 6.

The coupled cell model is extended to study the effects of altered levels of SERCA, IP_3R, RyR and gap junctional coupling on the propagation of intracellular calcium in VSMCs. The wave velocity and the penetration depth are analysed to describe the effects of each component investigated. The wave velocity and the penetration depth are calculated based on the regenerative calcium rise in the non-stimulated cells. The coupled results are discussed in the context of diabetes at the end of this chapter.

Finally, the whole thesis is summarised in chapter 7. The contributions of the research to the proposed research aims are explained from the model results. The possible directions of future works are also suggested.

Chapter 3

VSMC Model Development

3.1 Introduction

The recent increasing experimental study in VSMCs is bringing new insights to the VSMC calcium dynamics. It is so important to advance the existing mathematical models as they provided significant understandings to the calcium dynamics in VSMCs. We have used Kapela et al. [83] model as a building block to develop the new mathamatical model for VSMC. We have included new or modified description to NCX exchanger, IP_3R channel, NSC channel, agonist-induced IP_3 production, SR structure, and functioning.

In the past, the experimental difficulties to determine the SR structure drove researchers to use functional studies to understand the arrangement of SR. The functional studies have shown that SR is sensititive to calcium and IP_3. Some studies reported that the calcium-sensitive depletion via RyR of internal calcium store did not affect the IP_3-sensitive calcium release via IP_3R. It was interpreted as there would be two separate stores in VSMC, calcium-sensitive store contains only RyR and IP_3-sensitive store contains only IP_3R [174, 57, 77]. In contradiction to this, some researchers proposed that SR is a single calcium store with both IP_3R and RyR expressed in it [133, 178]. In their experiments, RyR-mediated depletion of the internal calcium store terminated the IP_3R-mediated calcium release.

Goldbeter et al. [52] assumed internal calcium store as a combination of two physically separate stores of which one is IP_3-sensitive and the other one is IP_3-insensitive in their minimal model for agonist-induced calcium oscillations. Similar to Goldbeter et al. [52] model, Parthimos et al. [135] developed a minimal mathematical model for VSMC by assuming two distinct internal calcium stores, ryanodine-sensitive and IP_3-sensitive. Kapela et al. [83] modelled SR as a single store but with two compartments, uptake compartment and release compartment. The uptake compartment contains a SERCA pump and a IP_3R channel whereas RyR is the main calcium release channel in the release compartment.

The recent development of advanced digital imaging techniques has improved the understanding about the structural organisation of SR. Picht et al. [139] showed that there is no major temporal delay in calcium recovery between junctional and longitudinal parts of SR. The calcium diffusion in the SR lumen is rapid, which nullifies the spatial calcium gradient in the SR during cell excitation. A recent experiment of McCarron and Olson [117] confirms that SR is a luminally continuous entity in which both IP_3R and RyR are expressed. The same level of intra-SR calcium is freely accessed by both IP_3R and RyR [142, 117]. Therefore, there is no need to model SR as two compartments with differential expression of calcium handling proteins on each compartments. One can assume that the SR is a single luminaly continuous store with homogeneous luminal calcium. This concept is used in the current study to model SR.

IP_3R is tetrameric with four subunits forming a single calcium-conducting channel. The opening of the IP_3R channel is regulated by calcium ions and IP_3 molecules. Calcium-mediated regulation of IP_3R is biphasic; it enhances channel opening at low calcium concentrations and deactivates channels at high calcium concentrations.

Goldbeter et al. [52] modelled the IP_3-sensitive calcium release as a “constant" and the value of “constant” was changed to represent the IP_3-sensitive calcium release for different agonist concentrations; similar to Parthimos et al. [135]. Koenigsberger et al. [89] used an equation similar to the Michaelis-Menten equation to model IP_3R-mediated calcium release, which is directly proportional to the IP_3 concentration. Bennett et al. [15] has included the biphasic regulation of IP_3R channel along with the IP_3 activation; the same is used in the Kapela et al. [83] model.

According to a detailed review on the existing IP_3R models by Shuai et al. [164], sequential-binding of calcium and IP_3 messengers should be included in the IP_3R model in order to fit the open probability to experimental observation. They have compared the existing model results with the patch clamp experiments for single IP_3R channels in Xenopus oocyte to draw the given conclusion. None of the existing VSMC models has implemented sequential binding of calcium and IP_3 for the activation of IP_3R. We have incorporated a simplified sequential-binding IP_3R model in our VSMC model since calcium is the central attention of the study.

The equation of the NCX is modified by incorporating the allosteric factor. A different description is given to the ionic current equation of the NSC channel. The Lemon et al. [101] model for agonist-induced IP_3 production is simplified by eliminating receptor activity regulation. The details of these modifications can be found in the respective sections of this chapter.

The VSMC model contains only the most relevant channels, pupms and exchangers for the agonist-induced calcium dynamics. For the specific study we are doing, we have eliminated the following components of the original Kapela et al. [83] model; NO/cGMP signalling, sodium-potassium pump (NaK), voltage-dependent potassium channel (K_V), potassium leak channel (K_{leak}) and NaKCl.

In this chaper, the model components and their respective model equations are discussed in the first sections. Following that, the numerical methods used and numerical algorithm developed are discussed. The model response to varying agonist concentrations is discussed in the start of the results section. The model response is compared against the available experimental results. The responses of the model to varying extracellular concentrations are tested against experimental results. The intracellular calcium signalling mechanism of the model is detailed in the discussion section. We propose that this model (in comparison with [83]) is minimal in that it provides the required phenomena of Ca^{2+} dynamics with a reduced number of parameters and ion channels. The model limitations are listed at the end of the chapter.

3.2 Model Development

A schematic representation of the model is shown in Figure 3.1. The model contains three fluid compartments, extracellular space (e), cytosol (cyt), and SR, which are separated by cell and SR membranes. Ion transport across cell membrane is given by four ion channels, a large conductance calcium-activated potassium channel (BK_{Ca}), a voltage-operated calcium channel (VOCC), a NSC channel and a calcium-activated chloride channel (CACC), one plasma membrane calcium ATPase pump (PMCA), and one Na/Ca exchanger (NCX). Three calcium channels, an IP_3R channel, an RyR channel, an SR leak channel (SR_{leak}), and a SERCA pump are included in the SR membrane. Calcium buffering in the cytosol is considered as the sum of calmodulin and other buffers. The buffering of intra-SR calcium is ignored in the current study [197, 135]. Action of an agonist on adrenergic receptor cascade and the resulting formation of IP_3 and DAG are included in the model. In contrast to other models such as [83, 85] the SR is treated as a single domain and we have not included the NO/cGMP pathway mediating the BK_{Ca} channel.

We define an ionic current, I, specific to a channel k by I_k. For an ion channel in the cell membrane,

$$I_k = G_k P_k (V_m - E_{ion}) \tag{3.1}$$

Where G_k is whole cell conductance, P_k is open probability and E_{ion} is Nernst potential of the ion.

$$E_{ion} = \frac{RT}{z_{ion}F} \ln\left(\frac{[ion]_e}{[ion]_{cyt}}\right) \tag{3.2}$$

Where 'ion' represents Ca^{2+}, K^+ or Cl^-, F is Faraday's constant, R is universal gas constant, z is ion valency and T is temperature.

For an ion pump,

$$I_k = Q_k f\left(\left[Ca^{2+}\right]_{cyt}\right) \tag{3.3}$$

Where Q_k is the maximum rate of calcium flux and 'f' is a function of intracellular calcium.

For an ion channel in the SR,

$$I_k = Q_k P_k\left(\left[Ca^{2+}\right]_{cyt} - \left[Ca^{2+}\right]_{SR}\right) \tag{3.4}$$

The membrane potential of the cell is defined based on the lumped Hodgkin-Huxley formulation using ionic currents (I) across the cell membrane.

$$\frac{dV_m}{dt} = \frac{-1}{C_m}\left(I_{BK_{Ca}} + I_{VOCC} + I_{NCX} + I_{PMCA} + I_{NSC} + I_{CACC}\right) \tag{3.5}$$

Calcium levels in the cytosol and in the SR are estimated by balancing fluxes of calcium channels, pumps and exchangers across the cell membrane and the SR membrane respectively.

$$\frac{d\left[Ca^{2+}\right]_{cyt}}{dt} = \frac{-1}{\rho\alpha}\left(I_{SERCA} - I_{IP_3R} - I_{RyR} - I_{SR_{leak}} - 2I_{NCX} + I_{VOCC} + I_{PMCA}\right) \tag{3.6}$$

$$\frac{d\left[Ca^{2+}\right]_{SR}}{dt} = \frac{1}{\beta}\left(I_{SERCA} - I_{IP_3R} - I_{RyR} - I_{SR_{leak}}\right) \tag{3.7}$$

Where ρ is a calcium buffering parameter.

$$\rho = 1 + \frac{B_{CM}k_{CM}}{\left(k_{CM} + \left[Ca^{2+}\right]_{cyt}\right)^2} + \frac{B_F k_B}{\left(k_B + \left[Ca^{2+}\right]_{cyt}\right)^2} \tag{3.8}$$

Where B_{CM} and B_F are the concentrations of calmodulin and other buffers, respectively. k_{CM} and k_B are the dissociation constants of calmodulin and other buffers, respectively.

$$\alpha = z_{Ca}FVol_{cyt} \text{ and } \beta = z_{Ca}FVol_{SR} \tag{3.9}$$

Where Vol_{SR} is the volume of SR and Vol_{cyt} is the volume of cytosol.

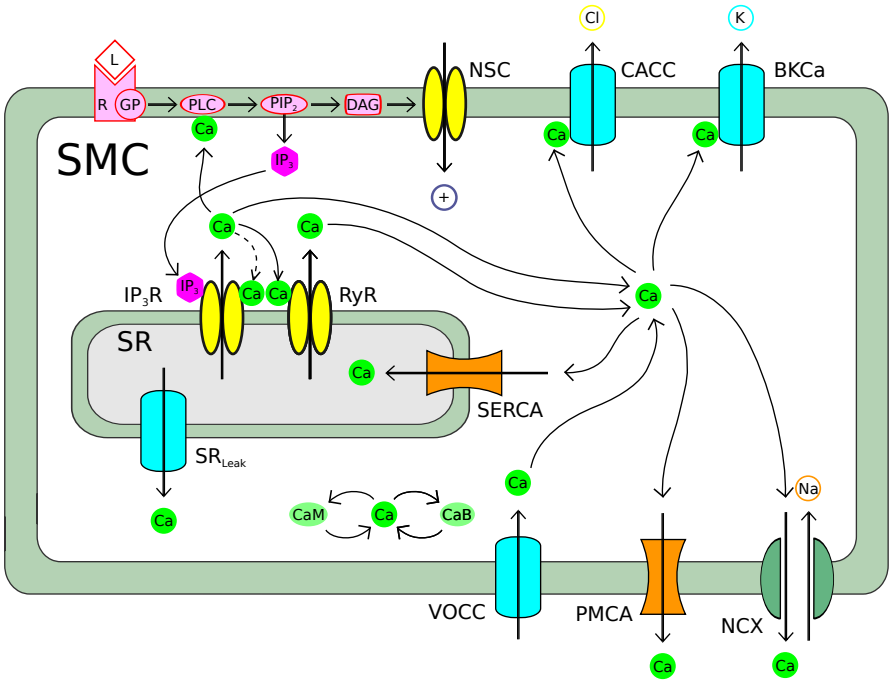

Fig. 3.1 Schematic diagram of SMC model: BK_{Ca} - large conductance calcium-activated potassium channel, PMCA - plasma membrane calcium ATPase, VOCC - voltage-operated calcium channel, NCX - Na/Ca exchanger, NSC -non-selective cation channel, CACC - calcium-activated chloride channel, IP_3R - IP_3 receptor channel, RyR - Ryanodine receptor channel, SR_{leak} - SR leak channel, SERCA - SR calcium ATPase, L - agonist, GP - G-protein, R - receptor, CaM - calmodulin, CaB - other calcium buffers.

3.2.1 Cell membrane channels, pumps and exchangers

3.2.1.1 Large conductance calcium-activated potassium channel (BK_{Ca})

The BK_{Ca} channel plays an important role in setting the membrane potential and is the main repolarizing current in the VSMC [134, 31]. Its ability to sense two controlling variables of contraction, $\left[Ca^{2+}\right]_{cyt}$ and V_m, allows this channel to coordinate electrochemical signals. The increased intracellular calcium during stimulation will trigger the BK_{Ca} channel and results in an outward flux of potassium ions (K^+). This is considered as a spontaneous transient outward current (STOC) forcing the V_m to return to its basal level. BK_{Ca} channels are known to be important for myogenic activities of VSMC and in the pathophysiology of hypertension [199, 183]. The model equation for BK_{Ca} current is given below,

$$I_{BK_{Ca}} = G_{BK_{Ca}} P_{BK_{Ca}} (V_m - E_K) \tag{3.10}$$

Where $G_{BK_{Ca}}$ and $P_{BK_{Ca}}$ are the whole cell conductance and open probability of the BK_{Ca} channel. E_K is the Nernst potential of potassium. The open probability of the BK_{Ca} channel is modelled as a combination of fast and slow activation processes. The empirical equation for the open probability of the BK_{Ca} channel is taken from the Kapela et al. [83] model.

$$P_{BK_{Ca}} = 0.17 p_f + 0.83 p_s \tag{3.11}$$

Where p_f and p_s are the fast and slow activation variables which are modelled based on the kinetic behaviour of the open and closed states of the channel, refer to Section A.6 for a general discussion.

$$\frac{dp_f}{dt} = \frac{\bar{p}_o - p_f}{\tau_{p_f}}, \qquad \frac{dp_s}{dt} = \frac{\bar{p}_o - p_s}{\tau_{p_s}} \tag{3.12}$$

Where τ_{p_f} and τ_{p_s} are the fast and slow activation time constants. $\bar{p_o}$ is the steady state open probability of the BK_{Ca} channel.

$$\bar{p}_o = \frac{1}{1 + Exp\left(-\frac{V_m - V_{0.5BK_{Ca}}}{C_1}\right)} \tag{3.13}$$

Where $C_1 = 18.25$ mV. The $V_{0.5BK_{Ca}}$ provides the calcium dependency of the BK_{Ca} channel.

$$V_{0.5BK_{Ca}} = -41.7\log_{10}\left(\left[Ca^{2+}\right]_{cyt}\right) - C_2 \tag{3.14}$$

Where $C_2 = 128.2$ mV.

3.2.1.2 Voltage-operated calcium channel (VOCC)

The VOCC channel is a key channel which is responsible for the influx of calcium into the cell from the extracellular space. VOCC channels respond to membrane potential signals and release calcium to the cytosol accordingly. The L-type VOCC is found to be responsible for myogenic activities in VSMCs of the microcirculation [124, 34]. Modulation of L-type VOCCs is identified as a major pathway that controls myogenic contraction in cerebrovascular smooth muscle cells [116]. The model equation for VOCC is as follows,

$$I_{VOCC} = G_{VOCC} d_L f_L (V_m - E_{Ca}) \tag{3.15}$$

Where G_{VOCC} is the whole cell conductance of VOCC and is calculated from the whole-cell voltage-current (V-I) curve published in Nikitina et al. [129]. d_L and f_L represent activation and inactivation variables of the VOCC respectively. E_{Ca} is the Nernst potential of the calcium ion. The activation and inactivation of VOCC are modelled as, (refer to Section A.6 for a general expression).

$$\frac{dd_L}{dt} = \frac{\bar{d_L} - d_L}{\tau_{d_L}}, \qquad \frac{df_L}{dt} = \frac{\bar{f_L} - f_L}{\tau_{f_L}} \tag{3.16}$$

Where $\bar{d_L}$ and $\bar{f_L}$ are the steady state activation and inactivation variables of the VOCC respectively. τ_{d_L} and τ_{f_L} are the activation and inactivation time constants respectively. The empirical equations of $\bar{d_L}$, $\bar{f_L}$, τ_{d_L} and τ_{f_L} are taken from the Kapela et al. [83] model.

$$\bar{d_L} = \frac{1}{1 + \mathrm{Exp}\left(-\frac{V_m}{C_3}\right)} \qquad \bar{f_L} = \frac{1}{1 + \mathrm{Exp}\left(\frac{V_m + C_4}{C_5}\right)}, \tag{3.17}$$

Where $C_3 = 8.3$ mV, $C_4 = 42$ mV, and $C_5 = 9.1$ mV.

$$\tau_{d_L} = 2.5\text{Exp}\left(-\left(\frac{V_m + C_6}{C_7}\right)^2\right) + 1.15\ (ms) \tag{3.18}$$

$$\tau_{f_L} = 65\text{Exp}\left(-\left(\frac{V_m + C_8}{C_9}\right)^2\right) + 45\ (ms) \tag{3.19}$$

Where $C_6 = 40$ mV, $C_7 = 30$ mV, $C_8 = 35$ mV, and $C_9 = 25$ mV.

3.2.1.3 Sodium/Calcium exchanger (NCX)

The NCX channel exchanges three sodium ions (Na^+) into the cell and one calcium ion out of the cell [143]. This electrogenic transfer causes depolarization of the cell at the expense of intracellular calcium. This bidirectional exchange mechanism and its increased activity at higher calcium concentrations after agonist stimulation is identified in VSMCs [126]. The NCX channel is a low affinity-high capacity calcium efflux pathway. The NCX is allosterically regulated by calcium. The calcium binds to the allosteric site of the NCX at low calcium concentrations and changes the activity of the NCX. The full equation for NCX is obtained by incorporating allosteric factors into the electrochemical term [186].

$$I_{NCX} = \bar{I}_{NCX} P_{NCX,allo} P_{NCX,elec} \tag{3.20}$$

Where $\bar{I}_{NCX}$ is the scaling factor of NCX. NCX is alloseterically regulated in a way that NCX can get deactivated at low calcium concentrations [121]. The allosteric factor, $P_{NCX,allo}$, through binding of calcium to the regulatory site is expressed as a Hill equation, (refer to section A.7 for a general description).

$$P_{NCX,allo} = \frac{\left[Ca^{2+}\right]^2_{cyt}}{\left[Ca^{2+}\right]^2_{cyt} + k^2_{NCX}} \tag{3.21}$$

Where k_{NCX} is the dissociation constant for the allosteric component and fixed to 125 nM based on the study of Weber et al. [186]. The equation for the electrochemical term, $P_{NCX,elec}$, stands for the exchange of ions due to electrochemical potential [83, 35, 186]. The mathematical expression of $P_{NCX,elec}$ is taken from the Kapela et al. [83] model.

$$P_{NCX,elec} = \frac{[Na^+]^3_{cyt}\left[Ca^{2+}\right]_e \phi_F - [Na^+]^3_e\left[Ca^{2+}\right]_{cyt}\phi_R}{1 + d_{NCX}\left([Na^+]^3_e\left[Ca^{2+}\right]_{cyt} + [Na^+]^3_{cyt}\left[Ca^{2+}\right]_e\right)} \tag{3.22}$$

Where $d_{NCX} = 0.0003$, ϕ_F and ϕ_R represent the dependency of the model on the membrane potential as NCX is an electrogenic exchanger.

$$\phi_F = Exp\left(\frac{\gamma V_m F}{RT}\right), \qquad \phi_R = Exp\left(\frac{(\gamma - 1) V_m F}{RT}\right) \tag{3.23}$$

Where γ is the position of the energy barrier of the NCX in the membrane electric field.

3.2.1.4 Calcium-activated chloride channel (CACC)

An increase in intracellular calcium by the calcium activated chloride (Cl^{-1}) channel is observed following agonist stimulation [189, 140]. CACC currents have been reported to be activated spontaneously. These spontaneous CACC currents are produced in synchronization with BK_{Ca} currents [80, 97]. The CACC seems to be activated mainly by intracellular calcium and is also sensitive to cyclic guanosine monophosphate (cGMP) [76]. Since the cGMP calcium signalling pathway is not included in the model, the open probability of CACC is assumed to depend on intracellular calcium only. The model equation of the CACC is,

$$I_{CACC} = G_{CACC} P_{CACC} (V_m - E_{Cl}) \tag{3.24}$$

Where G_{CACC} and P_{CACC} are the whole cell conductance and open probability of CACC. G_{CACC} is calculated from the whole cell V-I data in Matchkov et al. [114]. E_{Cl} is the Nernst potential of the chloride ion. A Hill equation, (refer to Section A.7), is used to model P_{CACC}.

$$P_{CACC} = \frac{\left[Ca^{2+}\right]^2_{cyt}}{\left[Ca^{2+}\right]^2_{cyt} + k^2_{CACC}} \tag{3.25}$$

Where k_{CACC} is dissociation constant of CACC. The dissociation constant (k_{CACC}) reported in the literature varies from 63 nM [28, 4] to several μMs [152]. Ni et al. [127] used an experimental protocol to have negligible channel run down of CACC which is considered as

one of the main reasons for the discrepancies of k_{CACC} in the literature. This is the reason for choosing k_{CACC}, 587 nM, from Ni et al. [127]. A similar k_{CACC} value is reported by Angermann [3] for CACC in pulmonary arterial smooth muscle cells. It is well known that the Hill coefficient of CACC is larger than one. The Hill coefficient of CACC in the Ni et al. [127] study equals 3.8 at -40 mV, whereas in Angermann [3], it varies from 2 to 2.5 for a change of membrane potential from -40 mV to 0 mV. For the same voltage range, the Hill coefficient is given as less than 1.5 in the Arreola et al. [4] study and is less than 3 in the Kuruma and Hartzell [93] study. The Hill coefficient of 3.8 in the Ni et al. [127] study is high compared to the other above mentioned studies. Based on the above observations we have therefore fixed the Hill coefficient of CACC to 2. Interestingly, the same Hill coefficient is used in the Kapela et al. [83] model of VSMCs.

3.2.1.5 Non-selective cation channel (NSC)

Agonist stimulation in smooth muscle cells induces a cation current which is not activated by calcium and is different from the BK_{Ca} and CACC currents. This cation current causes depolarization of the cell and plays an important role in the influx of calcium [2, 72]. Experiments by Soboloff et al. [166] show that when the L-type Ca channel (VOCC) is inhibited, transmembrane calcium influx induced by DAG is blocked. Intracellular calcium rise due to DAG activation of the NSC channel is contributed mainly by the VOCC channel and not by the calcium flux through the NSC channel. Thus, we have not included the direct contribution of calcium flux through NSC channel. The transient receptor potential cation channel, (TRPC6), is identified as an alpha-adrenoceptor evoked NSC channel in VSMC [79, 38]. Membrane potential and diacylglycerol (DAG) regulate the opening of the NSC channel. The model equation of the NSC channel current is given below,

$$I_{NSC} = G_{NSC} P_{NSC,V_m} P_{NSC,DAG} (V_m - E_{NSC}) \tag{3.26}$$

Where G_{NSC} is the whole cell conductance of the NSC channel and is determined from the whole cell V-I data given in Helliwell and Large [63]. E_{NSC} is the reverse potential of the NSC channel. P_{NSC,V_m} and $P_{NSC,DAG}$ represent the dependency of channel open probability on V_m and DAG respectively. P_{NSC,V_m} is fitted to the V-I relationship reported in Helliwell and Large [63] as below,

$$P_{NSC,V_m} = \frac{1}{1 + Exp(-(V_m + C_{10})/C_{11})} \tag{3.27}$$

Where $C_{10} = 78$ mV and $C_{11} = 45$ mV. A Hill equation is used to model $P_{NSC,DAG}$.

$$P_{NSC,DAG} = \frac{[DAG]}{([DAG] + k_{NSC})} \tag{3.28}$$

There is a scarcity of experimental data that discusses the open probability of the NSC channel with respect to DAG concentration. When oleoyl-2-acetyl-sn-glycerol (OAG), a DAG analogue, is used, activation of TRPC6 is obtained with micromolar concentrations of OAG [63, 166]. Based on these observations, the dissociation constant for the NSC is assumed as 1 μM.

3.2.1.6 Plasma membrane calcium ATPase (PMCA)

PMCA plays a vital role in maintaining the resting concentration of intracellular calcium. PMCA removes calcium from intracellular space at the expense of energy from ATP hydrolysis [23]. PMCA has high affinity to calcium but its pumping capacity is low [122, 111]. It can operate in a concentration range where NCX is relatively inactive. Michaelis-Menten kinetics is used to model PMCA current and the model equation of PMCA is,

$$I_{PMCA} = \alpha Q_{PMCA} P_{PMCA} \tag{3.29}$$

Where Q_{PMCA} is the maximum rate of calcium efflux by PMCA.

$$P_{PMCA} = \frac{\left[Ca^{2+}\right]_{cyt}}{\left[Ca^{2+}\right]_{cyt} + k_{PMCA}} \tag{3.30}$$

Where k_{PMCA} is the Michaelis constant of the PMCA pump. As noted, PMCA has a high affinity to calcium and is the main component responsible for maintaining the resting calcium concentration. The PMCA operates at a low calcium range where the NCX is relatively inactive [23]. Kapela et al. [83] used a Michaelis constant of 170 nM whereas Jacobsen et al. [76] used a value of 200 nM. In Jacobsen et al. [76] study, the intracellular calcium at the resting state was 100 nM which is slightly higher than the corresponding value of 80 nM in our model. To account the difference in intracellular concentration with Jacobsen et al. [76] study, Michaelis constant, k_{PMCA}, of 150 nM is used for PMCA and to satisfy the experimental observation of the high affinity to calcium and the k_{PMCA} is within the range of values used in the previous models.

3.2.2 Sarcoplasmic Reticulum (SR) channels and pump

3.2.2.1 Sarcoplasmic reticulum calcium ATPase (SERCA) pump

SERCA pumps utilize energy from ATP to pump calcium back to the SR. The SERCA pump is activated at high cytosolic calcium levels to bring back both intracellular and intra-SR calcium concentrations to basal conditions. Thus the pump helps to complete the cycle of contraction and relaxation [137]. SERCA activity is controlled mainly by changes in intracellular calcium [9, 91]. A Michaelis-Menten kinetics equation is used to model the SERCA pump.

$$I_{SERCA} = \alpha Q_{SERCA} P_{SERCA} \tag{3.31}$$

Where α is defined by Equation 3.9. Q_{SERCA} is the maximum rate of calcium efflux of the SERCA and is equal to 210×10^3 nM s^{-1} [9].

$$P_{SERCA} = \frac{\left[Ca^{2+}\right]^2_{cyt}}{\left[Ca^{2+}\right]^2_{cyt} + k^2_{SERCA}} \tag{3.32}$$

Where, k_{SERCA} is the Michaelis constant of the SERCA pump. The value of Q_{SERCA} is taken from the experiment of Balke et al. [9]. In their experiment, the Michaelis-Menten equation was fitted to two slope factors of 2 and 4. Wimsatt et al. [191] reported a Michaelis constant of 500 nM with a slope factor of 1.6. Based on these observations, we have used a Michaelis constant of 500 nM and a slope factor of 2.

3.2.2.2 SR leak channel (SR_{leak})

SR_{leak} is the calcium release that is different from the calcium release due to cell excitation and is more prevalent during the relaxation phase. SR_{leak} acts as a counterbalance to the SERCA pump and plays an important role in maintaining the intra-SR calcium load [202, 22, 17]. SR_{leak} is significantly raised at high intra-SR calcium. The change of SR_{leak} with respect to intra-SR calcium is matched to an exponential function in the Zima et al. [202] study. In our model, an exponential equation is used to model the SR_{leak} channel.

$$I_{SR_{leak}} = \beta\lambda \mathrm{Exp}\left(\frac{\left[Ca^{2+}\right]_{SR}}{k_{leak}}\right) \tag{3.33}$$

Where λ is maximum rate of calcium leak and k_{leak} is a growth factor of the exponential function, 145 μM [202] .

3.2.2.3 IP_3 receptor channel (IP_3R)

A sequential-binding four state model developed by Swaminathan et al. [170] is used to find the open probability of IP_3R. In this, IP_3R is modelled as having four equal and independent subunits. Each subunit has three distinct binding sites, one for IP_3 activation, one for calcium activation and the third one for binding inhibitory calcium. Calcium can bind to its activation site only if IP_3 is bound to the subunit; calcium binding is a sequential step following IP_3 binding.

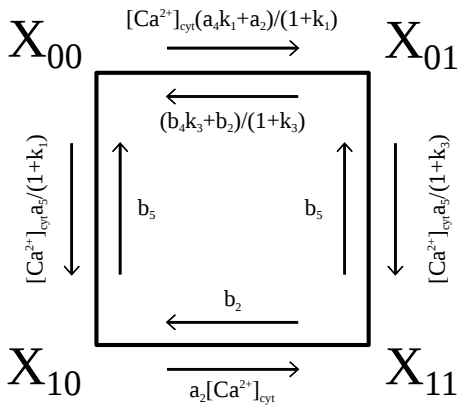

Fig. 3.2 Schematic representation of sequential-binding IP_3 model [170]. X_{00}, X_{10}, X_{01} and X_{11} are the four states of a subunit.

Figure 3.2 shows the schematic diagram of the sequential-binding four state model. $X_{i,j}$ represents the different intermediate states and the probability of IP3R in the corresponding state (i,j). For $X_{i,j}$, the first subscript "i" represents the calcium activating site and "j" the calcium inhibiting site. "0" means not bound and "1" means bound. $X_{1,0}$ is the open state among the 4 states of IP3R. Other states can be read based on the value of "i" and "j". $X_{0,0}$ is the state with no calcium bound to the sites, $X_{0,1}$ is the state with calcium bound to only an inhibition site and $X_{1,1}$ is the state with calcium bound to both sites. Transition from one state to another depends on the concentrations of IP_3 and calcium. Subunit dynamics of the IP_3R model are given by the following differential equations [170].

$$\frac{dX_{00}}{dt} = (b_4k_3 + b_2)\frac{X_{01}}{1+k_3} + b_5X_{10} - (a_4k_1 + a_5 + a_2)\left[Ca^{2+}\right]_{cyt}\frac{X_{00}}{1+k_1} \tag{3.34}$$

$$\frac{dX_{10}}{dt} = b_2X_{11} + a_5\left[Ca^{2+}\right]_{cyt}\frac{X_{00}}{1+k_1} - \left(a_2\left[Ca^{2+}\right]_{cyt} + b_5\right)X_{10} \tag{3.35}$$

$$\frac{dX_{01}}{dt} = (a_4k_1 + a_2)\left[Ca^{2+}\right]_{cyt}\frac{X_{00}}{1+k_1} + b_5X_{11} - \left(b_4k_3 + b_2 + a_5\left[Ca^{2+}\right]_{cyt}\right)\frac{X_{01}}{1+k_3} \tag{3.36}$$

$$X_{11} = 1 - X_{00} - X_{01} - X_{10} \tag{3.37}$$

$$k_j = \frac{b_j}{a_j\left[IP_3\right]}, \quad j=1,2,3 \tag{3.38}$$

Where a_i and b_i are binding and dissociation constants as given by Swaminathan et al [170] as given in Table E.5. The IP_3R channel opens when all four or any three subunits are in the open state. The single channel open probability of IP_3R (P_{IP_3R}) is given by,

$$P_{IP_3R} = \left(X_{10}^4 + 4X_{10}^3(1 - X_{10})\right) \tag{3.39}$$

The calcium and IP_3 regulation of IP_3R opening are shown in the left and right-hand panels of Figure 3.3 respectively. The open probability variation with IP_3 is monotonic increasing, reaching a maximum value of 1.7×10^{-2} at IP_3R = 10 μM [172, 185]. The open probability of IP_3R with respect to calcium gives a bell-shaped curve [18], as expected for biphasic regulation. The open probability of IP_3R increases at low calcium concentrations and decreases at high calcium concentrations. Peak open probability is obtained at $\left[Ca^{2+}\right]_{cyt}$ ~250 nM which matches the experimental studies [86, 18].

The total calcium flux through the IP_3R channels is defined as follows,

$$I_{IP_3R} = \beta Q_{IP_3R}P_{IP_3R}\left(\left[Ca^{2+}\right]_{SR} - \left[Ca^{2+}\right]_{cyt}\right) \tag{3.40}$$

Where β is defined by equation 3.9. Q_{IP_3R} is the maximum rate of the IP_3R channel. Swaminathan [169] used 4625 s^{-1} for Q_{IP_3R} and 0.5 mM for intra-SR calcium concentration

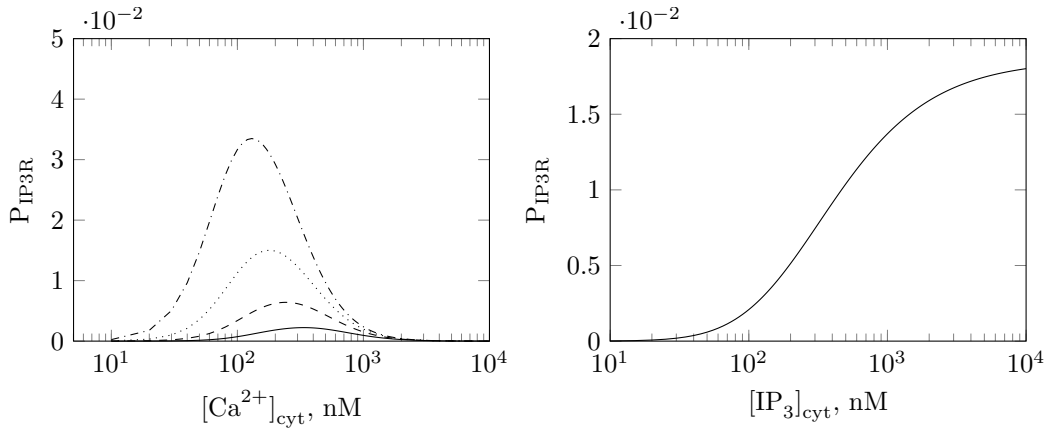

Fig. 3.3 (Left) Variation of steady state open probability of IP_3R channel with respect to $\left[Ca^{2+}\right]_{cyt}$ for different IP_3 concentrations, $[IP_3]$ = 1000 nM (dash dotted), $[IP_3]$ = 400 nM (dotted), $[IP_3]$ = 200 nM (dashed), $[IP_3]$ = 100 nM (solid). (Right) Variation of steady state open probability of IP_3R channel with respect to $[IP_3]$ at $\left[Ca^{2+}\right]_{cyt}$ = 1000 nM.

to obtain calcium puffs lifetimes and amplitudes consistent with the experiments. In our model, intra-SR calcium equals to 1.2 mM at the resting state. A value of 2000 s^{-1} is used for the Q_{IP_3R} in order to account the difference in intra-SR calcium with the Swaminathan et al. [170] study.

3.2.2.4 Ryanodine receptor channel (RyR)

RyR channels are functionally and structurally comparable to IP_3R channels and are sensitive to intracellular calcium concentrations. These channels get activated when intracellular calcium increases from nM to μM, whilst at mM levels of intracellular calcium, RyR is inhibited. A multiple state kinetic model proposed by Yang et al. [197] is used to find calcium activation of RyR. The four states of the RyR in the model are R_{00} is free receptor, R_{01} is the receptor with a calcium ion bound to the inactivation site, R_{11} is the state with a calcium ion bound to both the activation and inactivation sites and R_{10} is the state with a calcium ion bound to the activation site. Two calcium activation sites are assumed in a single RyR. The multi-state RyR model equations are given below,

$$\frac{dR_{10}}{dt} = K_{r1}\left[Ca^{2+}\right]_{cyt}^{2} R_{00} - \left(K_{-r1} + K_{r2}\left[Ca^{2+}\right]_{cyt}\right) R_{10} + K_{-r2} R_{11} \tag{3.41}$$

$$\frac{dR_{11}}{dt} = K_{r2}\left[Ca^{2+}\right]_{cyt} R_{10} - \left(K_{-r1} + K_{-r2}\right) R_{11} + K_{r1}\left[Ca^{2+}\right]_{cyt}^{2} R_{01} \tag{3.42}$$

$$\frac{dR_{01}}{dt} = K_{r2}\left[Ca^{2+}\right]_{cyt} R_{00} + K_{-r1}R_{11} - \left(K_{-r2} + K_{r1}\left[Ca^{2+}\right]^2_{cyt}\right) R_{01} \tag{3.43}$$

$$R_{00} = 1 - R_{01} - R_{10} - R_{11} \tag{3.44}$$

Where K_{r1} and K_{r2} are the activation and inactivation rate constants, respectively. K_{-r1} and K_{-r2} are unbinding rate constants from activation and inactivation, respectively.

The open probability of the RyR channel, P_{RyR}, is given by the solution of the time-dependent equations of the four states and the open probability of the RyR is a quadratic function of the variable R_{10} as shown below,

$$P_{RyR} = R^2_{10} \tag{3.45}$$

Total calcium flux through the RyR channels is defined as follows,

$$I_{RyR} = \beta Q_{RyR} P_{RyR}\left(\left[Ca^{2+}\right]_{SR} - \left[Ca^{2+}\right]_{cyt}\right) \tag{3.46}$$

Where Q_{RyR} is the maximum rate of RyR. β is defined as before.

3.2.3 G-protein cascade and IP_3 formation

We have used a simplified mathematical model of Lemon et al. [101] eliminating receptor activity regulation to model G-protein activation and subsequent IP_3 formation. The agonist ligand (L) gets bound to the receptor and forms a ligand occupied receptor, LR. The G-protein is activated by the ligand occupied receptor. The rate of G-protein activation is dependent on the number of active receptors (LR) and the number of inactive G-proteins, see the Eq.3.47. The deactivation of G-protein is related to the amount of active G-protein present.

$$\frac{dGP}{dt} = k_a\left(\delta + \rho_r\right)\left(GP_T - GP\right) - k_d GP \tag{3.47}$$

Where GP denotes G-protein, k_a is the rate of G-protein activation, k_d is the rate of G-protein inactivation, GP_T is the total number of G-protein molecules in a VSMC, δ is G-protein intrinsic activity parameter and ρ_r is the ratio of agonist-bound receptors to the total receptors.

$$\rho_r = \frac{[L]}{k_R + [L]} \tag{3.48}$$

Where [L] is the agonist concentration and k_R is the unphosphorylated receptor dissociation constant.

PLC is fully activated only when it binds to the G-protein and to calcium. Therefore, the activation of PLC is modelled as dependent on intracellular calcium and the G-protein, see the Eq.3.49 to Eq.3.51. This helps to build a positive feedback system between IP_3 production and intracellular calcium. Activated PLC hydrolyses PIP_2 and the rate of PIP_2 hydrolysis is equated to $r_h [PIP_{2,T}]$. The concentration of PIP_2 is kept constant based on the assumption that the degradation of PIP_2 is equal to the replenishment from the cytosol [100]. The hydrolysis of PIP_2 produces one molecule of each DAG and IP_3. The model equations of IP_3 and DAG are given below,

$$\frac{d[IP_3]_{cyt}}{dt} = \frac{r_h}{N_{AV} Vol_{SMC}} PIP_{2,T} - k_{deg,IP_3} [IP_3]_{cyt} \tag{3.49}$$

$$\frac{d[DAG]}{dt} = \frac{r_h}{N_{AV} Vol_{SMC}} PIP_{2,T} - k_{deg,DAG} [DAG] \tag{3.50}$$

Where N_{AV} is Avogadro's constant, $PIP_{2,T}$ is the total number of PIP2 molecules in a VSMC, k_{deg,IP_3} is rate of IP_3 degradation, $k_{deg,DAG}$ is rate of DAG degradation and r_h is the rate coefficient of PIP_2 hydrolysis.

$$r_h = \eta \frac{\left[Ca^{2+}\right]_{cyt}}{\left[Ca^{2+}\right]_{cyt} + k_{PLC}} GP \tag{3.51}$$

Where η is effective signal gain parameter and k_{PLC} is the dissociation constant for calcium binding to PLC.

3.3 Numerical Method

There are a number of ways in which the coupled system of ODEs can be solved. However, we have based the solution procedure on numerical methods developed by Rempe and Chopp's algorithm [145]. This is because for future work we have adapted the code to

investigate coupled cells in branched structures such as bifurcating arteries. This makes the transition to coupled cell systems easier.

Mascagni [112] developed a numerical procedure to solve Hodgkin-Huxley equations using a backward Euler method and fixed point iteration, see Appendix B for a general description. Later on, Rempe and Chopp [145] implemented it in a branched neural network. A similar procedure is implemented in our study as follows. The model equations can be written in a general form, for a particular state variable x_{i}.

$$\dot{x_i} = x_i g_i\left(x_1, ..., x_n\right) + h_i\left(x_1, ..., x_n\right) \tag{3.52}$$

In the interests of brevity we provide an example of the procedure based on the variable membrane potential $\mathrm{V_m}$.

The backward Euler method is used to discretize the differential equations, see Appendix C for the discretized model equations. For $\mathrm{V_m}$ the membrane potential, the discretized equation is given as ,

$$\begin{aligned}\mathrm{C_m}\frac{\mathrm{V_m^{t+\Delta t}} - \mathrm{V_m^t}}{\Delta \mathrm{t}} = &-\mathrm{G_{BK_{Ca}}P_{BK_{Ca}}^{t+\Delta t}}\left(\mathrm{V_m^{t+\Delta t}} - \mathrm{E_K}\right) - \mathrm{G_{VOCC}d_L^{t+\Delta t}f_L^{t+\Delta t}}\left(\mathrm{V_m^{t+\Delta t}} - \mathrm{E_{Ca}^{t+\Delta t}}\right)\\ &- \mathrm{G_{NSC}P_{NSC,V_m}^{t+\Delta t}P_{NSC,DAG}^{t+\Delta t}}\left(\mathrm{V_m^{t+\Delta t}} - \mathrm{E_{NSC}}\right) - \mathrm{G_{NCX}P_{NCX,allo}^{t+\Delta t}P_{NCX,elec}^{t+\Delta t}}\\ &- \mathrm{G_{CACC}P_{CACC}^{t+\Delta t}}\left(\mathrm{V_m^{t+\Delta t}} - \mathrm{E_{Cl}}\right) - \alpha Q_{\mathrm{PMCA}}\mathrm{P_{PMCA}^{t+\Delta t}}\end{aligned} \tag{3.53}$$

The $\mathrm{V_m^{t+\Delta t}}$ terms are collected together on the left hand side, giving

$$\begin{aligned}&\mathrm{V_m^{t+\Delta t}}\left(\mathrm{G_{BK_{Ca}}P_{BK_{Ca}}^{t+\Delta t}} + \mathrm{G_{VOCC}d_L^{t+\Delta t}f_L^{t+\Delta t}} + \mathrm{G_{NSC}P_{NSC,V_m}^{t+\Delta t}P_{NSC,DAG}^{t+\Delta t}} + \mathrm{G_{CACC}P_{CACC}^{t+\Delta t}} + \frac{\mathrm{C_m}}{\Delta \mathrm{t}}\right)\\ &\quad = \mathrm{V_m^t}\frac{\mathrm{C_m}}{\Delta \mathrm{t}} + \mathrm{G_{BK_{Ca}}P_{BK_{Ca}}^{t+\Delta t}E_K} + \mathrm{G_{VOCC}d_L^{t+\Delta t}f_L^{t+\Delta t}E_{Ca}^{t+\Delta t}} + \mathrm{G_{NSC}P_{NSC,V_m}^{t+\Delta t}P_{NSC,DAG}^{t+\Delta t}E_{NSC}}\\ &\quad - \mathrm{G_{NCX}P_{NCX,allo}^{t+\Delta t}P_{NCX,elec}^{t+\Delta t}} + \mathrm{G_{CACC}P_{CACC}^{t+\Delta t}E_{Cl}} - \alpha Q_{\mathrm{PMCA}}\mathrm{P_{PMCA}^{t+\Delta t}}\end{aligned} \tag{3.54}$$

In this case the function g_i is written as

$$-\left(\mathrm{G_{BK_{Ca}}P_{BK_{Ca}}^{t+\Delta t}} + \mathrm{G_{VOCC}d_L^{t+\Delta t}f_L^{t+\Delta t}} + \mathrm{G_{NSC}P_{NSC,V_m}^{t+\Delta t}P_{NSC,DAG}^{t+\Delta t}} + \mathrm{G_{CACC}P_{CACC}^{t+\Delta t}}\right)\frac{1}{\mathrm{C_m}} \tag{3.55}$$

and the function h_i is written as

$$\Big(\mathrm{G_{BK_{Ca}}P^{t+\Delta t}_{BK_{Ca}}E_K + G_{VOCC}d^{t+\Delta t}_{L}f^{t+\Delta t}_{L}E^{t+\Delta t}_{Ca} + G_{NSC}P^{t+\Delta t}_{NSC,V_m}P^{t+\Delta t}_{NSC,DAG}E_{NSC}}$$
$$\mathrm{- G_{NCX}P^{t+\Delta t}_{NCX,allo}P^{t+\Delta t}_{NCX,elec} + G_{CACC}P^{t+\Delta t}_{CACC}E_{Cl} - \alpha Q_{PMCA}P^{t+\Delta t}_{PMCA}}\Big)\frac{1}{\mathrm{C_m}} \tag{3.56}$$

As shown in the supplementary material, for the state variable $\mathrm{X_{00}}$, Eq 3.34 gives $g_i = -\left(\mathrm{a_4k_1 + a_5 + a_2}\right)\left[Ca^{2+}\right]_{cyt}\frac{1}{1+\mathrm{k_1}}$ and $h_i = \left(\mathrm{b_4k_3 + b_2}\right)\frac{\mathrm{X_{01}}}{1+\mathrm{k_3}} + \mathrm{b_5X_{10}}$. Similarly, g_i and h_i functions are obtained for all 16 model equations. The discretized equations of all state variables can written in the form to give,

$$x_i\left(t+\Delta t\right)\left(1-\Delta t\ g_i\left(x_1\left(t+\Delta t\right),....,x_n\left(t+\Delta t\right)\right)\right) = x_i\left(t\right)+\Delta t\ h_i\left(x_1\left(t+\Delta t\right),....,x_n\left(t+\Delta t\right)\right) \tag{3.57}$$

A fixed point iteration method is used to solve the above equation at a given time step [145, 112]. Functions g and h are calculated explicitly at each iteration using x_i from the previous iteration. The resultant equation of x_i for the iterative procedure is obtained as follows,

$$x_i^{(k+1)} = \frac{x_i\left(t\right)+\Delta t\ h_i\left(x_1^{(k)},....,x_n^{(k)}\right)}{1-\Delta t\ g_i\left(x_1^{(k)},....,x_n^{(k)}\right)} \tag{3.58}$$

Where superscript k represents the iteration number. For $k=1$, we choose $x_i^k = x_i(t)$ and a series of approximations x_i^k $(k=2,3,\ldots)$ to $x_i(t+\Delta t)$ is obtained using the equation 3.58. When the fixed point iterations converge, x_i^{k+1} is a solution to the equation 3.57. In the current model, iteration is continued until all the state variables converge to an error tolerance limit such that $x_i^{k+1} - x_i^k \leq 10^{-4}$ for all i and time step is fixed to 0.1 ms.

3.3.1 Running time and Error analysis

The time step required to obtain estimated relative error of 10^{-4} with the proposed numerical method is obtained from the relative error plot, (Figure 3.4). This plot shows how the relative error changes with the time step (Δt). The relative error is calculated by taking the result with $\Delta t = 10^{-7}$ seconds and tolerance limit 10^{-6} as the exact solution. The relative error decreases as the time step decreases. Error is always higher if no iteration is used. Iteration significantly improves the accuracy of the result.

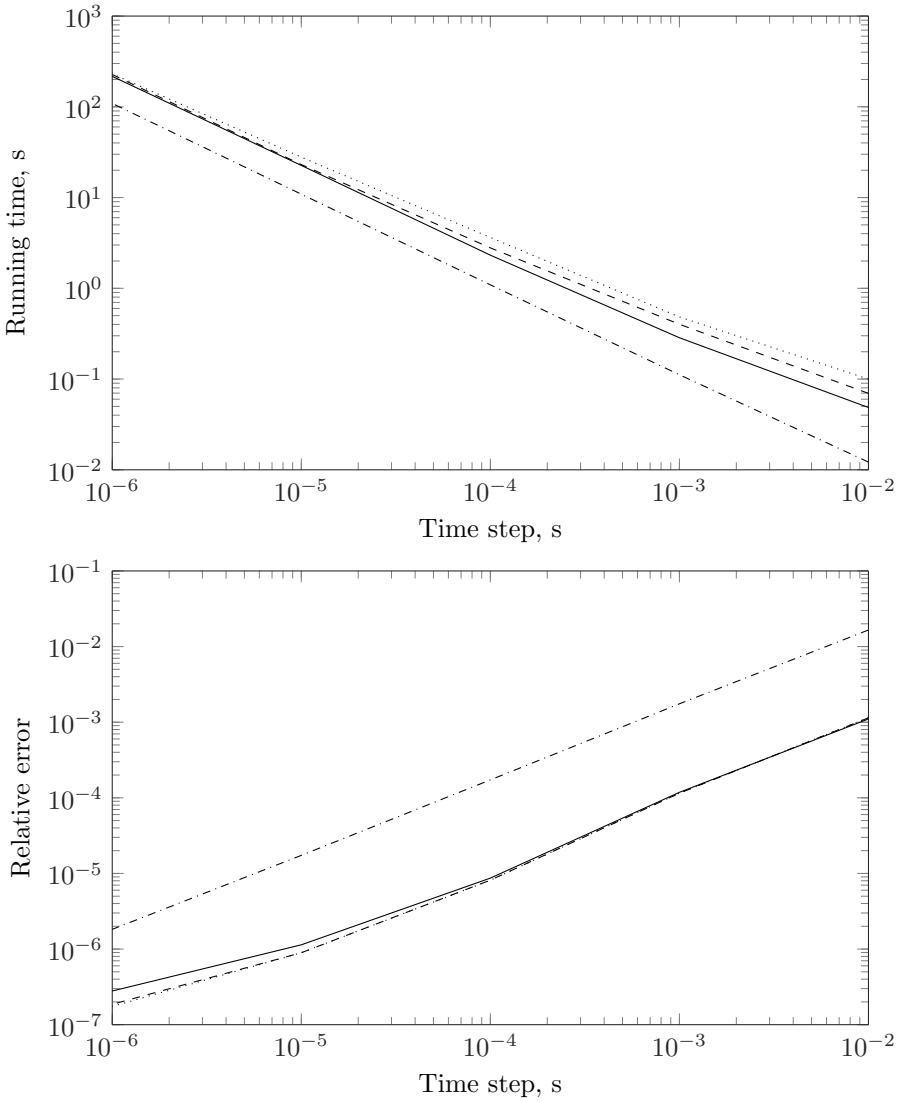

Fig. 3.4 Solver dependency: Running time (top) and relative error (bottom) of the solver is plotted against time step at different tolerance values of iteration, 10^{-2} (solid), 10^{-4} (dashed) and 10−6 (dotted) and with no iteration (dashdotted).

Running time is calculated as the total CPU time required to finish 150 seconds real time simulation. CPU time increases when time step is decreased, (see Figure 3.4). Similarly, the decreasing tolerance limit raises the required CPU time. For any time step, running time is low if no iteration is used. Though reducing the time step improves the accuracy, it slows the simulation. To get the required accuracy in a reasonable running time, we have used a time step of 10^{-4} seconds and a tolerance limit of 10^{-4}.

3.3.2 Computer algorithm

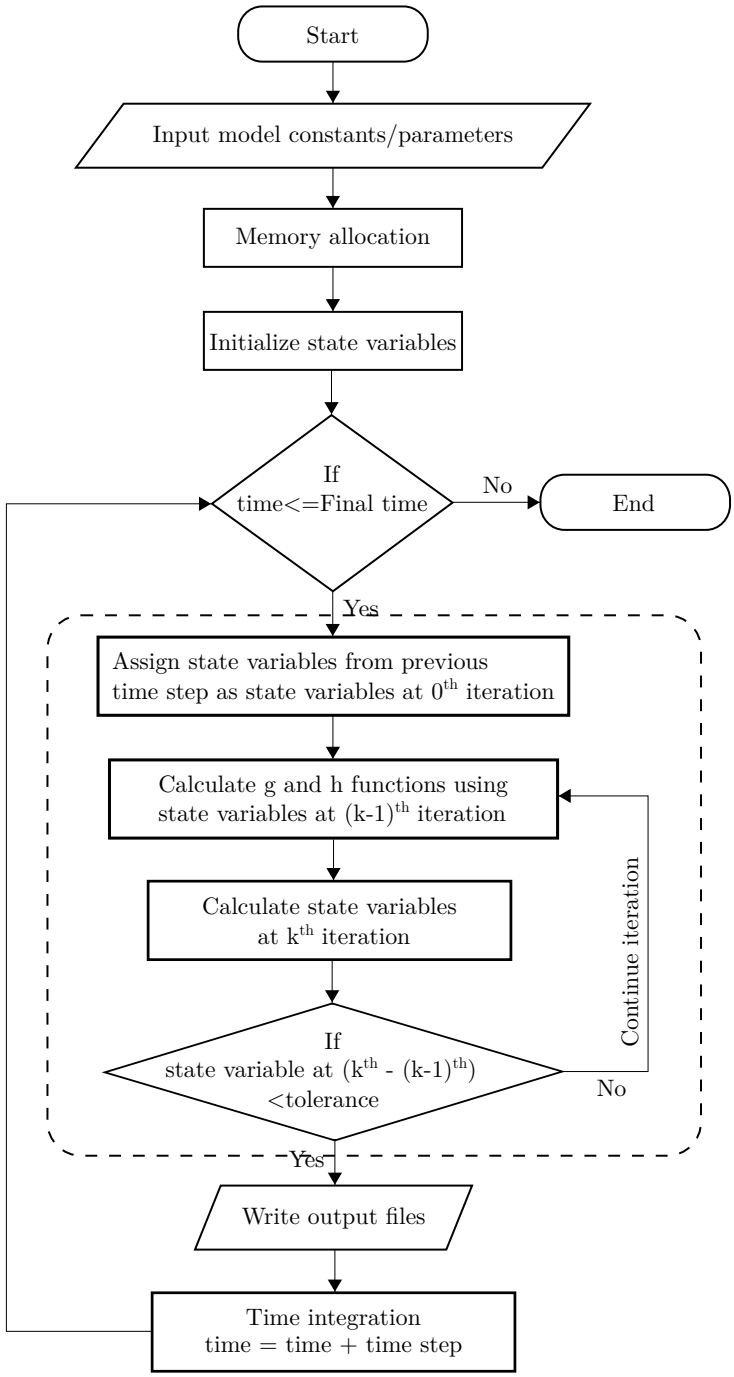

Fig. 3.5 Computer algorithm: Contains 5 parts 1) define model constants/parameters, 2) memory allocation, 3) initialization, 4) fixed point iteration and 5) writing output data. Part of the algorithm for fixed point iteration is given in the dashed box.

A computer code is developed in 'C' language using Eclipse software, version: Juno service release 2 from http://eclipse.org/, to run the VSMC model. The developed computer algorithm is divided into 5 parts, (see Figure 3.5). The first part of the code defines the model constants and parameters. All the model constants given in the Appendix E are defined globally, so that they can be accessed at any part of the program. The simulation control parameters such as final time, time step tolerance limit, file writing frequency etc. are defined locally in the main file. The second part is allocating memory for the assigned variables in the code. All the state variables are initialized in the third part using the values given in Appendix D.

Once initialization is complete, the solution of the problem is calculated using a fixed point iteration algorithm, (refer to Figure 3.5). All the operations inside the dashed line box in Figure 3.5 represent the iteration algorithm. At the start of the algorithm, g and h functions are calculated using the state variables from the previous iteration, $(k\text{-}1)^{th}$. To calculate the g and h functions for the first iterative step, state variables from the previous time step are used. Using these g and h values, state variables are calculated in the new iteration, k^{th}. The state variables calculate in the $(k\text{-}1)^{th}$ and k^{th} iterations are compared to check for tolerance limit. If the tolerance limit is not satisfied, iteration algorithm is repeated.

The last part of the code is to save the results in the desired formats. The code saves the output data in two formats, .txt and .vtk. Vtk files are used to visualize the problem and .txt files are imported into Matlab for plotting and analysing the results. The frequency of saving output data is based on the file writing frequency defined in the first step. The last two parts of the code, fixed point iteration and writing files, are repeated until the final time is reached. We have uploaded the source code to a public area of the Github repository; the link is "https://github.com/BlueFern/VSMC-SC".

3.4 Model parameters and resting state values

The values of state variables at resting state (no agonist) are given in Table D. Experimental studies show that intracellular calcium at the resting state is less than or equal to 100 nM [128, 200, 55]. We use this evidence to choose 80 nM in our model. Studies by Picht et al. [139] and Esfandiarei et al. [44] show that intra-SR calcium concentration at resting state stays in between 1 mM and 1.3 mM. Therefore, we have adjusted the SR leak parameter to obtain a value of 1.2 mM. The initial value of Vm is fixed to -54 mV based on the experimental observation of Harder and Sperelakis [62] in VSMCs of mesenteric artery. Once intracellular calcium, intra-SR calcium and V_m are fixed, other state variables, GP, IP_3, DAG, R_{10}, R_{01}, R_{00}, X_{10}, X_{01}, X_{00}, p_f, p_s, d_L and f_L, at resting state are calculated based on

the steady state equations given in Appendix D. The $[Na^{+}_{cyt}]$ value is taken from the model of Kapela et al [83] and this value is used to find the NCX current.

All model parameters appear in Tables E.1, E.2, E.3, E.4, and E.5. The SR_{leak} parameter, λ, is obtained from the intra-SR calcium balance at resting state. All the other terms in the intra-SR calcium equation (see Equation 3.7), are known at resting state. The maximum rate of calcium efflux of PMCA, Q_{PMCA}, is calculated by solving the intracellular calcium balance at resting state, (refer to Equation 3.6). The NCX current at resting state is almost negligible. The BK_{Ca} channel parameter, $G_{BK_{Ca}}$, is obtained by balancing membrane potential equation at resting state, (refer to Equation 3.5). The scaling factor of NCX, $\bar{I}_{NCX}$, is fixed by adjusting it to get the intracellular calcium concentration within the physiological range, less than 1μM, [128, 200, 55] upon agonist stimulation.

3.5 Results

3.5.1 Model response to varying agonist concentrations

The simulations are carried out for varying concentrations of agonist, zero nM to 800 nM. At the beginning of the simulation, zero agonist is set, so the VSMC will be in the resting state. The agonist concentration is imposed from the first time step onwards.

The temporal variations of intracellular calcium, membrane potential, intra-SR calcium, IP_3, and DAG at 350 nM and 600 nM for the first 100 seconds are shown in Figure 3.6. Below [L] = 237 nM concentrations, intracellular calcium increases gradually with respect to agonist concentration with no oscillations. However, calcium transients show a repeating oscillatory behaviour at medium agonist concentrations, greater than 237 nM. With 350 nM, the peak amplitude of the first transient intracellular calcium wave attains a value close to 500 nM. The maximum and minimum values of regular intracellular calcium oscillations are 445 nM and 71.57 nM respectively. For the same agonist concentrations, V_m (-43.12 mV, -50.70 mV), intra-SR calcium (1.12 mM, 0.06 mM), IP_3 (69.68 nM, 22.37 nM) and DAG(84.9 nM, 27.99 nM) oscillate with the respective maximum and minimum values (given in the brackets).

The temporal variations of ionic currents of the VOCC, NSC, BK_{Ca}, CACC, PMCA, NCX, RyR, IP_3R, SERCA, SR_{leak}, and the net calcium current in the SR at 350 nM are shown in Figure 3.7. The spontaneous BK_{Ca} currents are well aligned with the CACC currents; both of them have matching magnitudes as well. Similar to this, the CACC currents were synchronized with BK_{Ca} currents in the studies of Kamouchi et al. [80] and Large and Wang [97]. At the start of the oscillation, the IP_3R current is slightly larger than the RyR current. However, before intracellular calcium reaches a peak, the RyR current overtakes the IP_3R

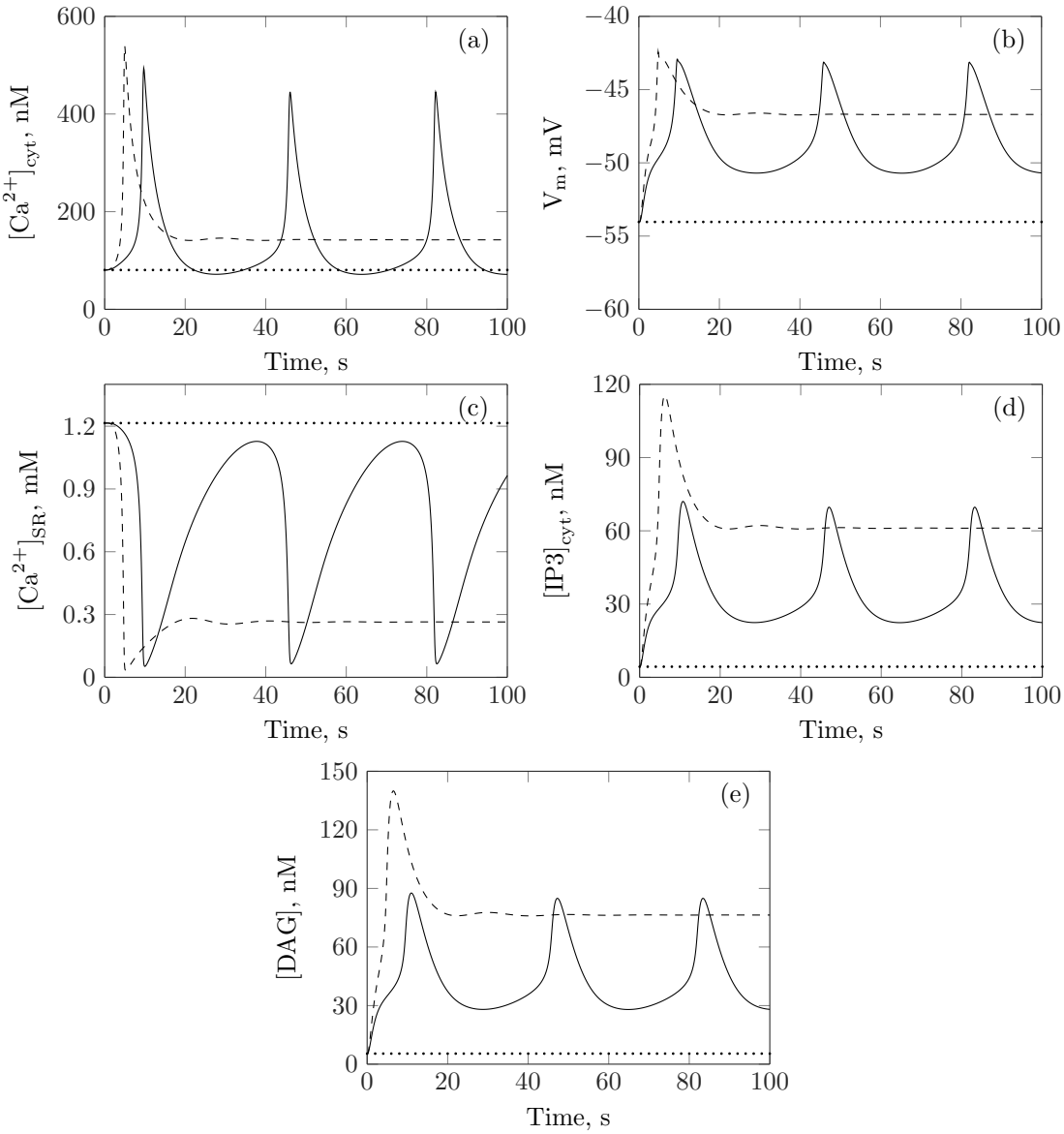

Fig. 3.6 Temporal variations of intracellular calcium (a), membrane potential (b), intra-SR calcium (c), IP_3 (d) and DAG (e) are plotted at 350 nM (solid line) and 600 nM (dashed line) concentrations of agonist. Dotted line indicates values of respective variables when no agonist is present.

current. IP_3R current shows a sharp decline at 45 seconds unlike the RyR current, (refer to Figure 3.7 (d)). The peak current of RyR is two-fold larger than the peak IP_3R current. The peak amplitude of the SERCA current is slightly larger than the RyR current peak. Both IP_3R and RyR currents become negligible at around 60 seconds.

The net calcium SR-current becomes negative at the time when IP_3R current overtakes RyR current. The net calcium current from SR shows a sharp increase in magnitude at around

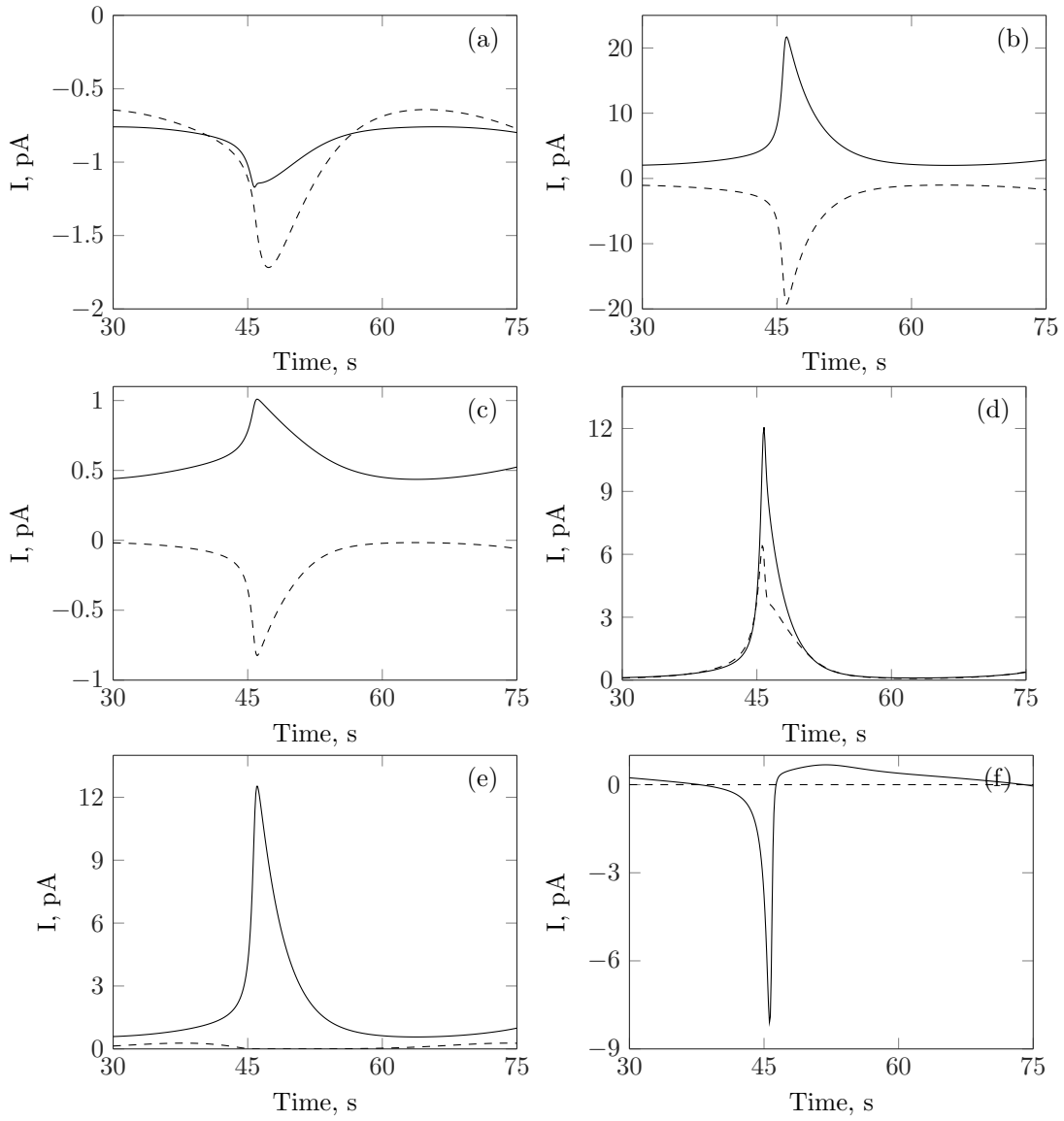

Fig. 3.7 Temporal variations of ionic currents: Shows variation of different ionic currents at 350 nM concentration of agonist. (a) VOCC (solid) and NSC (dashed), (b) BK_{Ca} (solid) and CACC (dashed), (c) PMCA (solid) and NCX (dashed), (d) RyR (solid) and IP_3R (dashed), (e) SERCA (solid) and SR leak (dashed) and (f) Net calcium current in SR (solid) and zero reference (dashed).

45 seconds. Then it goes back to positive values and stays there up to 75 seconds. The net SR calcium current stays in the positive values for a long time compared to the short period of negative values, (refer to Figure 3.7 (f)). The VOCC current is always negative and never reaches zero. The NCX current is zero at low intracellular calcium concentrations whereas the PMCA current is comparatively higher. The magnitudes of the NCX current and the

PMCA current are alomst equal to each other during the activation period. The magnitude of the NSC current peak is larger than the currents of the VOCC, NCX and PMCA.

At high concentration of agonist of 600 nM, intracellular calcium shows a single oscillation with a sharp peak, greater than 500 nM, immediately after agonist stimulation and within 10 seconds mostly, (see Figure 3.6 (a)). Intracellular calcium is then gradually reduced and reaches a steady value, 142.31 nM, which is higher than the intracellular calcium at the resting state. A similar temporal pattern of intracellular calcium was reported in experimental work on VSMCs of male Wistar rats by Lamboley et al. [95]. The steady state values of V_m, intra-SR, IP_3 and DAG at 600 nM are equal to -46.69 mV, 0.26 mM, 61.10 nM, and 76.37 nM respectively.

Figure 3.8 shows bifurcation diagrams as functions of agonist concentration. Bifurcation diagrams of different state variables are plotted by finding the maximum and minimum values at a fixed agonist concentration. The simulations are carried out for 800 seconds at a fixed agonist concentration. The maximum and minimum values of oscillations are taken as the average of all the oscillations which happened in between 500 seconds and 800 seconds. We should note however that this method of finding bifurcation points is an approximate one, but is adequate for this particular model. However, we have used MATCONT package (version: matcontp63), a Matlab toolbox for the bifurcation study of discrete and continuous dynamical systems, in order to understand the type of bifurcation of the given system. The MATCONT analysis has shown that the two bifurcations are both of a Hopf type and these points are equal to 237 nM and 545 nM.

The intracellular calcium reaches a value less than the resting condition after each peak in oscillations when the agonist concentration is less than 425 nM in agreement with the experimental studies of Hamada et al. [61] and Guibert et al. [55]. With other concentrations of agonist, minimum calcium is higher than the resting value matching with the Ruehlmann et al. [147]'s study. The peak intracellular calcium of oscillations increases up to the agonist concentration equals 324 nM, then it decreases as agonist concentration increases. The minimum values of intracellular calcium increase only slightly in the whole oscillatory region (within the bifurcation points).

The maximum and minimum values of both IP_3 and DAG increase as agonist concentration gets higher. The minimum intra-SR calcium value is almost unchanged in the oscillatory region except the agonist concentrations near the highest bifurcation point, 545 nM. The minimum V_m value increases significantly against agonist concentration but the peak V_m values are mostly unchanged.

Frequency of intracellular calcium oscillations are plotted in Figure 3.9 top-pane. Frequency is directly related to the agonist concentration. A steep increase in frequency is

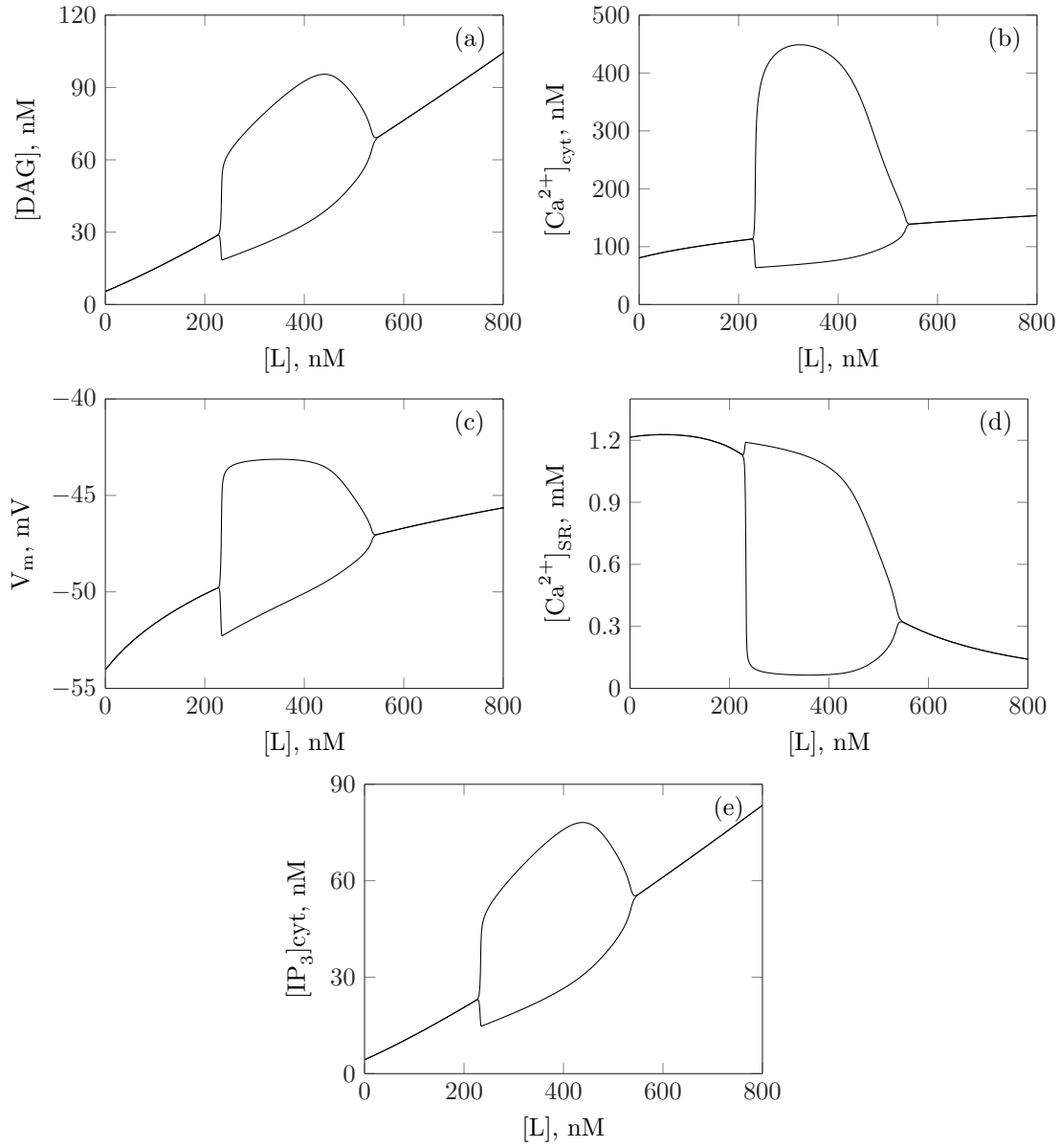

Fig. 3.8 Bifurcation diagrams of (a) DAG, (b) intracellular calcuim, (c) membrane potential, (d) intra-SR calcium and (e) IP_3.

obtained near the bifurcation points. Away from the bifurcation points, frequency increases gradually with agonist concentration. The maximum frequency of oscillations equals 2.75 cycles/min.

The time period of the activation phase and relaxation phase of the intracellular calcium oscillations are shown in Figure 3.9 bottom-pane. The time period of the activation phase is defined as the time taken for the intracellular calcium to go from the minimum value to the maximum value. The time period of the relaxation phase is the time duration at which

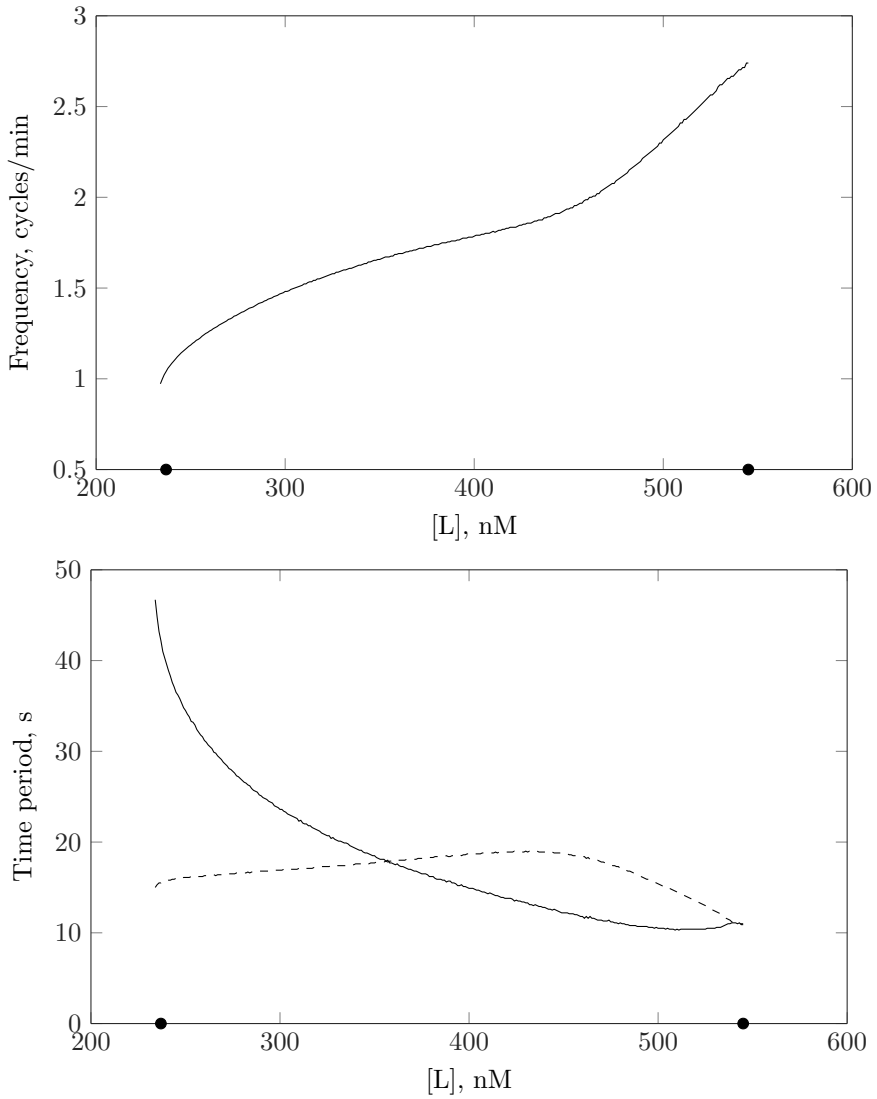

Fig. 3.9 Frequency (top) and time periods (bottom) of activation (solid) and relaxation (dashed) phases of intracellular calcium oscillations against agonist concentration. Black dots are used to represent the bifurcation points.

intracellular calcium of the cell decreases from the maximum value to the minimum value, (refer to Appendix F for a general explanation). The time period of activation phase decreases significantly as the agonist concentration increases. At an agonist concentration of 357.5 nM, the time period of the activation phase equals the relaxation time period. The time period of relaxation phase increases gradually and reaches a maximum at an agonist concentration of 433 nM, then it decreases. At the highest bifurcation point, the time periods of the activation and relaxation phases are equal.

3.5.2 Model response to varying extracellular concentrations

The response of the VSMC to different extracellular calcium concentrations is shown in Figure 3.10. Extracellular calcium concentration is varied from 0.5 mM to 4 mM at a fixed agonist concentration of 350 nM. Changes in extracellular calcium could not stop calcium oscillations and only a slight change in amplitude is obtained. This is due to the fact that the major contribution of the calcium rise emanates from SR rather than extracellular space.

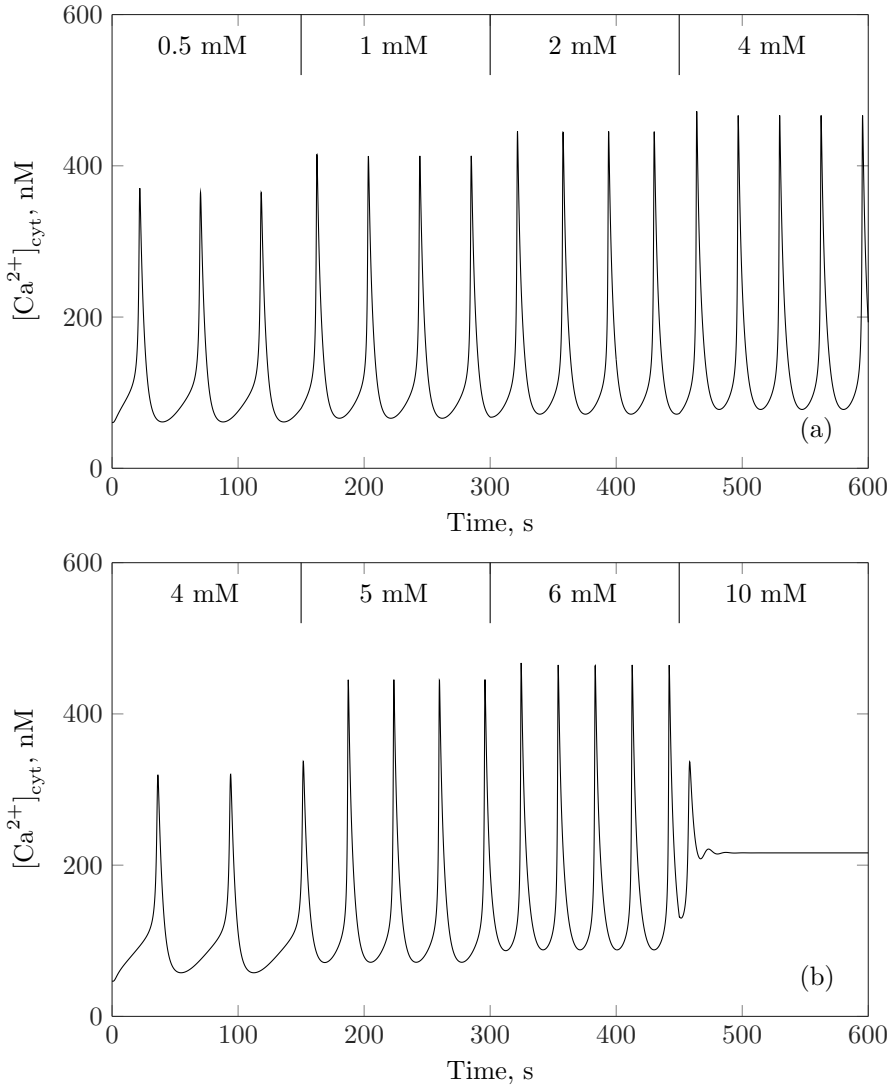

Fig. 3.10 Response of the VSMC model to varying extracellular concentrations: agonist concentration is equal to 350 mM (a) Temporal variations of intracellular calcium at different extracellular calcium concentrations. Extracellular calcium is equal to 0.5 mM at 0-150 seconds, 1 mM at 150-300, 2 mM at 300-450 and 4 mM at 450-600. (b) Temporal variations of intracellular calcium at varying extracellular potassium concentrations, 4 mM (0-150 seconds), 5 mM (150-300 seconds), 6 mM (300-450 seconds) and 10 mM (450-600 seconds)

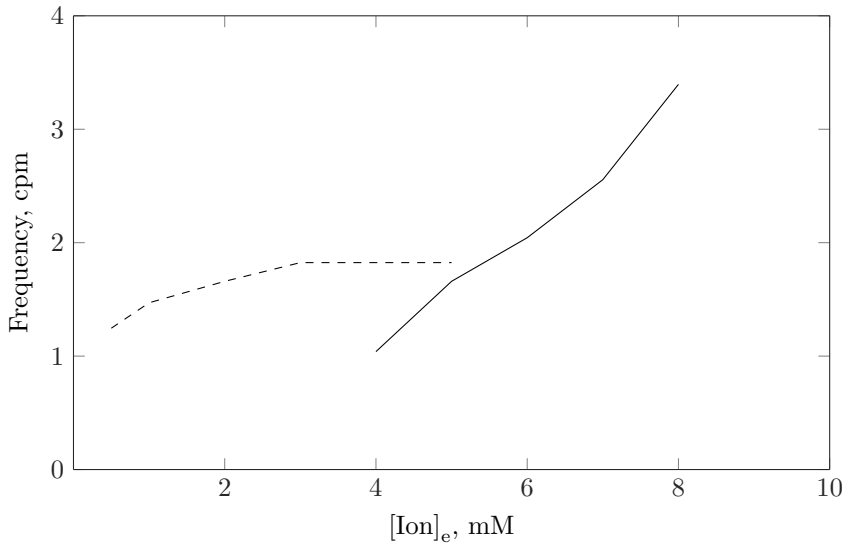

Fig. 3.11 Frequency of intracellular calcium oscillations at different extracellular potassium (solid) and extracellular calcium concentrations (dashed). The control values of extracellular potassium and calcium are 5 mM and 2 mM, respectively. cpm means cycles per minute.

Increasing the extracellular potassium from 4 mM to 10 mM at a fixed agonist concentration raises the peak calcium concentration and the frequency of oscillations, (as shown in Figure 3.10 (bottom panel)). However, when extracellular potassium is increased, the BK_{Ca} current is reduced due to the reduction in the potassium concentration gradient across the membrane. This causes an increased depolarization of the VSMC, thereby bringing more calcium through the VOCC channel leading to an increase in the calcium amplitude. Calcium oscillations disappear at potassium concentrations of the order of 10 mM and above.

To highlight the frequency changes as a function of extracellular ion concentrations, a frequency plot for varying extracellular potassium and extracellular calcium is shown in Figure 3.11. There is only a minimal frequency change with extracellular calcium, but extracellular potassium significantly alters the frequency of calcium oscillations.

3.6 Discussions

We first make some comments on the model response compared to others, notably that of Kapela et al. [83]. Although care should be taken in comparing since the equation sets modelling the phenomena are different, the frequencies and maximum values of intracellular calcium compare well with those of other work (c.f. Fig 5 (b) of Kapela et al. [83] with Figures 3.8 (b) and 3.9 (top panel) of the present work). However the presented work shows lower frequencies than that of Kapela et al. [83]. We also note that the values of external K^+_{ext}

at which oscillations begin are significantly different. For the presented work oscillations occur at 4mM and cease at 10 mM whereas for Kapela [83] oscillations exist in the range $K_e^+ > 30$mM. The location of the right-hand bifurcation point (a Hopf bifurcation) differs in the two numerical models. Kapela's point occurs at an agonist concentration of 400 nM whilst the present model shows a bifurcation at 545 nM agonist concentration. This may be due to the inclusion in Kapela's model of the nitric oxide pathway including the CGMP concentration mediation of the BKCa channel.

It is reported that the characteristics of agonist induced intracellular calcium dynamics in VSMC is mainly subjected to the agonist concentration. The intracellular calcium oscillations are obtained at medium agonist concentrations, 237 nM $<$ [L] $<$ 545 nM. This is similar to Lamboley et al. [95] and Schuster et al. [153] experiments where mesenteric arteries show calcium oscillations and vasomotion at medium concentrations of agonists, 400 nM to 800 nM of PE and 300 nM to 500 nM of NE respectively. Although in the experimental case the SMCs tended to "flash" and only became synchronised at relatively high concentrations. Our comparison here is that the numerical simulations show oscillations at the experimentally found agonist concentrations but clearly the numerical results are a regular oscillation whereas experiments show noisy data of calcium peaks.

The first peak of oscillations is obtained in less than 15 seconds in agreement to the study of Nicholls et al. [128]. Repetitive calcium oscillations with constant frequency and constant peak are obtained after the first peak, (refer to Figure 3.6). The peak of repetitive oscillations is less than the first calcium peak [128, 55]. Both frequency and peak of calcium oscillations increase with respect to the concentration of agonist near the first bifurcation point, 225 nM [61]. For the agonist concentrations around 320 nM, only the frequency increases and the calcium peak stays unchanged [147, 95, 136]. Near the second bifurcation point, 545 nM, frequency continues to increase with agonist concentration but calcium peak decreases. The frequency of oscillations ranges from 0.85 to 2.75 cycles/min. This is consistent with the experimental study of Hamada et al. [61] using cultured VSMCs from pulmonary artery. In their study, frequency of calcium oscillations was varied from 0.5 to 1.36 cycles/min when stimulated with 0.1 to 10 μM of PE.

Extracellular calcium does not have a significant effect on intracellular calcium oscillations. This is consistent with the experimental observations of Baro and Eisner [10] and Bolton et al. [20]. However, extracellular potassium modulation of intracellular calcium strongly affects the peak and frequency of oscillations. Oscillatory state of intracellular calcium is shifted to steady state at higher potassium concentrations. The modulation of intracellular calcium by extracellular potassium is similar to the experimental results of Lamboley et al. [95].

Agonist-induced calcium signalling mechanism

The model respnse of intracellular calcium oscillations are the result of calcium cycling between the SR & cytosol and the cytosol & extracellular space. The former calcium cycling is composed of intra-SR calcium release and recovery phases and the later one consists of depolarization and repolarization phases. The agonist binding to the G-protein coupled receptor leads to the activation of PLC and subsequent hydrolysis of PIP_2 into IP_3 and DAG molecules. The DAG molecules activate the NSC channel. The opening of the NSC channel depolarizes the VSMC. The cell depolarization increases VOCC current causing an initial rise of intracellular calcium, (see the Figure 3.7 (a)). The positive feedback mechanism between PLC, NSC and VOCC (PLC-NSC-VOCC) causes mutual rise of intracellular calcium and IP_3.

At medium concentrations of agonist, the mutual rise of IP_3 and intracellular calcium in the cytosol magnifies the open probability of the IP_3R leading to IP_3-induced calcium release (IICR). The increased calcium will then activate RyR as well as further activation of IP_3R causing calcium-induced calcium release (CICR). The combined IICR and CICR mechanisms mediated by RyR and IP_3R produce a sharp increase in intracellular calcium. This is clear from the sharp change in SR net current during calcium rise as shown in Figure 3.7 (f). Furthermore, intra-SR calcium is sharply declined and is analogous to the sharp increase of intracellular calcium, in agreement to the study of Picht et al. [139]. Also, the change in extracellular calcium showed only limited influence on the peak intracellular calcium. These observations suggest that the major calcium influx for intracellular calcium rise in this model is the calcium release from the SR mediated by IICR and CICR mechanisms [20, 99].

However, at higher intracellular calcium concentrations, the open probability of IP_3R is quickly reduced due to the effect of calcium inactivation of the IP_3R. This causes a sharp decreased calcium release through the IP_3R channel, (see Figure 3.7 (d)). At the same time, high calcium boosts the pumping rate of SERCA. These two actions, inactivation of IP_3R and increased pumping of SERCA, stop a further release of calcium to the cytosol and also the rise of intracellular calcium. The function of SERCA is to recover intra-SR calcium and return intracellular calcium to its basal values.

During the period of calcium rise, the calcium influx to the cytosol through the VOCC is small compared to the combined calcium efflux by the NCX and the PMCA. This means there will be calcium loss to the extracellular space at the expense of intra-SR calcium. Therefore, calcium influx through the VOCC is necessary for bringing the intra-SR calcium back to the resting state level [163].

As the intracellular calcium increases, the CACC current further depolarizes the cell. However, the counteraction of the BK_{Ca} channel keeps the membrane potential within physiological levels, (see Figure 3.7 (b)). Similarly, the NCX maintains the intracellular calcium in the physiological range by increasing the pumping rate at high intracellular calcium levels.

As the agonist concentration increases, intra-SR calcium retained in the recovery phase of regular oscillations is gradually reduced. At an agonist concentration higher than the highest bifurcation point, 545 nM, the increased production of IP_3 along with the enhanced calcium influx through the VOCC due to the DAG-mediated depolarization sustained activation of IP_3R and RyR. At this condition, the SERCA fails to bring the intra-SR calcium after the first drop immeditely after the agonist stimulation to a threshold level necessary for intracellular oscillations to occur. Therefore, after the first calcium rise, further calcuim rise and subsequent calcium oscillations are completely disappeared.

3.7 Model limitations

Like previous mathematical models, the cytosol is assumed to be a homogeneous domain which is not physiologically correct and we recognise this as a limitation of our model. There are experimental observations which support spatial heterogeneity in VSMCs. Although the SR is a single continous lumen, spatial distribution and organization of SERCA, IP_3R and RyR proteins are varied in longitudinal and junctional parts of the SR. The intracellular calcium waves are generated at the point of simulation on the cell membrane or at the SR and spread to other parts of the intracellular space [200, 16]. This creates microdomains in the cytosol which can regulate cellular processes in different regions of the cell. Since calcium signalling pathways due to beta-adrenergic agonists are not directly related to SR function the action of beta-adrenergic agonists on he VSMC is not included in the model. This model has not included cell membrane channels such as a store-operated channel, stretch operated channel and also has not included nitric oxide (NO) or cyclic guanosine monophosphate (cGMP) signaling pathways. In addition to that, the presence of mitochondria, Golgi apparatus, a nucleus and other cellular components may have a role in the development of calcium microdomains, particularly the mitochondria. Further improvements will be made to the model by adding the above mentioned cellular components and signalling pathways to the current model.

3.8 Conclusions

As a powerful tool to investigate extremely complex biological systems, we have developed a mathematical model of VSMC to accomplish the research aims. In the model, we have defined new or modified descriptions to NCX exchanger, IP_3R channel, NSC channel, agonist-induced IP_3 production, SR structure, and functioning. The SR was modelled as a single luminally continuous store which contains both IP_3R and RyR and with homogeneous luminal calcium. None of the VSMC mathematical models has used sequential binding of calcium and IP_3 for the activation of IP_3R. We have incorporated a simplified 4-state sequential-binding IP_3R model in our VSMC model since calcium is the central attention of the study. The model equations were solved using a numerical model developed based on Backward-Euler method and fixed point iteration. The time period and tolerance limit for getting required accuracy was fixed by analysing the relative error. The code for the model is written 'C' code and was implemented on a local machine.

The model results were compared qualitatively against the experimental studies. The temporal occurrence of intracellular calcium oscillations, amplitude and frequency of intracellular calcium oscillations, the response of the model to varying extracellular concentrations of potassium and calcium and bifurcation points of the agonist stimulation are matching with the experiments in VSMCs. The intracellular calcium signalling mechanism of the model is discussed to know how the model responses to different agonist concentrations. The developed model will then be used for studying the effects of SERCA, IP_3R, RyR and GJIC. The next chapter (chapter 4) will focus on the effects of altered levels of SERCA, IP_3R and RyR in a single VSMC.

Chapter 4

The effects of altered levels of SERCA, RyR and IP_3R: Single VSMC

4.1 Introduction

Agonist induced intracellular calcium dynamics depends on the functional interaction between SERCA, IP_3R and RyR [53, 194, 13]. We have already seen that the intracellular calcium dynamics of the VSMC are modified in diabetes along with altered regulation of the calcium handling proteins in the SR such as SERCA, IP_3R and RyR. The altered expression of these proteins were found in other pathological as well as physiological conditions. The SERCA expression was found to be downregulated in proliferating VSMC [106] and the supression of IP_3R activity reduced proliferation in cerebral VSMC [190]. VSMCs failed to contract when RyR and SERCA were not present in the SR [180]. Interestingly, proliferation and migration are found to be significantly increased in VSMCs of a diabetic origin [46] whilst the contractility is decreased [138]. In addition intracellular calcium dynamics and contractility of VSMC were altered with a reduction of SERCA and IP_3R levels in the development of atherosclerosis [45, 113]. Therefore, the current study to understand the effects of altered levels of SERCA, IP_3R and RyR on the intracellular calcium dynamics can be used to investigate not only diabetes but also other relevant normal or disease conditions.

We have used the new VSMC mathematical model developed in our dry lab (discussed in the chapter 4) to investigate the consequences of altered levels of SERCA, IP_3R and RyR on the intracellular calcium dynamics of VSMCs in combination with agonist stimulation. The level of a protein is altered in the model by changing the maximum rate of the corresponding protein function. The responses of the model to different combinations of SERCA, IP_3R and RyR levels at a fixed agonist concentration and for varying agonist concentrations are

discussed. The model results are compared with the experimental studies and discussed with an interest to diabetes (at the end of the discussion section).

The model results will provide information about how the intracellular calcium dynamics of a VSMC are altered due to SERCA, IP_3R and RyR. This may help to understand the impaired calcium dynamics in pathological condition such as diabetes. Also, this study will help to understand the combinations of SERCA, IP_3R and RyR levels required to obtain desired intracellular calcium dynamics when the agonist concentration is changed. Based on that, our hypothesis is that if an external environment influences the agonist-induced calcium transients, the VSMC may alter the levels of SERCA, IP_3R and/or RyR expressed in the SR to restore intracellular calcium transients matched with the functional need. The model results based on diabetic condition leads to the fact that reduced SERCA level is probably the primary factor responsible for the reduced intracellular calcium transients and the reduced contractility in diabetes even though all the three IP_3R, SERCA and RyR are varied in diabetic VSMCs.

4.2 Results

The functional role of a particular calcium handling protein may depend on the total number of that protein expressed in the SR. Changing Q_{SERCA}, Q_{RyR} and Q_{IP_3R} values qualitatively provide varying levels of SERCA, RyR and IP_3R activity. For the control case, Q_{SERCA}, Q_{RyR} and Q_{IP_3R} are equal to 2.1×10^4 nM s^{-1}, 4000 s^{-1} and 2000 s^{-1} respectively. The level of SERCA, IP_3R and RyR are presented as percentages of Q_{SERCA}, Q_{IP_3R} and Q_{RyR} compared to the control case.

4.2.1 Effects of varying levels of SERCA

The response of the model to varying levels of SERCA at a fixed agonist concentration 320 nM is shown in Figure 4.1. At this agonist concentration, the VSMC shows oscillations of intracellular calcium with 100% SERCA level. When the SERCA level is decreased to 0% or increased to 200%, the oscillatory state disappears and the intracellular concentration becomes steady. For the given system, the bifurcation points are 45% and 178% SERCA levels, (refer to Figures 4.1 (a) and (b)). These values are an approximation as we determine them based on the maximum and minimum values of oscillations, but is satisfactory for the kind of study we do. The simulations are carried out for 800 seconds at a fixed SERCA level. The maximum and minimum values of oscillations are taken as the average of all the oscillations which happened in between 500 seconds and 800 seconds. The same procedure

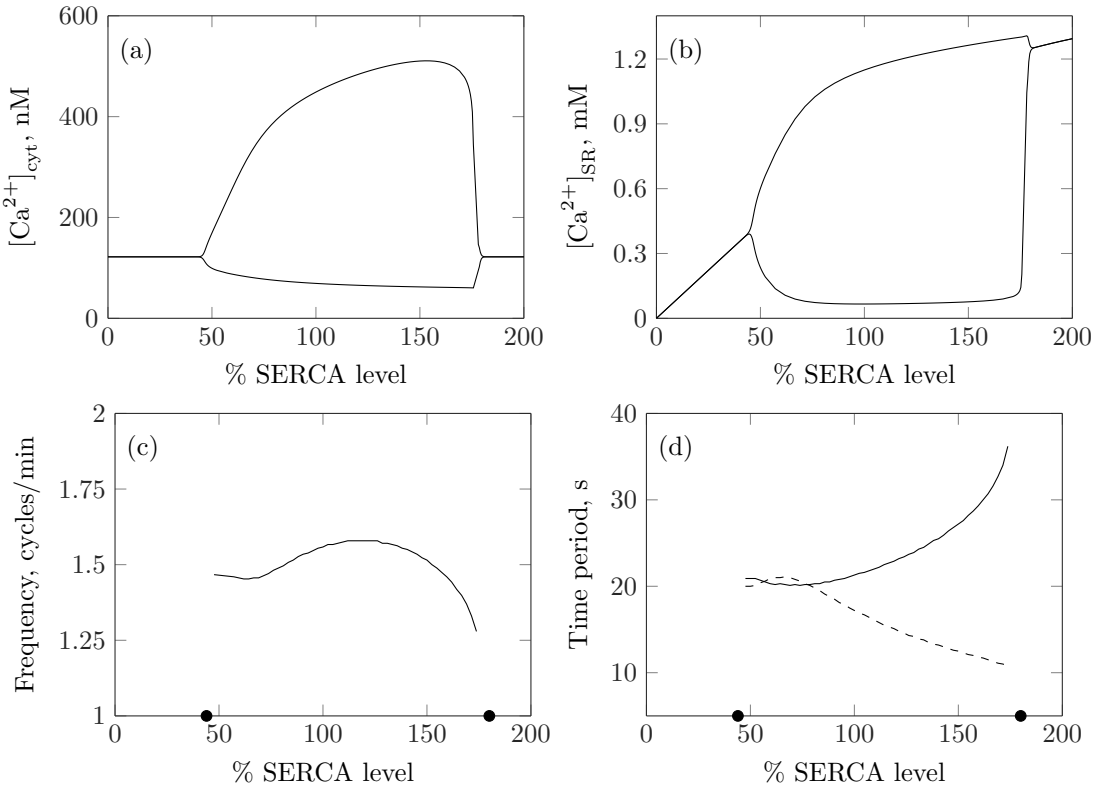

Fig. 4.1 Intracellular calcium (a), intra-SR calcium (b), frequency (c) and time periods of activation (solid) and relaxation (dashed) phases of intracellular calcium oscillations (d). SERCA is varied from 0% to 200%. IP_3R and RyR levels are kept constant at 100%. Agonist concentration is fixed to 320 nM. Black dots are used to represent the bifurcation points.

is followed for IP_3R and RyR as well. At any SERCA levels outside the bifurcation points, the intracellular calcium is steady and almost constant, 121.9 nM while intra-SR calcuim shows an increasing trend as SERCA level increases. The intra-SR calcium at the lowest bifurcation point is ≈0.35 mM, smaller than the 1.2 mM at the highest bifurcation point.

The frequency of intracellular calcium oscillations is unchanged between 45% and ≈75% SERCA levels. Then, the SERCA level regulation of frequency is biphasic. For less than 121% SERCA levels, frequency increases and for SERCA levels higher than 121%, frequency decreases, (refer to Figure 4.1 (c)). The frequency decrease is sharp just before the oscillation turns to a steady state.

Figure 4.1 (d) shows the time periods of activation and relxation phases, refer to Appendix F for definitions of activation and relaxation phases. The relaxation and activation time periods are almost equal for SERCA levels less than ≈75%. As the SERCA level increases further, the time period of activation phase is getting bigger than the relaxation time period. The time period of the activation phase increases continuously and the curve is concave up.

The relaxation time period shows a steady decrease. At higher SERCA levels, the change of the activation time period is higher than the corresponding change of the relaxation time period.

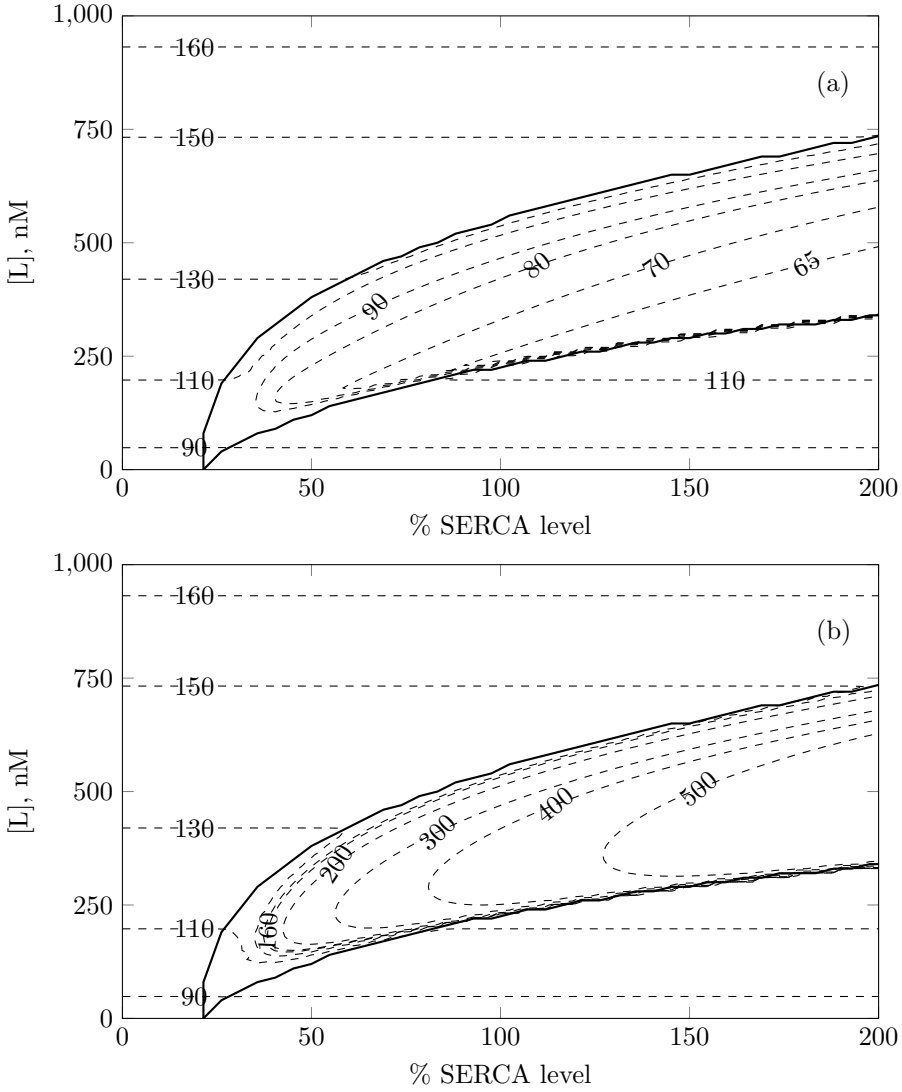

Fig. 4.2 Contour plots of minimum (a) and maximum (b) values of intracellular calcium oscillations for different combinations of agonist concentration and SERCA level are given. IP_3R and RyR levels are fixed to 100%. Solid line shows the bifurcation points for different SERCA levels and agonist concentrations.

The contour plots of maximum and minimum values of intracellular concentration for different combinations of agonist concentration and SERCA level are shown in Figure 4.2. The figure also shows the bifurcation points for different SERCA levels and agonist concentrations. The agonist concentration is varied from zero nM to 1000 nM. The SERCA

level is changed from 0% to 200%. The calcium oscillations are not seen at SERCA levels lower than ≈20%.

The bifurcation points increase monotonically as the SERCA level increases. The bifurcation points at 50% SERCA levels equals [L] = 120 nM and [L] = 380 nM. Increasing SERCA level to 200% lifted the bifurcation points to [L] = 340 nM and [L] = 735 nM. For any agonist concentration higher than the highest bifurcation point, an increase of SERCA level may shift the steady state of the VSMC to an oscillatory state. For example, at [L] = 500 nM, the increase of SERCA level from 30% to 100% shifts the intracellular calcium state from steady to oscillatory. Similarly, if the agonist concentration is lower than the lowest bifurcation point, a decrease in the SERCA level may change the intracellular calcium dynamics from a steady state to an oscillatory state.

When SERCA level is reduced, the area of the oscillatory region decreases with the maximum and minimum values of the calcium oscillations also decreasing. The overall maximum of intracellular calcium oscillations across the entire range of agonist concentrations decreases as the SERCA level is reduced. The definition of overall maximum is given in Appendix F. At 100% SERCA level, the overall maximum by varying agonist concentration is greater than 400 nM whereas the overall maximum is less than 300 nM with 50% SERCA level. At the same time, overall minimum of calcium oscillations is increased with decreasing SERCA levels.

4.2.2 Effects of varying levels of IP_3R

The effects of altered levels of IP_3R on the intracellular calcium, intra-SR calcium, frequency and time period of relaxation and activation phases at a fixed agonist concentration, 320 nM, are shown in Figure 4.3. The level of IP_3R is varied from 0% to 200%. The intracellular calcium equals ≈121.9 nM at 0% IP_3R and is unchanged until ≈30% IP_3R. The intracellular calcium oscillations are produced when IP_3R level is greater than ≈30%. When the level of IP_3R is increased to 200%, the oscillations of intracellular calcium and intra-SR calcium are almost unchanged.

The frequency of intracellular calcium oscillations increases monotonically with IP_3R level. The frequency is increased from ≈ 1 cycles/min to 1.62 cycles/min when the IP_3R level is varied from 30% to 200%. At low IP_3R levels, the frequency shows a great dependency on IP_3R level, while at higher IP_3R levels, frequency is almost unchanged.

The relaxation time period increases steadily as the IP_3R level increases. The time period of the activation phase decreases faster at low IP_3R levels compared to that at the higher IP_3R levels. At the same time, the time period of activation phase changes at a high rate compared

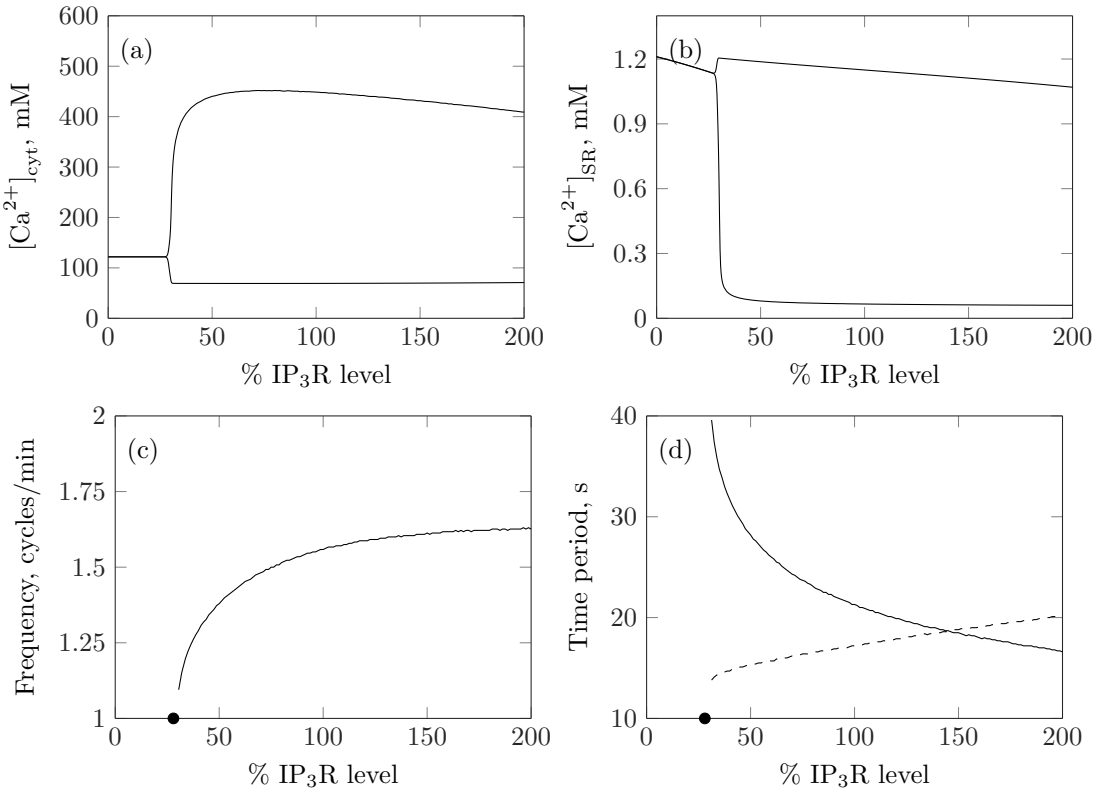

Fig. 4.3 Intracellular calcium (a), intra-SR calcium (b), frequency (c) and time periods of activation (solid) and relaxation (dashed) phases of intracellular calcium oscillations as a function of IP_3R level. SERCA and RyR levels are kept constant at 100%. Agonist concentration is fixed to 320 nM. Black dots are used to represent the bifurcation points.

to the relaxation phase time period at low IP_3R levels. The time periods of relaxation and activation phases are equal at 145% IP_3R.

Figure 4.4 shows the contour plots of maximum and minimum values of intracellular calcium oscillations for different combinations of IP_3R level and agonist concentration. The bifurcation points decreases as the IP_3R level increases. A strong influence of IP_3R level on the bifurcation points is seen at lower IP_3R levels compared to higher IP_3R levels. For 200% IP_3R level, the bifurcation points are equal to [L] = 460 nM and [L] = 180 nM whereas at 20% IP_3R level, they are equal to [L] = 890 nM and [L] = 330 nM.

The overall maximum of intracellular calcium oscillations by varying agonist concentration for the given range is considerably higher at low IP_3R levels than at high IP_3R levels. For 20% IP_3R level, the overall maximum of calcium oscillations is greater than 500 nM whereas the overall maximum is smaller than 450 nM at 100% IP_3R level.

For any agonist concentration higher than the highest bifurcation point, a decrease of IP_3R shifts the steady state of the VSMC to an oscillatory state. For example, the reduction of IP_3R

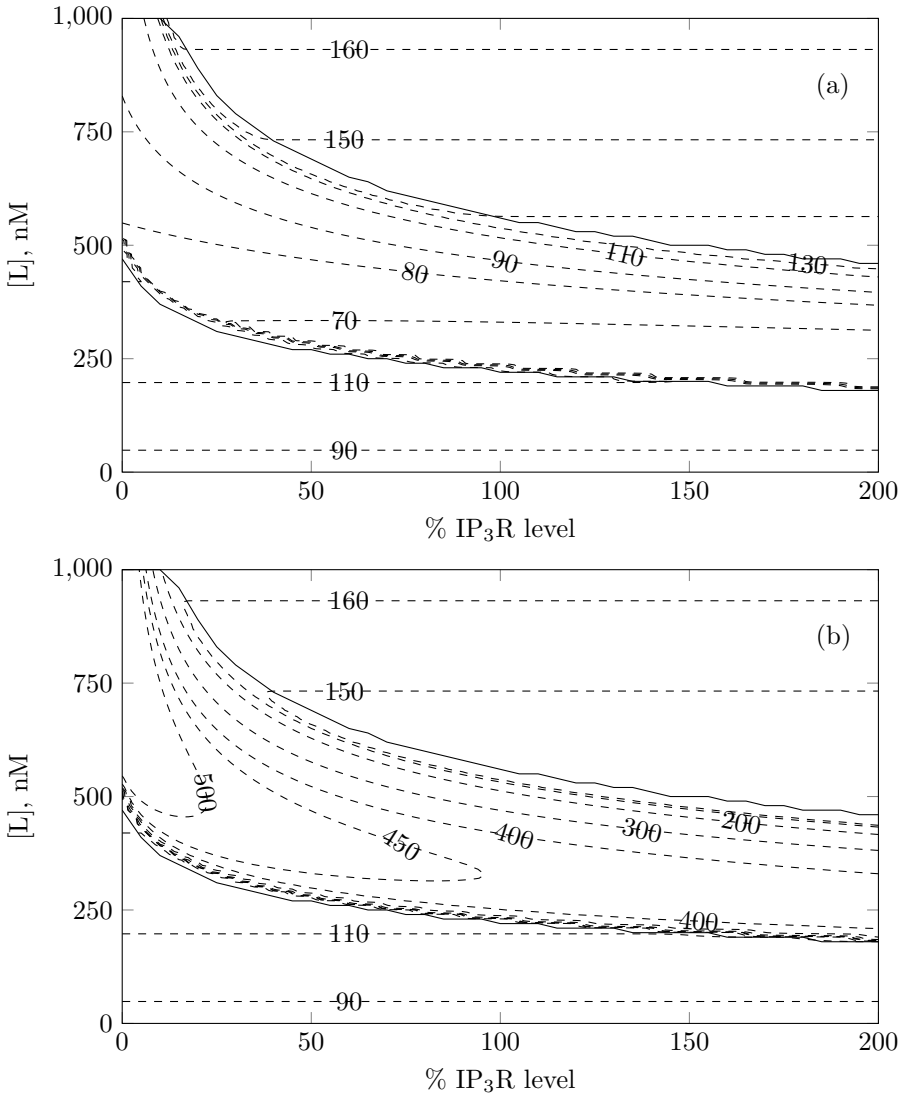

Fig. 4.4 Contour plots of minimum (a) and maximum (b) values of intracellular calcium for different combinations of agonist concentration and IP_3R level are shown. 100% SERCA and 100% RyR levels are used. Solid line shows the bifurcation points for different IP_3R levels and agonist concentrations.

level from 100% to 20% produces calcium oscillations at 750 nM of agonist concentration. On the other hand, if the agonist concentration is smaller the lowest bifurcation point, an increase of IP_3R level shifts the VSMC dynamics from steady state to an oscillatory state. For 300 nM of agonist concentration, an increase of IP_3R level from 20% to 100% produces calcium oscillations.

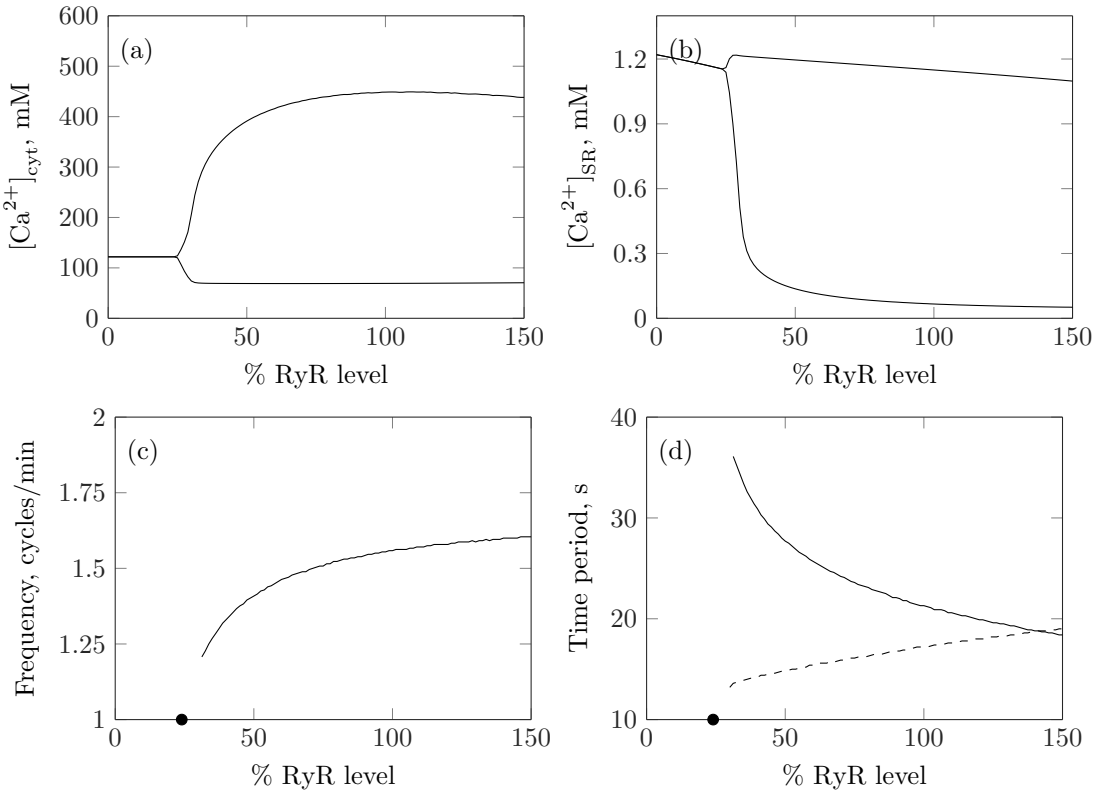

Fig. 4.5 Intracellular calcium (a), intra-SR calcium (b), frequency (c) and time periods of activation (solid) and relaxation (dashed) phases of intracellular calcium oscillations (d) as a function of RyR level. SERCA and IP_3R levels are kept constant at 100%. Agonist concentration is fixed to 320 nM. Black dots are used to represent the bifurcation points.

4.2.3 Effects of varying levels of RyR

Figure 4.5 shows the influence of RyR level on the intracellular calcium, intra-SR calcium, frequency and time periods of activation and relaxation phases at an agonist concentration of 320 nM. The RyR level is changed from 0% to 150%. The VSMC exhibits a steady state of intracellular calcium at 0% RyR level. As the RyR level increases, the intracellular calcium is unaffected until ≈25% RyR level, then it starts to oscillate. The maximum and minimum values of intracellular calcium and intra-SR calcium are unchanged for RyR levels greater than 70%. Below 70% RyR level, peak intracellular calcium increases with RyR level.

The frequency of oscillation increases significantly at low RyR level, (refer to Figure 4.5 (c)). However at high RyR levels, the frequency tends to be constant. The frequency is increased from 1.21 to 1.5 cycles/min for an increase of RyR level from 30% to 70%, whereas only an 0.05 cycles/min increase in frequency is obtained for a rise of RyR level from 100% to 150%.

The graph of relaxation and activation time periods with RyR looks similar to that with IP_3R. The activation time period decreases continuously as the RyR level increases whereas the relaxation time period increases. The decrease of activation time period is more significant at low RyR levels, (refer to Figure 4.5 (d)). The change of activation time period is large compared to the relaxation time period at low RyR levels. The relaxation and activation time periods are matching at 141% RyR level.

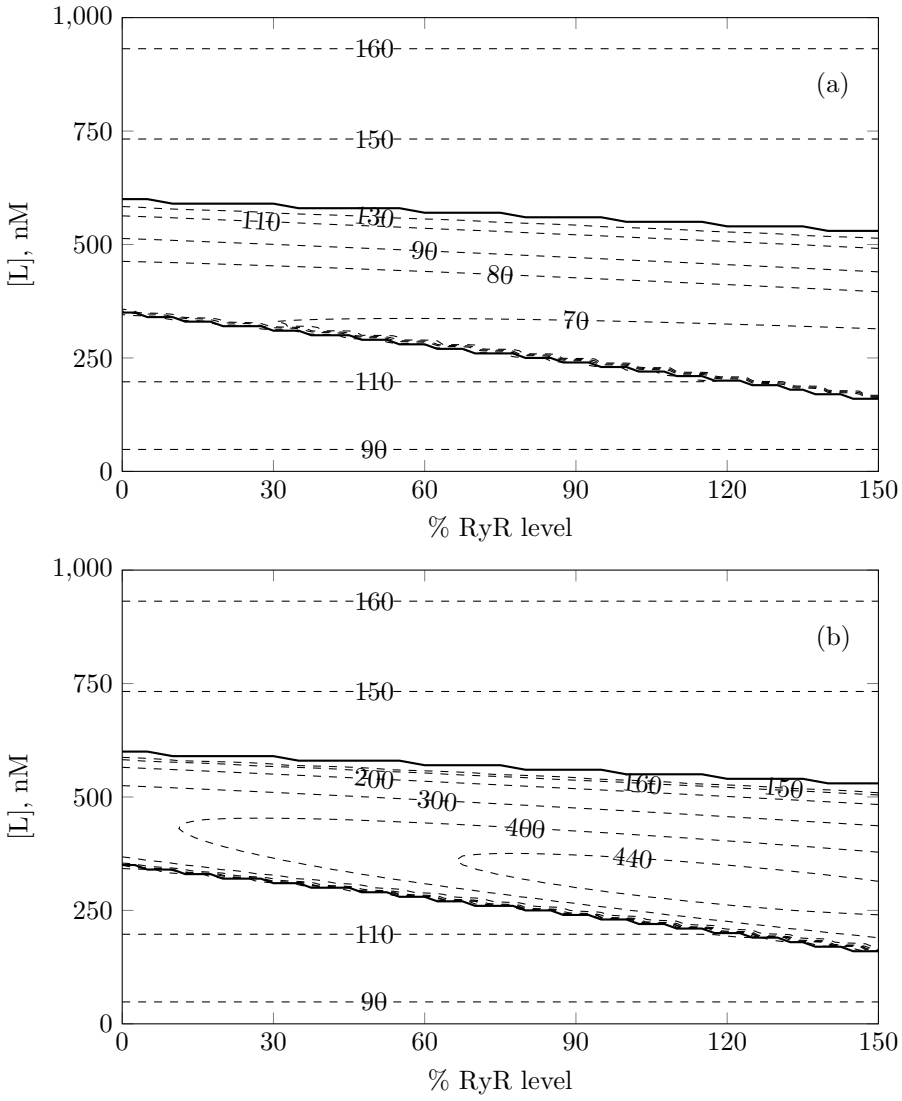

Fig. 4.6 Contour plots of minimum (a) and maximum (b) values of intracellular calcium for different combinations of agonist concentration and RyR level with 100% SERCA and 100% IP_3R levels. Solid line shows the bifurcation points for different RyR levels and agonist concentrations.

Figure 4.6 presents the effect of different combinations of RyR level and agonist on the maximum and minimum values and the bifurcation points of intracellular calcium oscillations. The bifurcation points increase linearly with RyR levels. At 0% RyR level, the bifurcation points are [L] = 600 nM and [L] = 350 nM of agonist concentrations. When the RyR level is increased to 150% RyR level, the bifurcation points are [L] = 530 nM and [L] = 160 nM.

The overall maximum of calcium oscillations increases as the RyR level increases. The 20% RyR level produces an overall maximum less than 300 nM whereas the overal maximum is greater than 440 nM for an RyR level of 80%. If the agonist concentration is smaller than the lowest bifurcation point, an increase of RyR level may shift the VSMC dynamics from the steady state to the oscillatory state. For example, At [L] = 250 nM, intracellular calcium is not oscillating at 30% RyR level but increasing the RyR level to 150% makes the calcium oscillate.

4.2.4 Effects of varying combinations of SERCA, IP_3R and RyR levels

The maximum and minimum values of intracellular calcium oscillations at different combinations of SERCA & IP_3R and SERCA & RyR are shown in Figures 4.7 and 4.8. The bifurcation points of intracellular calcium oscillations are also plotted in these figures. The agonist concentration is fixed to 320 nM. The intracellular calcium oscillations are obtained in the absence of IP_3R and RyR but not in the absence of SERCA. The upper limit of the SERCA level required for intracellular calcium oscillations increases significantly as the levels of IP_3R or RyR increase whereas the change of the lower limit of the SERCA level is minimal. For an increase of IP_3R or RyR level from 25% to 70%, the upper limit of the SERCA level is increased from $\approx$100% to $\approx$150% respectively. For the same change in IP_3R level or RyR level, the lower limit of SERCA level shows only a small change from 36.04% to 39.99% for IP_3R and 34.53% to 39.68% for RyR.

The overall maximum of calcium oscillations produced by varying IP_3R or RyR for the given range increases as SERCA level increases, refer to the upper panes of Figures 4.7 and 4.8. For example, at 50% SERCA level, the overall maximum of calcium oscillations produced by varying IP_3R level from 0% to 200% is less than 350 nM while the overall maximum is higher than 550 nM at 200% SERCA level. Similarly, the overall maximum of clacium oscillations by varying RyR levels from 0% to 150% at 50% SERCA level is smaller than that at 100% SERCA level.

The overall minimum of calcium oscillations produced by varying IP_3 or RyR for the given range decreases as SERCA level increases, refer to lower panes of the figures 4.7 and 4.8. At 50% SERCA level, the overall minimum of calcium oscillations by varying IP_3R or

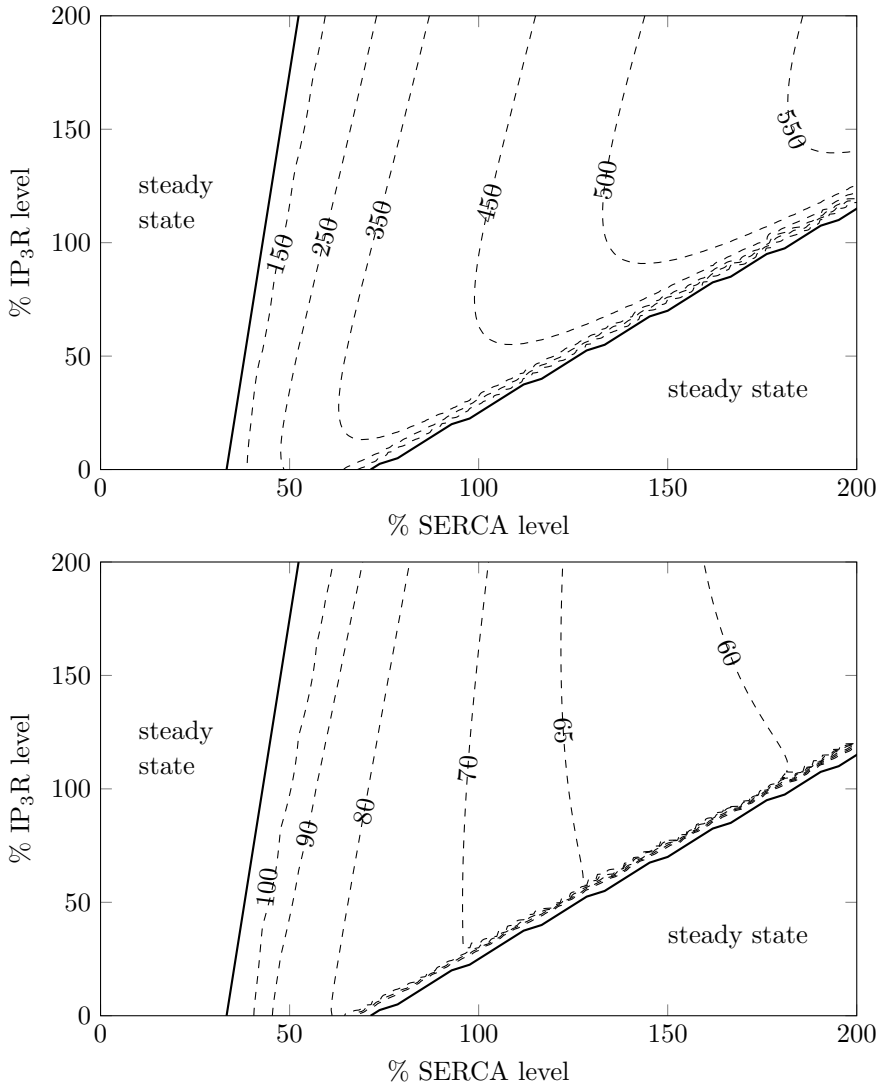

Fig. 4.7 Contour plots of maximum (top) and minimum (bottom) values of intracellular calcium for different combinations of SERCA and IP_3R levels with 100% RyR level and [L] = 320 nM. Solid line shows the bifurcation points for different SERCA and IP_3R levels.

RyR level is greater than 80 nM. The overall minimum value is smaller than 60 nM at 200% SERCA level.

The maximum and minimum values of intracellular calcium oscillations at different combinations of IP_3R and RyR are shown in Figure 4.9. The overall maximum or minimum of calcium oscillations is not changing much with IP_3R or RyR level. The RyR level required for calcium oscillations decreases as the IP_3R level increases. Similarly, the IP_3R level required for calcium oscillations decreases as the RyR level increases. When the IP_3R level is increased from 0% to 50%, the required RyR levels for calcium oscillations are 127.5%

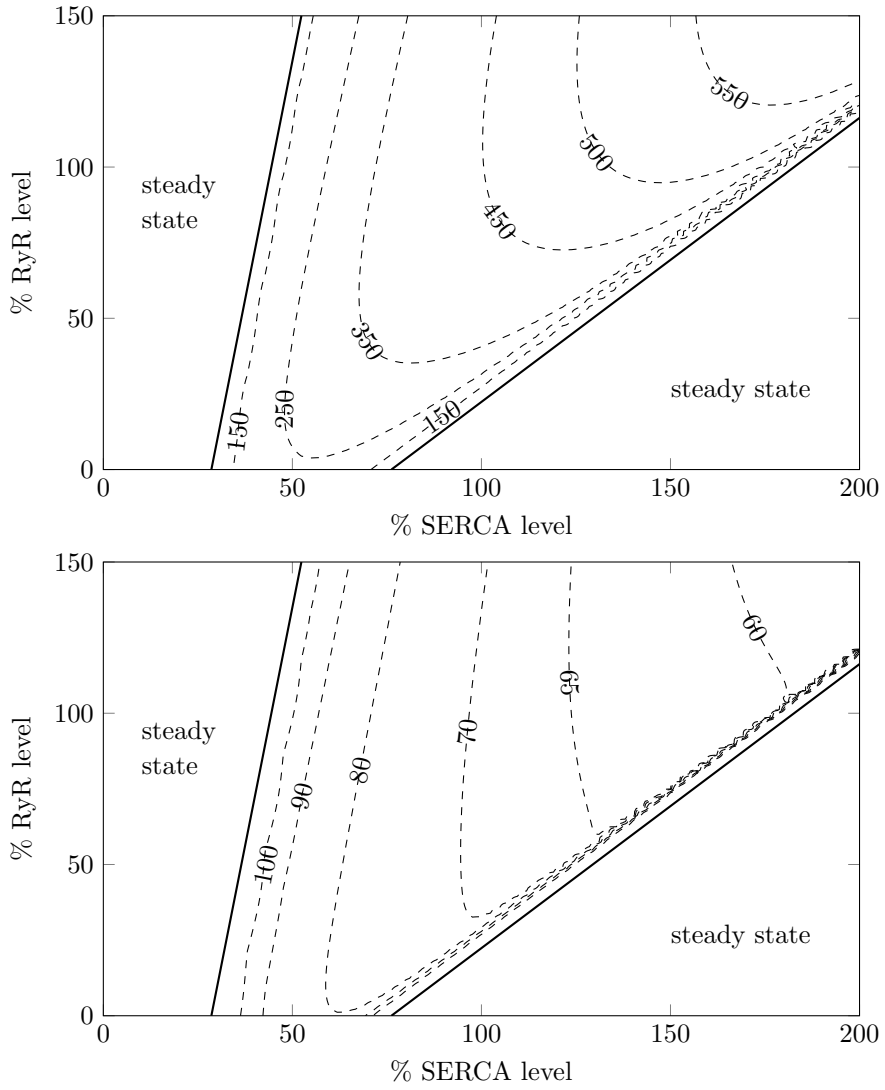

Fig. 4.8 Contour plots of maximum (top) and minimum (bottom) values of intracellular calcium for different combinations of SERCA and RyR with 100% IP_3R level and [L] = 320 nM. Solid line shows the bifurcation points for different SERCA and RyR levels.

to 75% respectively. For the similar increase of RyR level, from 0% to 50%, required IP_3R level decreases from 122.5% to 72.5%.

The top and bottom panes of the figure 4.10 shows contour plots of frequency of calcium oscillations with different combinations of SERCA & IP_3R and SERCA & RyR respectively at a an agonist concentration of 320 nM. The shape of the contours with different combinations of SERCA and IP_3R looks similar to that with SERCA and RyR. For any IP_3R or RyR level, the shape of the frequency curve for varying SERCA level looks similar to the Figure 4.1 (c).

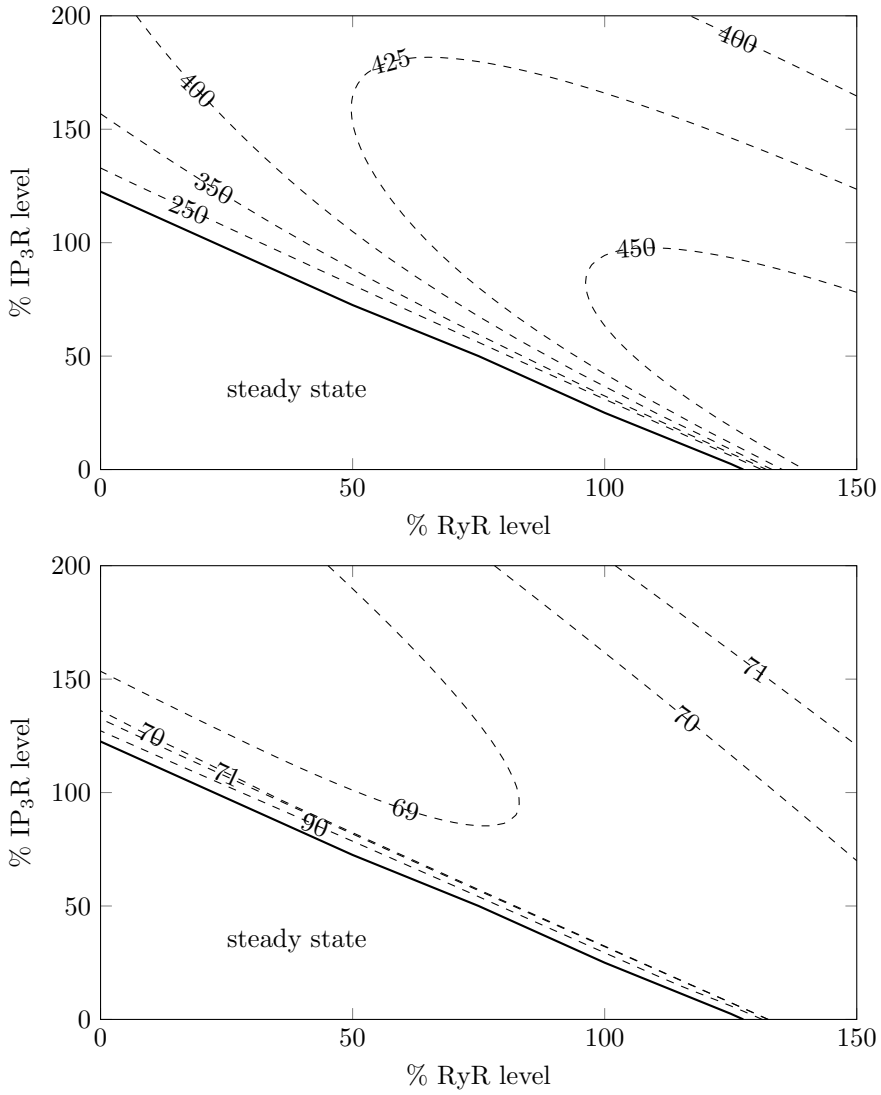

Fig. 4.9 Contour plots of maximum (top) and minimum (bottom) values of intracellular calcium for different combinations of IP_3R and RyR with 100% SERCA level and [L] = 320 nM. Solid line shows the bifurcation points for different IP_3R levels and RyR levels.

The overall frequency of calcium oscillations for the given range of SERCA levels increases as the IP_3R level or RyR level increases. The overall frequency is smaller than 1.4 cpm for 50% IP_3R level and is increasing up to 1.7 cpm for an IP_3R level of 150%. The overall frequency of calcium oscillation at 30% RyR level is less than 1.4 cpm and at 150% is going greater than 1.6 cpm.

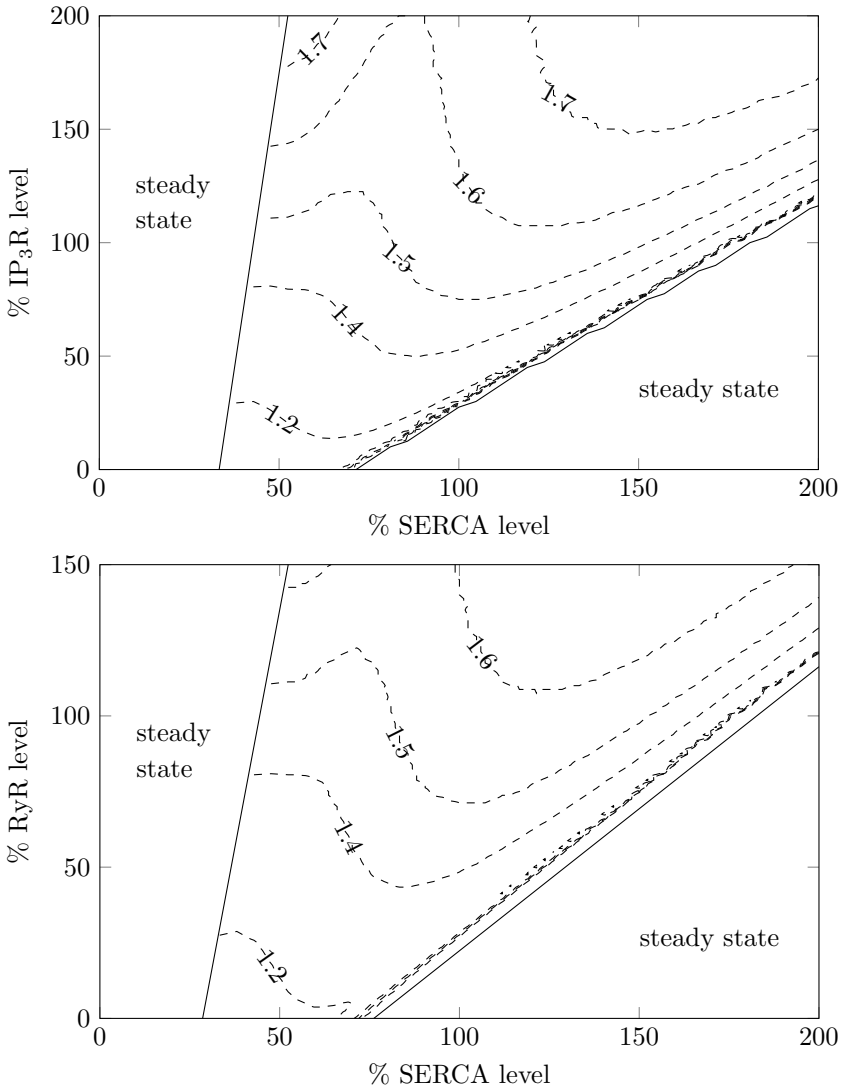

Fig. 4.10 Contour plots of frequency of intracellular calcium oscillations for different combinations of SERCA and IP_3R with 100% RyR level (top) and different combinations of SERCA and RyR with 100% IP_3R level (bottom). Agonist concentration is fixed to 320 nM. Solid line shows the bifurcation points for different combinations of SERCA, IP_3R and RyR.

4.3 Discussions

In the absence of IP_3R or RyR

The SR is responsible for a major contribution to agonist induced intracellular calcium oscillations in the VSMC. Some of the studies reported that SR calcium release is initiated by IP_3R leading to subsequent activation of RyR to produce a large amount of calcium release to the cytosol [19, 147]. In their studies, blocking of RyR activity abolished agonist-induced

calcium oscillations. In contrast to this, other studies reported that activity of IP_3R alone produces agonist induced calcium oscillations without RyR contribution [115].

Our model results show that the agonist induced calcium oscillations are attainable in the absence of either RyR or IP_3R. IP_3R and RyR share a common calcium pool. A complete blockage of either of these channels provides the full calcium potential available for the other channel. This keeps a sufficient calcium flux through the unblocked channel to produce intracellular calcium rise. When RyR is absent, IP_3R-mediated IICR and CICR produce intracellular calcium rise in the VSMC. On the other hand, when IP_3R is absent, intracellular calcium rise is obtained due to the activation of the RyR-mediated CICR mechanism.

The blocking of IP_3R or RyR can not produce calcium oscillations at the same agonist concentration at which calcium oscillations are possible in the presence of IP_3R or RyR. This is because of insufficient calcium influx through the VOCC to activate RyR-mediated or IP_3R-mediated calcium release at the same agonist concentration. At a higher agonist concentration, the increased production of DAG further depolarizes the cell, releasing enough calcium to the cytosol through the VOCC needed for RyR-mediated CICR or IP_3-mediated IICR and CICR. The calcium activation of IP_3R happens at low calcium concentrations, (refer to Figure 3.3). However, the activation of RyR-mediated CICR happens only at considerably higher intracellular calcium concentrations. Therefore, the IP_3R-mediated IICR and CICR are activated at a lower agonist concentration compared to the case in the absence of IP_3R. In the absence of RyR, intracellular calcium oscillations are obtained for an agonist concentration of 400 nM. However the agonist concentration should be greater than 500 nM for getting intracellular calcium oscillations in the absence of IP_3R.

The contradictory statements in the experiments regarding the occurrence of intracellular calcium oscillations in the absence of IP_3R or RyR are most probably due to the different types of agonist used for the stimulation or the use of same type of agonist in different concentrations. The model results indicate that using same agonist concentration for studying the existence of intracellular concentrations in the absence of IP_3R or RyR may lead to contradictory findings because of the shift of oscillatory region.

Frequency regulation

The frequency of oscillation depends on combined action of SERCA, IP_3R and RyR. If the level of any of these components is changed, it will affect both the relaxation and activation time periods. If the level of IP_3R or RyR increases, the calcium flux through these channels to the cytosol also increases. This helps the cell to achieve the calcium peak, as a faster rate leads to reduced activation time. This is the main reason for the increase of frequency while IP_3R or RyR level increases.

When the SERCA level increases, pumping of calcium back to the SR is leading to decreased relaxation time. However, if the SERCA pumping increases further, the net calcium flux to the cytosol during the activation time decreases which leads to a longer activation time to get a similar rise of intracellular calcium. These opposing effects of SERCA level causes biphasic SERCA regulation of frequency.

Shift between steady and oscillatory states

Phenotypic diversity is one of the characteristics of VSMCs. Based on the contractile properties, VSMCs are classified into either phasic or tonic. Phasic contraction is the rhythmic contractile activity, which is a distinctive property of arterioles to control blood pressure and flow [107]. As the contraction of VSMCs is related to intracellular calcium, the alteration of calcium dynamics may shift the phenotypic state of VSMCs from phasic to tonic or vice versa. The shift of oscillatory state and steady state at different combinations of SERCA, IP_3R and RyR levels may cause the phenotypic switching of VSMCs from phasic to tonic or vice versa.

Regis et al. [144] showed that increasing SERCA expression in human coronary artery smooth muscle cells shifts agonist-induced calcium release from steady to an oscillatory state. This is associated with increased intra-SR calcium load. The current model produces results similar to these experimental observations. In addition, the model results show that a reduction of SERCA level would shift the intracellular calcium state in the opposite direction [98, 107] and supports the fact that reduction or blocking of SERCA expression/function stops calcium oscillations in the smooth muscle cell. Therefore, the SERCA level acts as a controlling parameter for the intracellular calcium oscillation. Similar to SERCA, IP_3R and RyR levels also significantly affect the switching of oscillatory to steady states and vice versa of VSMCs.

One could assume that SERCA, IP_3R and RyR levels are the regulating parameters for enabling calcium oscillations at different agonist concentrations. Especially, increasing SERCA level move the oscillatory region to high agonist concentrations whereas increasing IP_3R or RyR level shift the oscillatory region to lower agonist concentrations. The shift of oscillatory region is large at low SERCA levels. At low IP_3 levels, the shift of oscillatory region is more significant than compared with low RyR levels.

Hypothesis

The current model results suggest that altered levels of SERCA, IP_3R and RyR modulate agonist-induced intracellular calcium dynamics significantly. If an external environment

influences the agonist-induced intracellular calcium transients in VSMCs, that may affect the activities of VSMCs such as contraction. Our hypothesis is that, in such situations, VSMC may alter the levels of SERCA, IP_3R and/or RyR expressed in the SR to restore intracellular calcium transients matched with the functional need.

Discussion in the context of diabetes

Several studies indicate that the impaired calcium dynamics in diabetic VSMCs is related to the altered levels of calcium handling proteins in the SR such as SERCA, IP_3R and RyR. The experimental study of Searls et al. [154] in VSMCs from the aorta of diabetic rats showed that the levels of SERCA and IP_3R are significantly lowered with an approximate reduction of 25% - 50% and 50% - 75% respectively. Sharma et al. [161] and Ma et al. [109] stated 50% and 30% reduction of IP_3R respectively in diabetic VSMCs from the aorta. The RyR was downregulated in the studies of Rueda et al. [146] using diabetic VSMCs from the aorta and Ma et al. [109] to almost 30%. In contrast to that, Searls et al. [154] reported upregulation of RyR to several folds.

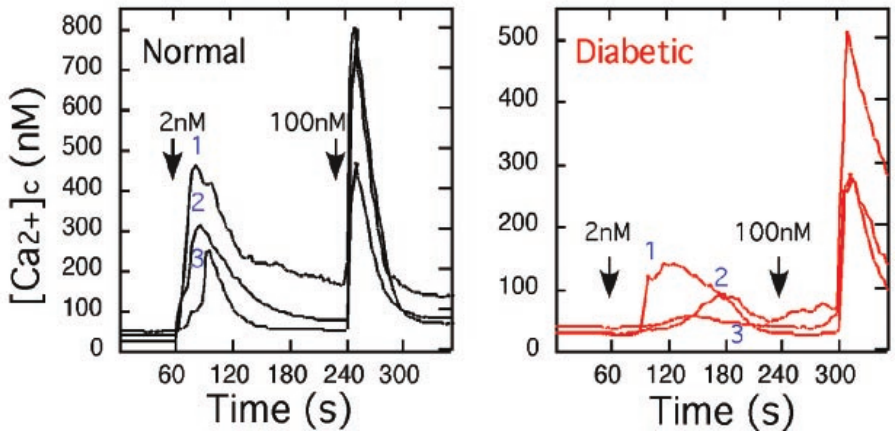

Fig. 4.11 Angiotensin II-induced intracellular calcium transients in normal and diabetic VSMCs from aorta. Reproduced from Sharma et al. [161] paper.

Searls et al. [154] and Sharma et al. [161] reported temporal variation of intracellular calcium in diabetic VSMCs as a response to an agonist stimulation, (see Figures 4.12 and 4.11). According to them, diabetic VSMCs show “smoothed" calcium transients with a decline in the overall calcium maximum. Similar to that, temporal variation of intracellular calcium from model results looks like low amplitude oscillations effectively “smoothed" with 50% reduction of SERCA level, (see Figure 4.13 (a)). The agonist concentration is fixed to 320 nM. The calcium transients seems to be less smoothed when either the IP_3R or

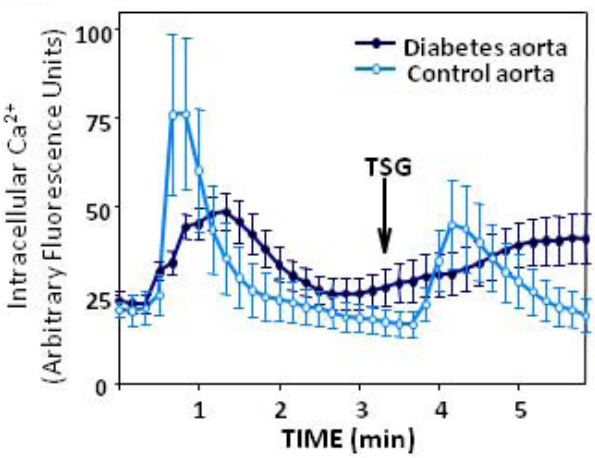

Fig. 4.12 Vasopressin and thapsigargin (TSG)-induced intracellular calcium transients in control and diabetic VSMCs. Reproduced from Searls et al. [154] paper.

RyR levels are reduced to 25% along with a 50% reduction of SERCA level than the case with only 50% reduction in SERCA level, (see Figure 4.13 (a)). These model responses suggest that the reduced SERCA level is one possible mechanism for the “smoothed" calcium transients.

The peak intracellular calcium with 50% SERCA level shows 60% reduction compared to that of the control case. This is closely matching with the 65% reduction of the intracellular calcium peak in diabetic VMSCs in the study of Sharma et al. [161]. When either the IP_3R or RyR levels are reduced to 25% along with a 50% reduction of SERCA level, only 35% reduction in the intracellular calcium peak is obtained. This is in good agreement with the calcium peak reduction of 33% obtained in the Searls et al. [154] study in diabetic VSMCs. When the level of RyR is upregulated to 150% along with 75% reduction of IP_3R and unchanged SERCA level, peak intracellular calcium is unaffected. The reduction of calcium release due to the downregulation of IP_3R would be compensated by the upregulation of RyR.

When agonist concentration is varied from zero nM to 600 nM, the overall maximum of calcium oscillations is reduced 36% for a reduction of 50% in SERCA level as shown in Figure 4.13 (b). The reduced overall maximum is unchanged with an additional 75% reduction of either IP_3R or RyR. When the SERCA level is kept at 100%, the reduction of IP_3R to 75% along with an increased RyR level of 150% shows no reduction in the overall maximum, meaning to say the overall maximum is matching with control case. These results indicate that the reduction of SERCA level is one possible reason for the decrease of calcium in VSMCs.

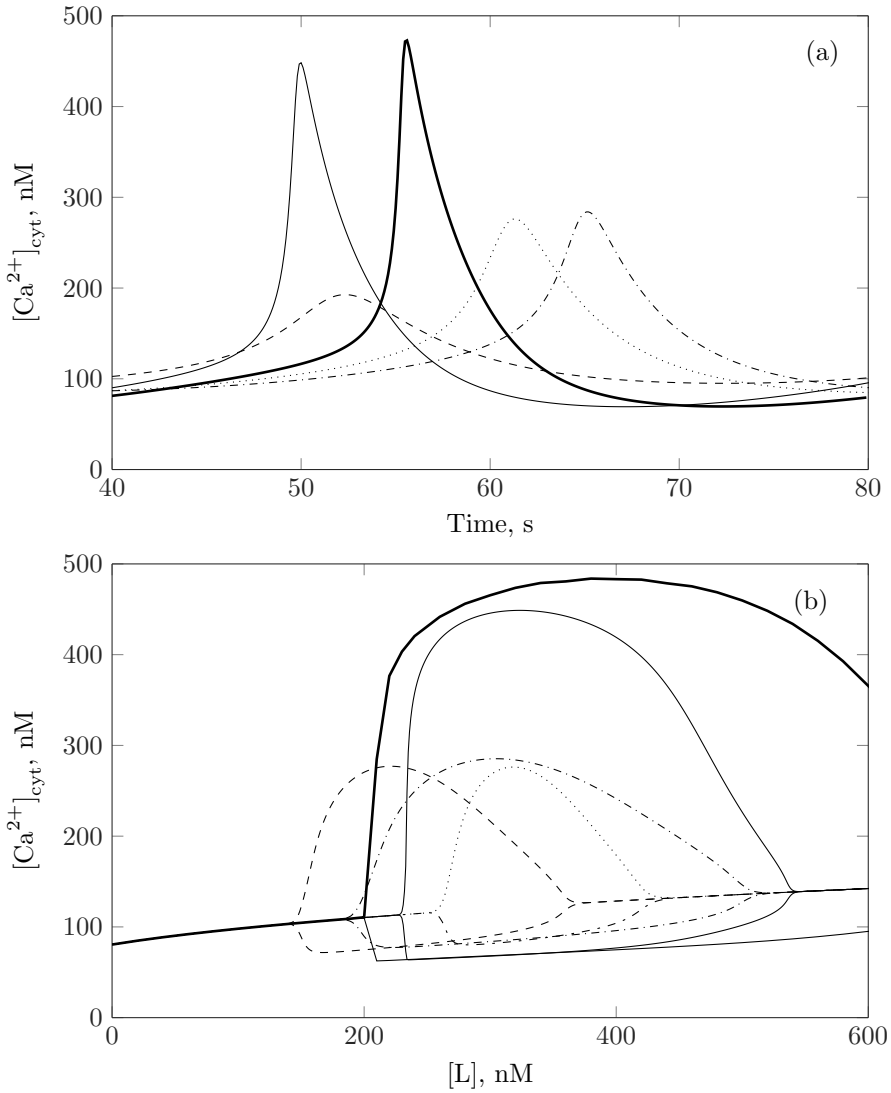

Fig. 4.13 (a) Temporal variations of intracellular calcium at [L] equals 320 nM and (b) bifurcation diagrams for control case (thin solid), for 50% reduction of SERCA (dashed), for 50% reduction of SERCA and 75% reduction of IP_3R (dash-dotted), for 50% reduction of SERCA and 75% reduction of RyR (dotted), and for 75% reduction of IP_3R and 50% increase of RyR (thick solid)

The figure 4.13 (b) shows that a reduction in SERCA level will shift the upper and lower limits of agonist concentration for oscillation to smaller values than the control case. However, an additional reduction of IP_3R or RyR level will raise the limits of the oscillatory region close to the control case. This means that reducing the IP_3R or RyR level would make the VSMC produce continuous intracellular calcium oscillations at similar agonist concentrations of the control case. The shift of the oscillatory region due to changed SERCA level can be re-established by altering the right amount of IP_3R or RyR level.

The model results show that intracellular calcium lowering as well as intracellular calcium rising in VSMCs is significantly affected by SERCA level changes. If the SERCA pumping is reduced, the intracellular calcium is raised in the relaxation phase. At the same time, the reduced reloading of intra-SR calcium causes decreases calcium influx through IP_3R and RyR, which leads to decreased intracellular calcium peaks. SERCA level is one regulating factor of intracellular calcium in both the activation and relaxation phases of oscillations.

The altered levels of SERCA, IP_3R and RyR modulate the intracellular calcium dynamics in diabetic VSMCs. The functional implications of altered levels of IP_3R or RyR in diabetic VSMCs might be regulated by changing the levels of the other protein. The proposed hypothesis points out this fact as a general scenario. However, the impaired intracellular calcium dynamics due to reduced SERCA levels can not be restored by changing IP_3R or RyR levels because of the reduced intra-SR calcium load.

Diabetes leads to reduced agonist-induced vascular contractility [138]. Since altered levels of SERCA, IP_3R and RyR are observed in VSMCs of diabetics [154, 118], it was not clear which of these components leads to reduced contractility. Our results shows that reduced SERCA level is probably the primary factor responsible for the reduced intracellular calcium transients and the reduced contractility in diabetics.

4.4 Conclusions

We have used the mathematical model developed during the course of our research (detailed in the chapter 3) to investigate the effects of altered levels of SERCA, IP_3R and RyR in a single VSMC. The level of a particular channel or pump was altered by changing the maximum rate of the corresponding channel or pump function. The responses of the model to the altered levels of SERCA, IP_3R and RyR at a fixed agonist concentration and for varying agonist concentrations were studied.

The frequency of intracellular calcium oscillations is significantly influenced by IP_3R and RyR at its low levels. The SERCA regulation of frequency is biphasic. At low SERCA levels, frequency increases with SERCA levels whereas at higher SERCA levels, the relation reversed.

The role of IP_3R and RyR in the occurrence of intracellular calcium oscillations was not fully clear in the literature. Some studies claimed the need of RyR for the existence of calcium oscillations whereas others proposed IP_3R alone is enough. The model results showed that the agonist induced calcium oscillations are feasible in the absence of RyR or IP_3R. However, higher stimulating strength is required to produce intracellular calcium oscillations in the absence IP_3R or RyR. The change in IP_3R or RyR level shifts the bifurcation points of agonist-

induced calcium oscillations. This might have been the reason for not getting the calcium oscillations in experiments when either IP_3R or RyR was blocked with the stimulation strength. These findings provide a possible explanation for the contradictory statements published in existing experimental studies.

The change of SERCA, IP_3R or RyR level shifted the oscillatory state of intracellular calcium to steady and vice versa at a constant agonist concentration. Especially, increasing SERCA level move the oscillatory region to high agonist concentrations whereas increasing IP_3R or RyR level shift the oscillatory region to lower agonist concentrations. The shift of oscillatory region was more significant at low SERCA levels and at low IP_3 levels. Based on this, our hypothesis is that if an external environment influences the agonist-induced calcium transients, the VSMC may alter the levels of SERCA, IP_3R and/or RyR expressed in the SR to restore intracellular calcium transients matched with the functional need.

We have done a set of simulations with altered levels of SERCA, IP_3R and RyR reported in the experiments using diabetic VSMCs. The model responses suggest that the reduced SERCA level is one possible mechanism for the “smoothed" calcium transients in VSMC. The intracellular calcium lowering as well as intracellular calcium rising in VSMC are significantly affected by the altered SERCA level. SERCA level tends to be the regulating factor of intracellular calcium in both the activation and relaxation phases of oscillations. The functional implications due to the altered level of IP_3R in diabetic VSMCs might be regulated by changing the level of RyR and vice versa. However, if the SERCA level is low, the alteration of IP_3R or RyR level can not restore the calcium dynamics in the VSMC because of the reduced intra-SR calcium load. These results leads to the fact that reduced SERCA level is probably the primary factor responsible for the reduced intracellular calcium transients and the reduced contractility in diabetes even though all the three IP_3R, SERCA and RyR are varied in diabetic VSMCs.

Chapter 5

Propagation of intracellular calcium oscillations: Coupled VSMCs

5.1 Introduction

Propagation of intracellular calcium is a spatiotemporal event with a high-level complexity in signal transduction. The GJIC exchanges information in the form of chemical and electrical signals. Advanced experimental techniques were developed to visualize and quantify intracellular calcium propagation [21, 175, 60]. However, in the context of the difficulty in tracking the individual coupling components with the available experimental methods, mathematical modelling has emerged as a powerful tool to understand the mechanisms behind the propagation of calcium oscillations.

Seppey et al. [157] hypothesized that opening of VOCCs due to the propagation of a depolarization from the stimulated cells to the non-stimulated cells is the pathway of the propagation of intracellular calcium. At the same time, they have reported that propagation was not seen until the artery were globally stimulated with a minimum agonist concentration. The production of IP_3 was increased when the artery was globally stimulated. Therefore, IP_3 concentration might have also been involved in the intercellular signalling pathway. This needs further study to understand the individual roles of V_m and IP_3 in the propagation of intracellular calcium.

Halidi et al. [60] has shown that two distinctive calcium waves propagate with different velocities and amplitudes, a fast calcium wave with low amplitude and a slow calcium wave with high amplitude. According to them, the opening of VOCCs due to the rapid propagation of depolarization results in fast calcium waves and the slow calcium waves require functional IP_3R. Coupling between VOCC and IP_3R is observed in their study. The amplitude of slow

calcium waves was reduced when the VOCC was blocked. However, they could not explain the cellular mechanism that connects VOCC and IP_3R; This needs a further study.

In this chapter, we have investigated propagation of intracellular calcium in coupled VSMCs. A numerical method is developed to solve the coupled cell simulations by incorporating the numerical method of single cell and tridiagonal matrix algorithm (TDMA). The coupled cells simulations are carried out in 100 serially coupled cells with a sigmoidal distribution of agonist. The simulations are carried out by coupling both V_m and IP_3, V_m alone and IP_3 alone to know the importance of V_m and IP_3 -mediated intercellular signalling mechanisms. The simulations are conducted in the presence and absence of IP_3R and RyR. The coupled cells results are qualitatively validated against the available experimental studies. The signalling pathways of propagation of intracellular calcium mediated by IP_3 and V_m and the dominant cellular mechanisms are discussed.

5.2 Gap junctional intercellular communication (GJIC)

GJIC is the result of the passage of cytosolic molecules and ions through the gap junction. The gap junction pore is large enough to allow the passage of cytosolic ions and many secondary messengers such as IP_3. It is necessary to know the relevance of gap-junctional diffusion of each intercellular messenger in the physiological environment.

It is reported that diffusion of calcium ions is slower than IP_3 in the cytosol even though the calcium ion is smaller in size [1]. According to Allbritton et al. [1], diffusion coefficients of IP_3 and Ca^{2+} in the cytosol are approximately 285 $\mu m^2/s$ and 13 $\mu m^2/s$ respectively. Strong buffering of calcium in the cytosol restricts the movement of calcium ions because calcium binds with immobile or slow mobile buffers. For a single VSMC size, IP_3 may act as a global messenger but the action of Ca^{2+} is limited to restricted domains.

The Young et al. [200] study on the propagation of intracellular calcium in colonic SMCs indicates that a cell may not show a calcium rise even if all the adjacent cells have a significant calcium increase. Clair et al. [30] shows that the diffusion of calcium across gap junctions is negligible in connected hepatocytes, (refer to Figure 5.1). In their experiments, though calcium concentration in one cell was kept at a high value for at least 3 minutes by applying high agonist concentration, no rise in calcium was observed in the other cell. The experiment was able to detect the concentration of calcium at nanomolar levels. The role of the undetected small amount of calcium to generate calcium oscillation in the neighbouring cell was ruled out in their study. Koenigsberger et al. [90] has shown that only electrical coupling between VSMCs produces propagation of intracellular calcium matching with the

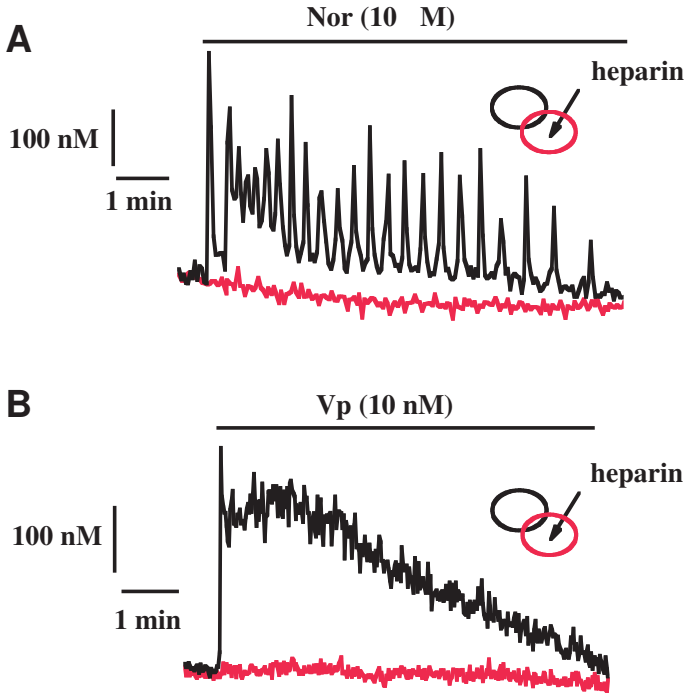

Fig. 5.1 Absence of calcium diffusion between two connected hepatocytes: High concentrations of noradrenaline or vasopressin are used to induce intracellular calcium rise. Heparin was added to one of the cells. Heparin inhibits the binding of IP_3 and IP_3-induced calcium release. The application of agonist produced high intracellular calcium rise in one of the cells. Though the calcium rise was for 3 minutes in one of the cells, calcium diffusion to the other cell was negligible. Reproduced from Clair et al. [30] paper (permission granted from The Company of Biologists Ltd to reuse in the thesis, license number: 3850010553260).

experiments in VSMCs [157]. Therefore, it is reasonable to assume negligible diffusion of calcium across the gap junction based on the above studies.

5.2.1 Modelling equations of GJIC

The passage of chemical species between two VSMCs is influenced by both potential difference and concentration difference. In our model, we have assumed calcium transport between two cells is negligible and assumed constant intracellular concentrations for other cytosolic ions such as Na^+, K^+ and Cl^-. Therefore, ionic flux carried by Na^+, K^+ and Cl^- across gap junctions between two VSMCs depends only on the potential difference. Jacobsen et al. [75] used an additive electrodiffusion to model the GJIC due to the passage of an ion between two cell compartments. This equation is a representation of a Nernst-Plank equation, (refer to Equation 2.1), to model ionic current between two cells. Kapela et al. [85]

used the GHK equation, (refer to Equation 2.2), to model the ionic currents throughout the gap junctions. The reduced form of the equation with our model assumptions, no calcium transport across the gap junctions and constant concentrations for other ions, the is given below,

$$I_{GJ} = -N_{GJ} A_{GJ} \frac{F^2}{RT} \Delta V_m \sum_{ions} P_{ion} z_{ion}^2 [ion] \tag{5.1}$$

Where 'GJ' denotes gap junction, ΔV_m is the membrane potential difference between two VSMCs, A_{GJ} is the cross-sectional area of a gap junctional pore, N_{GJ} is the total number of gap junctions between two VSMCs, P_{ion} is the permeability of the gap junction to an ion and [ion] represents ion concentration in molar (moles/litre). The unit I_{GJ} is coulombs per second (C/s). All the terms except ΔV_m are constants. Therefore, Equation 5.1 is rewritten for ionic current as follows,

$$I_{GJ} = -N_{GJ} g_{GJ} \Delta V_m \tag{5.2}$$

Where g_{GJ} is the unitary conductance of a gap junction. This relation represents an ohmic behaviour for the gap junction. The gap junctional current is directly proportional to the difference in V_m between the adjacent cells, similar to the studies of Koenigsberger et al. [89] and Diep et al. [37].

Like ions, IP_3 is an intercellular messenger which is also allowed to pass through gap junctions. IP_3 is not an ion; therefore, the IP_3 flux across the gap junctions depends only on the concentration difference. Based on Fick's law of diffusion, IP_3 transport, J_{GJ,IP_3}, between two cell compartments is written as,

$$J_{GJ,IP_3} = -N_{GJ} \frac{A_{GJ} P_{IP_3}}{Vol_{cyt}} \Delta [IP_3]_{cyt} \tag{5.3}$$

$$J_{GJ,IP_3} = -N_{GJ} d_{IP_3} \Delta [IP_3]_{cyt} \tag{5.4}$$

Where P_{IP_3} is the permeability of the gap junction to IP_3, Vol_{cyt} is the cytosol volume, and d_{IP_3} is the unitary IP_3 coupling coefficient of a gap junction. The unit of J_{GJ,IP_3} is molar/s. IP_3 transport equation is linearly related to the concentration difference between two cells. A similar kind of coupling equation for IP_3 is used in the studies of Koenigsberger et al. [89] and Kapela et al. [84].

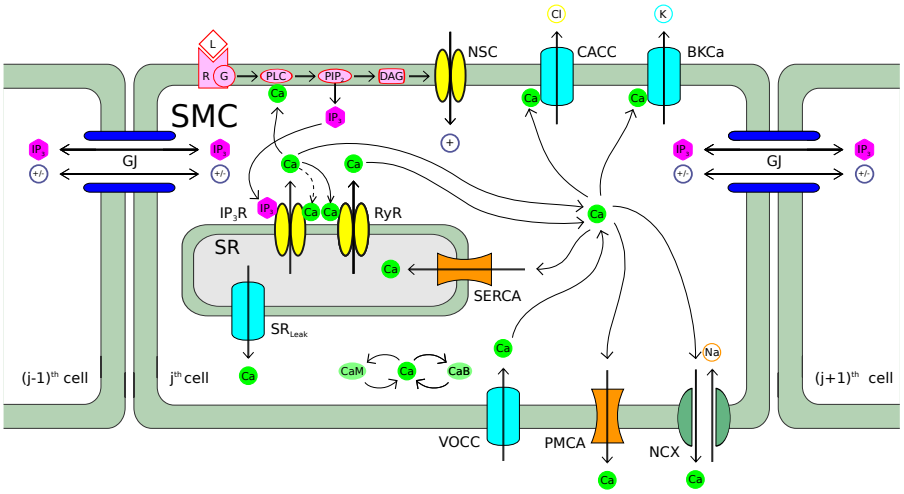

Fig. 5.2 Graphical representation of the coupled VSMC model: IP_3 and V_m are coupled between VSMCs. 'gj' represents gap junction.

In the current model, VSMCs are connected serially to mimic a straight VSMC strip. One VMSC is coupled to two adjacent VSMCs. A schematic representation of the cell coupling is shown in Figure 5.2. Each cell is assumed as a compartment with homogenous cytosol. For the serially coupled VSMCs, Equation 5.2 becomes,

$$I_{GJ} = -G_{GJ}(V_{m,j} - V_{m,j\pm1}) \tag{5.5}$$

$$G_{GJ} = N_{GJ} g_{GJ} \tag{5.6}$$

Where 'j' denotes current cell and G_{GJ} is whole cell conductance between two VSMCs. Similarly for IP_3 flux,

$$J_{GJ,IP_3} = -D_{IP_3}([IP_3]_{cyt,j} - [IP_3]_{cyt,j\pm1}) \tag{5.7}$$

$$D_{IP_3} = N_{GJ} d_{IP_3} \tag{5.8}$$

Where D_{IP_3} is the whole cell IP_3 coupling coefficient between two VSMCs.

Now, we have to find the values of N_{GJ}, g_{GJ} and $d_{[IP_3]}$. In VSMCs, the most abundantly expressed connexin is Cx43 [24, 181, 58, 78]. van Kempen and Jongsma [181] reported the confined and differentiated expression of Cx43 in VSMCs of an aorta and coronary arteries. Based on this, we assume that the gap junction in VSMC is made up of Cx43. The characteristics of Cx43 are then used to model the gap junction between VSMCs.

The unitary conductance of Cx43 is quantified in experiments, and it is approximately 60 pS [125, 179]. Emerson and Segal [42] reported that the whole cell gap junctional conductance between two VSMCs of a hamster feed artery was equal to 178.57 nS. In previous work, the same research group has reported the dominant expression of Cx43 in VSMCs of a hamster feed artery [59]. Based on that, we assume 178.57 nS as the whole cell conductance of gap junctions made up of Cx43. By using 5.6, the average number of gap junctions per VSMC is calculated as follows,

$$\mathrm{N_{GJ}} = \frac{\mathrm{G_{GJ}}}{\mathrm{g_{GJ}}} \approx 1100 \tag{5.9}$$

According to our knowledge, there is no experimental data available in the literature that provides values of $\mathrm{d_{IP_3}}$ and $\mathrm{D_{IP_3}}$. In this model, we have used a value of 2 $\mathrm{s^{-1}}$ as the whole cell $\mathrm{IP_3}$ coupling coefficient, which is close to that suggested in Kapela et al. [85] and Ghanim et al. [51]. The value of $\mathrm{d_{IP_3}}$ is calculated by dividing the value of $\mathrm{D_{IP_3}}$ with the total number of gap junctions, $\mathrm{N_{GJ}}$,

$$\mathrm{d_{IP_3}} = \frac{\mathrm{D_{IP_3}}}{\mathrm{N_{GJ}}} \approx 1.81 \times 10^{-3} s^{-1} \tag{5.10}$$

Weber et al. [187] calculated the permeability of Alexa dye through homotypic gap junction channels of Cx43. According to them, the single channel permeability of homotypic Cx43 gap junction channel equals 0.5×10^{-9} $\mathrm{mm^3/s}$. The corresponding value of $\mathrm{d_{IP_3}}$ is 1.267×10^{-9} $\mathrm{mm^3/s}$, which is not different from the experimental values of permeability of Alexa dye through homotypic Cx43 gap junction. The permeability of Cx43 depends on several physiological parameters and this would be a subject of study in the future.

5.3 Numerical Method

The coupling equations of $\mathrm{V_m}$ and $\mathrm{IP_3}$, 5.7 and 5.5, are added to the corresponding single cell equations, 3.5 and 3.49, respectively. The resultant model equations for coupled VSMCs can be written in a general form, refer to section 3.3 for details, we get,

For $j = 2, 3, ..., \mathrm{N_{SMC}} - 1$

$$\dot{x}_{i,j} = x_{i,j}\left(g_{i,j}\left(x_{1,j}, ..., x_{n,j}\right) - 2\mathrm{D}_i\right) + h_{i,j}\left(x_{1,j}, ..., x_{n,j}\right) + \mathrm{D}_i x_{i,j-1} + \mathrm{D}_i x_{i,j+1} \tag{5.11}$$

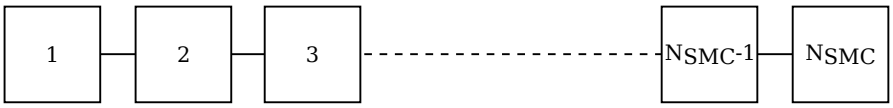

Fig. 5.3 Serially connected VSMCs representing a single straight VSMC strip. N_{SMC} denotes the number of VSMCs coupled.

For $j = 1$

$$\dot{x}_{i,j} = x_{i,j}\left(g_{i,j}\left(x_{1,j},....,x_{n,j}\right) - \mathrm{D}_i\right) + h_{i,j}\left(x_{1,j},....,x_{n,j}\right) + \mathrm{D}_i x_{i,j+1} \tag{5.12}$$

For $j = \mathrm{N_{SMC}}$

$$\dot{x}_{i,j} = x_{i,j}\left(g_{i,j}\left(x_{1,j},....,x_{n,j}\right) - \mathrm{D}_i\right) + h_{i,j}\left(x_{1,j},....,x_{n,j}\right) + \mathrm{D}_i x_{i,j-1} \tag{5.13}$$

Where subscript 'j' denotes cell number and 'i' is used to represent 16 state variables in each coupled VSMCs. $x_{i,j}$ means the i^{th} variable in j^{th} VSMC. N_{SMC} is the total number of VSMCs couped and D is the coupling coefficient of a variable. D_i represents the coupling coefficient of the i^{th} variable between two VSMCs. For variables other than V_m and IP_3, D is equal to zero. For V_m, D equals G_{GJ}/C_m. High resistance is assumed at two ends, which means no flux going out of the cells at the two ends. The backward Euler method is used to discretize the model equations of all state variables. This will give,

For $j = 2,3,....,\mathrm{N_{SMC}} - 1$

$$\begin{aligned} &x_{i,j}(t+\Delta t)\left(1 + 2\Delta t \mathrm{D}_i - \Delta t\ g_{i,j}\left(x_{1,j}(t+\Delta t),....,x_{n,j}(t+\Delta t)\right)\right) - \Delta t \mathrm{D}_i x_{i,j+1} - \Delta t \mathrm{D}_i x_{i,j-1} \\ &= x_{i,j}(t) + \Delta t\ h_{i,j}\left(x_{1,j}(t+\Delta t),....,x_{n,j}(t+\Delta t)\right) \end{aligned} \tag{5.14}$$

For $j = 1$

$$\begin{aligned} &x_{i,j}(t+\Delta t)\left(1 + \Delta t \mathrm{D}_i - \Delta t\ g_{i,j}\left(x_{1,j}(t+\Delta t),....,x_{n,j}(t+\Delta t)\right)\right) - \Delta t \mathrm{D}_i x_{i,j+1} = x_{i,j}(t) \\ &+ \Delta t\ h_{i,j}\left(x_{1,j}(t+\Delta t),....,x_{n,j}(t+\Delta t)\right) \end{aligned} \tag{5.15}$$

For $j = \mathrm{N_{SMC}}$

$$\begin{aligned} &x_{i,j}(t+\Delta t)\left(1 + \Delta t \mathrm{D}_i - \Delta t\ g_{i,j}\left(x_{1,j}(t+\Delta t),....,x_{n,j}(t+\Delta t)\right)\right) - \Delta t \mathrm{D}_i x_{i,j-1} = x_{i,j}(t) \\ &+ \Delta t\ h_{i,j}\left(x_{1,j}(t+\Delta t),....,x_{n,j}(t+\Delta t)\right) \end{aligned} \tag{5.16}$$

A fixed point iteration method whose details are given in Appendix B is used to solve the above equations for coupled cells at a given time step [145, 112]. Functions g and h are calculated explicitly at each iteration using x_i from the previous iteration. The resultant equation of x_i, other than V_m and IP_3, for the iterative procedure is obtained as follows,

$$x_{i,j}^{(k+1)} = \frac{x_{i,j}(t) + \Delta t\ h_{i,j}\left(x_{1,j}^{(k)}, ..., x_{n,j}^{(k)}\right)}{1 - \Delta t\ g_{i,j}\left(x_{1,j}^{(k)}, ..., x_{n,j}^{(k)}\right)} \tag{5.17}$$

Where superscript k represents iteration number. V_m and IP_3 equations for the iterative procedure are as follows,

For $j = 2, 3, ..., N_{SMC} - 1$

$$x_{i,j}^{(k+1)}\left(1 + 2\Delta t D_i - \Delta t\ g_{i,j}\left(x_{1,j}^{(k)}, ..., x_{n,j}^{(k)}\right)\right) - \Delta t D_i x_{i,j+1}^{(k+1)} - \Delta t D_i x_{i,j-1}^{(k+1)} = x_{i,j}(t) + \Delta t\ h_{i,j}\left(x_{1,j}^{(k)}, ..., x_{n,j}^{(k)}\right) \tag{5.18}$$

For $j = 1$

$$x_{i,j}^{(k+1)}\left(1 + \Delta t D_i - \Delta t\ g_{i,j}\left(x_{1,j}^{(k)}, ..., x_{n,j}^{(k)}\right)\right) - \Delta t D_i x_{i,j+1}^{(k+1)} = x_{i,j}(t) + \Delta t\ h_{i,j}\left(x_{1,j}^{(k)}, ..., x_{n,j}^{(k)}\right) \tag{5.19}$$

For $j = N_{SMC}$

$$x_{i,j}^{(k+1)}\left(1 + \Delta t D_i - \Delta t\ g_{i,j}\left(x_{1,j}^{(k)}, ..., x_{n,j}^{(k)}\right)\right) - \Delta t D_i x_{i,j-1}^{(k+1)} = x_{i,j}(t) + \Delta t\ h_{i,j}\left(x_{1,j}^{(k)}, ..., x_{n,j}^{(k)}\right) \tag{5.20}$$

The equations of V_m and IP_3 represent a tridiagonal system of linear equations. V_m and IP_3 are solved using a tridiagonal matrix algorithm (TDMA) integrated iterative method. For each iterative step, a tridiagonal system of equations is solved using TDMA, refer to Appendix B, based on Gaussian elimination [33].

For $k = 1$, we choose $x_{i,j}^k = x_{i,j}(t)$ and a series of approximations $x_{i,j}^k$ $(k = 2, 3, \ldots)$ to $x_{i,j}(t + \Delta t)$ is obtained using the Eqn. 5.17 and solving TDMA (composed of Eqn. 5.18, Eqn. 5.19 and Eqn. 5.20). When the fixed point iterations converge, $x_{i,j}^{k+1}$ is a solution to the discretized equation. In the current model, iteration is continued until all the state variables have converged to an error tolerance limit such that $| x_{i,j}^{(k+1)} - x_{i,j}^k | \leq 10^{-4}$ for all i and j. The time step is fixed at 0.1 ms. We have used the same computer algorithm of single cell

model, (refer to Figure 3.5), to solve coupled cell simulations by incorporating the fixed point iteration method for coupled cells.

Running time and relative error plots for the coupled cell model is shown in Figure 5.4. The relative error is calculated by taking the results from the simulation with a time step of 10^{-7} seconds as the correct solution. Simulation running time increases linearly as the time step decreases. The minimum time step needed for the coupled cell model to get a relative error of $\mathcal{O}(10^{-5})$ is 10^{-4} s. Total simulation running time to solve 150 seconds real time with a time step of 10^{-4} s is approximately 15 seconds.

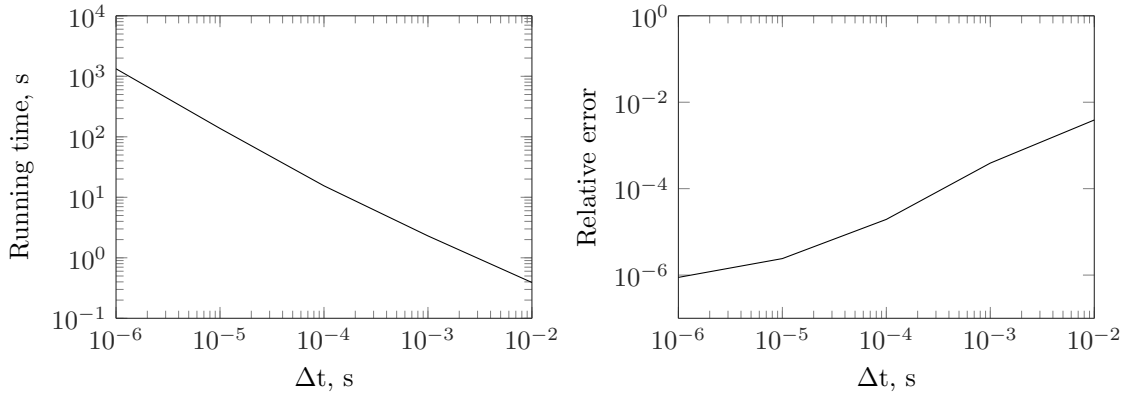

Fig. 5.4 Simulation running time (left) and relative error (right) plots for coupled cell model. The total time required to solve a system of 5 cells for 150 s real time is plotted as running time. The relative error is calculated as the error value compared to the solution with a time step of 10^{-7} s.

5.4 Results

Coupled VSMCs simulations are carried out on a total of 100 VMSCs connected serially. Assuming an VSMC width of 5 μm, 100 VSMCs correspond to a distance of 500 μm that matches with the measurement distance used in the experiment of Emerson and Segal [42]. At the beginning of the simulation, all the VSMCs are in the resting state, meaning zero agonist concentration. As the simulation starts, a sigmoidal distribution of agonist concentration is imposed over the coupled cells as shown in Figure 5.5. This kind of spatial distribution will help us to investigate the propagation of calcium oscillations in both constant and 'linearly varying' agonist concentrations [160]. To study the propagation of calcium oscillations, the agonist concentration is distributed in such a way that some of the cells will experience agonist concentrations greater than lowest bifurcation point, [L] = 237 nM, and the rest of the cells have agonist concentrations smaller than the lowest bifurcation point.

In order to get that, the agonist concentrations at two ends are kept at 400 nM and 100 nM, respectively. With the given distribution of the agonist, the first 51 cells show an oscillatory state if VSMCs are uncoupled. Therefore, the first 51 cells are referred as stimulated cells and next 49 cells as non-stimulated cells.

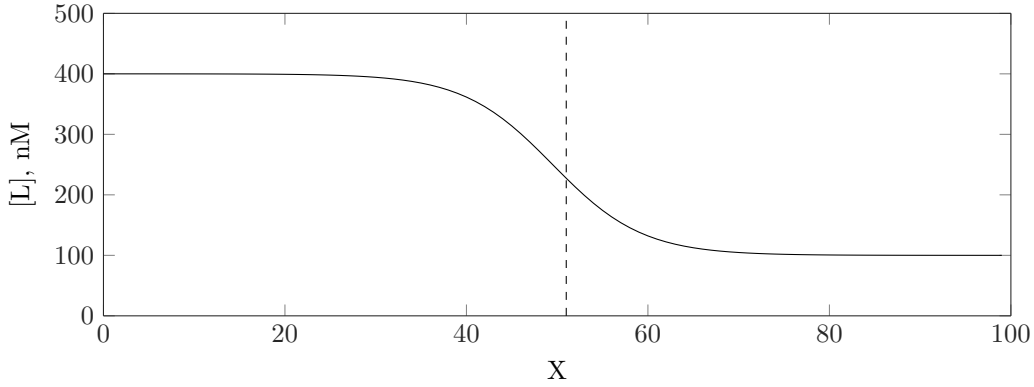

Fig. 5.5 Sigmoidal distribution of agonist (solid) over the 100 VSMCs coupled serially. Dashed line is used to separate stimulated cells and non-stimulated cells. With this spatial distribution of agonist, all the cells (51 cells) on the left side of the dashed line show oscillatory state when uncoupled and rest of the cells are in steady state.

5.4.1 Model response to spatial distribution of agonist: sigmoidal

Figure 5.6 shows contour plots of intracellular calcium, V_m and IP_3 in coupled 100 VSMCs for the first 200 seconds of simulation. Contour plots provide a spatiotemporal profile of the corresponding variable. The maximum and minimum values of the intracellular calcium, intra-SR calcium, V_m and IP_3 in the coupled cells are plotted in Figure 5.7. The maximum and minimum values of oscillations are taken as the average of all the oscillations which happened in the first 500 seconds excluding the first oscillation.

Once VSMCs are coupled, calcium oscillations are seen not only in the first 51 cells but also in all the non-stimulated cells. The calcium oscillations in non-stimulated cells, which are located far from the stimulated cells, are not visible on the scale of the figure 5.6, but are clear in the figure 5.7. Though intracellular calcium oscillations are obtained in all the non-stimulated cells, the amplitude of these oscillations are not equal. If the peak intracellular calcium in the non-stimulated cell is equal or greater than 75% of the peak intracellular calcium of the stimulated cells, it is called a regenerative calcium rise. The propagation of regenerative calcium rise is called regenerative calcium propagation. With the specified agonist distribution, the regenerative calcium propagation ends at the 59^{th} cell, refer to Figure 5.7 (a). The agonist concentration of the 59^{th} cell equals 145 nM. Beyond this

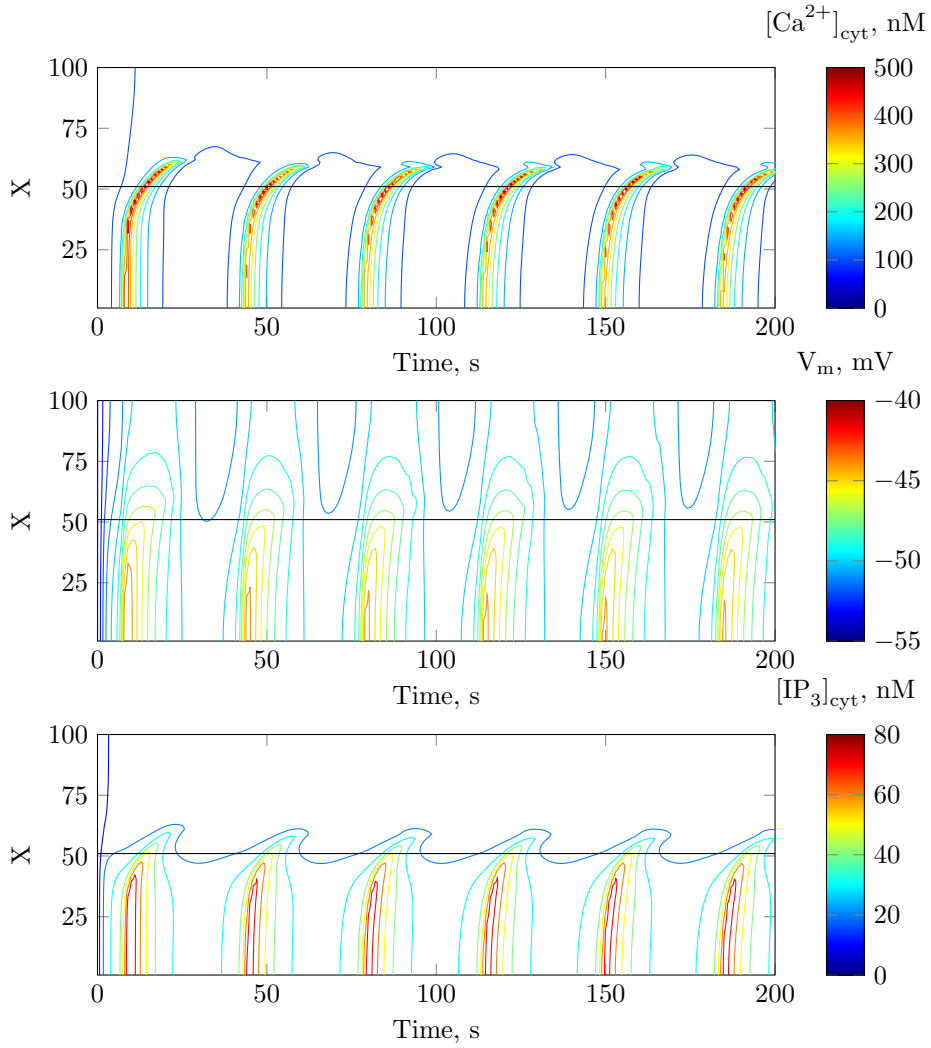

Fig. 5.6 Countour plots of intracellular calcium (top), V_m (middle) and IP_3 (bottom): 100 VMSCs are coupled serially through V_m and IP_3. The black line is used to show the boundary between steady state and oscillatory state in uncoupled VSMCs.

cell, calcium rise due to cell coupling is minimal, and only small amplitude oscillations are seen. The minimum value of calcium oscillation in the cells beyond the 59^{th} cell is equal to the steady state calcium of these cells when uncoupled.

Similar to intracellular calcium, intra-SR calcium, V_m and IP_3 also oscillate in the non-stimulated cells. Maximum and minimum values of intra-SR calcium oscillations in the stimulated cells are unaffected by coupling. Maximum and minimum values of intra-SR calcium oscillations in the cells from the 51^{st} cell up to the 59^{th} cell are matching with that of the stimulated cells, (refer to Figure 5.7 (c)). In all the non-stimulated cells beyond 59^{th}

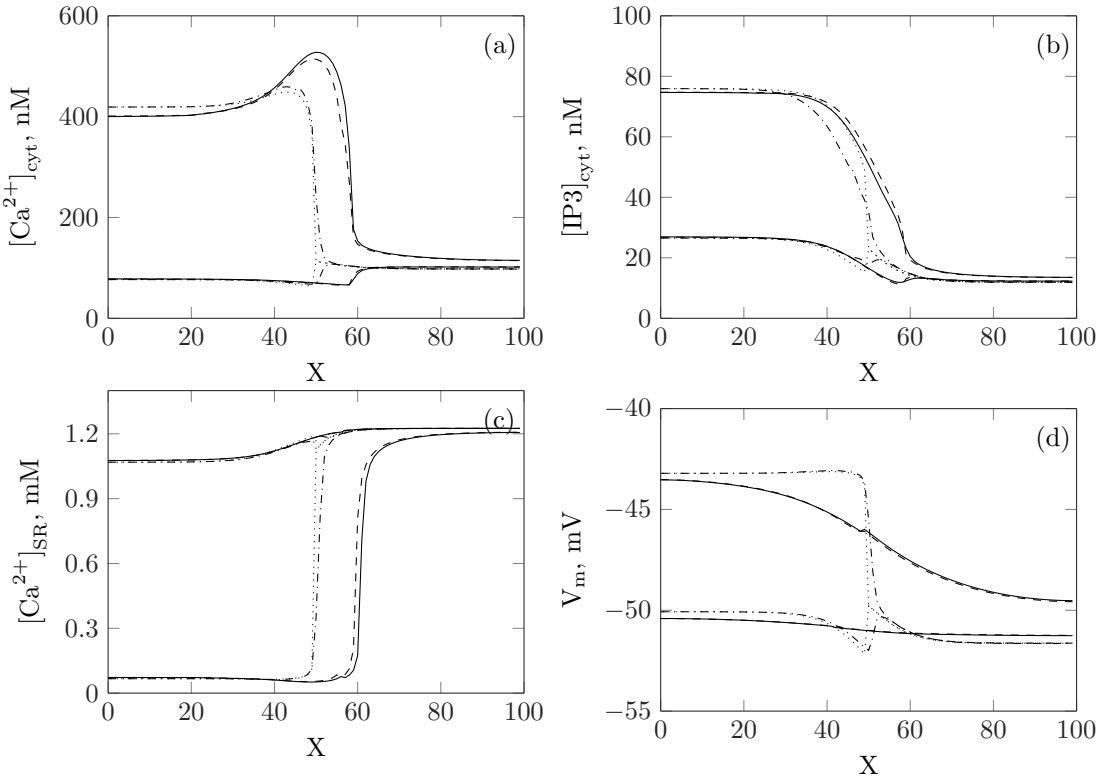

Fig. 5.7 Maximum and minimum plots of intracellular calcium (a), IP_3 (b), intra-SR calcium (c) and V_m (d) of 100 VMSCs coupled with V_m and IP_3 (solid), coupled with V_m alone (dashed), coupled with IP_3 alone (dash-dotted) and uncoupled (dotted).

cell, intra-SR calcium oscillates with a small amplitude and the maximum intra-SR calcium is identical to the steady state intra-SR calcium of the cells when uncoupled.

The peak amplitude of oscillations of V_m and IP_3 are decreasing gradually in the non-stimulated cells. In the case of IP_3, maximum and minimum of calcium oscillation of the first 50 cells are matching with that of the cells when uncoupled. Beyond the 59^{th} cell, the amplitude of IP_3 oscillation is small, and the minimum IP_3 concentration is the same as the steady state IP_3 concentration of the cells when uncoupled.

In the case of V_m, the maximum value of calcium oscillations in the stimulated cells is lowered due to coupling compared to the uncoupled case (Figure 5.7 (d)). In those cells, the minimum value of oscillations is almost unchanged except for some cells close to the 51^{st} cell. However, the peak value of V_m of the non-stimulated cells is increased significantly. In the entire set of cells, maximum membrane potential decreases gradually as the cell position is getting farther from the first cell, whereas the change of minimum membrane potential is nominal. The peak value of V_m oscillations in all the non-stimulated cells beyond the 59^{th} cell is not diminished like intracellular calcium, intra-SR calcium and IP_3. V_m oscillates with

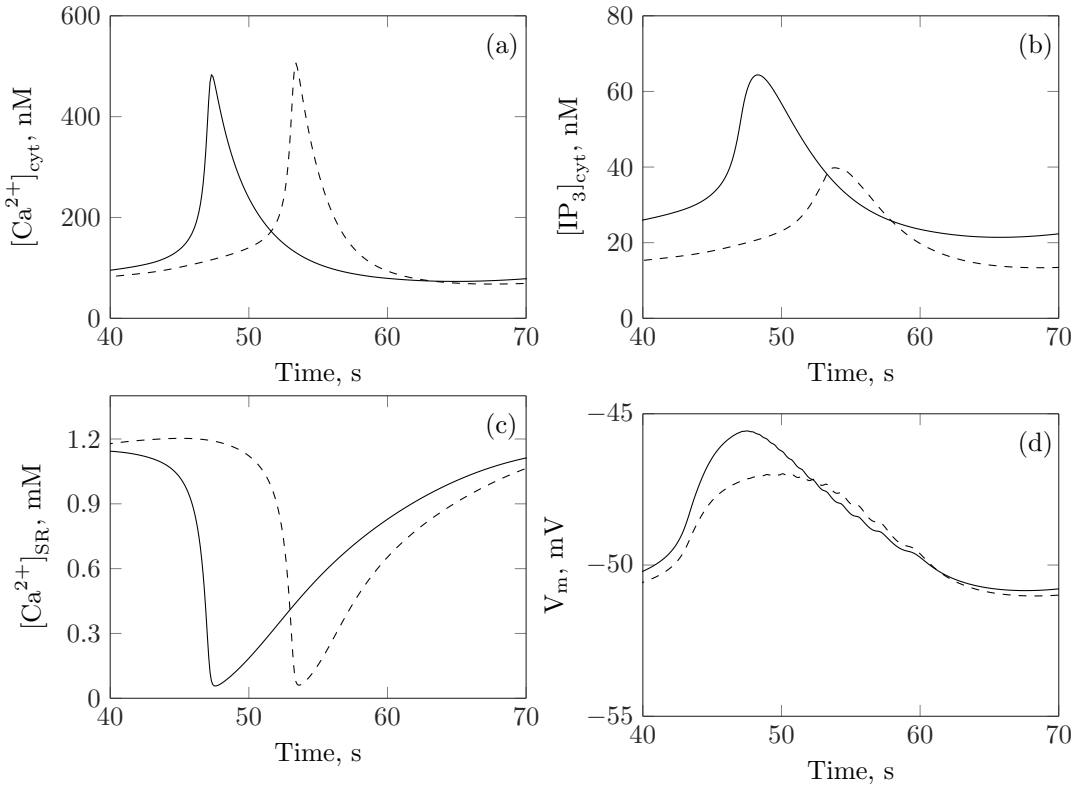

Fig. 5.8 Time series plots of intracellular calcium (a), IP_3 (b), intra-SR calcium (c) and V_m (d) for the 45th cell (solid), and the 55th cell (dashed) in 100 coupled VMSCs.

a considerable amplitude in the cells from the 60th cell up to the 100th cell. The intracellular calcium, intra-SR calcium and IP_3 experience more than 90% reduction in amplitude whereas the V_m amplitude reduction is less than 65%.

Time series plots of intracellular calcium, IP_3, intra-SR calcium and V_m for a stimulated cell (45th cell), and for a non-stimulated cell (55th cell) are shown in Figure 5.8. The time at which the intracellular calcium peak is obtained in the stimulated cell is matching with the time at which the intra-SR calcium attains its minimum, and IP_3 and V_m attain their maxima. For the non-stimulated cell, intracellular calcium peak, IP_3 peak and intra-SR calcium minimum are reached at the same time. However the peaks of V_m happen before the peaks of intracellular calcium.

The net calcium current from the SR and the VOCC of the 55th cell and the 70th cell are given in Figure 5.9. The 55th cell and the 70th cell are selected to compare net SR calcium and VOCC currents in regenerative and small amplitude intracellular calcium oscillations respectively. The net SR calcium current of the 55th cell during the period of intracellular calcium rise is much higher than the VOCC current. The major calcium influx to cytosol for regenerative calcium rise is therefore contributed by the SR. Regarding the 70th cell,

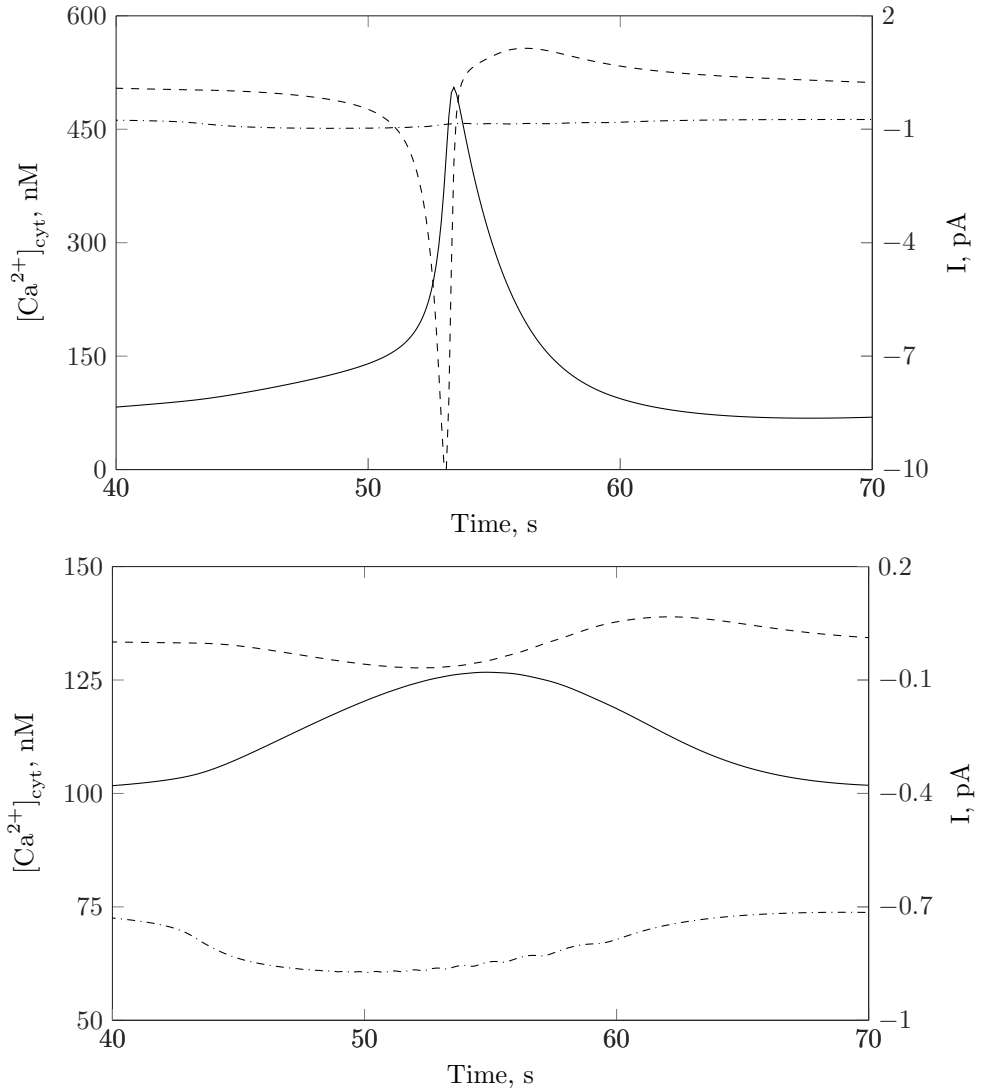

Fig. 5.9 Time series plots of intracellular calcium (solid), net SR current (dashed) and VOCC current (dashdotted) are plotted for the 55th cell (top) and the 70th cell (bottom).

the intracellular calcium rise is mainly supplied by the VOCC. However, the intracellular calcium rise in the 70th is relatively small compared to the regenerative calcium rise in the 55th cell, (refer to Figure 5.7).

The time lag of the calcium oscillations with respect to the oscillation of the first cell is shown in Figure 5.10. The time lag increases gradually with respect to the cell position from the first cell until the regenerative calcium rise ends, up to the 59th cell. The time lag sharply decreases beyond the 59th cell and slowly reaches a constant value. Frequency of calcium oscillations are almost equal for all the cells coupled. The frequency of intracellular calcium oscillations is taken as the average of all the oscillations which happened in the first 500

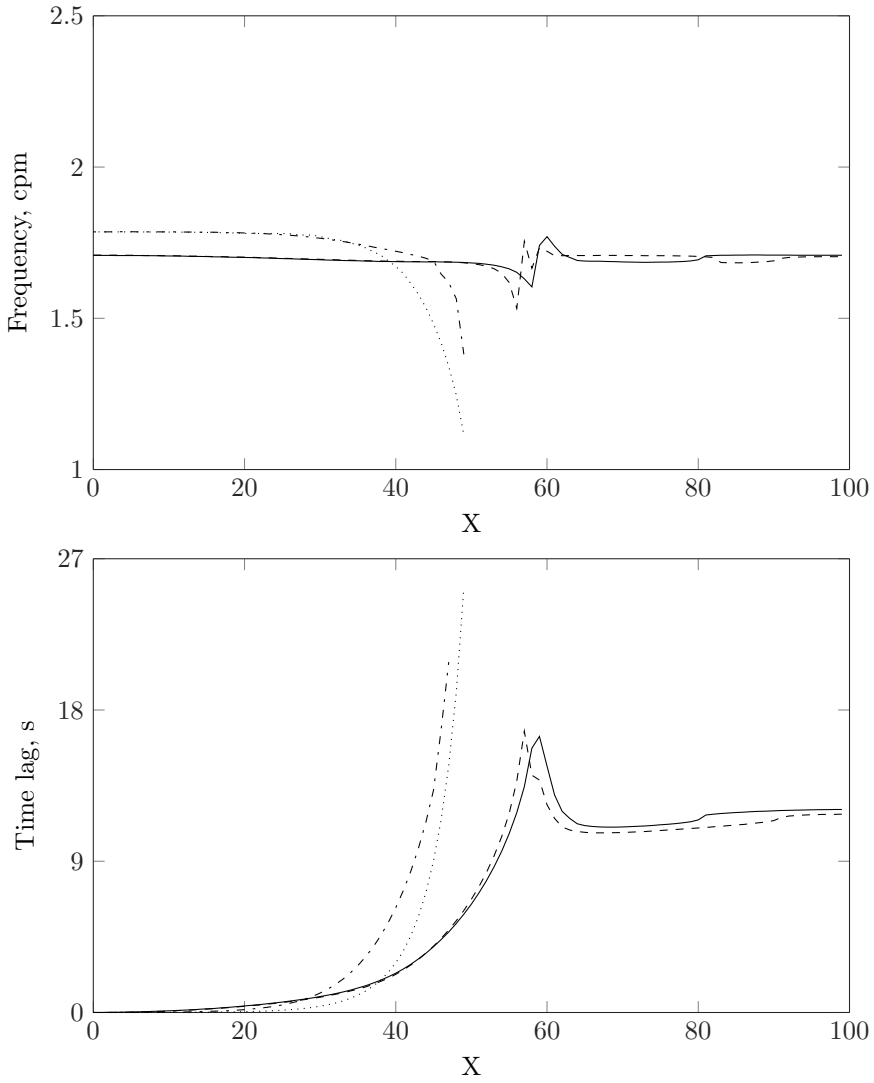

Fig. 5.10 Frequency (top) and Time lag (bottom) plots of intracellular calcium oscillations in 100 VMSCs coupled with both V_m and IP_3 (solid), coupled with V_m alone (dashed), coupled with the IP_3 alone (dash-dotted) and uncoupled (dotted). cpm means cycles per minute. Time lag is calculated by subtracting time at which intracellular calcium peak is obtained in a cell with the time at which intracellular calcium is obtained in the first cell.

seconds excluding the first oscillation. The frequency of coupled cells calcium oscillation is smaller than the frequency of first 40 cells when uncoupled. These cells have the highest agonist concentration in the system.

The characteristics of propagation of intracellular calcium in all the coupled cells are unchanged when only V_m coupling is used, (refer to Figures 5.7 and 5.11). Maximum and minimum values of intracellular calcium, intra-SR calcium, IP_3, and V_m oscillations are unaffected when IP_3 coupling between the cells is switched off. Also, the frequency and the

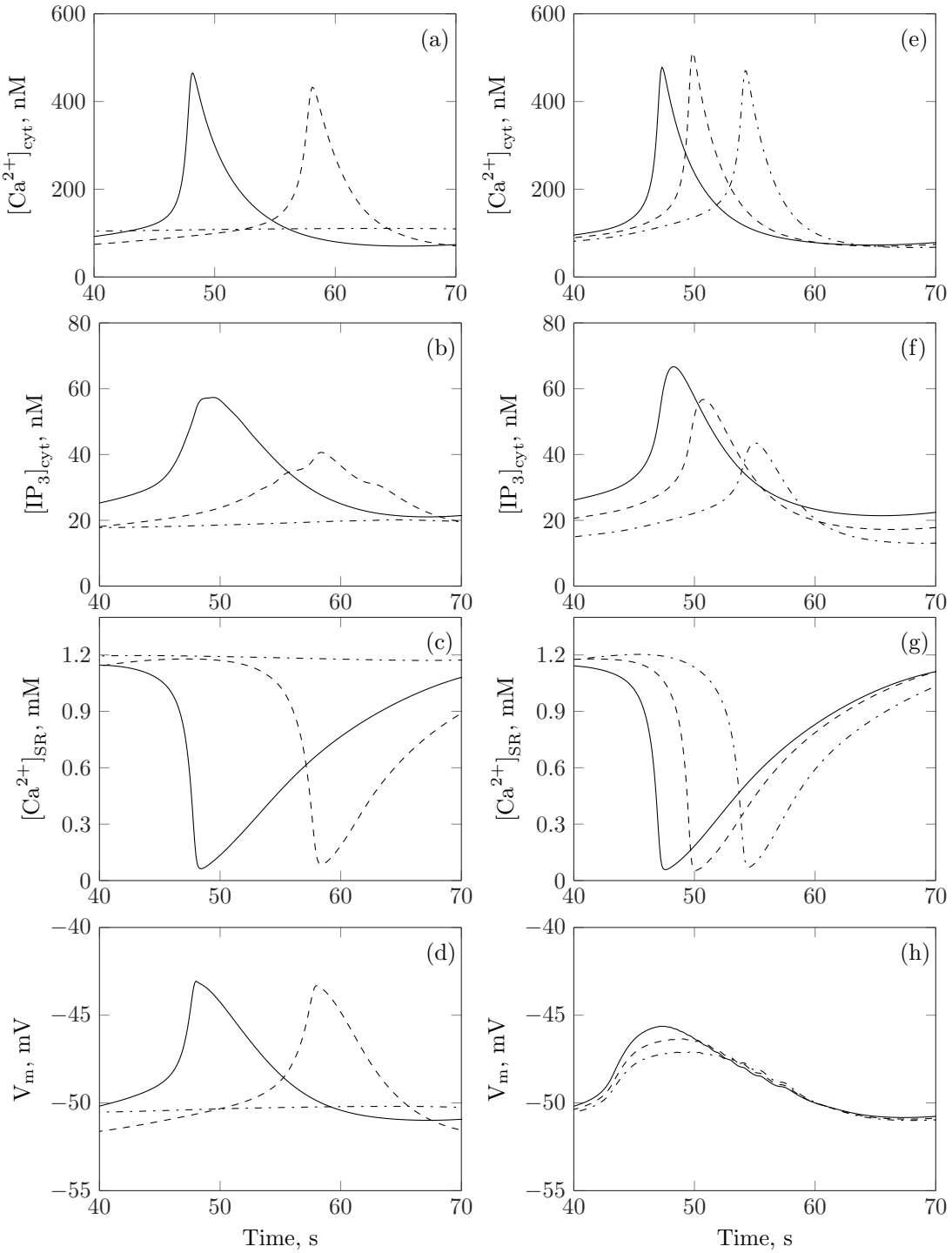

Fig. 5.11 Time series plots of intracellular calcium (a,e), IP_3 (b,f), intra-SR calcium (c,g) and V_m (d,h) for the 45^{th} (solid), 50^{th} (dashed) and 55^{th} (dash-dotted) cell in VMSCs with only IP_3 coupled (a-d) and with only V_m coupled (e-h).

time lag of intracellular calcium oscillations with V_m coupling alone are matching well with the simulation results when both V_m and IP_3 are coupled.

With the given sigmoidal distribution of agonist, IP_3 coupling alone is not enough to propagate regenerative intracellular oscillations, (refer to Figure 5.7). The small amplitude calcium oscillations disappeared when V_m coupling is blocked. The level of state variables in the coupled cells with IP_3 coupling alone matches with single cell simulations. The time lag of oscillations in the stimulated cells increases significantly in those cells which are located close to the 51^{st} cell, mostly cells numbered 30 to 50, (refer to Figure 5.10). The frequency of intracellular calcium oscillations in the first 30 cells matches closely with when these cells are uncoupled. In other cells, the frequency of oscillations is higher compared to the uncoupled cells.

Figure 5.11 shows the time series of intracellular calcium, IP_3, intra-SR calcium and V_m for two coupling cases, one with only IP_3 coupling and the another with only V_m coupling. The time series are taken from the 45^{th} cell, 50^{th} cell and 55^{th} cell. The regenerative intracellular calcium oscillations are aligned with the oscillations of IP_3 and intra-SR calcium. When IP_3 alone is coupled, the peak of V_m is obtained at the same time as the intracellular calcium peak. This is not happening when cells are coupled with V_m alone and coupled with both V_m and IP_3. In all three different coupling cases, intracellular calcium rising is associated with a corresponding decrease of intra-SR calcium, (refer to Figures 5.11 and 5.8).

5.4.2 Absence of IP_3R and RyR

Coupled cell model responses in the absence of IP_3R and RyR are shown in Figure 5.12. It is clear from the single VSMC simulation results that, (see Figures 4.4 and 4.6), bifurcation points change in the absence of IP_3R or RyR. For the same distribution of agonist concentration, the first 42 cells show intracellular calcium oscillations when uncoupled in the absence of RyR. When the cells are coupled, five cells exhibit regenerative calcium propagation. The regenerative calcium rise is limited to 4 cells when IP_3 alone is coupled. The intra-SR calcium concentration of these cells is declined analogous to their intracellular calcium rise.

With the given sigmoidal distribution, none of the cells are in the oscillatory state in the absence of IP_3R, coupled or uncoupled. To have calcuim oscillations in the absence of IP_3R, the agonist concentration should be greater than 500 nM (see Figure 4.4). Based on this fact, agonist concentrations of the cells at two boundaries are increased to 650 nM and 250 nM respectively. Using these boundary conditions, a new sigmoidal distribution of agonist is imposed on the coupled cells in the absence of IP_3R, (refer to Figure 5.13).

With the new distribution of agonist concentration shown in Figure 5.13, the first 46 cells oscillates in the absence of IP_3R when uncoupled. The regenerative propagation

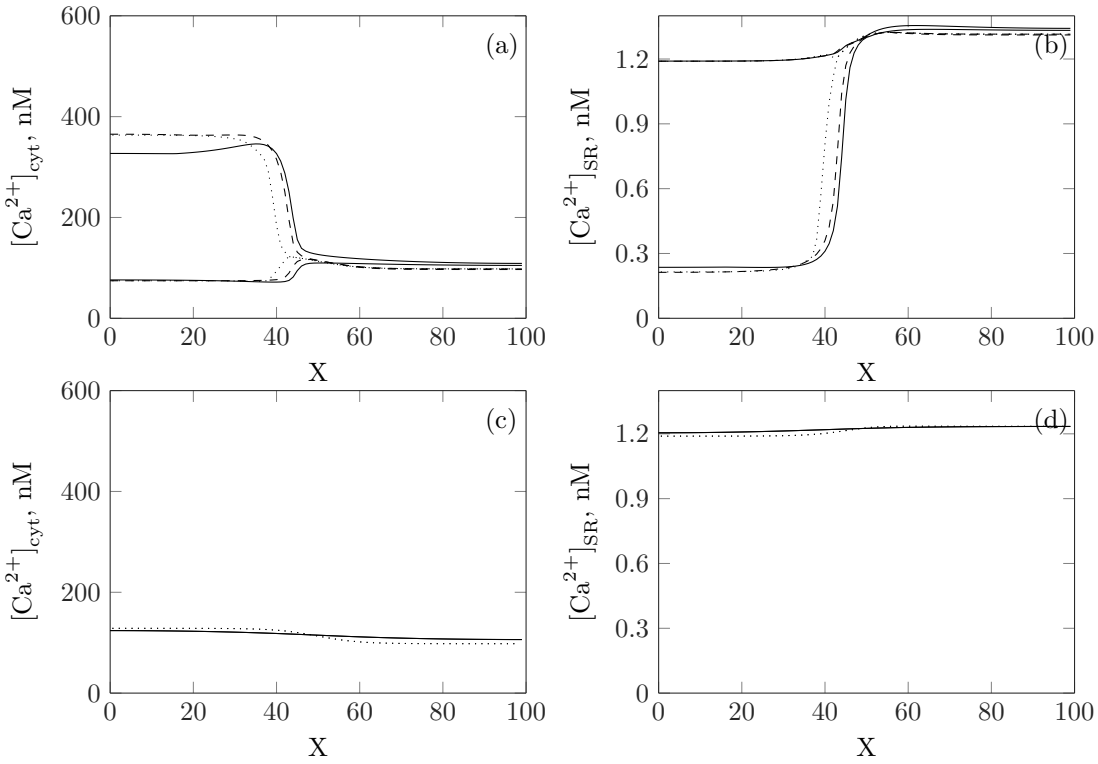

Fig. 5.12 Maximum and minimum plots of intracellular calcium (a,c) and intra-SR calcium (b,d) of 100 VMSCs coupled in the absence of RyR (a,b) and in the absence of IP_3R (c,d) with a sigmoidal distribution of agonist concentration given in the figure 5.5. Both V_m and IP_3 coupled (solid), IP_3 alone coupled (dashed) and uncoupled (dotted).

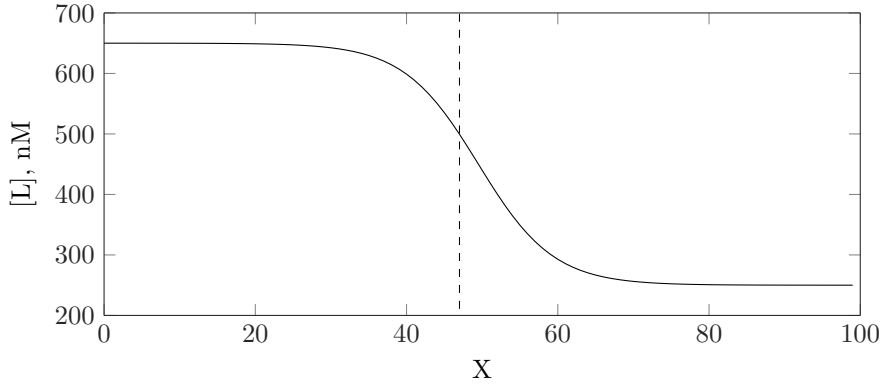

Fig. 5.13 Sigmoidal distribution of agonist (solid) over the 100 VSMCs coupled for the set of simulations with absence of IP_3R. The dashed line is used to show the number of cells in oscillatory state when uncoupled.

of intracellular calcium oscillations are obtained in 23 cells (Figure 5.14). Analogous to intracellular calcium increase observed in regenerative calcium oscillations, intra-SR calcium

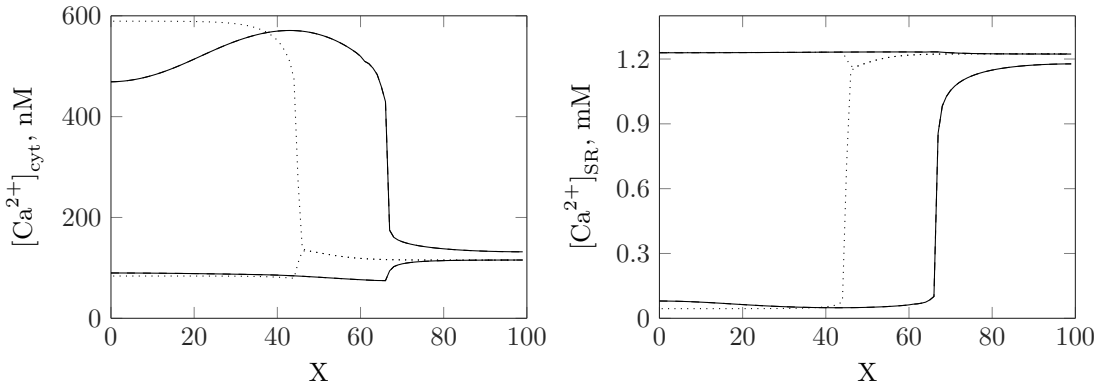

Fig. 5.14 Maximum and minimum plots of intracellular calcium (left) and intra-SR calcium (right) of 100 VMSCs coupled in the absence of IP_3R with a sigmoidal distribution of agonist given in Figure 5.13. Coupled (solid) and uncoupled (dotted).

decreases. The range of intra-SR calcium reduction in the regenerative oscillations looks similar to that in the stimulated cells.

5.5 Discussions

Regenerative intracellular calcium propagation

The regenerative intracellular calcium propagation is observed in experimental studies of Young et al. [200] and Seppey et al. [157]. In the Young et al. [200] study, intracellular calcium oscillations were seen in all the cells of the visual field and over a distance up to 180 μm away from the stimulated cell. It is also evident from the Seppey et al. [157] study that the propagation of calcium rise can be regenerative, (see Figure 5.15). In their study, the regenerative calcium oscillations are stopped after a certain distance away from the stimulated region. Similar to these studies, model results establish the fact that intracellular calcium propagation could be regenerative, but the regenerative nature of propagation is not attainable in all the coupled cells, only some cells next to the stimulated cells.

Presence of large amplitude and small amplitude calcium oscillations

In all the different simulations, regenerative (large amplitude) intracellular calcium rise is strongly related to the declination of intra-SR calcium. This is evident from the matching time series plots of intracellular and intra-SR calcium, (refer to Figures 5.11 and 5.8). In addition to that, the dominant calcium flux to the cytosol during regenerative calcium rise is

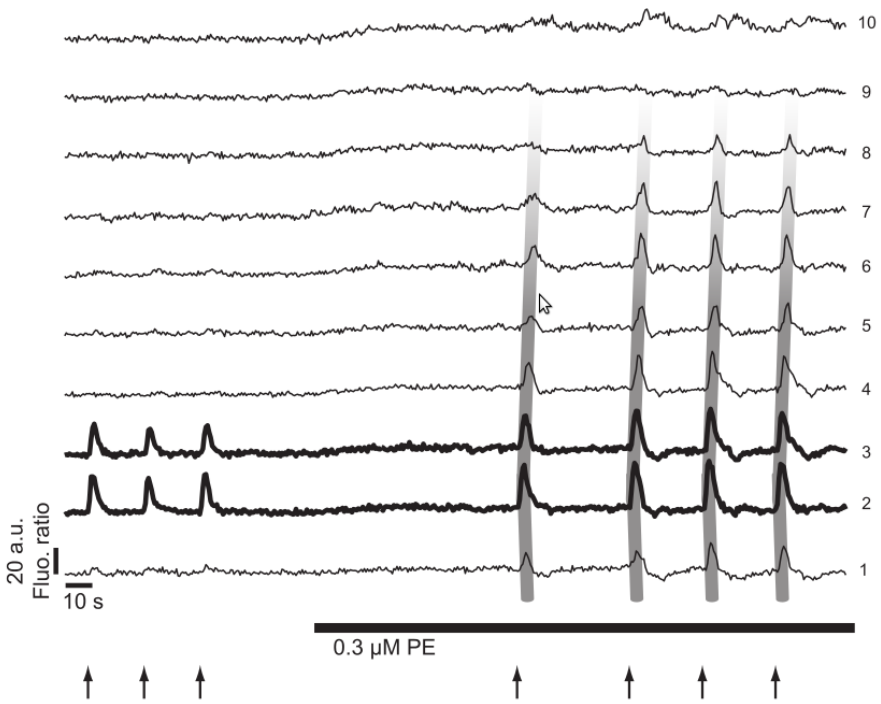

Fig. 5.15 Regenerative intracellular calcium rise in mesenteric arterial strip of VSMCs. Reproduced from Seppey et al. [157] paper (Permission is not required to reuse in a thesis/dissertation).

contributed by the SR, (refer to Figure 5.9). So, the regenerative or large amplitude calcium rise is the result of calcium release from the SR through IP_3R and RyR.

Small amplitude oscillations are obtained in the cells far from the stimulated cells. The small amplitude calcium oscillations are seen when V_m alone is coupled and not seen with only IP_3 coupling. The amplitude of membrane potential oscillations in the far cells are not significantly reduced as the amplitude of IP_3 oscillations and intra-SR calcium oscillations are reduced. It is evident from Figure 5.9 that the VOCC is the major contributor of the calcium flux into the cytosol in the cells far from the stimulated cells. These finding imply that small amplitude intracellular calcium oscillations are the result of electrical coupling and the calcium rise in the far cells are primarily coming from extracellular calcium through the VOCC.

As a whole, there are large amplitude and small amplitude calcium oscillations in the coupled VSMCs. The large amplitude oscillations are obtained in the cells nearby to the stimulated cells. The calcium release from the SR is the main contributor of large amplitude calcium oscillations. Small amplitude oscillations occur in the distant cells, and calcium release through the VOCC is the primary source of small amplitude oscillations. Halidi

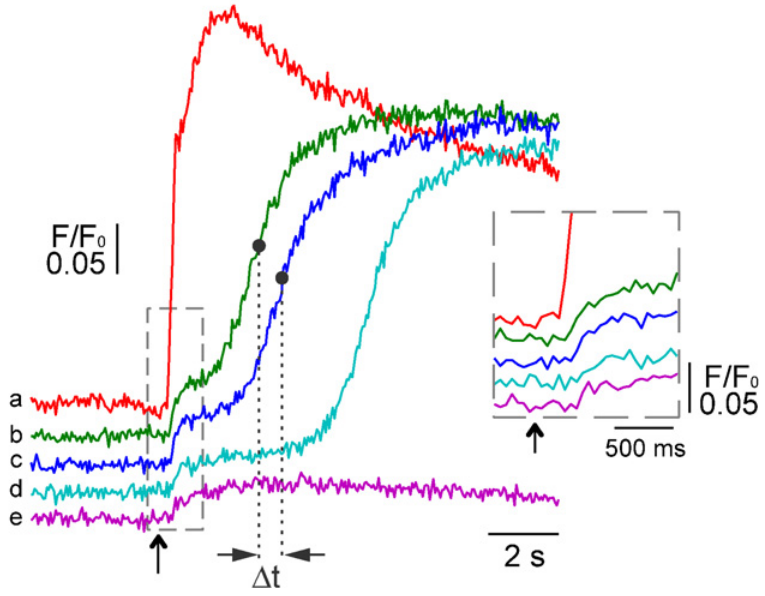

Fig. 5.16 Large and small amplitude intracellular calcium waves in mesenteric SMCs. Points 'a' and 'b' represents two points in the stimulated cell, points 'c' and 'd' from the adjacent cell to the stimulated cell and point 'e' from the 5th cell next to the stimulated cell. Reproduced from Halidi et al. [60] paper (permission granted from Elsevier to reuse in the thesis, license number: 3855101478578).

et al. [60] observed large amplitude and small amplitude oscillations in the experiments of cultured VSMCs from the mesenteric artery, (refer to Figure 5.16). According to them, large amplitude oscillations were spatially limited, and small amplitude oscillations were seen in all the cells of the field of view. The model results are in good agreement with the study of Halidi et al. [60].

In the absence of IP_3R or RyR

Young et al. [200] and Halidi et al. [60] reported that inhibition of RyR has no effect on the propagation of calcium in coupled VSMCs. Likewise, regenerative propagation of intracellular calcium is unaffected by the blocking of RyR in the model results. Further, the regenerative intracellular calcium oscillations are possible with V_m alone coupling and with IP_3 alone coupling in the absence of RyR. In both cases, the rise of calcium is analogous to the reduction of intra-SR calcium. In the absence of RyR, IP_3R needs to be activated to produce regenerative calcium oscillations as the SR is the major calcium contributor. This leads to the fact that V_m and IP_3 -mediated separate intercellular signalling mechanisms are possible in the absence of RyR to produce regenerative calcium rise.

According to Halidi et al. [60], no regenerative calcium propagation was seen when IP_3R was blocked. There was no calcium rise even in the stimulated cell in their study. Halidi et al. [60] used the same stimulation strength in the absence and the presence of IP_3R. In agreement to this, none of the coupled cells exhibit intracellular calcium oscillations when the same spatial distribution of agonist concentration is used in our model, (refer to Figure 5.12). The single cell model results show that higher stimulating strength is required to produce calcium oscillation in the absence of IP_3R. This was the reason for not getting calcium rise in the absence of IP_3R. By increasing the range of agonist concentration applied over the cells, the regenerative propagation is possible in the absence of IP_3R, (refer to Figure 5.14). In the absence of IP_3R, the dominant contributor to calcium rise is the RyR channel. Since IP_3 has no role in propagation in the absence of IP_3R, one could say that V_m coupling alone can mediate an intercellular signalling mechanism to generate regenerative calcium propagation by activating RyR.

V_m-mediated intercellular signalling mechanism

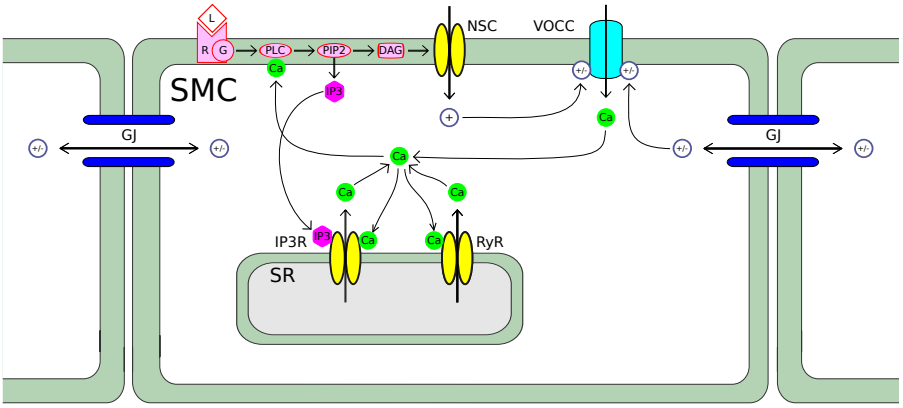

Fig. 5.17 V_m-mediated intercellular signalling mechanism in coupled VSMCs.

V_m mediated intercellular signalling mechanism in our coupled VSMCs model is depicted in Figure 5.17. When V_m is coupled, electrical coupling between a stimulated cell and a non-stimulated cell causes depolarization of the non-stimulated cell, which leads to an initial calcium rise through the activation of the VOCC. The calcium increase enhances PLC activation, which leads to the increased production of IP_3 and DAG. DAG depolarizes the cell further by opening the NSC channel, which leads to increased activation of the VOCC. This positive feedback mechanism between PLC-NSC-VOCC enables the mutual rise of

intracellular calcium and IP_3. The increased concentrations of calcium and IP_3 activate IICR and CICR mechanisms by enhancing the opening of IP_3R and RyRs. The activation of IICR and CICR produce regenerative calcium rise in the cell. In agreement to this, Koenigsberger et al. [90] reported that sufficient amount of calcium influx should enter through VOCC to activate CICR and to induce a regenerative calcium rise.

IP_3-mdiated intercellular signalling mechanism

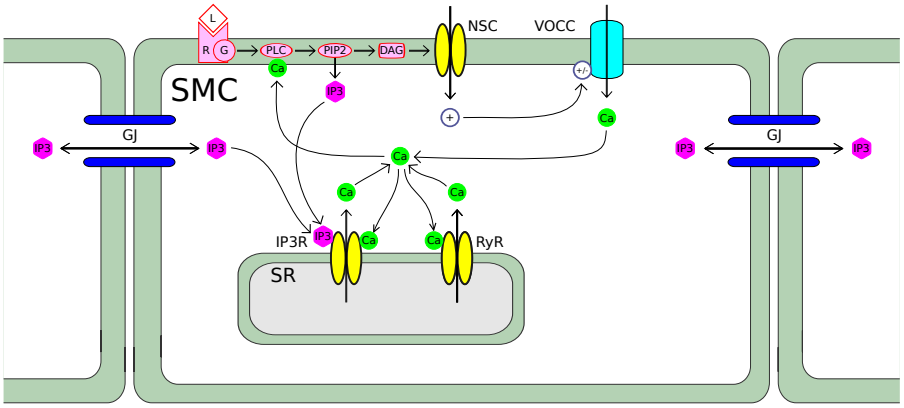

Fig. 5.18 IP_3-mediated intercellular signalling mechanism in coupled VSMCs.

Figure 5.18 shows IP_3 mediated intercellular signalling in the coupled VSMCs. If the IP_3 coupling between two cells attains a sufficiently high IP_3 concentration in the non-stimulated cell to activate the IP_3R channel, that may lead to an initial calcium rise. The increase in calcium boosts the activation of PLC which produces more IP_3 and DAG and initiates the positive feedback mechanism between PLC-NSC-VOCC. The simultaneous rise of calcium and IP_3 activates IICR and CICR mechanisms to generate regenerative calcium rise.

Dominant role of V_m coupling

The main difference between IP_3-mediated and V_m-mediated intercellular signalling mechanisms is the calcium amplification mechanism that initiates the calcium rise. In the IP_3-mediated calcium signalling mechanism, IP_3R should be activated to get an initial calcium rise. The opening of IP_3R depends on sequential binding of IP_3 and calcium. The IP_3R channel needs to be activated for the initiation of IP_3 -mediated signalling mechanism. The IP_3R is activated only if both IP_3 and calcium are bound to its respective activation sites.

Also, in the absence of IP_3 bound to its activation site, calcium can not bind to its respective activating site. This means that sufficiently high calcium and IP_3 concentrations should be present in the system to activate the IP_3R channel. Since the calcium concentration in the non-stimulated cell is low, the open probability of IP_3 would be limited to low values, (refer to Figure 3.3). Therefore, the increased IP_3 concentration due to coupling alone would not be enough to activate IP_3R. This limitation makes IP_3 mediated calcium signalling mechanisms less effective in the coupled VSMCs.

In the case of V_m-mediated regenerative calcium rise, the VOCC is responsible for the initial calcium increase. The opening of the VOCC depends only on V_m. If the electrical coupling depolarizes the non-stimulated cell, the open probability of the VOCC increases and there would be a calcium rise in the cell. There are no other prerequisites for the activation of the VOCC. The dominant role of the V_m-mediated intercellular signalling mechanism is the primary reason for getting unchanged coupled cells responses in the absence of IP_3 coupling, (refer to Figure 5.7). Koenigsberger et al. [90] showed that the V_m coupling alone reproduces the characteristics of propagation of intracellular calcium, which are observed in the experiments. In addition to this, our study illustrates the reason for the dominant role of V_m coupling.

The activation of IICR and CICR mechanisms is essential for the regenerative calcium rise. IP_3 and calcium are the two regulators of IICR and CICR mechanisms. To generate regenerative calcium rise in a non-stimulated cell, there should be an initial rise of IP_3 and/or calcium in the cytosol to a level enough for the activation of IICR and CICR mechanisms. V_m-mediated and IP_3-mediated intercellular signalling mechanisms are responsible for the initial calcium rise. For the given coupled VSMC system, V_m-mediated signalling mechanism plays a dominant role in the propagation of regenerative calcium.

5.6 Conclusions

We have extended our single cell VSMC model to coupled VSMCs model by adding appropriate model equations for the GJIC between VSMCs. A numerical method was developed to solve the coupled cell simulations by incorporating the numerical method of single cell and TDMA. The accuracy of the numerical method was checked with the relative error analysis. We have investigated the propagation of intracellular calcium in 100 serially coupled cells with a sigmoidal distribution of agonist. The simulations were carried out by coupling both V_m and IP_3, V_m alone and IP_3 alone to know the importance of V_m and IP_3 -mediated intercellular signalling mechanisms. The simulations were performed in the presence and absence of IP_3R and RyR.

In agreement to the experimental studies, the model results establish the fact that intracellular calcium propagation could be regenerative and the regenerative calcium propagation is not attainable in all the coupled cells but up to some cells next to the stimulated cells. The calcium release from SR is the main contributor of calcium rise in the large amplitude or the regenerative calcium oscillations. The small amplitude calcium oscillations occur in the distant cells and the calcium release through VOCC is the primary source of calcium rise in these oscillations.

The activation of IICR and CICR mechanisms is essential for the regenerative calcium rise. IP_3 and calcium are the two regulators of IICR and CICR mechanisms. To generate regenerative calcium rise in a non-stimulated cell, there should be an initial rise of IP_3 and/or calcium in the cytosol to a level enough for the activation of IICR and CICR mechanisms.

V_m and IP_3 -mediated intercellular mechanisms for the propagation of intracellular calcium were detailed. The V_m and IP_3 -mediated mechanisms could separately generate regenerative calcium propagation in coupled VSMCs. However, Vm-mediated signalling mechanism plays a dominant role. The calcium and IP_3 should bind to its respective activation site on the IP_3R. This limiting factor plays the major role to suppress the IP_3-mediated regenerative calcium propagation.

For a fixed agonist distribution, the regenerative propagation depends on the GJIC, and therefore the number of gap junctions. If the number of gap junctions and the agonist concentration are fixed in each coupled cell, then the regenerative calcium rise may depend on the activation of IICR and CICR mechanisms. The influence of these parameters on the regenerative calcium propagation will be discussed in the next chapter.

Chapter 6

The effects of altered levels of SERCA, IP_3R, RyR and GJIC: Coupled VSMCs

6.1 Introduction

The GJIC, SERCA, IP_3R and RyR levels are altered in diabetic VSMCs [154, 146, 161, 25, 71]. GJIC controls the intracellular calcium dynamics of a cell in coupled VSMCs. Gap junctional communication depends on the number of gap junctions, N_{GJ}, present in the VSMCs and the permeability of the connexins present at the gap junctions. There is a scarcity of studies to confirm the selective permeability of different connexins to cytoplasmic chemical species. Therefore, we define no selective permeability to gap junctions. However, this can be a subject of study in future. As the number of gap junctions change, both G_{GJ} and D_{IP_3} change accordingly, see Equations 5.6 and 5.8. This would alter the GJC between VSMCs.

In chapter 4, we have seen that the altered levels of SERCA, IP_3R and RyR would define the intracellular calcium state of VSMC. The altered levels of these proteins may influence the propagation of intracellular calcium oscillations. None of the studies has reported in the literature that deals with the importance of SERCA, IP_3R and RyR on the propagation of intracellular calcium. In order to fully understand the impaired vascular function in diabetic VSMCs, the roles of altered levels of SERCA, IP_3R and RyR on the propagation of intracellular calcium need to be investigated as well.

We have based the coupled cell model discussed in the chapter 5 to study the effects of altered levels of GJC, SERCA, IP_3R and RyR on the propagation of intracellular calcium. The number of coupled cells are fixed to 100 and a sigmoidal distrubtion of agonist, (refer to the figure 5.5) is imposed on the cells. The number of gap junctions between the cells is

altered and the resultant propagation of intracellular calcium dynamics is studied. We have analysed the influences of N_{GJ} on the penetration depth and wave velocity of regenerative calcium propagation. The variation of penetration depth against the varying levels of SERCA, IP_3R, and RyR is also investigated. The model results are discussed in general and on the basis of diabetes at the end of the chapter.

6.2 Results

6.2.1 Altered levels of gap junctions

100 VSMCs are connected serially, and a sigmoidal distribution of agonist is imposed over the cells as shown in Figure 5.5. The number of gap junctions, N_{GJ}, is varied to get increased coupling strengths for both V_m and IP_3. For the control case, N_{GJ} equals 1100 (refer to Equation 5.9). The level of GJIC is represented as the percentage change in the number of gap junctions compared to the control case.

At the beginning of the simulation, all the cells are in resting state. The spatial distribution of agonist and the specified N_{GJ} are imposed over the coupled cells from the first time step onwards. Contour plots of intracellular calcium for 20% N_{GJ}, 100% N_{GJ} and 1000% N_{GJ} are given in Figure 6.1. These plots show the spatiotemporal pattern of intracellular calcium for the first 150 seconds. The spatiotemporal pattern of intracellular calcium looks like the sigmoidal distribution of agonist as shown in Figure 5.5. In other words, the pattern is closely matching with the spatial distribution of agonist at high N_{GJ}.

Figure 6.2 shows the variation of penetration depth as N_{GJ} changes. The penetration depth, (δ_{RP}), is defined as the number of cells that show regenerative calcium rise. As the N_{GJ} increases, the penetration depth increases. With 20% N_{GJ}, regenerative propagation is seen only in five cells. When N_{GJ} is increased to 600%, regenerative propagation is extended to all the cells. For the cases with 100% N_{GJ} and 500% N_{GJ}, the 52^{nd} cell to 59^{th} cell (8 cells) and the 52^{nd} cell to 81^{th} cell (30 cells) show regenerative propagation, (see Figures 6.2 and 6.1).

The slope of the penetration depth curve is smaller for N_{GJ} less than 400%. Regenerative calcium propagation extends up to the 75^{th} cell for 400% N_{GJ}. This indicates that change in penetration depth is slow until the regenerative calcium propagation reaches the 72^{rd} cell (21 cells). For N_{GJ} greater than 400%, the regenerative calcium rise propagates at a faster rate as the N_{GJ} increases.

The agonist concentration at which regenerative propagation stops is also given in Figure 6.2. With 20% N_{GJ}, regenerative propagation stops at an agonist concentration of 174 nM.

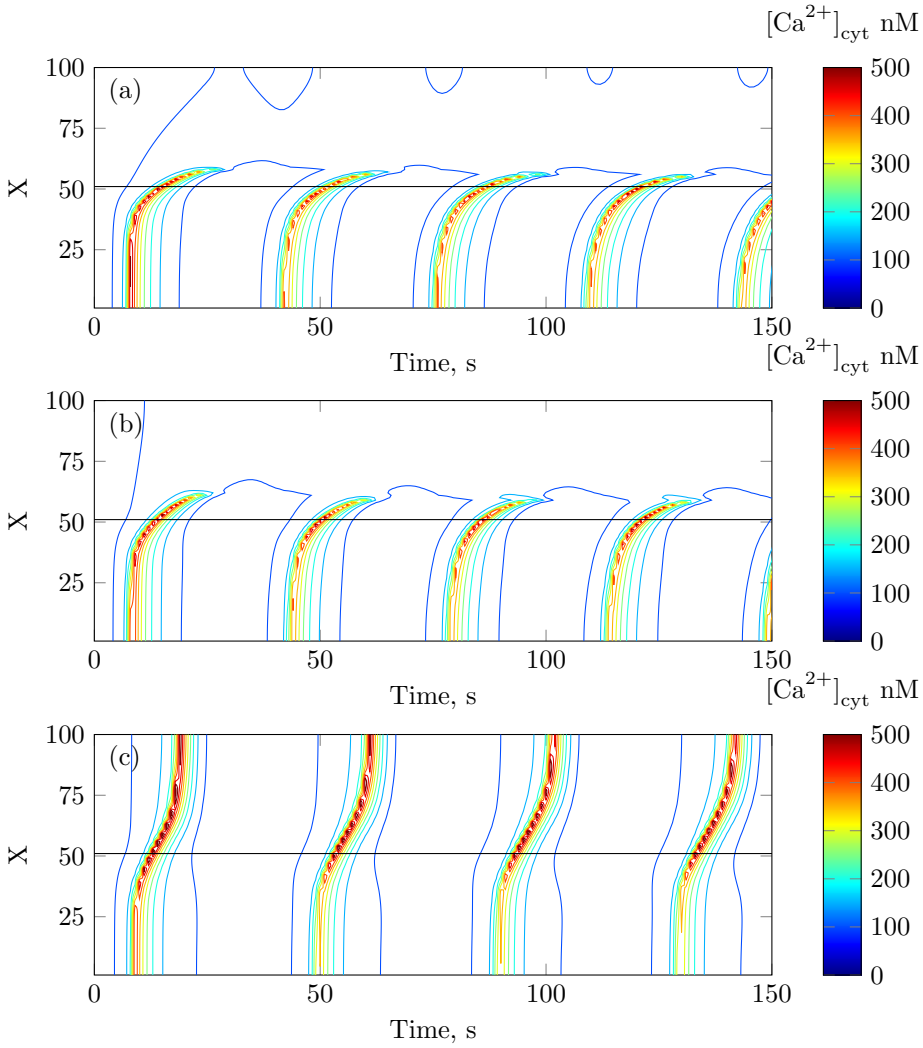

Fig. 6.1 Varying number of gap junctions: Contour plots of intracellular calcium in 100 VSMCs coupled with different levels of gap junctional coupling, 20% (a), 100% (b) and 1000% (c). Y-axis shows cell position. Sigmoidal distribution of agonist is applied over the cells (figure 6.4). The black line is used to distinguish cells that show steady and oscillatory states when uncoupled.

Regenerative calcium propagation is continued to lower agonist concentrations of 145 nM and 102 nM when N_{GJ} is increased to 100% and 400% respectively. For N_{GJ} greater than 400%, penetration depth increases as N_{GJ} increases, but the agonist concentration where regenerative caclium propagation ends is almost unchanged.

The wave velocity of the cells, except those cells which show small amplitude calcium rise, is shown in Figure 6.3. Wave velocity, U, is calculated as the inverse of the time lag between two adjacent cells. The time lag is calculated as the time difference between two adjacent cells to reach peak intracellular calcium. The unit of wave velocity is cell/s. Wave

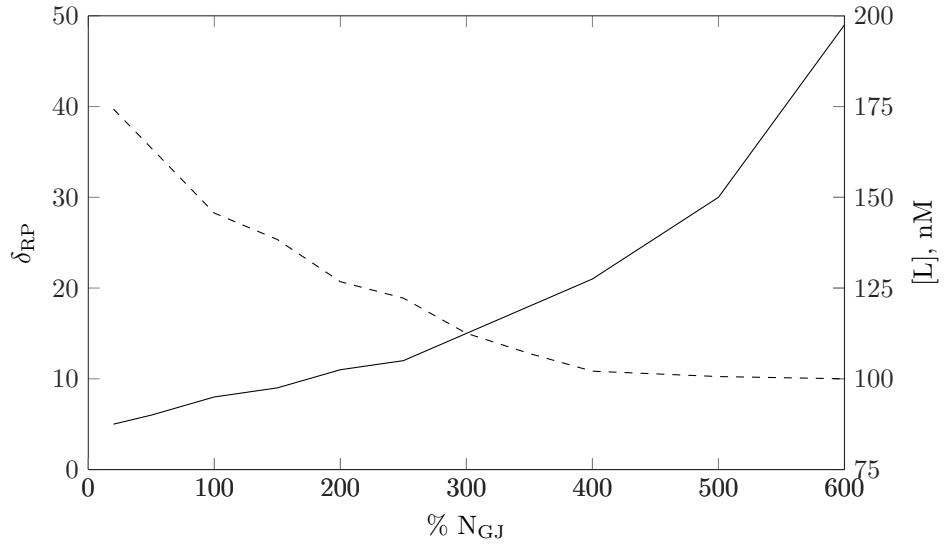

Fig. 6.2 Penetration length (solid) and the agonist concentration (dashed) of the cell at which regenerative calcium rise ends are plotted against the level of gap junctional coupling which is expressed as the percentage average number of gap junctions.

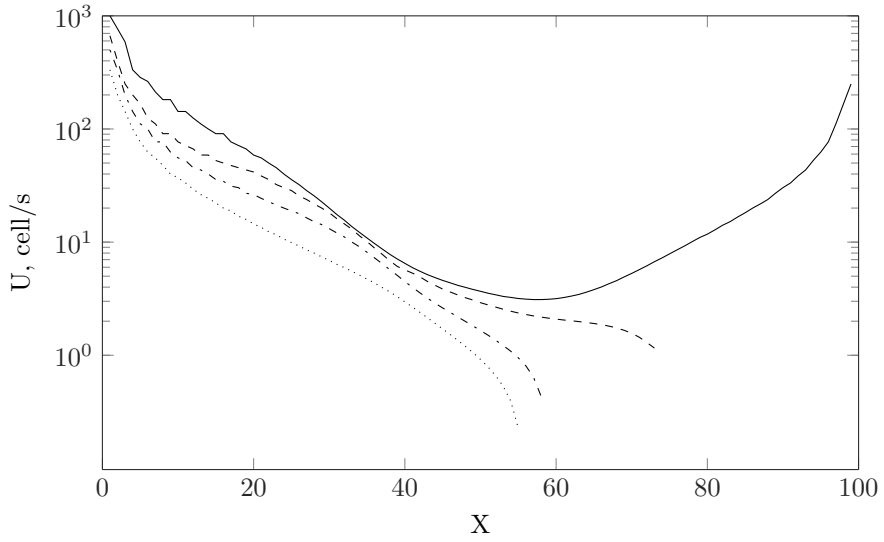

Fig. 6.3 Wave velocity is plotted against cell position in 100 VSMCs coupled with varying levels of N_{GJ}, 20% (dotted), 100% (dash-dotted), 500% (dashed) and 1000% (solid). X-axis shows cell position. A sigmoidal distribution of agonist is applied over the cells (Figure 6.4).

velocity decreases as the position of the cell relative to the first cell increases. A sharp decrease in wave velocity is seen in the cells which show regenerative propagation. However, the sharp decline of wave velocity in the regenerative calcium propagation is not seen with high N_{GJ} of 1000%. Instead, the wave velocity increases as the position of the cell gets further from the stimulated cells.

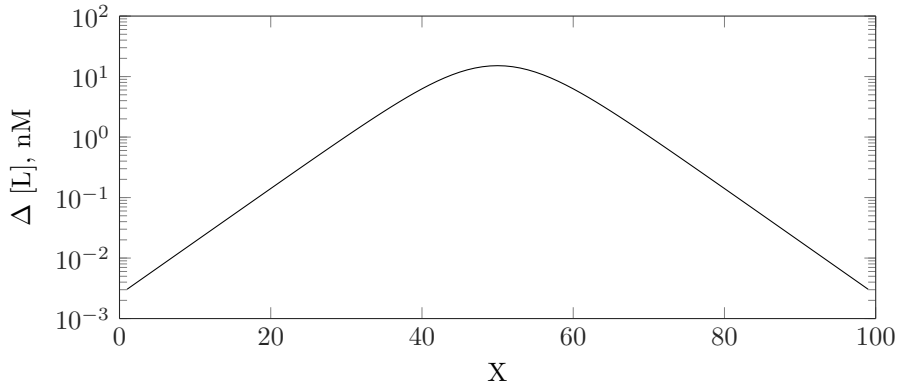

Fig. 6.4 Agonist concentration difference between two adjacent cells over the coupled 100 VSMCs

Based on the spatial distribution of agonist, (refer to Figure 5.5), the agonist concentration difference between the adjacent cells is plotted in Figure 6.4. The profile of propagation velocity at higher N_{GJ} is correlated with the profile of agonist concentration difference between the adjacent cells, (refer to Figures 6.3 and 6.4). The agonist concentration difference graph is symmetrical about the center cell. Similar to this, the velocity plot for 1000% N_{GJ} is symmetrical and the centre of symmetry is around the 60^{th} cell.

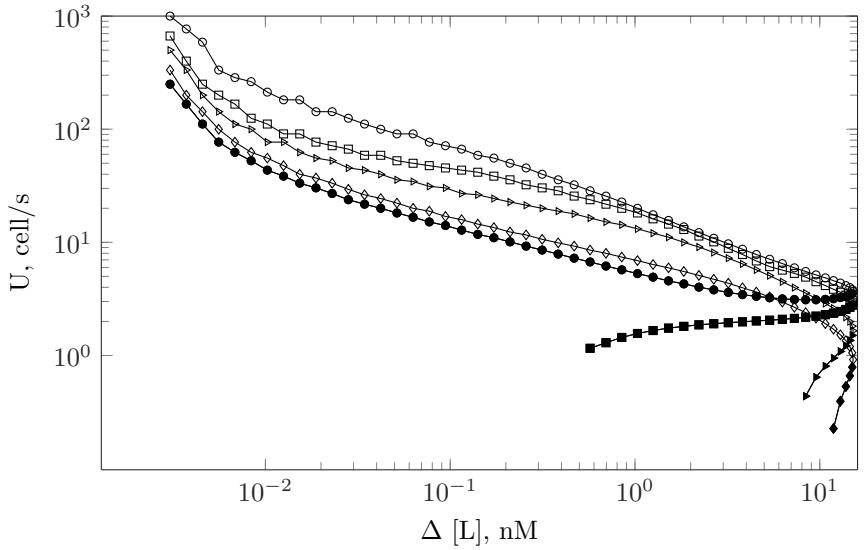

Fig. 6.5 Wave velocity plots of 100 VSMCs coupled with 20% (diamond), 100% (right triangle), 500% (square) and 1000% (circle) levels of gap junctional coupling. A sigmoidal distribution of agonist is applied over the cells (Figure 6.4). Closed markers are used to differentiate the velocity of regenerative propagation in the non-stimulated cells.

Figure 6.5 shows the variation of wave velocity with respect to agonist concentration difference between two adjacent cells as shown in the figure 6.4. For 1000% N_{GJ}, wave velocity of a cell is inversely proportional to the agonist concentration difference. However, for a few cells next to the 51^{st} cell, the relationship is opposite. For 20% N_{GJ}, 100% N_{GJ} and 500% N_{GJ}, wave velocity and agonist concentration difference are inversely related in the first 51 cells. However, the wave velocity of the rest of the cells which exhibit regenerative propagation is reversed and is directly proportional to the agonist concentration difference. Noticeably, at lower N_{GJ}, the cells in the regenerative propagation state show a sharp decline in wave velocity. Wave velocity of a cell within the first 51 cells is greater than that of a cell in the regenerative calcium propagation block with same agonist concentration difference for any N_{GJ}. For example, the 30^{th} cell and the 70^{th} cell experience the same agonist concentration difference. With 1000% N_{GJ}, the wave velocity of the 30^{th} and the 70^{th} cells are 18 cells/s and 1.5 cells/s, respectively.

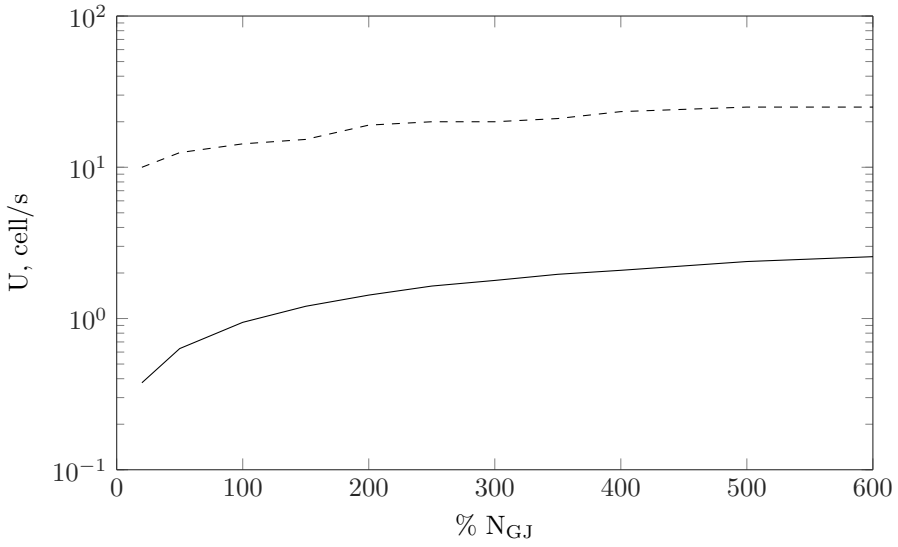

Fig. 6.6 Wave velocity of the 56^{th} cell (solid) and the 30^{th} cell are plotted against the number of gap junctions which is expressed as percent of the total number of gap junctions. A sigmoidal distribution of agonist is applied over the cells (Figure 6.4).

For any cell, the wave velocity increases as the N_{GJ} increases. For the 55^{th} cell, which shows regenerative calcium propagation, the wave velocity increases significantly at lower values of N_{GJ}, (refer to Figure 6.6). The wave velocity is almost doubled when N_{GJ} is increased from 50% to 150%. As the N_{GJ} is increased to a higher value, a further increase in gap junctional coupling does not change wave velocity significantly. Similar variation in wave velocity with respect to N_{GJ} is observed for a cell in the first 51 cells. For example, wave velocity of the 30^{th} cell is given in Figure 6.6. However, at lower values of N_{GJ}, the

change in wave velocity with respect to N_{GJ} is minimal in the 30^{th} cell compared to the 55^{th} cell.

6.2.2 Altered levels of SERCA, IP_3R, and RyR

In this section, we will study the effects of altered levels of SERCA, IP_3R and RyR on the propagation of regenerative calcium rise. To examine this, the levels of SERCA, IP_3R and RyR are changed only in the non-stimulated cell. The levels of SERCA, IP_3R, and RyR in the stimulated cells, (the first 51 cells), are unchanged and are equal to the control case. The coupling strength is kept constant at 100% N_{GJ}.

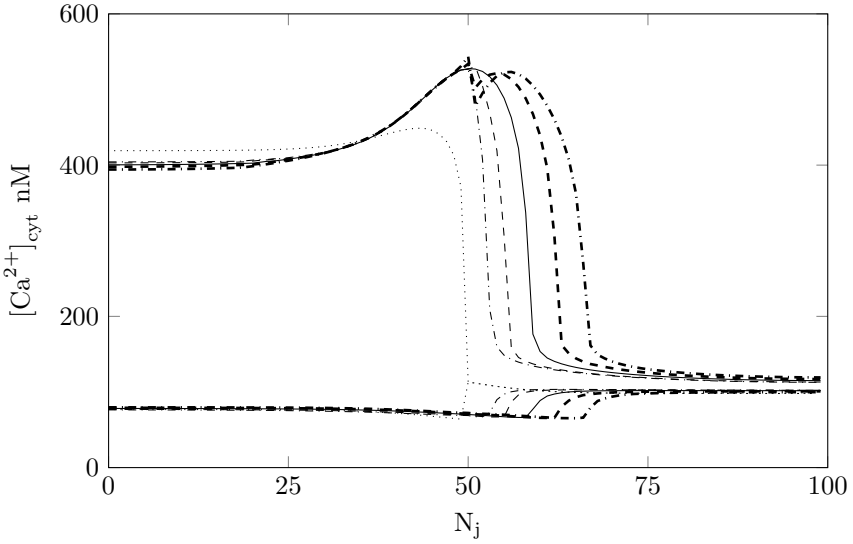

Fig. 6.7 Maximum and minimum values of intracellular calcium: (dotted) Uncoupled, (solid) Control case with 100% levels of SERCA, IP_3R, and RyR. In other simulations, IP_3R levels of the 52^{nd} cell to the 100^{th} cell are changed to 30% (thin dash-dotted), 50% (thin dashed), 150% (thick dashed) and 200% (thick dash-dotted). SERCA and RyR levels are unchanged.

Maximum and minimum values of intracellular calcium oscillations in the coupled cells when the IP_3R level in the cells from the 52^{nd} cell to the 100^{th} cell are varied is shown in Figure 6.7. The minimum calcium concentration of oscillations in a cell is unchanged if the same cell shows regenerative calcium rise for a different IP_3R level. When the IP_3R level is increased to 150% and 300%, regenerative calcium oscillations are produced in twelve and twenty-five cells respectively, (refer to Figure 6.8). The agonist concentration of the cell at which regenerative calcium rise stops for 150% and 300% IP_3R cases are 122 nM and 102 nM respectively. Regenerative calcium rise is obtained in all the non-stimulated cells when the IP_3R level is increased to 400%. For a decrease of 50% and 70% of IP_3R

level, regenerative propagation is restricted to only five cells and two cells, respectively. The regenerative calcium rise stops at 174 nM and 212 nM for 50% and 70% levels of IP_3R, respectively.

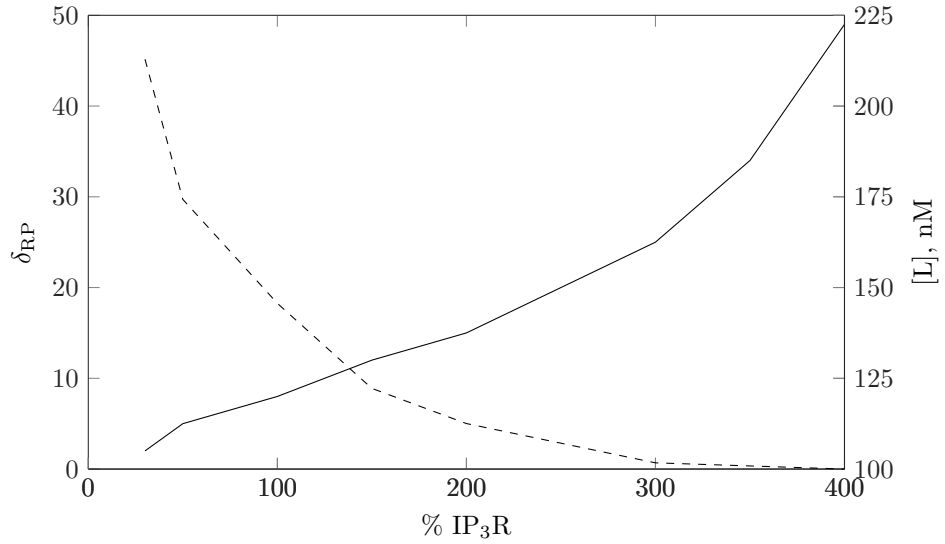

Fig. 6.8 Penetration length (solid) and the agonist concentration (dashed) of the cell at which regenerative calcium rise ends are plotted against IP_3R level

Figure 6.9 shows maximum and minimum values of intracellular calcium oscillations in the coupled cells when RyR levels in the cells from 52^{nd} cell to 100^{th} cell are changed. The minimum calcium concentration of oscillations in a cell is unchanged if the same cell shows regenerative calcium rise for a different RyR level. The altered levels of RyR in the non-stimulated cells cause no impact on the maximum and minimum of calcium oscillations in the stimulated cells. The penetration depth is significantly changed with RyR level. Increasing RyR level to 110% and 120% causes regenerative calcium oscillations in 10 and 15 cells respectively, (refer to Figure 6.10). A further increase to 130% produces regenerative calcium rise in all the non-stimulated cells. With 85% RyR level, only five cells show regenerative propagation. This number is further reduced to 4 cells with 75% RyR level. The regenerative propagation stops at an agonist concentration of 174 nM and 186 nM for 85% and 75% RyR levels respectively. When the RyR level is raised to 110% and 120%, regenerative calcium rise is extended to 126 nM and 110 nM, respectively.

Figure 6.11 shows maximum and minimum values of intracellular calcium in the coupled cells when the SERCA level is changed in the cells from the 52^{nd} cell to the 100^{th} cell. The penetration depth of regenerative calcium rise with 100% SERCA level is 8cells. The penetration depth is reduced as the SERCA level increases in non-stimulated cells. For 125% SERCA level, regenerative propagation is reduced to only five cells, and the corresponding

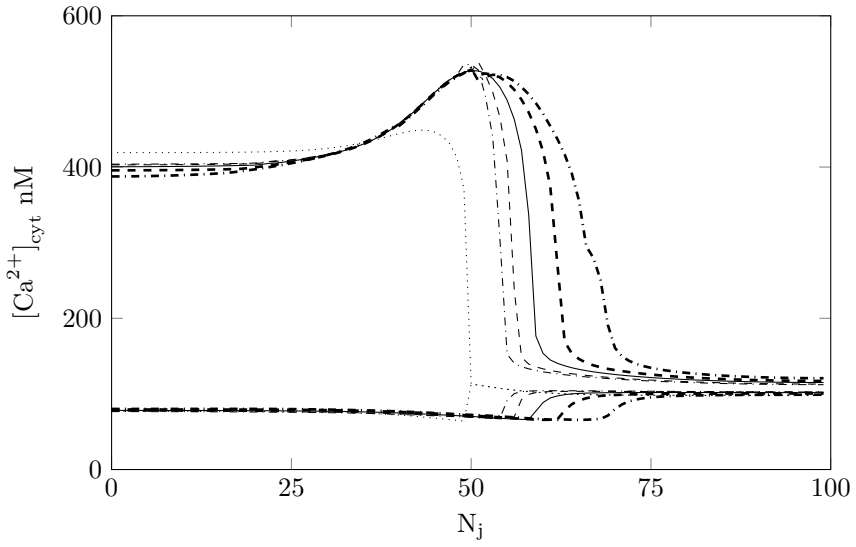

Fig. 6.9 Maximum and minimum values of intracellular calcium: (dotted) Uncoupled, (solid) Control case with 100% levels of SERCA, IP_3R, and RyR. In the other four simulations, RyR levels of the 52^{nd} cell to the 100^{th} cell are changed to 75% (thin dash-dotted), 85% (thin dashed), 110% (thick dashed) and 120% (thick dash-dotted). SERCA and IP_3R levels are unchanged.

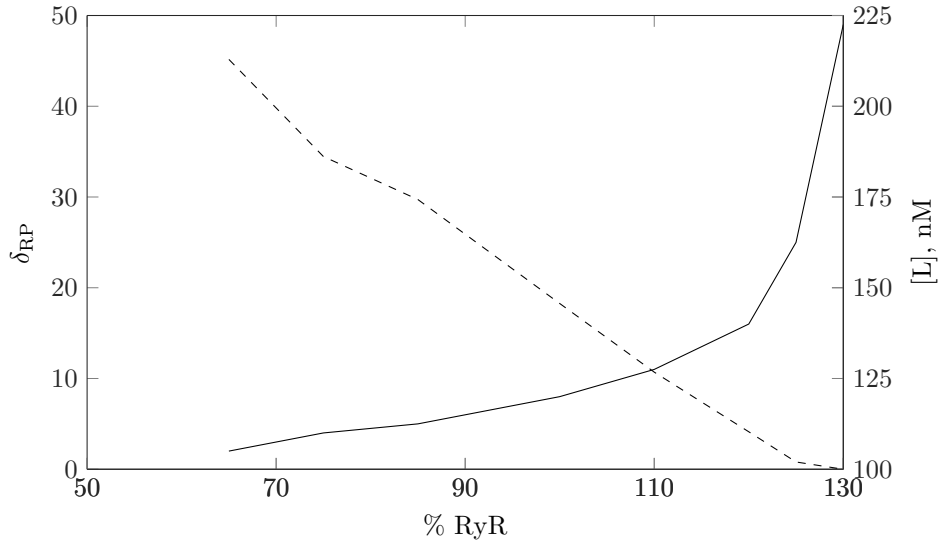

Fig. 6.10 Penetration length (solid) and the agonist concentration (dashed) of the cell at which regenerative calcium rise ends are plotted against RyR level.

regenerative calcium rise stops at an agonist concentration of 174 nM, (see Figure 6.12). Regenerative propagation is then restricted to only three cells when the SERCA level is increased to 135%. The regenerative propagation for 135% SERCA ends at 199 nM.

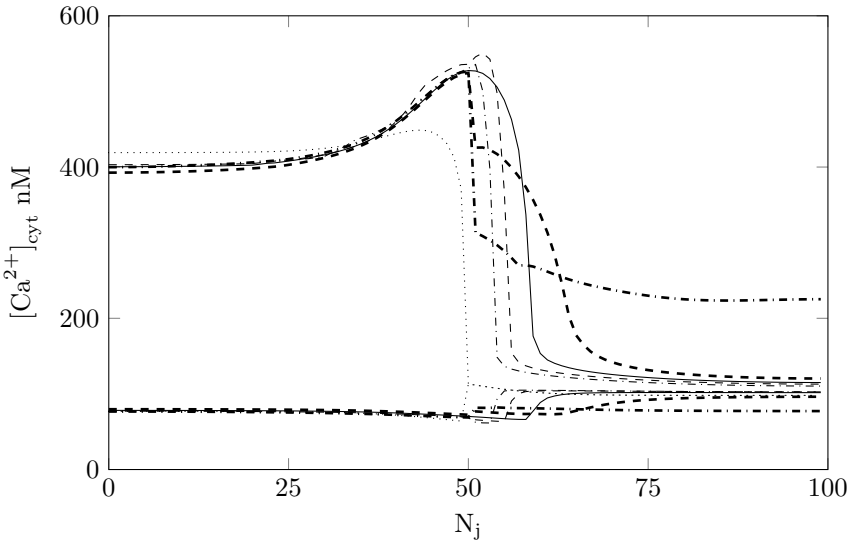

Fig. 6.11 Maximum and minimum values of intracellular calcium: (dotted) Uncoupled, (solid) Control case with 100% levels of SERCA, IP_3R, and RyR. In the other four simulations, SERCA levels of the 52^{nd} cell to the 100^{th} cell are changed to 150% (thin dash-dotted), 125% (thin dashed), 70% (thick dashed) and 50% (thick dash-dotted). RyR and IP_3R levels are unchanged.

On the other hand, when the SERCA level is reduced to 70%, the regenerative calcium oscillations are obtained in eleven cells, three cells more than the control case. Though reduction of SERCA level increases penetration depth, peak intracellular calcium is relatively low. However, for 50% SERCA level, regenerative calcium oscillations are seen only in 4 cells. The calcium rise in the rest of the non-stimulated cells is increased compared to a higher SERCA level. Further reduction of the SERCA level suppresses calcium rise in all the non-stimulated cells. For 70% and 50% SERCA levels, regenerative calcium rise ends at 126 nM and 186 nM respectively. For the SERCA levels greater than 70%, penetration depth decreases as SERCA level increases whereas for SERCA levels lower than 70%, penetration depth increases as the SERCA level increases, (refer to Figure 6.12).

6.3 Discussions

We have studied the effects of N_{GJ}, SERCA, IP_3R and RyR on the propagation of regenerative calcium waves in coupled VSMCs. The study mainly focused on the penetration depth and the wave velocity of regenerative calcium oscillations, which are the two important characteristics of calcium propagation.

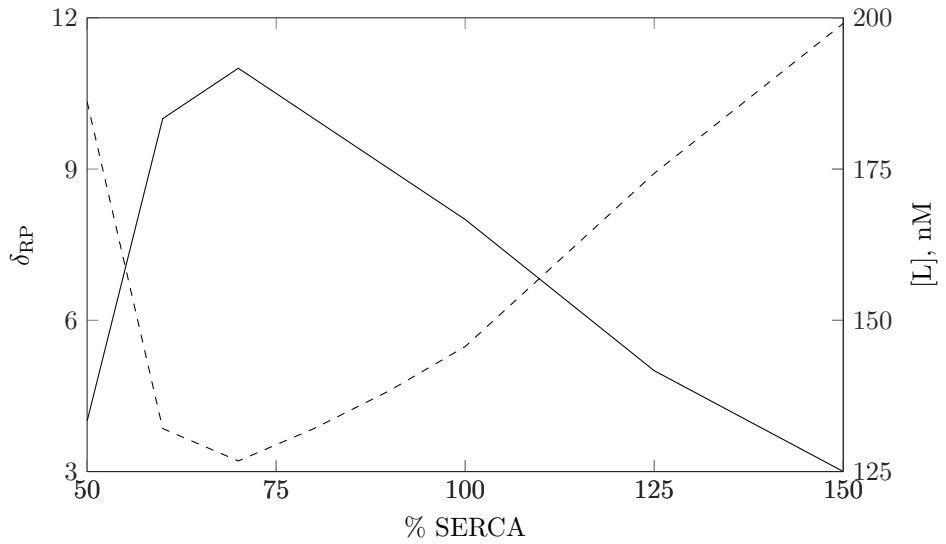

Fig. 6.12 Penetration length (solid) and the agonist concentration (dashed) of the cell at which regenerative calcium rise ends are plotted against SERCA level.

Wave velocity of the cells close to the two boundaries of the coupled cell system is considerably high compared to the other cells. This might be due to the boundary effects. There are no neighbouring cells for two ends cells to damp the coupling components such as V_m and IP_3. The absence of one adjacent cell makes the ends cells attain a higher depolarization and an increased IP_3 concentration, which leads to an enhanced wave propagation. The boundary effects are limited to only a few cells.

Regulation of penetration depth and wave velocity by GJIC

It is clear from the model results that penetration depth is proportional to the coupling strength. This has to be read along with the agonist concentration at which regenerative propagation ends, because, the increased coupling extended the regenerative calcium rise to a cell with a lower agonist concentration. The combined effect of agonist concentration and coupling strength is clearly visible in Figure 6.2. The increased coupling strength helps the cells with low agonist concentration to attain increased depolarization and a greater concentration of IP_3. The increased depolarization in the cells enhances the opening of the VOCC leads to increased intracellular calcium and the subsequent rise of IP_3. If the increased calcium and IP_3 are enough to enable IICR and CICR mechanisms, the cells at low agonist concentration exhibit regenerative calcium rise at a higher coupling strength.

The regenerative calcium rise is propagated to all the cells when the coupling strength is increased to 600% N_{GJ}. In the study of Koenigsberger et al. [90], fully regenerative

calcium waves were achieved at an increased coupling strength of 180%. The difference in the minimum coupling strength required to produce fully regenerative calcium waves might be because of the difference in the VSMC systems studied. The stimulated cells were depolarized to ≈-30 mV in Koenigsberger et al. [90]'s study which is comparatively high compared to ≈-43 mV in our model (refer to Figure 5.7). The large difference in membrane potential between the stimulated and non-stimulated cells might have enhanced the propagation of regenerative calcium waves in Koenigsberger et al. [90] study.

Irrespective of the cell position and agonist concentration, the wave velocity increases as the N_{GJ} increases. The dependency on the N_{GJ} is more prevalent in the cells which are located at the end of regenerative propagation. However, the wave velocity reaches a constant at higher coupling strength in all the cells irrespective of their position. At a high value of N_{GJ}, coupled cells would attain a maximum possible GJIC in the given system. This might cause no change in wave velocity at high coupling strengths. If the value of N_{GJ} is high enough to produce the regenerative calcium rise in all the coupled cells, the wave velocity is inversely proportional to the difference in agonist concentration between the adjacent cells. The wave velocity profile is simply the mirror image of the profile of the agonist concentration difference between the adjacent cells.

It seems that the penetration depth and the wave velocity of intracellular calcium oscillations in coupled VSMCs are strongly related to the N_{GJ}. Therefore, one could say that GJIC between VSMCs plays an essential role in the propagation of intracellular calcium.

Dominant role of RyR in the propagation of regenerative calcium rise

Regenerative calcium propagation is enhanced when IP_3R or RyR level is increased. In these cases, the regenerative calcium propagation extends to lower agonist concentrations. IP_3R and RyR are integral parts of IICR and CICR mechanisms. When IP_3R level or RyR is increased, it may enhance the activation of IICR and CICR mechanisms to generate regenerative calcium rise for the same agonist concentration. Therefore, the increased levels of IP_3R and RyR boost the regenerative calcium rise in VSMCs, which leads to greater penetration depth. Interestingly, the level of IP_3R required to enhance the same penetration length is high compared to the RyR level. For getting regenerative calcium rise in almost 11 cells, the level of IP_3R should be 150% whereas 110% level of RyR is enough. This means that influence of RyR is dominant on the propagation of regenerative calcium rise compared to IP_3R. This is expected as the maximum rate of RyR function is assumed two-fold higher than that of IP_3R.

Biphasic regulation of penetration depth by SERCA

The effect of reduced a SERCA level produces dual effects on the propagation of regenerative intracellular calcium rise. For high SERCA levels, greater than 70%, SERCA blocks regenerative calcium propagation whereas at low SERCA levels, lower than 70%, SERCA enhances regenerative calcium propagation, (refer to Figure 6.12). If the SERCA level is low, it reduces the intra-SR calcium concentration due to diminished SERCA pumping of calcium back to the SR. The reduction in intra-SR calcium creates a decreased concentration gradient between the SR and the cytosol available for IP_3R and RyR. This would cause reduced intracellular calcium release from the SR and a subsequent reduction in intracellular calcium. Therefore, the VSMC fails to attain regenerative calcium rise at a low SERCA level. As the SERCA level increases, intra-SR calcium load also increases, which leads to enough calcium influx to the cytosol to produce regenerative calcium rise. So that, the increasing SERCA level enhances penetration depth. However, further increase of the SERCA level lowers the net calcium release to the cytosol. The increased pumping of SERCA keeps the intracellular calcium low and blocks the calcium-induced activation of RyR and IP_3R. This may stop regenerative calcium rise at the same agonist concentration, leads to the shortening of the penetration depth. The regenerative calcium rise would be reestablished at a higher agonist concentration as the opening of IP_3R and RyR are enhanced to overcome the effect of increased SERCA level.

Discussion in the context of diabetes

According to Kuroki et al. [92], the function of Cx43 is inhibited in a high glucose medium, which leads to reduced GJIC. To study the role of GJIC, Lucifer yellow dye was injected into a single cell of a culture of VSMCs, (refer to Figure 6.13). The number of cells in which the injected dye was propagated is used as a measure of GJIC. Li et al. [103] reported the same in retinal pericytes. These experiments show that the penetration depth in VSMCs was reduced in a high glucose medium. In agreement to this, the reduced coupling strength shortened the penetration depth in the model results. This is expected as coupling strength is related to the GJIC.

In the cases of IP_3R and RyR, downregulation of both proteins restricts the propagation of regenerative calcium oscillations to a smaller number of cells. Searls et al. [154] observed upregulation of RyR along with downregulation of IP_3R. Since both of these proteins have the same effect on the propagation of calcium rise, the upregulation of RyR restores the penetration depth of the propagation that is narrowed by the downregulation of IP_3R, (refer to Figure 6.14). This observation in coupled cells matches with the hypothesis that we

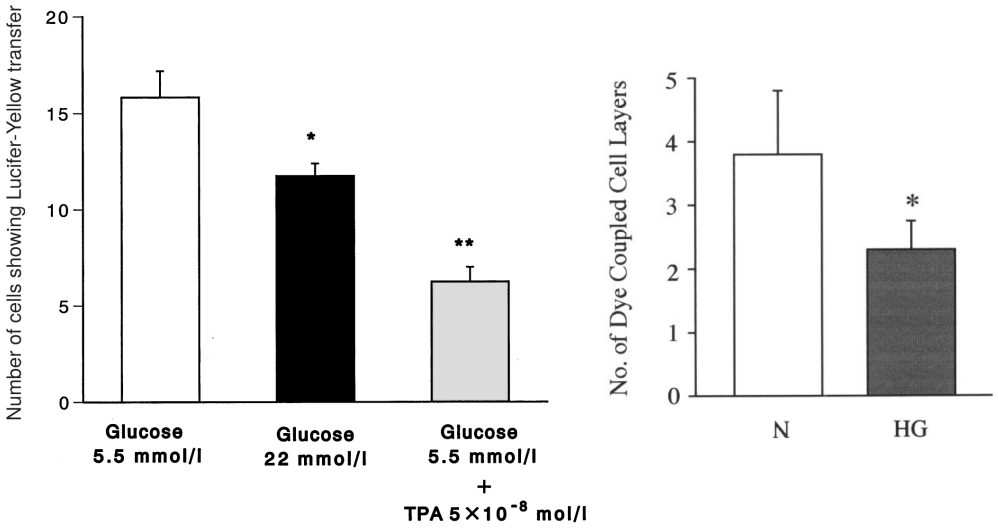

Fig. 6.13 The number of dye-coupled cells as a measure of GJIC. (left) VSMCs of a bovine thoracic aorta during exposed to a high glucose medium. Reproduced from Kuroki et al. [92] paper (permission granted from American Diabetes Association to reuse in the thesis, licence number: 3852141143899). (right) Bovine retinal pericytes exposed to a high glucose medium. HG stands for high glucose. Reproduced from Li et al. [103] paper (permission granted from Association for Research in Vision and Ophthalmology (ARVO) by email contact). Lucifer yellow dye is used in both experiments.

have suggested in the chapter 4, section 4.3. The impairment of penetration depth due to altered level of IP_3R or RyR might be corrected by changing the level of the other protein. However, the downregulation of both IP_3R and RyR reduces penetration of regenerative calcium oscillations in diabetic VSMCs.

According to the model results, downregulation of SERCA level to between 25% and 50% of the control case, as seen in diabetic VSMCs [154], has mixed effects on the penetration depth of calcium oscillations. In the model results, a 25% reduction of the SERCA level extends the penetration depth. However, 50% reduction of SERCA level halved the penetration depth. If the level of IP_3R or RyR is lowered along with the reduced level of SERCA, the penetration depth is further shortened, (refer to Figure 6.14). Though the reduction of SERCA level in diabetic VSMCs has mixed effects on the propagation of regenerative calcium oscillations, the combined reduction of SERCA and IP_3 or RyR levels diminishes the penetration depth.

In our knowledge, there are no experimental studies, which discuss the propagation of vasomotor response in diabetic VSMCs available in the literature. Most of the studies focused on the signal conduction in diabetic hearts. Ventricular conduction is significantly reduced in diabetes. The slowed conduction is related to the downregulation of Cx43 [173].

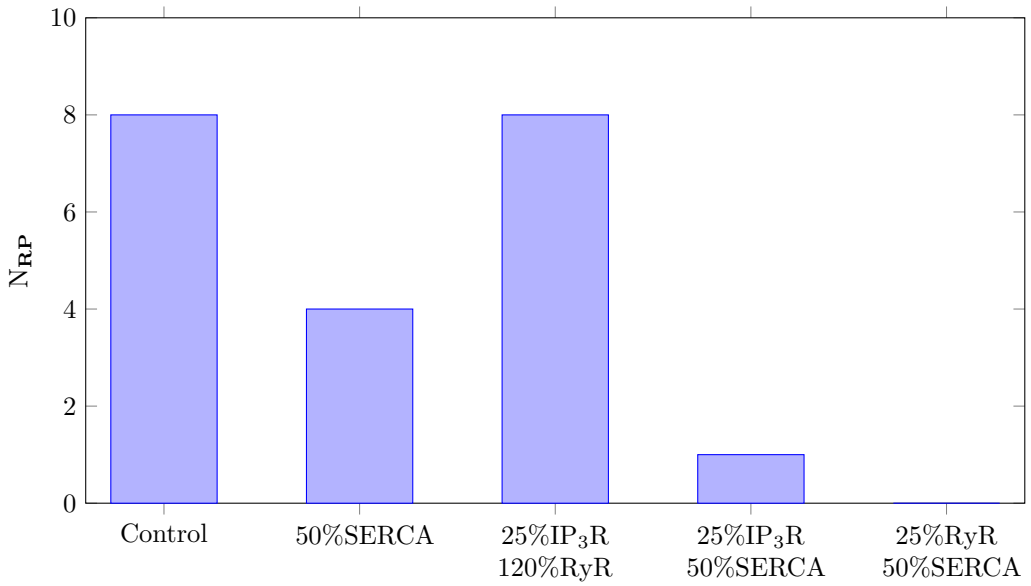

Fig. 6.14 Penetration length for different combinations of SERCA, IP_3R and RyR.

Signal conduction is slowed down in diabetic hearts compared to the normal heart, though the expression of Cx43 is unchanged in diabetic heart but associated with enhanced lateralization of Cx43. This leads to non-functional gap junctions [130]. As the function of Cx43 is inhibited, the conduction of signal reduces. Similar to these experimental observations, the model results show that the reduced coupling strength slows down the wave velocity of calcium oscillations.

The calcium oscillations are essential for the contraction-relaxation of the artery. The impaired calcium propagation may affect the long distance conduction of vasomotor response. One could say that the reduced GJIC due to the reduced Cx43 function, lower levels of SERCA, IP_3R and RyR affects the propagation of the vasomotor response, causing impaired propagation of vasoconstriction/vasodilation in diabetes.

6.4 Conclusions

We have evaluated the effects of altered levels of GJIC, SERCA, IP_3R and RyR on the propagation of intracellular calcium using the coupled cell model discussed in the chapter 5. We have analysed the influences of N_{GJ} on the penetration depth and wave velocity of regenerative calcium propagation. The level of SERCA, IP_3R, and RyR in the non-stimulated cells were altered and the results were investigated for the consequences on penetration depth.

The regenerative propagation is possible only if the coupling generates enough calcium and IP_3 required for the activation of IICR and CICR mechanisms, irrespective of the agonist concentration or the position of the cell.

It seems that the penetration depth and the wave velocity of intracellular calcium oscillations in coupled VSMCs are strongly related to the N_{GJ} if the regenerative propagation was not extended to the all the non-stimulated cells. Otherwise, the wave velocity profile is simply the mirror image of the profile of the agonist concentration difference between the adjacent cells.

The increased levels of IP_3R and RyR enhanced the the propagation of regenerative calcium rise in VSMCs leading to a greater penetration depth. The level of IP_3R required to enhance the same penetration length is high compared to the RyR level. Interestingly, the SERCA regulation of the propagation of regenerative intracellular calcium rise is biphasic. At high SERCA levels, SERCA blocks regenerative calcium propagation whereas at low SERCA levels, SERCA enhances regenerative calcium propagation.

The reduced GJIC due to the decreased Cx43 in diabetes slows down the wave velocity of intracellular calcium oscillations. Though the reduction of SERCA level in diabetic VSMCs have mixed effects on the propagation of regenerative calcium oscillations, combined reduction of SERCA and IP_3 or RyR levels diminishes the penetration depth. However, the suppression of penetration depth due to decreased level of IP_3R could be restored by increasing the level of RyR and vice versa. One could say that the reduced GJIC due to the reduced Cx43 function is a possible factor that affect the long distance conduction as well as propagation velocity of vasomotor response in diabetes.

Chapter 7

Concluding Remarks

Vascular dysfunction in diabetes causes vast complications in the circulatory system including the regulation of blood flow to the tissues. The cellular mechanisms of vascular dysfunction in diabetes are not completely elucidated because of the high-level complexity involved. The functioning of VSMCs is impaired in microcirculation as well as in macrocirculation of diabetic patients [123]. The experimental studies imply that impaired intracellular calcium dynamics in diabetic VSMC is related to the alterations of functions of GJIC and calcium handling proteins such as SERCA, IP_3R, and RyR. The main purpose of the thesis was to explore the importance of SERCA, IP_3R, RyR and GJIC as modulating factors of intracellular calcium dynamics in VSMCs and investigate the related consequences in the perspective of diabetes.

As a powerful tool to investigate the extremely complex biological systems, we have developed a mathematical model of VSMC which accomplishes our research aims. Kapela et al. [83] VSMC model was used as a building block to develop the new model. We have defined new or modified descriptions to NCX exchanger, IP_3R channel, NSC channel, agonist-induced IP_3 production, SR structure, and functioning. The SR was modelled as a single luminally continuous store with homogeneous luminal calcium. None of the VSMC mathematical models has used sequential binding of calcium and IP_3 for the activation of IP_3R. We have incorporated a simplified 4-state sequential-binding IP_3R model since calcium is the central attention of the study. The model equations were solved using a numerical model developed based on Bakward-Euler method and fixed point iteration. The time period and tolerance limit for getting required accuracy was fixed by analysing the relative error. The code for the model is written in 'C' language and was implemented in the desktop PC.

The response of the VSMC model to varying agonist concentrations were analysed on the basis of corresponding experimental studies. The temporal occurrence, amplitude and frequency of intracellular calcium oscillations, and bifurcation points of the agonist

stimulation were matching with the experiments in VSMCs. The response of the model to varying extracellular concentrations of potassium and calcium were also qualitatively matching with experiments. The developed model was then used for studying the effects of SERCA, IP_3R, RyR and GJIC.

We have extended our single cell VSMC model to coupled VSMCs model by adding appropriate model equations for GJIC between VSMCs. The transport of calcium through gap junctions was assumed negligible. V_m and IP_3 were coupled between VSMCs to model GJIC. The model equations were solved using TDMA along with the numerical method used for the single cell. We have investigated the propagation of intracellular calcium in 100 serially coupled cells with a sigmoidal distribution of agonist. The simulations were carried out by coupling both V_m and IP_3, V_m alone and IP_3 alone. The simulations were performed in the presence and absence of IP_3R and RyR.

In agreement to the experimental studies, the model results established the fact that intracellular calcium propagation could be regenerative, however the regenerative calcium propagation was not attainable in all the coupled cells but up to some cells next to the stimulated cells. The calcium release from SR is the main contributor of calcium rise in the large amplitude or the regenerative calcium oscillations. The small amplitude oscillations were obtained in the cells far from the stimulated cells and the calcium release through VOCC is the primary source of calcium rise in the these calcium oscillations.

The activation of IICR and CICR mechanisms are essential for the regenerative calcium rise in the non-stimulated cells. If the intercellular coupling generates enough calcium and IP_3 concentrations in the non-stimulated cell, regenerative calcium rise will result.

V_m and IP_3 -mediated intercellular signalling mechanisms for the propagation of intracellular calcium were detailed. The V_m and IP_3 -mediated mechanisms could separately generate regenerative calcium propagation in coupled VSMCs. However, Vm-mediated signalling mechanism plays a dominant role. The IP_3R channel, needed for the initiation of IP_3 -mediated signalling mechanism, is activated only if both IP_3 and calcium are bound to its respective activation sites. This limitation makes IP_3 mediated calcium signalling mechanisms less effective in the coupled VSMCs. Our study could illustrate the reason for the dominant role of the V_m coupling, which was observed in the experiments.

7.1 Findings with regard to the research questions

We investigated the effects of altered levels of SERCA, IP_3R and RyR in a single cell as well as coupled cells. The level of a particular channel or pump was altered by changing the maximum calcium flux of the corresponding channel or pump. The responses of the model to

the altered levels of SERCA, IP_3R and RyR at a fixed agonist concentration and for varying agonist concentrations were studied.

The frequency of intracellular calcium oscillations is significantly influenced by IP_3R and RyR at its low levels. The SERCA regulation of frequency is biphasic. At low SERCA levels, frequency increases with SERCA levels whereas at higher SERCA levels, the relation inverted.

The role of IP_3R and RyR for the occurrence of intracellular calcium oscillations is not fully clear in the literature. Some studies claimed the need of RyR for the existence of calcium oscillations whereas others proposed IP_3R alone is enough. The model results showed that the agonist induced calcium oscillations are feasible in the absence of RyR or IP_3R. However, higher stimulating strength is required to produce intracellular calcium oscillations in the absence IP_3R or RyR. The change in IP_3R or RyR level shifts the bifurcation points of agonist-induced calcium oscillations. This might have been the reason for not getting the calcium oscillations in experiments when either IP_3R or RyR was blocked with the stimulation strength. These findings provide explanation for the contradictory statements published in experiments.

The change of SERCA, IP_3R or RyR level shifted the oscillatory state of intracellular calcium to steady and vice versa at a constant agonist concentration. Especially, increasing SERCA level move the oscillatory region to high agonist concentrations whereas increasing IP_3R or RyR level shift the oscillatory region to lower agonist concentrations. The shift of oscillatory region was significant at low SERCA levels and at low IP_3 levels. Based on this, our hypothesis is that if an external environment influences the agonist-induced calcium transients, the VSMC may alter the levels of SERCA, IP_3R and/or RyR expressed in the SR to restore intracellular calcium transients matched with the functional need.

The SERCA regulation of the propagation of regenerative intracellular calcium rise is biphasic. At high SERCA levels, SERCA blocks regenerative calcium propagation whereas at low SERCA levels, SERCA enhances regenerative calcium propagation. The downregulation of IP_3R and RyR reduced penetration of regenerative calcium oscillations in diabetic VSMCs. The influence of RyR is dominant on the propagation of regenerative calcium rise compared to IP_3R. The suppression of penetration depth due to decreased level of IP_3R could be restored by increasing the level of RyR and vice versa.

It seems that the penetration depth and the wave velocity of intracellular calcium oscillations in coupled VSMCs are strongly related to the GJIC if the regenerative propagation was not extended to the all the non-stimulated cells. Otherwise, the wave velocity profile is simply the mirror image of the profile of the agonist concentration difference between the

adjacent cells. The wave velocity of a cell is unchanged at higher GJIC irrespective of their position.

The levels of GJIC, SERCA, IP_3R and RyR are found altered in VSMCs of diabetes [154, 118] along with impaired intracellular calcium dynamics. The reduced GJIC due to the reduced Cx43 function is one possible factor that affect the long distance conduction as well as propagation velocity of vasomotor response in diabetes. The model results showed that the functional implications due to the altered level of IP_3R in diabetic VSMCs might be regulated by changing the level of RyR and vice versa. However, the impaired intracellular calcium dynamics due to reduced SERCA levels can not be restored by changing IP_3R or RyR levels because of the reduced intra-SR calcium load. There is no other kinds of calcium pump expressed in the SR to replace the functioning of SERCA.

The model responses suggest that the reduced SERCA level is a possible mechanism for the “smoothed" calcium transients in VSMC. The intracellular calcium lowering as well as intracellular calcium rising in VSMC are significantly affected with altered SERCA level. The SERCA level tends to be the regulating factor of intracellular calcium in both the activation and relaxation phases of oscillations. These findings lead to the fact that reduced SERCA level is probably the primary factor responsible for the reduced intracellular calcium transients and the reduced contractility in diabetes even though all the three IP_3R, SERCA and RyR are varied in diabetic VSMCs.

7.2 Future works

- The agonists induce several signalling mechanisms in VSMC by activating different G-proteins like Gq, Gs and Gi protein. For example, NE activate Gq, Gs and Gi protein. The activation of Gs-protein enhance the production of cAMP whereas activation of Gi-protein suppresses the production of cAMP. Gq-protein activates PLC and leads to the generation of IP_3 and DAG. In the present study, we have included only the PLC activation and subsequent signalling transduction. Adding the signalling transduction leading to change the production of cAMP will help us to fully understand the complex signalling mechanism and intracellular calcium dynamics in VSMC following agonist stimulation.

- The model can be extened further by including nitric oxide (NO) or cyclic guanosine monophosphate (cGMP) signaling pathways. NO is known as an important vasodilation factor causing relaxation of the artery. NO is synthesized from the ECs and from there diffuses to the neighbouring VSMCs. The cGMP is produced in the VSMC when NO activates NO-sGC-GTP pathway.

- We have solved the model equations using constant time-step. One can think of converting the constant-time step to adaptive time step which is considered to be more efficient. This may further reduce the simulation time useful for coupling larger number of cells.

- This model can be further extended by including selective permeability of gap junctions.

- The cellular pathways that leads to the alteration of GJIC, SERCA, IP_3R and RyR in diabetic VSMCs.

  Diabetes increases PKC activity [70], transforming growth factor (TGF)-β production [161] and expression of Bcl-2 and Bcl-x_L [182] in VSMCs. The TGF-β inhibits intracellular calcium transients by reducing IP_3 sensitivity in VSMCs [201]. The IP_3 sensitivity is related to the TGF-β -induced downregulation of IP_3R [162]. TGF-β downregulation of IP_3R expression was found in diabetic VSMCs of aorta by Sharma et al. [161].

  Kuroki et al. [92] showed reduced GJIC in VSMC exposed to the high-glucose medium is related to the increased PKC activity. Similar findings were reported by Inoguchi et al. [71] in the cardiac cells of diabetic rats, (refer to Figure 1.10). The reduction of the expression of Cx43 in high-glucose medium was also reported in aortic ECs [92], microvascular ECS, and retinal pericytes [103]. Altogether, high-glucose leads to Cx43 function inhibition and is related to the increased PKC activity.

  The Bcl-2 and Bcl-x_L proteins are upregulated in the VSMCs of diabetic patients and exposed to a high-glucose medium [148, 149, 105]. The interaction of Bcl-2 and the Bcl-x_L proteins with IP_3R enhances the IP_3-dependent activation of IP_3R [104, 182]. Velmurugan and White [182] observed Bcl-2-dependent increases in the IP_3R-dependent calcium release in diabetic VSMCs.

  We have studied the effects of altered levels of GJIC, SERCA, IP_3R and RyR by changing the maximum rate of calcium flux. One could think of modelling the cellular pathways that leads to the alteration of GJIC, SERCA, IP_3R and RyR in diabetic VSMCs. Some of the suggestions are,

  - High-glucose activation of PKC - PKC-mediated phosphorylation of Cx43 - effect of Cx43 phosphorylation to GJIC
  - High-glucose activation of PKC - PKC-mediated activation of TGF-β production [56] - TGF-β -mediated alteration of IP_3R expression

- High-glucose and diabetes upregulation of the Bcl-2 and Bcl-x_L proteins - Bcl-2 and Bcl-x_L-mediated increase in IP_3-dependent activation of IP_3R channel
- Altered SERCA regulation in high-glucose medium

References

[1] Allbritton, N. L., Meyer, T., and L, S. (1992). Range of messenger action of calcium ion and inositol 1,4,5-trisphosphate. *Science*, 258:1812–1815.

[2] Amedee, T. and Large, A. (1989). Microelectrode study on the ionic mechanisms which contribute to the noradrenaline-induced depolarization in isolated cells of the rabbit portal vein. *British Journal of Pharmacology*, 97:1331–1337.

[3] Angermann, J. E. (2006). Mechanism of the Inhibition of Ca2+-Activated Cl- Currents by Phosphorylation in Pulmonary Arterial Smooth Muscle Cells. *The Journal of General Physiology*, 128(1):73–87.

[4] Arreola, J., Melvin, J. E., and Begenisich, T. (1996). Activation of calcium-dependent chloride channels in rat parotid acinar cells. *The Journal of general physiology*, 108(1):35–47.

[5] Ashida, T. and P, B. M. (1987). Regulation of cell calcium and contraction in mammalian arterial smooth muscle: The role of sodium-calcium exchange. *Journal of Physiology*, 392:617–635.

[6] Austin, C. and Wray, S. (2015). Interactions Between Ca^{2+} and H^{+} and Functional Consequences in Vascular Smooth Muscle. *Circulation Research*, pages 355–363.

[7] Australia, D. (2016). Diabetes in Australia. https://www.diabetesaustralia.com.au/diabetes-in-australia.

[8] Bai, Y., Edelmann, M., and Sanderson, M. J. (2009). The contribution of inositol 1,4,5-trisphosphate and ryanodine receptors to agonist-induced Ca(2+) signaling of airway smooth muscle cells. *American journal of physiology. Lung cellular and molecular physiology*, 297(2):L347–L361.

[9] Balke, C. W., Egan, T. M., and Wier, W. G. (1994). Processes that remove calcium from the cytoplasm during excitation-contraction coupling in intact rat heart cells FsRjleak. *Journal of Physiology*, 474:447–462.

[10] Baro, I. and Eisner, D. A. (1995). Factors controlling changes in intracellular Ca2 + concentration produced by noradrenaline in rat mesenteric artery smooth muscle cells. *Journal of Physiology*, 482:247–258.

[11] Barrio, L. C., Capel, J., Jarillo, J. A., Castro, C., and Revilla, A. (1997). Species-specific voltage-gating properties of connexin-45 junctions expressed in Xenopus oocytes. *Biophysical journal*, 73(2):757–769.

[12] Bartlett, I. S. and Segal, S. S. (2000). Resolution of smooth muscle and endothelial pathways for conduction along hamster cheek pouch arterioles. *American Journal of Physiology - Heart and Circulatory Physiology*, 278(2):H604—-H612.

[13] Bayguinov, O., Hagen, B., Bonev, A. D., Nelson, M. T., and Sanders, K. M. (2000). Intracellular calcium events activated by ATP in murine colonic myocytes. *American Journal of Physiology - Cell Physiology*, 279:126–135.

[14] Bedner, P., Niessen, H., Odermatt, B., Kretz, M., Willecke, K., and H, H. (2006). Gap junction channels exhibit connexin-specific permeability to cyclic nucleotides. *Journal of Biological Chemistry*, 281:6673–6681.

[15] Bennett, M. R., Farnell, L., and Gibson, W. G. (2005). A quantitative description of the contraction of blood vessels following the release of noradrenaline from sympathetic varicosities. *Journal of theoretical biology*, 234(1):107–22.

[16] Berridge, M. J. (2006). Calcium microdomains: organization and function. *Cell calcium*, 40(5-6):405–412.

[17] Bers, D. M. (2014). Cardiac sarcoplasmic reticulum calcium leak: basis and roles in cardiac dysfunction. *Annual review of physiology*, 76:107–27.

[18] Bezprozvanny, I., Watras, J., and Ehrlich, B. E. (1991). Bell-shaped calcium-response curves of Ins(1,4,5)P_3- and calcium-gated channels from endoplasmic reticulum of cerebellum. *Nature*, 351:751–754.

[19] Boittin, F.-X., Macrez, N., Halet, G., and Mironneau, J. (1999). Norepinephrine-induced Ca^{2+} waves depend on InsP_3 and ryanodine receptor activation in vascular myocytes. *American Journal of Physiology - Cell Physiology*, 277(in mM):139–151.

[20] Bolton, B. Y. T. B., Lang, R. J., and Takewaki, T. (1984). Mechanisms of Action of Noradrenaline and Carbachol on Smooth Muscle of Guinea-pig anterior Mesentric Artery. *Journal of Physiology*, 351:549–572.

[21] Bootman, M. D., Rietdorf, K., Collins, T., Walker, S., and Sanderson, M. (2013). *Ca^{2+}-sensitive fluorescent dyes and intracellular Ca^{2+} imaging*. Cold Spring Harbor Protocol.

[22] Bovo, E., Mazurek, S. R., Blatter, L. A., and Zima, A. V. (2011). Regulation of sarcoplasmic reticulum Ca^{2+} leak by cytosolic Ca^{2+} in rabbit ventricular myocytes. *The Journal of physiology*, 589(Pt 24):6039–50.

[23] Brini, M. and Carafoli, E. (2011). The plasma membrane Ca^{2+} ATPase and the plasma membrane sodium calcium exchanger cooperate in the regulation of cell calcium. *Cold Spring Harbor perspectives in biology*, 3(2).

[24] Brink, P. R., Ricotta, J., and Christ, G. J. (2000). Biophysical characteristics of gap junctions in vascular wall cells: implications for vascular biology and disease. *Brazilian Journal of Medical and Biological Research*, 33:415–422.

[25] Brink, P. R., Valiunas, V., Wang, H. Z., Zhao, W., Davies, K., and Christ, G. J. (2006). Experimental diabetes alters connexin43 derived gap junction permeability in short-term cultures of rat corporeal vascular smooth muscle cells. *Journal of Urology*, 175(1):381–386.

[26] Brisset, A. C., Isakson, B. E., and Kwak, B. R. (2009). Connexins in vascular physiology and pathology. *Antioxidants & redox signaling*, 11(2):267–282.

[27] Callendera, H. L., Horn, M. A., DeCamp, D. L., C, S. P., and Brown, H. A. (2010). Modeling Species-Specific Diacylglycerol Dynamics in the RAW 264.7 Macrophage. *Journal of Theorytical Biololgy*, 262(4):679–690.

[28] Chen, Y., An, H., Li, T., Liu, Y., Gao, C., Guo, P., Zhang, H., and Zhan, Y. (2011). Direct or indirect regulation of calcium-activated chloride channel by calcium. *Journal of Membrane Biology*, 240(3):121–129.

[29] Christ, G. J., Spray, D. C., El-Sabban, M., Moore, L. K., and Brink, P. R. (1996). Gap junctions in vascular tissues. Evaluating the role of intercellular communication in the modulation of vasomotor tone. *Circulation Research*, 79:631–646.

[30] Clair, C., Chalumeau, C., Tordjmann, T., Poggioli, J., Erneux, C., Dupont, G., and Combettes, L. (2001). Investigation of the roles of ca(2+) and insp(3) diffusion in the

coordination of ca(2+) signals between connected hepatocytes. *Journal of cell science*, 114:1999–2007.

[31] Cox, R. H., Lozinskaya, I., and Dietz, N. J. (2001). Differences in K+ Current Components in Mesenteric Artery Myocytes From WKY and SHR. *American Journal of Hypertension*, pages 897–907.

[32] Creager, M. a., Lüscher, T. F., Cosentino, F., and Beckman, J. a. (2003). Diabetes and vascular disease. Pathophysiology, clinical consequences, and medical therapy: Part I. *Circulation*, 108(12):1527–1532.

[33] Datta, B. N. (2010). *Numerical Linear Algebra and Applications*, page 162. SIAM.

[34] Davis, M. J. and Hill, M. A. (1999). Signaling Mechanisms Underlying the Vascular Myogenic Response. *Physiological Reviews*, 79(2).

[35] Demir, S. S., Clark, J. W., R., M. C., and R., G. W. (1994). A mathematical model of a rabbit sinoatrial node. *American Journal of Physiology - Cell Physiology*, 266:C832–C852.

[36] Dhein, S. (1998). Gap junction channels in the cardiovascular system: Pharmacological and physiological modulation. *Trends in pharmacological sciences*, 19(6):229–241.

[37] Diep, H. K., Vigmond, E. J., Segal, S. S., and Welsh, D. G. (2005). Defining electrical communication in skeletal muscle resistance arteries: a computational approach. *The Journal of physiology*, 568(Pt 1):267–281.

[38] Dietrich, A., Mederos, M., Gross, V., Storch, U., Obst, M., Yildirim, E., Salanova, B., Kalwa, H., Essin, K., Pinkenburg, O., Friedrich, C., Gudermann, T., Birnbaumer, L., Dietrich, A., Mederos, M., Gollasch, M., Gross, V., Storch, U., Dubrovska, G., Obst, M., Yildirim, E., Salanova, B., Kalwa, H., Essin, K., Pinkenburg, O., Luft, F. C., Gudermann, T., and Birnbaumer, L. (2005). Increased Vascular Smooth Muscle Contractility in TRPC6$^{-/-}$ Mice. *Molecular and Cellular Boilogy*, 25:6980 – 6989.

[39] Dietrich, H. H. (1989). Effect of locally applied epinephrine and norepinephrine on blood flow and diameter in capillaries of rat mesentery. *Microvascular Research*, 38(2):125–135.

[40] Duling, B. R. and Berne, R. M. (1970). Propagated Vasodilation in the Microcirculation of the Hamster Cheek Pouch. *Circulation Research*, 26(2):163–170.

[41] Eggermont, J. a., Wuytack, F., Verbist, J., and Casteels, R. (1990). Expression of endoplasmic-reticulum Ca2(+)-pump isoforms and of phospholamban in pig smooth-muscle tissues. *The Biochemical journal*, 271(3):649–53.

[42] Emerson, G. G. and Segal, S. S. (2000). Electrical coupling between endothelial cells and smooth muscle cells in hamster feed arteries: role in vasomotor control. *Circulation research*, 87:474–479.

[43] Endo, M., Iino, M., and Kobayashi, T. (1989). *Essential Hypertension 2*, chapter Calcium Mobilization Mechanisms in Smooth Muscle, pages 111–119. Springer Japan, Tokyo.

[44] Esfandiarei, M., Fameli, N., Choi, Y. Y. H., Tehrani, A. Y., Hoskins, J. G., and van Breemen, C. (2013). Waves of Calcium Depletion in the Sarcoplasmic Reticulum of Vascular Smooth Muscle Cells: An Inside View of Spatiotemporal Ca2+ Regulation. *PLoS ONE*, 8(2).

[45] Ewart, M.-A., Kennedy, S., MacMillan, D., Raja, A. L., Watt, I. M., and Currie, S. (2014). Altered vascular smooth muscle function in the ApoE knockout mouse during the progression of atherosclerosis. *Atherosclerosis*, 234:154–161.

[46] Faries, P. L., Rohan, D. I., Takahara, H., Wyers, M. C., Contreras, M. A., Quist, W. C., King, G. L., and Logerfo, F. W. (2001). Human vascular smooth muscle cells of diabetic origin exhibit increased proliferation, adhesion, and migration. *Journal of vascular surgery : official publication, the Society for Vascular Surgery [and] International Society for Cardiovascular Surgery, North American Chapter*, 33:601–607.

[47] Figueroa, X. F., Isakson, B. E., and Duling, B. R. (2013). Connexins : Gaps in Our Knowledge of Vascular Function Connexins : Gaps in Our Knowledge of Wall : The Processes. *Physiology*, 19:277–284.

[48] for the Diabetes Study, N. Z. S. (2010). Diabetes. http://www.nzssd.org.nz/education/diabetes.html.

[49] Franzini-Armstrong, C. and Protasi, F. (1997). Ryanodine receptors of striated muscles: a complex channel capable of multiple interactions. *Physiological Reviews*, 77(3):699–729.

[50] Furukawa, K.-I., Tawada-Iwata, Y., and Shigekawa, M. (1989). Modulation of plasma membrane ca2+ pump by membrane potential in cultured vascular smooth muscle cells. *Journal of Biochemistry*, 106(6):1068–1073.

[51] Ghanim, U., Peter, J., and Cornell-Bell, A. H. (2006). Anti-phase calcium oscillations in astrocytes via inositol (1, 4, 5)-trisphosphate regeneration. *Cell Calcium*, 39:197–208.

[52] Goldbeter, A., Dupont, G., and Berridge, M. J. (1990). Minimal model for signal-induced Ca^{2+} oscillations and for their frequency encoding through protein phosphorylation. *Proceedings of the National Academy of Sciences of the United States of America*, 87(4):1461–5.

[53] Gordienko, D. V. and Bolton, T. B. (2002). Crosstalk between ryanodine receptors and IP3 receptors as a factor shaping spontaneous Ca^{2+}-release events in rabbit portal vein myocytes. *The Journal of Physiology*, 542(3):743–762.

[54] Gu, H., Ek-Vitorin, J. F., Taffet, S. M., and Delmar, M. (2000). Coexpression of Connexins 40 and 43 Enhances the pH Sensitivity of Gap Junctions : A Model for Synergistic Interactions Among Connexins. *Circulation Research*, 86(10):e98–e103.

[55] Guibert, C., Marthan, R., and Savineau, J. P. (1996). Angiotensin II-induced Ca(2+)-oscillations in vascular myocytes from the rat pulmonary artery. *The American journal of physiology*, 270(4):637–642.

[56] Ha, H., Mi Ra Yu, and Hi Bahl Lee (2001). High glucose-induced PKC activation mediates TGF-β1 and fibronectin synthesis by peritoneal mesothelial cells. *Kidney International*, 59(2):463–470.

[57] Haddock, R. E. and Hill, C. E. (2002). Differential activation of ion channels by inositol 1,4,5-trisphosphate (IP3)- and ryanodine-sensitive calcium stores in rat basilar artery vasomotion. *The Journal of Physiology*, 545(2):615–627.

[58] Haefliger, J., Nicod, P., and Meda, P. (2004). Contribution of connexins to the function of the vascular wall. *Cardiovascular research*, 62(2):345–356.

[59] Hakim, C. H., Jackson, W. F., and Segal, S. S. (2008). Connexin isoform expression in smooth muscle cells and endothelial cells of hamster cheek pouch arterioles and retractor feed arteries. *Microcirculation (New York, N.Y. : 1994)*, 15:503–514.

[60] Halidi, N., Boittin, F.-X., Bény, J.-L., and Meister, J.-J. (2011). Propagation of fast and slow intercellular Ca(2+) waves in primary cultured arterial smooth muscle cells. *Cell calcium*, 50(5):459–67.

[61] Hamada, H., Damron, D. S., Hong, S. J., Van Wagoner, D. R., and Murray, P. A. (1997). Phenylephrine-induced Ca^{2+} oscillations in canine pulmonary artery smooth muscle cells. *Circulation research*, 81(5):812–823.

[62] Harder, D. R. and Sperelakis, N. (1978). Membrane electrical properties of vascular smooth muscle from the guinea pig superior mesenteric artery. *Pflugers Archiv European Journal of Physiology*, 378(2):111–119.

[63] Helliwell, R. M. and Large, W. A. (1997). tz1-Adrenoceptor activation of a non-selective cation current in rabbit portal vein by 1,2-diacyl-*sn*-glycerol. *Journal of Physiology*, pages 417–428.

[64] Hisayama, T. and Takayanagi, I. (1988). Ryanodine: its possible mechanism of action in the caffeine-sensitive calcium store of smooth muscle. *Pfl{ü}gers Archiv*, 412(4):376–381.

[65] Hodgkin, A. L. and Huxley, A. F. (1952). A quantitative description of membrane current and its application to conduction and excitation in nerve. *Journal of Physiology*, 117:500–544.

[66] Höfer, T., Venance, L., and Giaume, C. (2002). Control and plasticity of intercellular calcium waves in astrocytes: a modeling approach. *The Journal of neuroscience : the official journal of the Society for Neuroscience*, 22(12):4850–4859.

[67] Hyvelin, J. M., Guibert, C., Marthan, R., and Savineau, J. P. (1998). Cellular mechanisms and role of endothelin-1-induced calcium oscillations in pulmonary arterial myocytes. *The American journal of physiology*, 275(2):L269–L282.

[68] Iino, M. (1990). Biphasic Ca2+ dependence of inositol 1,4,5-trisphosphate-induced Ca release in smooth muscle cells of the guinea pig taenia caeci. *The Journal of general physiology*, 95(6):1103–1122.

[69] Iino, M. and Tsukioka, M. (1994). Feedback control of inositol trisphosphate signalling bycalcium. *Molecular and Cellular Endocrinology*, 98(2):141–146.

[70] Inoguchi, T., Xia, P., Kunisaki, M., Higashi, S., Feener, E. P., and King, G. L. (1994). Insulin{\textquoteright}s effect on protein kinase C and diacylglycerol induced by diabetes and glucose in vascular tissues. *American Journal of Physiology - Endocrinology and Metabolism*, 267(3):E369—-E379.

[71] Inoguchi, T., Yu, H. Y., Imamura, M., Kakimoto, M., Kuroki, T., Maruyama, T., and Nawata, H. (2001). Altered gap junction activity in cardiovascular tissues of diabetes. *Medical Electron Microscopy*, 34(2):86–91.

[72] Inoue, B. Y. R. and Kuriyama, H. (1993). Fukluoka 812,. *Journal of Physiology*, 465:427–448.

[73] Ito, K., Takakura, S., Sato, K., and Sutko, J. L. (1986). Ryanodine inhibits the release of calcium from intracellular stores in guinea pig aortic smooth muscle. *Circ Res*, 58(5):730–734.

[74] JA, B., MA, C., and P, L. (2002). Diabetes and atherosclerosis: Epidemiology, pathophysiology, and management. *The Journal of the American Medical Association*, 287(19):2570–2581.

[75] Jacobsen, J. C. B., Aalkjaer, C., Nilsson, H., Matchkov, V. V., Freiberg, J., and Holstein-Rathlou, N.-H. (2007a). A model of smooth muscle cell synchronization in the arterial wall. *American journal of physiology. Heart and circulatory physiology*, 293(1):H229–H237.

[76] Jacobsen, J. C. B., Aalkjaer, C., Nilsson, H., Matchkov, V. V., Freiberg, J., and Holstein-Rathlou, N.-H. (2007b). Activation of a cGMP-sensitive calcium-dependent chloride channel may cause transition from calcium waves to whole cell oscillations in smooth muscle cells. *American journal of physiology. Heart and circulatory physiology*, 293(1):H215–28.

[77] Janiak, R., Wilson, S. M., Montague, S., and Hume, J. R. (2001). Heterogeneity of calcium stores and elementary release events in canine pulmonary arterial smooth muscle cells. *American journal of physiology. Cell physiology*, 280(1):C22–33.

[78] Joshi, C. N., Martin, D. N., Shaver, P., Madamanchi, C., Muller-Borer, B. J., and Tulis, D. a. (2012). Control of vascular smooth muscle cell growth by connexin 43. *Frontiers in Physiology*, 3 JUN(June):1–13.

[79] Jung, S., Strotmann, R., Schultz, G., and Plant, T. D. (2002). TRPC6 is a candidate channel involved in receptor- stimulated cation currents in A7r5 smooth muscle cells. *American Journal of Physiology - Cell Physiology*, 282:347–359.

[80] Kamouchi, M., Fujishima, M., Ito, Y., and Kitamura, K. (1998). Simultaneous activation of Ca(2+)-dependent K+ and Cl- currents by various forms of stimulation in the membrane of smooth muscle cells from the rabbit basilar artery. *Journal of Smooth Muscle Research*, 34:57–68.

[81] Kanaporis, G., Mese, G., Valiuniene, L., White, T. W., Brink, P. R., and V, V. (2008). Gap junction channels exhibit connexin-specific permeability to cyclic nucleotides. *Journal of General Physiology*, 131:293–305.

[82] Kang, M. and Othmer, H. G. (2007). The variety of cytosolic calcium responses and possible roles of PLC and PKC. *Physical biology*, 4(4):325–343.

[83] Kapela, A., Bezerianos, A., and Tsoukias, N. M. (2008). A mathematical model of Ca2+ dynamics in rat mesenteric smooth muscle cell: agonist and NO stimulation. *Journal of theoretical biology*, 253(2):238–260.

[84] Kapela, A., Bezerianos, A., and Tsoukias, N. M. (2009). A mathematical model of vasoreactivity in rat mesenteric arterioles: I. Myoendothelial communication. *Microcirculation*, 16:694–713.

[85] Kapela, A., Nagaraja, S., and Tsoukias, N. M. (2010). A mathematical model of vasoreactivity in rat mesenteric arterioles. II. Conducted vasoreactivity. *American journal of physiology. Heart and circulatory physiology*, 298(1):H52–H65.

[86] Kaznacheyeva, E., Lupu, V. D., and Bezprozvanny, I. (1998). Single-Channel Properties of Inositol (1,4,5)-Trisphosphate Receptor Heterologously Expressed in HEK-293 Cells. *Journal of General Physiology*, 111(June):847–856.

[87] Keener, J. and Sneyd, J. (2009). *Mathematical Physiology, 1. Cellular Physiology*, chapter 2, pages 54–55. Springer.

[88] Kim, H. W., Cho, Y. S., Lee, H. R., Park, S. Y., and Kim, Y. H. (2001). Diabetic alterations in cardiac sarcoplasmic reticulum Ca2+-ATPase and phospholamban protein expression. *Life Sciences*, 70(4):367–379.

[89] Koenigsberger, M., Sauser, R., Lamboley, M., Bény, J.-L., and Meister, J. (2004). Ca2+ dynamics in a population of smooth muscle cells: modeling the recruitment and synchronization. *Biophysical journal*, 87(1):92–104.

[90] Koenigsberger, M., Seppey, D., Bény, J.-L., and Meister, J.-J. (2010). Mechanisms of propagation of intercellular calcium waves in arterial smooth muscle cells. *Biophysical journal*, 99(2):333–43.

[91] Koivumäki, J. T., Takalo, J., Korhonen, T., Tavi, P., and Weckström, M. (2009). Modelling sarcoplasmic reticulum calcium ATPase and its regulation in cardiac myocytes. *Philosophical transactions. Series A, Mathematical, physical, and engineering sciences*, 367(1896):2181–202.

[92] Kuroki, T., Inoguchi, T., Umeda, F., Ueda, F., and Nawata, H. (1998). High glucose induces alteration of gap junction permeability and phosphorylation of connexin-43 in cultured aortic smooth muscle cells. *Diabetes*, 47(6):931–936.

[93] Kuruma, A. and Hartzell, H. C. (2000). Bimodal control of a Ca2+-activated Cl channel by different Ca2+ signals. *The Journal of General Physiology*, 115(1):59–80.

[94] Kwak, B. R. (2002). Altered Pattern of Vascular Connexin Expression in Atherosclerotic Plaques. *Arteriosclerosis, Thrombosis, and Vascular Biology*, 22(2):225–230.

[95] Lamboley, M., Schuster, A., Bény, J., and Meister, J. (2003). Recruitment of smooth muscle cells and arterial vasomotion. *American journal of physiology. Heart and circulatory physiology*, 285(2):H562–H569.

[96] Landsberg, J. W. and Yuan, J. X.-J. (2004). Calcium and TRP Channels in Pulmonary Vascular Smooth Muscle Cell Proliferation. *News in Physiological Sciences*, 19:44–50.

[97] Large, W. A. and Wang, Q. (1996). Characteristics and physiological role of the Ca(2+)-activated Cl- conductance in smooth muscle. *American Journal of Physiology - Cell Physiology*, 271:C435–C454.

[98] Larissa, L., Lahouaria, H., Jose, J. L., Roger, J. H., and Regis, B. (2013). Benefit of SERCA2a Gene Transfer to Vascular Endothelial and Smooth Muscle Cells: A New Aspect in Therapy of Cardiovascular Diseases. *Current Vascular Pharmacology*, 11:465–479.

[99] Leijten, P., Saida, K., and van Breemen, C. (1985). Norepinephrine-induced intracellular Ca^{2+} release from vascular smooth muscle. *Journal of Cardiovascular Pharmacology*, 7:S38–S42.

[100] Lemon, G., Brockhausen, J., Li, G.-H., Gibson, W. G., and Bennett, M. R. (2005). Calcium mobilization and spontaneous transient outward current characteristics upon agonist activation of P2Y2 receptors in smooth muscle cells. *Biophysical Journal*, 88(3):1507–23.

[101] Lemon, G., Gibson, W., and Bennett, M. (2003). Metabotropic receptor activation, desensitization and sequestration-I: modelling calcium and inositol 1,4,5-trisphosphate dynamics following receptor activation. *Journal of Theoretical Biology*, 223(1):93–111.

[102] Lewis, T. W. and Larry, R. J. (1983). Specific binding of the calcium antagonist [^{3}H]Nitrendipine to subcellular fractions isolated from canine myocardium. *The Journal of Biological Chemistry*, 258:5344–5347.

[103] Li, A. F., Sato, T., Haimovici, R., Okamoto, T., and Roy, S. (2003). High Glucose Alters Connexin 43 Expression and Gap Junction Intercellular Communication Activity in Retinal Pericytes. *Investigative Ophthalmology and Visual Science*, 44(12):5376–5382.

[104] Li, C., Wang, X., Vais, H., Thompson, C. B., Foskett, J. K., and White, C. (2007). Apoptosis regulation by Bcl-x(L) modulation of mammalian inositol 1,4,5-trisphosphate receptor channel isoform gating. *Proceedings of the National Academy of Sciences of the United States of America*, 104(30):12565–12570.

[105] Li, H., TeLe´maque, S., Miller, R. E., and Marsh, J. D. (2005). High Glucose Inhibits Apoptosis Induced by Serum Deprivation in Vascular Smooth Muscle Cells via. *Diabetes*, 54(February):540–545.

[106] Lipskaia, L., Del Monte, F., Capiod, T., Yacoubi, S., Hadri, L., Hours, M., Hajjar, R. J., and Lompré, A. M. (2005). Sarco/endoplasmic reticulum Ca2+-ATPase gene transfer reduces vascular smooth muscle cell proliferation and neointima formation in the rat. *Circulation Research*, 97:488–495.

[107] Lipskaia, L., Limon, I., Bobe, R., and Hajjar, R. (2012). *Calcium Cycling in Synthetic and Contractile Phasic or Tonic Vascular Smooth Muscle Cells. In Current Basic and Pathological Approaches to the Function of Muscle Cells and Tissues - From Molecules to Humans*, chapter 2, pages 27–43. InTech.

[108] Lompre, A. M. (1998). The sarco(endo)plasmic reticulum Ca2+-ATPases in the cardiovascular system during growth and proliferation. *Trends in Cardiovascular Medicine*, 8(2):75–82.

[109] Ma, L., Zhu, B., Chen, X., Liu, J., Guan, Y., and Ren, J. (2008). Abnormalities of sarcoplasmic reticulum Ca2+ mobilization in aortic smooth muscle cells from streptozotocin-induced diabetic rats. *Clinical and Experimental Pharmacology and Physiology*, 35:568–573.

[110] MacMillan, D., Chalmers, S., Muir, T. C., and McCarron, J. G. (2005). IP3-mediated Ca2+ increases do not involve the ryanodine receptor, but ryanodine receptor antagonists reduce IP3-mediated Ca2+ increases in guinea-pig colonic smooth muscle cells. *The Journal of physiology*, 569(Pt 2):533–44.

[111] Mangialavori, I., Ferreira-Gomes, M., Pignataro, M. F., Strehler, E. E., and Rossi, J. P. F. C. (2010). Determination of the dissociation constants for Ca2+ and calmodulin from the plasma membrane Ca2+ pump by a lipid probe that senses membrane domain changes. *The Journal of biological chemistry*, 285(1):123–30.

[112] Mascagni, M. (1990). The Backward Euler Method for Numerical Solution of the Hodgkin-Huxley Equations of Nerve Conduction. *SIAM Journal on Numerical Analysis*, 27(4):941–962.

[113] Massaeli, H., Austria, J. A., and Pierce, G. N. (1999). Chronic exposure of smooth muscle cells to minimally oxidized LDL results in depressed inositol 1,4,5-trisphosphate receptor density and Ca(2+) transients. *Circulation research*, 85:515–523.

[114] Matchkov, V. V., Aalkjaer, C., and Nilsson, H. (2004). A cyclic GMP-dependent calcium-activated chloride current in smooth-muscle cells from rat mesenteric resistance arteries. *The Journal of general physiology*, 123(2):121–34.

[115] McCarron, J. G., Bradley, K. N., MacMillan, D., and Muir, T. C. (2003). Sarcolemma agonist-induced interactions between InsP3 and ryanodine receptors in Ca2+ oscillations and waves in smooth muscle. *Biochemical Society Transactions*, 31:920–924.

[116] Mccarron, J. G., Crichton, C. A., Langton, P. D., Mackenzie, A., and Smith, G. L. (1997). Myogenic contraction by modulation of voltage-dependent calcium currents in isolated rat cerebral arteries. *Journal of Physiology*, pages 371–379.

[117] McCarron, J. G. and Olson, M. L. (2008). A single luminally continuous sarcoplasmic reticulum with apparently separate Ca2+ stores in smooth muscle. *The Journal of biological chemistry*, 283(11):7206–18.

[118] McGowan, T. A. and Sharma, K. (2000). Regulation of inositol 1,4,5-trisphosphate receptors by transforming growth factor-beta: implications for vascular dysfunction in diabetes. *Kidney International Supplements*, 77:S99–S103.

[119] McVeigh, G. E., Brennan, G. M., D, J. G., J, M. B., T, M. L., R, H. W., W, A. J., and R, H. J. (1992). Impaired endothelium-dependent and independent vasodilation in patients with type 2 (non-insulin-dependent) diabetes mellitus. *Diabetologia*, 35:771–776.

[120] Meyer, T. and Stryer, L. (1988). Molecular model for receptor-stimulated calcium spiking. *Proceedings of the National Academy of Sciences of the United States of America*, 85(July):5051–5055.

[121] Miura, Y. and Kimura, J. (1989). Sodium-Calcium Exchange Current Dependence on Internal Ca and Na and Competitive Binding of External Na and Ca. *The Journal of General Physiology*, 93(June):1129–1145.

[122] Monteith, G. R. and Roufogalis, B. D. (1995). The plasma membrane calcium pump - a physiological perspective on its regulation. *Cell Calcium*, 18:459–470.

[123] Montero, D., Walther, G., Pérez-Martin, A., Vicente-Salar, N., Roche, E., and Vinet, A. (2013). Vascular smooth muscle function in type 2 diabetes mellitus: A systematic review and meta-analysis. *Diabetologia*, 56(10):2122–2133.

[124] Moosmang, S., Schulla, V., Welling, A., Feil, R., Feil, S., Wegener, E. W., Hofmann, F., and Klugbauer, N. (2003). Dominant role of smooth muscle L-type calcium channel Ca_v 1.2 for blood pressure regulation. *The EMBO Journal*, 22(22):6027–6034.

[125] Moreno, a. P., Sáez, J. C., Fishman, G. I., and Spray, D. C. (1994). Human connexin43 gap junction channels. Regulation of unitary conductances by phosphorylation. *Circulation research*, 74:1050–1057.

[126] Nabel, E. G., Berk, B. C., Brock, T. a., and Smith, T. W. (1988). Na+-Ca2+ exchange in cultured vascular smooth muscle cells. *Circulation Research*, 62(3):486–493.

[127] Ni, Y.-L., Kuan, A.-S., and Chen, T.-Y. (2014). Activation and inhibition of TMEM16A calcium-activated chloride channels. *PloS one*, 9(1):e86734.

[128] Nicholls, J. A., Greenwell, J. R., and Gillespie, J. I. (1995). Agonist concentration influences the pattern and time course of intracellular Ca^{2+} oscillations in human arterial smooth muscle cells. *Pflüg. Arch.*, 429:477–484.

[129] Nikitina, E., Zhang, Z.-D., Kawashima, A., Jahromi, B. S., Bouryi, V. a., Takahashi, M., Xie, A., and Macdonald, R. L. (2007). Voltage-dependent calcium channels of dog basilar artery. *The Journal of physiology*, 580(Pt. 2):523–41.

[130] Nygren, a., Olson, M. L., Chen, K. Y., Emmett, T., Kargacin, G., and Shimoni, Y. (2007). Propagation of the cardiac impulse in the diabetic rat heart: reduced conduction reserve. *The Journal of physiology*, 580(Pt. 2):543–60.

[131] Organization, W. H. (2014). Fact sheet - Diabetes. http://www.who.int/mediacentre/factsheets/fs312/en/.

[132] Osada, Yoshihito; Okuzaki, Hidenori; Hori, H. (1992). © 19 9 2 Nature Publishing Group. *Nature*, 355:242–244.

[133] Pacaud, P. and Loirand, G. (1995). Release of Ca2+ by noradrenaline and ATP from the same Ca2+ store sensitive to both InsP3 and Ca2+ in rat portal vein myocytes. *Journal of Physiology*, 484(3):549–555.

[134] Park, W. S., Son, Y. K., Kim, N., Youm, J. B., Warda, M., Ko, J.-H., Ko, E. a., Kang, S. H., Kim, E., Earm, Y. E., and Han, J. (2007). Direct modulation of Ca(2+)-activated K(+) current by H-89 in rabbit coronary arterial smooth muscle cells. *Vascular Pharmacology*, 46(2):105–13.

[135] Parthimos, D., Edwards, D. H., and Griffith, T. M. (1999). Minimal model of arterial chaos generated by coupled intracellular and membrane Ca2 + oscillators. *American Journal of Physiology Heart and Circulatory Physiology*, 277:H1119–H1144.

[136] Perez, J. F. and Sanderson, M. J. (2005). The contraction of smooth muscle cells of intrapulmonary arterioles is determined by the frequency of Ca2+ oscillations induced by 5-HT and KCl. *The Journal of general physiology*, 125(June):555–567.

[137] Periasamy, M. and Huke, S. (2001). SERCA pump level is a critical determinant of Ca(2+)homeostasis and cardiac contractility. *Journal of molecular and cellular cardiology*, 33(6):1053–63.

[138] Pfaffman, M. A., Ball, C. R., Darby, A., and Hilman, R. (1982). Insulin reversal of diabetes-induced inhibition of vascular contractility in the rat. *American Journal of Physiology*, 242(4):H490–H495.

[139] Picht, E., Zima, A. V., Shannon, T. R., Duncan, A. M., Blatter, L. a., and Bers, D. M. (2011). Dynamic calcium movement inside cardiac sarcoplasmic reticulum during release. *Circulation research*, 108(7):847–56.

[140] Pollock, N. S., Kargacin, M. E., and Kargacin, G. J. (1998). Chloride channel blockers inhibit Ca2+ uptake by the smooth muscle sarcoplasmic reticulum. *Biophysical journal*, 75(4):1759–66.

[141] Purvis, J. E., Chatterjee, M. S., Brass, L. F., and Diamond, S. L. (2008). Amolecular signaling model of platelet phosphoinositide and calcium regulation during homeostasis and $P2Y_1$ activation. *Blood*, 112(10):4069–4079.

[142] Rainbow, R. D., Macmillan, D., and McCarron, J. G. (2009). The sarcoplasmic reticulum Ca2+ store arrangement in vascular smooth muscle. *Cell calcium*, 46(5-6):313–22.

[143] Reeves, J. P. and Hale, C. C. (1984). The Stoichiometry of the Cardiac Sodium-Calcium Exchange System. *The Journal of Biological Chemistry*, 2(12):7733–7739.

[144] Regis, B., Lahouaria, H., Jose, J. L., Yassine, S., Fabrice, A., Ioannis, K., Lifan, L., Isabelle, L., Anne-Marie, L., Stephane, N. H., Roger, J. H., and Lipskaia, L. (2011). SERCA2a controls the mode of agonist-induced intracellular Ca^{2+} signal, transcription factor NFAT and proliferation in human vascular smooth muscle cells. *Journal of Molecular and Cellular Cardiology*, 50:621–633.

[145] Rempe, M. J. and Chopp, D. L. (2006). A Predictor-Corrector Algorithm for Reaction-Diffusion Equations Associated with Neural Activity on Branched Structures. *SIAM Journal of Scientific Computing*, 28(6):2139–2161.

[146] Rueda, A., Fernández-Velasco, M., Benitah, J.-P., and Gómez, A. M. (2013). Abnormal Ca2+ spark/STOC coupling in cerebral artery smooth muscle cells of obese type 2 diabetic mice. *PloS one*, 8(1):e53321.

[147] Ruehlmann, D. O., Lee, C. H., Poburko, D., and van Breemen, C. (2000). Asynchronous Ca(2+) waves in intact venous smooth muscle. *Circulation research*, 86:E72–E79.

[148] Ruiz, E. (2006). Human Vascular Smooth Muscle Cells From Diabetic Patients Are Resistant to Induced Apoptosis Due to High Bcl-2 Expression. *Diabetes*, 55(5):1243–1251.

[149] Sakuma, H., Yamamoto, M., Okumura, M., Kojima, T., Maruyama, T., and Yasuda, K. (2002). High glucose inhibits apoptosis in human coronary artery smooth muscle cells by increasing bcl-xL and bfl-1/A1. *Am J Physiol Cell Physiol*, 283(2):C422–428.

[150] Sanders, K. M. (2001). Mechanisms of calcium handling in smooth muscles. *Journal of Applied Physiology*, 91:1438–1449.

[151] Scherberich, a., Campos-Toimil, M., Rondé, P., Takeda, K., and Beretz, a. (2000). Migration of human vascular smooth muscle cells involves serum-dependent repeated cytosolic calcium transients. *Journal of cell science*, 113 (Pt 4):653–662.

[152] Schroeder, B. C., Cheng, T., Jan, Y. N., and Jan, L. Y. (2008). Expression Cloning of TMEM16A as a Calcium-Activated Chloride Channel Subunit. *Cell*, 134:1019–1029.

[153] Schuster, A., Lamboley, M., Grange, C., and Oishi, H. (2004). Calcium Dynamics and Vasomotion in Rat Mesenteric Arteries. *Journal of Cardiovascular Pharmacology*, 43(4):539–548.

[154] Searls, Y. M., Loganathan, R., Smirnova, I. V., and Stehno-Bittel, L. (2010). Intracellular Ca2+ regulating proteins in vascular smooth muscle cells are altered with type 1 diabetes due to the direct effects of hyperglycemia. *Cardiovascular diabetology*, 9:8.

[155] Segal, S. S. and Duling, B. R. (1989). Conduction of vasomotor responses in arterioles: a role for cell-to-cell coupling? *American Journal of Physiology - Heart and Circulatory Physiology*, 256(3):H838—-H845.

[156] Segal, S. S., Welsh, D. G., and Kurjiaka, D. T. (1999). Spread of vasodilatation and vasoconstriction along feed arteries and arterioles of hamster skeletal muscle. *The Journal of physiology*, 516 (Pt 1:283–291.

[157] Seppey, D., Sauser, R., Koenigsberger, M., Bény, J., and Meister, J. (2010). Intercellular calcium waves are associated with the propagation of vasomotion along arterial strips. *American journal of physiology. Heart and circulatory physiology*, 298(2):H488–96.

[158] Seppey, D., Sauser, R., Koenigsberger, M., Beny, J. L., and Meister, J. J. (2008). Does the Endothelium Abolish or Promote Arterial Vasomotion in Rat Mesenteric Arteries? Explanations for the Seemingly Contradictory Effects. *Journal of Vascular Research*, 45(5):416–426.

[159] Severs, N. J., Rothery, S., Dupont, E., Coppen, S. R., Yeh, H. I., Ko, Y. S., Matsushita, T., Kaba, R., and Halliday, D. (2001). Immunocytochemical analysis of connexin expression in the healthy and diseased cardiovascular system. *Microscopy research and technique*, 52(3):301–322.

[160] Shaikh, M. a., Wall, D. J. N., and David, T. (2012). Macro-scale phenomena of arterial coupled cells: a massively parallel simulation. *Journal of The Royal Society Interface*, 9(70):972–987.

[161] Sharma, K., Deelman, L., Madesh, M., Kurz, B., Ciccone, E., Siva, S., Hu, T., Zhu, Y., Wang, L., Henning, R., Ma, X., and Hajnoczky, G. (2003). Involvement of transforming growth factor-beta in regulation of calcium transients in diabetic vascular smooth muscle cells. *American journal of physiology. Renal physiology*, 285(6):F1258–F1270.

[162] Sharma, K., Wang, L. W., Zhu, Y. Q., Bokkala, S., and Joseph, S. K. (1997). Transforming growth factor-beta 1 inhibits type I inositol 1,4,5-trisphosphate receptor expression and enhances its phosphorylation in mesangial cells. *J Biol Chem*, 272(23):14617–14623.

[163] Shmigol, A. V., Eisner, D. A., and Wray, S. (2001). Simultaneous measurements of changes in sarcoplasmic reticulum and cytosolic [Ca 2 +] in rat uterine smooth muscle cells. *Journal of Physiology*, 531:707–713.

[164] Shuai, J. W., Yang, D. P., Pearson, J. E., and Rüdiger, S. (2009). An investigation of models of the IP3 R channel in Xenopus oocyte. *Chaos*, 19(3):1–11.

[165] Smaili, S., Hirata, H., Ureshino, R., Monteforte, P. T., Morales, A. P., Muler, M. L., Terashima, J., Oseki, K., Rosenstock, T. R., Lopes, G. S., and Bincoletto, C. (2009).

Calcium and cell death signaling in neurodegeneration and aging. *Anais da Academia Brasileira de Ciencias*, 81:467–475.

[166] Soboloff, J., Spassova, M., Xu, W., He, L.-P., Cuesta, N., and Gill, D. L. (2005). Role of Endogenous TRPC6 Channels in Ca^{2+} Signal Generation in A7r5 Smooth Muscle Cells. *Journal of Biological Chemistry*, 280:39786–39794.

[167] Somlyo, a. V., Bond, M., Somlyo, a. P., and Scarpa, a. (1985). Inositol trisphosphate-induced calcium release and contraction in vascular smooth muscle. *Proceedings of the National Academy of Sciences of the United States of America*, 82(August):5231–5235.

[168] Suematsu, E., Hirata, M., Hashimoto, T., and Kuriyama, H. (1984). Inositol 1,4,5-trisphosphate releases Ca2+ from intracellular store sites in skinned single cells of porcine coronary artery. *Biochemical and Biophysical Research Communications*, 120(2):481–485.

[169] Swaminathan, D. (2010). *Mathematical Modeling of Intracellular Calcium Signaling: A Study of IP_3 Receptor Models*. PhD thesis, The College of Arts and Sciences of Ohio University.

[170] Swaminathan, D., Ullah, G., and Jung, P. (2009). A simple sequential-binding model for calcium puffs. *Chaos (Woodbury, N.Y.)*, 19(3):037109.

[171] Tabit, C. E., Chung, W. B., and Vita, J. a. (2010). Endothelial dysfungtion in diabetes mellitus : Molecular mechanisms and clinical implications. *Rev endocrine metabolism disorder*, 11(1):61–74.

[172] Taufiq-Ur-Rahman, Skupin, A., Falcke, M., and Taylor, C. W. (2009). Clustering of InsP3 receptors by InsP3 retunes their regulation by InsP3 and Ca2+. *Nature*, 458(7238):655–9.

[173] Thomas, S. A., Schuessler, R. B., Berul, C. I., Beardslee, M. A., Beyer, E. C., Mendelsohn, M. E., and Saffitz, J. E. (1998). Disparate Effects of Deficient Expression of Connexin43 on Atrial and Ventricular Conduction Evidence for Chamber-Specific Molecular Determinants of Conduction. *Circulation*, 97:686–691.

[174] Tribe, R. M., Borin, M. L., and Blaustein, M. P. (1994). Functionally and spatially distinct Ca2+ stores are revealed in cultured vascular smooth muscle cells. *Proceedings of the National Academy of Sciences of the United States of America*, 91(13):5908–5912.

[175] Tsien, R. Y. (1980). New calcium indicators and buffers with high selectivity against magnesium and protons: design, synthesis, and properties of prototype structures. *Biochemistry*, 19(11):2396–2404.

[176] Tsoukias, N. M. (2011). Calcium dynamics and signaling in vascular regulation: computational models. *Wiley interdisciplinary reviews*, 3:93–106.

[177] Tumelty, J., Hinds, K., Bankhead, P., McGeown, N. J., Scholfield, C. N., Curtis, T. M., and McGeown, J. G. (2011). Endothelin 1 stimulates Ca2+-sparks and oscillations in retinal arteriolar myocytes via IP3R and RyR-dependent Ca2+ release. *Investigative ophthalmology & visual science*, 52(6):3874–3879.

[178] Ureña, J., Smani, T., and López-Barneo, J. (2004). Differential functional properties of Ca2+ stores in pulmonary arterial conduit and resistance myocytes. *Cell Calcium*, 36(6):525–534.

[179] Valiunas, V., Beyer, E. C., and Brink, P. R. (2002). Cardiac gap junction channels show quantitative differences in selectivity. *Circulation Research*, 91(2):104–111.

[180] Vallot, O., Combettes, L., Jourdon, P., Inamo, J., Marty, I., Claret, M., and Lompré, A.-M. (2000). Intracellular Ca(2+) handling in vascular smooth muscle cells is affected by proliferation. *Arteriosclerosis, thrombosis, and vascular biology*, 20:1225–1235.

[181] van Kempen, M. J. and Jongsma, H. J. (1999). Distribution of connexin37, connexin40 and connexin43 in the aorta and coronary artery of several mammals. *Histochemistry and cell biology*, 112(6):479–86.

[182] Velmurugan, G. V. and White, C. (2012). Calcium homeostasis in vascular smooth muscle cells is altered in type 2 diabetes by Bcl-2 protein modulation of InsP3R calcium release channels. *Am J Physiol Heart Circ Physiol*, 302(1):H124–H134.

[183] Wan, E., Kushner, J. S., Zakharov, S., Nui, X.-W., Chudasama, N., Kelly, C., Waase, M., Doshi, D., Liu, G., Iwata, S., Shiomi, T., Katchman, A., D'Armiento, J., Homma, S., and Marx, S. O. (2013). Reduced vascular smooth muscle BK channel current underlies heart failure-induced vasoconstriction in mice. *FASEB journal : official publication of the Federation of American Societies for Experimental Biology*, 27(5):1859–67.

[184] Wang, Y., Chen, J., Wang, Y., Taylor, C. W., Hirata, Y., Hagiwara, H., Mikoshiba, K., Toyo-oka, T., Omata, M., and Sakaki, Y. (2001). Crucial Role of Type 1, but Not Type 3, Inositol 1,4,5-Trisphosphate (IP_3) Receptors in IP_3-Induced Ca_{2+} Release, Capacitative

Ca_{2+} Entry, and Proliferation of A7r5 Vascular Smooth Muscle Cells. *Circulation Research*, pages 202–209.

[185] Watras, J., Bezprozvanny, I., and Ehrlich, B. E. (1991). Inositol 1,4,5-Trisphosphate-gated Channels in Cerebellum: Presence of Multiple Conductance States. *The Journal of Neuroscience*, 11(October):3239–3245.

[186] Weber, C. R., Ginsburg, K. S., Philipson, K. D., Shannon, T. R., and Bers, D. M. (2001). Allosteric Regulation of Na / Ca Exchange Current by Cytosolic Ca in Intact Cardiac Myocytes. *American Journal of Physiology - Cell Physiology*, 117(February).

[187] Weber, P. A., Chang, H.-c., Spaeth, K. E., Nitsche, J. M., and Nicholson, B. J. (2004). The Permeability of Gap Junction Channels to Probes of Different Size Is Dependent on Connexin Composition and Permeant-Pore Affinities. *Biophysical Journal*, 87(August):958–973.

[188] Welsh, D. G. and Segal, S. S. (1998). Endothelial and smooth muscle cell conduction in arterioles controlling blood flow. *American Journal of Physiology - Heart and Circulatory Physiology*, 274(1):H178—-H186.

[189] White, C. R., Elton, T. S., Shoemaker, R. L., and Brock, T. A. (1995). Calcium-sensitive chloride channels in vascular smooth muscle cells. *Proc Soc Exp Biol Med*, 208:255–262.

[190] Wilkerson, M. K., Heppner, T. J., Bonev, A. D., Nelson, M. T., and Keith, M. (2006). Inositol trisphosphate receptor calcium release is required for cerebral artery smooth muscle cell proliferation. *The American Journal of Physiology - Heart and Circulatory Physiology*, pages 240–247.

[191] Wimsatt, D. K., Hohl, C. M., Brierley, G. P., and Altschuld, R. A. (1990). Calcium accumulation and release by the sarcoplasmic reticulum of digitonin-lysed adult mammalian ventricular cardiomyocytes. *Journal of Biological Chemistry*, 265(25):14849–14857.

[192] Wong, A. Y. and Klassen, G. A. (1993). A model of calcium regulation in smooth muscle cell. *Cell Calcium*, 14:227–243.

[193] Wong, A. Y. and Klassen, G. A. (1996). Mechanisms underlying spontaneous rhythmical contractions in irideal arterioles of the rat. *Annals of Biomedical Engineering*, 24:547–560.

[194] Wray, S. and Burdyga, T. (2010). Sarcoplasmic Reticulum Function in Smooth Muscle. *Physiological Review*, 90:113–178.

[195] Wu, K. D., Bungard, D., and Lytton, J. (2001). Regulation of SERCA Ca2+ pump expression by cytoplasmic Ca2+ in vascular smooth muscle cells. *American journal of physiology. Cell physiology*, 280:C843–C851.

[196] X, L. and M, F. J. (1996). Acetylcholine-induced Ca++-dependent chloride current oscillations are mediated by inositol 1,4,5-trisphosphate in tracheal myocytes. *Journal of Pharmacology and Experimental Therapeutics*, 277:796–804.

[197] Yang, J., Clark, J. W., Bryan, R. M., and Robertson, C. (2003). The myogenic response in isolated rat cerebrovascular arteries: smooth muscle cell model. *Medical Engineering & Physics*, 25(8):691–709.

[198] Yang, J., Clark, J. W., Bryan, R. M., and Robertson, C. S. (2005). Mathematical modeling of the nitric oxide/cGMP pathway in the vascular smooth muscle cell. *American journal of physiology. Heart and circulatory physiology*, 289(April 2005):H886–H897.

[199] Yang, Y., Li, P.-Y., Cheng, J., Mao, L., Wen, J., Tan, X.-Q., Liu, Z.-F., and Zeng, X.-R. (2013). Function of BKCa channels is reduced in human vascular smooth muscle cells from Han Chinese patients with hypertension. *Hypertension*, 61(2):519–25.

[200] Young, S. H., Ennes, H. S., and Mayer, E. A. (1996). Propagation of calcium waves between colonic smooth muscle cells in culture. *Cell Calcium*, 20:257–271.

[201] Zhu, Z., Tepel, M., Neusser, M., and Zidek, W. (1995). Transforming growth factor $\beta 1$ modulates angiotensin induced calcium influx in vascular smooth muscle. *European Journal of Clinical Investigation*, 25(5):317–321.

[202] Zima, A. V., Bovo, E., Bers, D. M., and Blatter, L. A. (2010). Ca^{2+} spark-dependent and -independent sarcoplasmic reticulum Ca^{2+} leak in normal and failing rabbit ventricular myocytes. *The Journal of physiology*, 588(Pt 23):4743–57.

Appendix A

Methodologies of mathematical modelling in cell physiology

Hodgkin and Huxley [65] had published their famous work on initiation and propagation of neuronal action potential. From then, mathematical modelling emerged as an important research tool in cell physiology. The development of high-speed digital computers has shifted the application of mathematical modelling from a single/many cell system to millions of cells or a full organ. A mathematical model of a cell is a system of ordinary differential equations to show the change of system variables over time. The differential equations are used to represent subcellular processes inside a cell. These processes are modelled based on appropriate kinetic laws such as the law of mass action for stoichiometric reactions and Michaelis-Menten and Hill equations for enzyme-substrate reactions. Transport of molecule/ion species due to concentration gradients and electric gradients are modelled using Ficks law of diffusion, the Nernst equation and the Nernst-Plank equation. Mass balance is used to account for the transport of molecule/ion species across the boundaries. All the above-mentioned modelling approaches are explained below in detail.

A.1 Law of mass action

According to the law of mass action, the rate of a chemical reaction is proportional to the product of masses of the reactants. For a stoichiometric reversible reaction of the following type,

$$\mathrm{aA} + \mathrm{bB} \underset{\mathrm{k^-}}{\overset{\mathrm{k^+}}{\rightleftharpoons}} \mathrm{cC} + \mathrm{dD} \tag{A.1}$$

The law of mass action for forward and backward reactions can be written as,

$$r_f = k^+[A]^a[B]^b \tag{A.2}$$

$$r_b = k^-[C]^c[D]^d \tag{A.3}$$

where k^+ and k^- are rate constants for forward and backward reactions. The equilibrium constant of the reversible reaction equals,

$$K = \frac{[C]^c[D]^d}{[A]^a[B]^b} \tag{A.4}$$

The commonly used unit of concentration of chemical species is moles per litre (mol/L). The unit of K depends on the order of the reaction.

A.2 Enzyme-substrate reaction

A.2.1 Michaelis-Menten equation

The Michaelis-Menten equation describes the rate of an enzymatic reaction using the concentration of the substrate, S. For the following enzyme-substrate reaction,

$$E + S \underset{k^-}{\overset{k^+}{\rightleftharpoons}} ES \xrightarrow{k^{cat}} E + P \tag{A.5}$$

the Michaelis-Menten equation for rate of product formation is written as,

$$\frac{d[P]}{dt} = V_{MAX}\frac{[S]}{K_M + [S]} \tag{A.6}$$

Where E represents enzyme, P represents product and ES represents enzyme-substrate complex. k^{cat} is the rate constant of enzyme-substrate conversion into a product and the enzyme.

The rate of product formation increases as the substrate concentration increases and reaches a maximum at a higher substrate concentration. V_{MAX} is the maximum possible reation rate. According to Equation A.6, the Michaelis constant, K_M, is the substrate concentration at which the reaction rate equals half-maximum.

A.2.2 Hill equation

The Hill equation is commonly used for quantifying the cooperative binding of a ligand to a receptor. If the binding of a ligand to a receptor is related to the concentration of the ligand in a non-linear manner, it is called cooperative binding. There are basically two types of cooperative bindings, positive and negative cooperativities. In the case of positive cooperative binding, if a ligand molecule binds to the receptor, the affinity of the receptor to bind next ligand molecule increases. This process continues untill all the binding sites of the receptor are bound to the ligand molecules. If the binding of a ligand molecule to the receptor reduces the affinity of the receptor to bind with another ligand molecule, it is called negative cooperativity.

The Hill equation helps us to find the fraction of ligand-bound sites on the receptors in the system. The general form of the Hill equation is given below,

$$\theta = \frac{[\mathrm{Ld}]^n}{K_d + [\mathrm{Ld}]^n} = \frac{[\mathrm{Ld}]^n}{[\mathrm{K_A}]^n + [\mathrm{Ld}]^n} \tag{A.7}$$

Where [Ld] is the concentration of ligand, n is the Hill coefficient, K_d is the rate constant of dissociation and K_A is the ligand concentration at which half of the binding sites are occupied. For positive cooperative binding, N is greater than 1 whereas N is smaller than 1 for negative cooperative binding. N equal to 1 indicates noncooperative binding, which means that the affinity of the receptor to bind to a ligand molecule is independent of the presence of any previously bound ligand on the receptor.

A.3 Diffusion of a molecule or an ion

A.3.1 Ficks law of diffusion

According to Fick's law of diffusion, movement of molecules from a high concentration region to a low concentration region is driven by a concentration gradient. The law states that the flux of the molecule, moles per unit area per second, is proportional to the spatial concentration gradient. For a one-dimensional problem, Fick's law of diffusion is written as,

$$J = -D\frac{dc}{dx} \tag{A.8}$$

Where c is the concentration of the molecule in moles per unit volume, D is the diffusion coefficient in unit area per unit time, x is the position and J is the molecular flux in moles per unit area per unit time.

A.3.2 Nernst-Plank equation

Indifferent to molecules, movement of an ion depends on the electric potential gradient in addition to the concentration gradient. The Nernst-Plank equation describes the motion of an ion under the influence of both a concentration gradient and an electric potential gradient. The steady state form of the Nernst-Plank equation for a one-dimensional problem is given below,

$$J = -D\left[\frac{dc}{dx} + \frac{Fzc}{RT}\frac{d\phi}{dx}\right] \tag{A.9}$$

Where F is Faraday's constant, R is the universal gas constant, T is temperature, z is valency of the ion and ϕ is the electric field. The second term of the equation represents the influence of the electric field on the movement of an ion. For a molecule, only the first term exists.

A.3.3 Nernst equation

The Nernst equation describes the distribution of an ion at electrochemical equilibrium between two compartments separated by a membrane. The membrane channels allow the passage of the ion of interest through it. The passage of ions across the membrane develops a potential difference across the membrane. The potential gradient grows in magnitude until it balances the concentration gradient. The ion is in electrochemical equilibrium when the potential gradient and concentration gradient are equal in magnitude. The membrane potential developed at electrochemical equilibrium is called equilibrium potential or Nernst potential.

When a membrane separates a particular type of ions, total chemical potential of the ions in the intracellular space equals,

$$\mu_i = \mu_0 + RTln[\text{ion}]_i + zFV_0 \tag{A.10}$$

Similarly, for the chemical potential of the ions in the extracellular space,

$$\mu_e = \mu_0 + RTln[\text{ion}]_e + zFV_i \tag{A.11}$$

At electrochemical equilibrium, the chemical potential of the ions in the intracellular and in the extracellular spaces are equal. Therefore,

$$\mu_0 + RTln[\text{ion}]_i + zFV_i = \mu_0 + RTln[\text{ion}]_e + zFV_0 \tag{A.12}$$

Simplying and rearranging Equation A.12 yields,

$$zF\,(V_i - V_0) = RTln\frac{[\text{ion}]_e}{[\text{ion}]_i} \tag{A.13}$$

Potential difference between the intracellular and extracellular compartments is defined as the membrane potential, V_m. Substituting V_m into Equation A.13, and solving for V_m, we get the Nernst equation,

$$V_m = \frac{RT}{zF}ln\frac{[\text{ion}]_e}{[\text{ion}]_i} \tag{A.14}$$

A.3.4 Goldman-Hodgkin-Katz (GHK) equation

The Goldman-Hodgkin-Katz (GHK) equation is used to determine the ionic flux across a cell membrane. It accounts for the contributions of transmembrane potential and concentration gradient to the ionic flux. The GHK equation is derived by assuming a constant electric field across a membrane [87]. Consider a case where a membrane with a thickness of L separates two solutions, named extracellular and intracellular solutions. The concentration of an ion, S, in the extracellular and intracellular solutions equal c_e and c_i respectively. If the electric potential difference across the membrane is V and constant electric field is assumed, then the term $\frac{d\phi}{dx}$ becomes $\frac{-V}{L}$.

At steady state and with no production of ions, ionic flux across the membrane is constant. We can rewrite the Nernst-Plank equation, (refer to Equation A.9), for this case as follows,

$$\frac{dc}{dx} - \frac{zFV}{RTL}c + \frac{J}{D} = 0 \tag{A.15}$$

The solution of this equation is,

$$J = \frac{D}{L}\frac{zFV}{RT}\frac{c_i - c_e Exp\left(\frac{-zFV}{RT}\right)}{1 - Exp\left(\frac{-zFV}{RT}\right)} \tag{A.16}$$

If we multiply Equation A.16 with zF, we will get an equation for ionic current density which is the famous GHK current equation.

$$I = \frac{D}{L}\frac{z^2F^2V}{RT}\frac{c_i - c_e Exp\left(\frac{-zFV}{RT}\right)}{1 - Exp\left(\frac{-zFV}{RT}\right)} \tag{A.17}$$

A.4 Mass balance

Mass balance is another form of conservation of mass based on the principle that, mass is neither created nor destroyed in a closed system. Mass balance is applied to physical systems such as a cell to calculate changes in concentration of a particular chemical species in the system by accounting for material entering the the system, material leaving the system, material generation and consumption within the system. A general form of a mass balance equation for a reactive system is as follows,

$$\text{Input} + \text{Generation} = \text{Output} + \text{Accumulation} + \text{Consumption} \tag{A.18}$$

Accumulation is the rate change of the material. For example, consider the calcium concentration balance of a cell as shown in the figure,

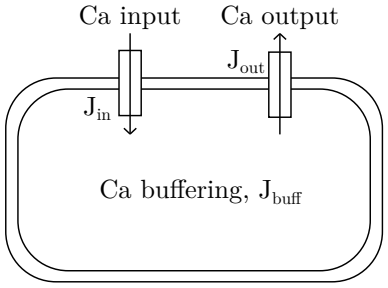

Fig. A.1 Mass balance in a simple cell system:

$$\frac{dCa}{dt} = J_{\text{in}} - J_{\text{out}} + J_{\text{buff}} \tag{A.19}$$

The channels, pumps and exchangers are the main membrane components that contribute to the calcium influx and calcium outflux. The release of calcium through these channels depends on the conductance and permeability of each membrane component as well as the concentration gradient and electric potential gradient across the cell membrane.

A.5 Whole cell current of a channel

In general, the whole cell current of a channel that allows the passage of a particular ion is,

$$I_k = N_k g_k P_k (V_m - E_{\text{ion}}) \tag{A.20}$$

Where N_k is the total number of channels, g_k is the conductance of a single channel, P_k is the open probability of the channel, E_{ion} is the Nernst potential of the ion and V_m is the membrane potential or the potential gradient across the membrane. g_k is constant unless there is extreme voltage dependent blocking or asymmetric conditions. Therefore, G of a particular channel is constant and is equal to N_k g_k. However, open probability of a channel is highly modulated by different cellular changes which result in a highly non-linear behaviour of the ionic current.

A.6 Open probability of an ion channel

A channel protein contains a pore which is guarded by a single gate or several gates. Gating of an ion channel represents the opening or closing of the channel pore. Different cellular components regulate the gating of a channel. The main gating mechanisms are,

- **Voltage gating:** The opening of voltage-gated channels depend on the membrane potential of the cell. The most common voltage-gated channels are voltage-operated calcium channels, and calcium-activated potassium channels.
- **Secondary messenger gating:** In some ion channels of the cell, the opening is regulated by secondary messengers. Calcium, inositol triphosphate (IP_3) and diacylglycerol

(DAG) are some of such secondary messengers. Calcium-activated potassium channels, IP_3 receptor (IP_3R) channels, Ryanodine (RyR) receptor channels and calcium-activated chloride channels (CACC) are the most common calcium-gated channels. IP_3R channels and non-selective cation (NSC) channels are gated by IP_3 and DAG respectively.

In general, an ion channel exists in one of two states; open state or closed state. The dynamic existence of these states depends on the kinetic behaviour of the chemical phenomenon between the two states of the channel. A simple model of the channel gating is shown below,

$$\mathrm{X_0} \underset{\mathrm{k^-}}{\overset{\mathrm{k^+}}{\rightleftharpoons}} \mathrm{X_1} \tag{A.21}$$

where 'X_0' represents closed state and 'X_1' represents open state. The fraction of total channels in the open state, f_1, is defined as,

$$f_1 = \frac{N_{X_1}}{N_{X_1} + N_{X_0}} \tag{A.22}$$

Where N_{X_1} is the number of channels in the open state and N_{X_0} is the number of channels in the closed state. Differentiate Equation A.22 with respect to time, we get,

$$\frac{df_1}{dt} = \frac{1}{N}\frac{dN_{X_1}}{dt} \tag{A.23}$$

Where N is the total number of channels. Applying the law of mass action to Equation A.21 and substituting that in Equation A.23, we obtain,

$$\frac{df_1}{dt} = \frac{1}{N}\left(k^+ N_{X_0} - k^- N_{X_1}\right) \tag{A.24}$$

$$= \left(k^+ + k^-\right)\left(\frac{k^+}{(k^+ + k^-)} - f_1\right) \tag{A.25}$$

Let,

$$\tau = \frac{1}{k^+ + k^-};\ f_\alpha = \frac{k^+}{k^+ + k^-} \tag{A.26}$$

Equation A.25 becomes,

$$\frac{d\mathrm{f_1}}{dt} = \frac{\mathrm{f}_\alpha - \mathrm{f_1}}{\tau} \tag{A.27}$$

Where τ is the time constant and f_α is the equilibrium open probability of the channel. These two functions may depend on the other cellular components. The values of these two variables are obtained from experiments.

A.7 Hodgkin-Huxley model

The Hodgkin-Huxley model is a continuous time model which describes the initiation and propagation of an action potential in excitable cells such as neurons and cardiac myocytes. In this model, an excitable cell is treated as an electrical circuit in which each component of the cell is an electrical component, (see Figure A.2). The lipid bilayer is represented as a membrane capacitor. Each channel in the membrane is represented as a fixed resistor or variable resistor. Voltage-gated channels are treated as variable resistors whereas a leak channel is treated as a fixed resistor.

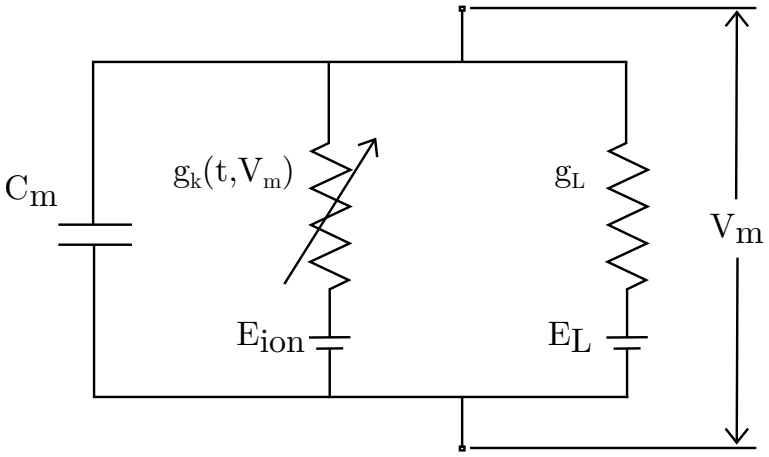

Fig. A.2 Hodgkin-Huxley model

Ohm's law is used to calculate the current flowing through each channel, which is driven by the voltage difference,

$$I_k = g_k(V_m - E_{ion}) \tag{A.28}$$

$$I_L = g_L(V_m - E_L) \tag{A.29}$$

Where g_k is the variable conductance of the channel, 'k', which allows the passage of a specific ion. E_{ion} is the Nernst potential of that specific ion. g_L and E_L are the conductance and Nernst potential of the leak channel.

The following mathematical equation is used to describe the total current passing through the membrane,

$$I = C_m \frac{dV_m}{dt} + I_k + I_L \tag{A.30}$$

Where I is the total membrane current. C_m and V_m are the conductance and membrane potential of the cell, respectively. By rearranging equation A.30, we get,

$$\frac{dV_m}{dt} = \frac{1}{C_m}(I - I_k - I_L) \tag{A.31}$$

If we know the current passing through each channel, pump and exchanger present in the membrane, we can use Equation A.31 to find the temporal variation in membrane potential of the cell.

Appendix B

Numerical methods used

B.1 Backward Euler discretization

Discretization is used to convert a continuous function to a discrete function. To determine a discrete function, we have to discretize the time domain into N evenly spaced points. The time difference between two points is called the time step or step size, Δt. Now, we have to use a discrete method for getting a discrete version of the ordinary differential equation (ODE) under consideration.

In the current study, we have used Backward Euler to discretize the ODEs of the model. Consider an ODE,

$$\frac{dy}{dt} = f(t,y) \quad y(t=0) = y_0 \tag{B.1}$$

A Backward Euler approximation of the equation B.1 gives,

$$\frac{y(t+\Delta t) - y(t)}{\Delta t} = f\left(t+\Delta t, y(t+\Delta t)\right) \tag{B.2}$$

$$y(t+\Delta t) = y(t) + \Delta t f\left(t+\Delta t, y(t+\Delta t)\right) \tag{B.3}$$

The discretized function is unknown as it depends on the future value of y. We have to solve an algebraic equation or fixed point iteration if the discrete function is non-linear.

B.2 Fixed-point iteration

To find the solution of the discretized Equation B.3, a fixed-point iteration method is used on the model. Each iterative step is denoted by superscript 'k'. To start the fixed point iteration, an approximation of the solution for the first iteration is taken as the initial value or previous time converged solution. For fixed-point iteration,

$$y^k(t+\Delta t) = y(t) + \Delta t f\left(t+\Delta t, y^{k-1}(t+\Delta t)\right) \tag{B.4}$$

For the first iteration,

$$y^1(t+\Delta t) = y(t) + \Delta t f\left(t+\Delta t, y(t)\right) \tag{B.5}$$

A tolerance limit is fixed to define the convergence of the fixed-point iteration. The converged value $y^k(t+\Delta t)$ is taken as the solution at t+Δt, $y(t+\Delta t)$.

B.3 Tridiagonal Matrix algorithm or Thomas algorithm

A tridiagonal matrix algorithm (TDMA) is an efficient way of solving tridiagonal matrices. This method is based on the LU decomposition. For the matrix system, MY=D, the system is rewritten as LUY=D, where A is a coefficient matrix, D is a constant matrix, U is an upper triangular matrix and L is a lower triangular matrix.

A TDMA is implemented in two steps. In the first step, the matrix M is decomposed into M=LU and solved for ρ using Lρ=D in a single forward sweep. In the second step, y is solved using the equation UY=ρ in the backward sweep. For example, consider a system of equations, My=D, as below,

$$\begin{bmatrix} b_1 & c_1 & 0 \\ a_2 & b_2 & c_2 \\ 0 & a_3 & b_3 \end{bmatrix} \begin{bmatrix} y_1 \\ y_2 \\ y_3 \end{bmatrix} = \begin{bmatrix} d_1 \\ d_2 \\ d_3 \end{bmatrix}$$

Take the first row and divide it by b_1,

$$y_1 + \frac{c_1}{b_1} y_2 = \frac{d_1}{b_1} \tag{B.6}$$

This can be written as,

$$y_1 + \gamma_1 y_2 = \rho_1, \quad \gamma_1 = \frac{c_1}{b_1}, \rho_1 = \frac{d_1}{b_1} \tag{B.7}$$

Similarly, take the second row,

$$a_2 y_2 + b_2 y_2 + c_2 y_3 = d_2 \tag{B.8}$$

Substracting Equation $a_2 \times$ B.7 from Equation B.8, we get,

$$(b_2 - a_2\gamma_1)\, y_2 + c_2 y_3 = d_2 - a_2\rho_1 \tag{B.9}$$

Divide Equation B.9 by $(b_2 - a_2\gamma_1)$,

$$y_2 + \frac{c_2}{b_2 - a_2\gamma_1} y_3 = \frac{d_2 - a_2\rho_1}{b_2 - a_2\gamma_1} \tag{B.10}$$

We can write the above equation as,

$$y_2 + \gamma_2 y_3 = \rho_2, \quad \gamma_2 = \frac{c_2}{b_2 - a_2\gamma_1}, \rho_2 = \frac{d_2 - a_2\rho_1}{b_2 - a_2\gamma_1} \tag{B.11}$$

Finally, take the third row,

$$a_3 y_2 + b_3 y_3 = d_3 \tag{B.12}$$

Substract Equation $a_3 \times$ B.11 from Equation B.12, we get,

$$(b_3 - a_3\gamma_2)\, y_3 = d_3 - a_3\rho_2 \tag{B.13}$$

Divide Equation B.13 by $(b_3 - a_3\gamma_2)$, we get,

$$y_3 = \frac{d_3 - a_3\rho_2}{(b_3 - a_3\gamma_2)} \tag{B.14}$$

This can be written as,

$$y_3 = \rho_3 \quad \rho_3 = \frac{d_3 - a_3\rho_2}{(b_3 - a_3\gamma_2)} \tag{B.15}$$

Here, we have finished the first step and the matrix is converted into the form UY=ρ as given below,

$$\begin{bmatrix} 1 & \gamma_1 & 0 \\ 0 & 1 & \gamma_2 \\ 0 & 0 & 1 \end{bmatrix} \begin{bmatrix} y_1 \\ y_2 \\ y_3 \end{bmatrix} = \begin{bmatrix} \rho_1 \\ \rho_2 \\ \rho_3 \end{bmatrix}$$

Now the solution of the matrix UY=D is straightforward. The solution is calculated in the second step of a backward sweep. We will start with the last row.

$$y_3 = \rho_3 \tag{B.16}$$

Substitute the value of y_3 in Equation B.11 and solve for y_2,

$$y_2 = \rho_2 - \gamma_2 x_3 \tag{B.17}$$

Similarly for y_1 by substituting y_2 in to Equation B.7,

$$y_1 = \rho_1 - \gamma_1 x_2 \tag{B.18}$$

This is the end of the TDMA as full solution of the problem is obtained. TDMA is stable if, the matrix form of the discretized ODEs in the model satisfy the condition of stability:

$$|b_i| > |a_i| + |c_i| \tag{B.19}$$

Appendix C

Discretization

The Backward Euler method is used to discretize the differential equations of 16 state variables.

1) For the membrane potential, V_m, the discretized equation is given as,

$$\begin{aligned} C_m \frac{V_m^{t+\Delta t} - V_m^t}{\Delta t} = & -G_{BK_{Ca}} P_{BK_{Ca}}^{t+\Delta t} \left(V_m^{t+\Delta t} - E_K \right) - G_{VOCC} d_L^{t+\Delta t} f_L^{t+\Delta t} \left(V_m^{t+\Delta t} - E_{Ca}^{t+\Delta t} \right) \\ & - G_{NSC} P_{NSC,V_m}^{t+\Delta t} P_{NSC,DAG}^{t+\Delta t} \left(V_m^{t+\Delta t} - E_{NSC} \right) - G_{NCX} P_{NCX,allo}^{t+\Delta t} P_{NCX,elec}^{t+\Delta t} \\ & - G_{CACC} P_{CACC}^{t+\Delta t} \left(V_m^{t+\Delta t} - E_{Cl} \right) - \alpha Q_{PMCA} P_{PMCA}^{t+\Delta t} \end{aligned} \tag{C.1}$$

The $V_m^{t+\Delta t}$ terms are collected together on the left hand side, giving

$$\begin{aligned} & V_m^{t+\Delta t} \left(G_{BK_{Ca}} P_{BK_{Ca}}^{t+\Delta t} + G_{VOCC} d_L^{t+\Delta t} f_L^{t+\Delta t} + G_{NSC} P_{NSC,V_m}^{t+\Delta t} P_{NSC,DAG}^{t+\Delta t} + G_{CACC} P_{CACC}^{t+\Delta t} + \frac{C_m}{\Delta t} \right) \\ & \quad = V_m^t \frac{C_m}{\Delta t} + G_{BK_{Ca}} P_{BK_{Ca}}^{t+\Delta t} E_K + G_{VOCC} d_L^{t+\Delta t} f_L^{t+\Delta t} E_{Ca}^{t+\Delta t} + G_{NSC} P_{NSC,V_m}^{t+\Delta t} P_{NSC,DAG}^{t+\Delta t} E_{NSC} \\ & \quad - G_{NCX} P_{NCX,allo}^{t+\Delta t} P_{NCX,elec}^{t+\Delta t} + G_{CACC} P_{CACC}^{t+\Delta t} E_{Cl} - \alpha Q_{PMCA} P_{PMCA}^{t+\Delta t} \end{aligned} \tag{C.2}$$

In a similar fashion the discretized equations for other variables are written below,

2) For the intracellular calcium, $\left[Ca^{2+}\right]_{cyt}$

$$\begin{aligned}\left[Ca^{2+}\right]_{cyt}^{t+\Delta t}\left(\frac{\rho^{t+\Delta t}Vol_{cyt}}{\Delta t}+Vol_{SR}V_{IP_3R}P_{IP_3R}^{t+\Delta t}+Vol_{SR}Q_{RyR}P_{RyR}^{t+\Delta t}\right)&=\frac{\left[Ca^{2+}\right]_{cyt}^{t}\rho^{t+\Delta t}Vol_{cyt}}{\Delta t}\\&+Vol_{SR}\lambda Exp\left(\frac{\left[Ca^{2+}\right]_{SR}^{t+\Delta t}}{k_{leak}}\right)+Vol_{SR}V_{IP_3R}P_{IP_3R}^{t+\Delta t}\left[Ca^{2+}\right]_{SR}^{t+\Delta t}+Vol_{SR}Q_{RyR}P_{RyR}^{t+\Delta t}\left[Ca^{2+}\right]_{SR}^{t+\Delta t}\\&-Vol_{cyt}Q_{SERCA}P_{SERCA}^{t+\Delta t}+2G_{NCX}P_{NCX,allo}^{t+\Delta t}P_{NCX,elec}^{t+\Delta t}-G_{VOCC}d_L^{t+\Delta t}f_L^{t+\Delta t}\left(V_m^{t+\Delta t}-E_{Ca}^{t+\Delta t}\right)\\&-\alpha Q_{PMCA}P_{PMCA}^{t+\Delta t}\end{aligned}\tag{C.3}$$

3) For the intra-SR calcium, $\left[Ca^{2+}\right]_{SR}$

$$\begin{aligned}\left[Ca^{2+}\right]_{SR}^{t+\Delta t}\left(\frac{1}{\Delta t}+V_{IP_3R}P_{IP_3R}^{t+\Delta t}+Q_{RyR}P_{RyR}^{t+\Delta t}\right)&=\frac{\left[Ca^{2+}\right]_{SR}^{t}}{\Delta t}+\frac{Vol_{cyt}}{Vol_{SR}}Q_{SERCA}P_{SERCA}^{t+\Delta t}\\&-\lambda Exp\left(\frac{\left[Ca^{2+}\right]_{SR}^{t+\Delta t}}{k_{leak}}\right)+V_{IP_3R}P_{IP_3R}^{t+\Delta t}\left[Ca^{2+}\right]_{cyt}^{t+\Delta t}+Q_{RyR}P_{RyR}^{t+\Delta t}\left[Ca^{2+}\right]_{cyt}^{t+\Delta t}\end{aligned}\tag{C.4}$$

4) For the IP_3, $[IP_3]_{cyt}$

$$[IP_3]_{cyt}^{t+\Delta t}\left(\frac{1}{\Delta t}+k_{deg,IP_3}\right)=\frac{[IP_3]_{cyt}^{t}}{\Delta t}+\frac{r_h^{t+\Delta t}}{N_{AV}Vol_{SMC}}PIP_{2,T}\tag{C.5}$$

5) For the DAG, [DAG]

$$[DAG]^{t+\Delta t}\left(\frac{1}{\Delta t}+k_{deg,DAG}\right)=\frac{[DAG]^{t}}{\Delta t}+\frac{r_h^{t+\Delta t}}{N_{AV}Vol_{SMC}}PIP_{2,T}\tag{C.6}$$

6) For the activation variable of the VOCC, d_L

$$d_L^{t+\Delta t}\left(\frac{1}{\Delta t}+\frac{1}{\tau_{d_L}^{t+\Delta t}}\right)=d_L^{t}\left(\frac{1}{\Delta t}\right)+\bar{d_L}^{t+\Delta t}\left(\frac{1}{\tau_{d_L}^{t+\Delta t}}\right)\tag{C.7}$$

7) For the inactivation variable of the VOCC, f_L

$$f_L^{t+\Delta t}\left(\frac{1}{\Delta t}+\frac{1}{\tau_{f_L}^{t+\Delta t}}\right)=f_L^{t}\left(\frac{1}{\Delta t}\right)+\bar{f_L}^{t+\Delta t}\left(\frac{1}{\tau_{f_L}^{t+\Delta t}}\right)\tag{C.8}$$

8) For the fast activation variable of the BK_{Ca} channel, p_f

$$p_f^{t+\Delta t}\left(\frac{1}{\Delta t}+\frac{1}{\tau_{p_f}}\right)=p_f^{t}\left(\frac{1}{\Delta t}\right)+\bar{p_o}^{\,t+\Delta t}\left(\frac{1}{\tau_{p_f}}\right) \tag{C.9}$$

9) For the slow activation variable of the BK_{Ca} channel, p_s

$$p_s^{t+\Delta t}\left(\frac{1}{\Delta t}+\frac{1}{\tau_{p_s}}\right)=p_s^{t}\left(\frac{1}{\Delta t}\right)+\bar{p_o}^{\,t+\Delta t}\left(\frac{1}{\tau_{p_s}}\right) \tag{C.10}$$

10) For the X_{10} state of the IP_3R channel

$$X_{10}^{t+\Delta t}\left(\frac{1}{\Delta t}+a_2\left[Ca^{2+}\right]_{cyt}+b_5\right)=\frac{X_{10}^{t}}{\Delta t}+b_2X_{11}^{t+\Delta t}+a_5\left[Ca^{2+}\right]_{cyt}^{t+\Delta t}\frac{X_{00}^{t+\Delta t}}{1+k_1^{t+\Delta t}} \tag{C.11}$$

11) For the X_{00} state of the IP_3R channel

$$X_{00}^{t+\Delta t}\left(\frac{1}{\Delta t}+\left(a_4k_1^{t+\Delta t}+a_5+a_2\right)\left[Ca^{2+}\right]_{cyt}^{t+\Delta t}\frac{1}{1+k_1^{t+\Delta t}}\right)=\frac{X_{00}^{t}}{\Delta t}+\left(b_4k_3^{t+\Delta t}+b_2\right)\frac{X_{01}^{t+\Delta t}}{1+k_3^{t+\Delta t}}+b_5X_{10}^{t+\Delta t} \tag{C.12}$$

12) For the X_{01} state of the IP_3R channel

$$X_{01}^{t+\Delta t}\left(\frac{1}{\Delta t}+\left(b_4k_3^{t+\Delta t}+b_2+a_5\left[Ca^{2+}\right]_{cyt}^{t+\Delta t}\right)\frac{1}{1+k_3^{t+\Delta t}}\right)=\frac{X_{01}^{t}}{\Delta t}+b_5X_{11}^{t+\Delta t}+\left(a_4k_1^{t+\Delta t}+a_2\right)\left[Ca^{2+}\right]_{cyt}^{t+\Delta t}\frac{X_{00}^{t+\Delta t}}{1+k_1^{t+\Delta t}} \tag{C.13}$$

13) For the R_{10} state of the RyR channel

$$R_{10}^{t+\Delta t}\left(\frac{1}{\Delta t}+K_{-r1}+K_{r2}\left[Ca^{2+}\right]_{cyt}^{t+\Delta t}\right)=\frac{R_{10}^{t}}{\Delta t}+k_{r1}\left(\left[Ca^{2+}\right]_{cyt}^{t+\Delta t}\right)^2R_{00}^{t+\Delta t}+K_{-r2}R_{11}^{t+\Delta t} \tag{C.14}$$

14) For the R_{11} state of the RyR channel

$$R_{11}^{t+\Delta t}\left(\frac{1}{\Delta t}+K_{-r1}+K_{-r2}\right)=\frac{R_{11}^{t}}{\Delta t}+k_{r2}\left[Ca^{2+}\right]_{cyt}^{t+\Delta t}R_{10}^{t+\Delta t}+K_{r1}\left(\left[Ca^{2+}\right]_{cyt}^{t+\Delta t}\right)^2R_{01}^{t+\Delta t} \tag{C.15}$$

15) For the R_{01} state of the RyR channel

$$R_{01}^{t+\Delta t}\left(\frac{1}{\Delta t}+K_{-r2}+K_{r1}\left(\left[Ca^{2+}\right]_{cyt}^{t+\Delta t}\right)^2\right)=\frac{R_{01}^{t}}{\Delta t}+k_{r2}\left[Ca^{2+}\right]_{cyt}^{t+\Delta t}R_{00}^{t+\Delta t}+K_{-r1}R_{11}^{t+\Delta t} \tag{C.16}$$

16) For the G-protein, [GP]

$$GP^{t+\Delta t}\left(\frac{1}{\Delta t}+k_a\left(\delta+\rho_r\right)+k_d\right)=\frac{GP^{t}}{\Delta t}+k_a\left(\delta+\rho_r\right)GP_T \tag{C.17}$$

Unknown terms in the above discretized equations (from different cell components) are given below,

1) VOCC

$$\bar{d_L}^{t+\Delta t}=\frac{1}{1+Exp\left(\frac{V_m^{t+\Delta t}+C_4}{C_5}\right)} \tag{C.18}$$

$$\bar{f_L}^{t+\Delta t}=\frac{1}{1+Exp\left(-\frac{V_m^{t+\Delta t}}{C_3}\right)} \tag{C.19}$$

$$\tau_{d_L}^{t+\Delta t}=2.5Exp\left(-\left(\frac{V_m^{t+\Delta t}+C_6}{C_7}\right)^2\right)+1.15 \tag{C.20}$$

$$\tau_{f_L}^{t+\Delta t}=65Exp\left(-\left(\frac{V_m^{t+\Delta t}+C_8}{C_9}\right)^2\right)+45 \tag{C.21}$$

$$E_{Ca}^{t+\Delta t}=\frac{RT}{z_{Ca}F}ln\left(\frac{\left[Ca^{2+}\right]_e}{\left[Ca^{2+}\right]_{cyt}^{t+\Delta t}}\right) \tag{C.22}$$

2) BK_{Ca} channel

$$P_{BK_{Ca}}^{t+\Delta t} = 0.17 p_f^{t+\Delta t} + 0.83 p_s^{t+\Delta t} \tag{C.23}$$

$$\bar{p_o}^{\,t+\Delta t} = \frac{1}{1 + \mathrm{Exp}\left(-\frac{V_m^{t+\Delta t} - V_{0.5BK_{Ca}}^{t+\Delta t}}{C_1}\right)} \tag{C.24}$$

$$V_{0.5BK_{Ca}}^{t+\Delta t} = -41.7 \log_{10}\left(\left[Ca^{2+}\right]_{cyt}^{t+\Delta t}\right) - C_2 \tag{C.25}$$

3) NSC channel

$$P_{NSC,V_m}^{t+\Delta t} = \frac{1}{1 + \mathrm{Exp}\left(-(V_m^{t+\Delta t} + C_{10})/C_{11}\right)} \tag{C.26}$$

$$P_{NSC,DAG}^{t+\Delta t} = \frac{[DAG]^{t+\Delta t}}{\left([DAG]^{t+\Delta t} + k_{NSC}\right)} \tag{C.27}$$

4) CACC

$$P_{CACC}^{t+\Delta t} = \frac{\left[Ca^{2+}\right]_{cyt,t+\Delta t}^2}{\left[Ca^{2+}\right]_{cyt,t+\Delta t}^2 + k_{CACC}^2} \tag{C.28}$$

5) NCX exchanger

$$P_{NCX,allo}^{t+\Delta t} = \frac{\left[Ca^{2+}\right]_{cyt,t+\Delta t}^2}{\left[Ca^{2+}\right]_{cyt,t+\Delta t}^2 + k_{NCX}^2} \tag{C.29}$$

$$P_{NCX,elec} = \frac{[Na]_{cyt}^3 [Ca]_e \phi_F - [Na]_e^3 \left[Ca^{2+}\right]_{cyt}^{t+\Delta t} \phi_R}{1 + d_{NCX}\left([Na]_e^3 [Ca]_{cyt}^{t+\Delta t} + [Na]_{cyt}^3 [Ca]_e\right)} \tag{C.30}$$

6) PMCA pump

$$P_{PMCA}^{t+\Delta t} = \frac{\left[Ca^{2+}\right]_{cyt}^{t+\Delta t}}{\left[Ca^{2+}\right]_{cyt}^{t+\Delta t} + k_{PMCA}} \tag{C.31}$$

7) IP_3R channel

$$X_{11}^{t+\Delta t} = 1 - X_{01}^{t+\Delta t} - X_{10}^{t+\Delta t} - X_{00}^{t+\Delta t} \tag{C.32}$$

$$P_{IP_3R}^{t+\Delta t} = \left(\left(X_{10}^{t+\Delta t} \right)^4 + 4 \left(X_{10}^{t+\Delta t} \right)^3 \left(1 - X_{10}^{t+\Delta t} \right) \right) \tag{C.33}$$

$$k_j^{t+\Delta t} = \frac{b_j}{a_j \left[IP_3 \right]^{t+\Delta t}}, \quad j=1,2,3 \tag{C.34}$$

8) RyR channel

$$R_{00}^{t+\Delta t} = 1 - R_{01}^{t+\Delta t} - R_{10}^{t+\Delta t} - R_{11}^{t+\Delta t} \tag{C.35}$$

$$P_{RyR}^{t+\Delta t} = \left(R_{10}^{t+\Delta t} \right)^2 \tag{C.36}$$

9) SERCA pump

$$P_{SERCA}^{t+\Delta t} = \left(\frac{\left(\left[Ca^{2+} \right]_{cyt}^{t+\Delta t} \right)^2}{\left(\left[Ca^{2+} \right]_{cyt}^{t+\Delta t} \right)^2 + k_{SERCA}^2} \right) \tag{C.37}$$

10) Cytosol buffering term

$$\rho^{t+\Delta t} = 1 + \frac{B_{CM} k_{CM}}{\left(k_{CM} + \left[Ca^{2+} \right]_{cyt}^{t+\Delta t} \right)^2} + \frac{B_F k_B}{\left(k_B + \left[Ca^{2+} \right]_{cyt}^{t+\Delta t} \right)^2} \tag{C.38}$$

11) G-protein cascade and IP_3 formation

$$\rho_r = \frac{[L]}{k_1 + [L]} \tag{C.39}$$

$$r_h^{t+\Delta t} = \eta \frac{\left[Ca^{2+} \right]_{cyt}^{t+\Delta t}}{\left[Ca^{2+} \right]_{cyt}^{t+\Delta t} + k_c} GP^{t+\Delta t} \tag{C.40}$$

Appendix D

VSMC model: Resting state values

Experimental studies show that intracellular calcium at the resting state is less than or equal to 100 nM [128, 200, 55]. We use this evidence to choose 80 nM in our model (This is done by adjusting PMCA parameters). The studies by Picht et al. [139] and Esfandiarei et al. [44] show that intra-SR calcium concentration at resting state stays in between 1 mM and 1.3 mM. Therefore, we have adjusted the SR leak parameter to obtain a value of 1.2 mM.

$$\left[Ca^{2+}\right]_{cyt} = 80.55 \text{ nM}$$

$$\left[Ca^{2+}\right]_{SR} = 1.2149 \text{ mM}$$

Once intracellular is fixed, the resting state values of the following state variables are calculated using the steady state equations of the corresponding variables.

$$GP = \frac{k_a \delta GP_T}{k_a \delta + k_d},$$

$$[IP_3]_{cyt} = \frac{r_h PIP_{2,T}}{k_{deg,IP_3} N_{AV} Vol_{SMC}},$$

$$[DAG]_{cyt} = \frac{r_h PIP_{2,T}}{k_{deg,DAG} N_{AV} Vol_{SMC}}$$

The resting state values of state variables of RyR and IP_3R channels are obtained by solving their steady state equations given below using the initial values of IP_3 and intracellular

calcium.

For IP_3R,

$$0 = (b_4k_3 + b_2)\frac{X_{01}}{1+k_3} + b_5X_{10} - (a_4k_1 + a_5 + a_2)\left[Ca^{2+}\right]_{cyt}\frac{X_{00}}{1+k_1} \tag{D.1}$$

$$0 = b_2X_{11} + a_5\left[Ca^{2+}\right]_{cyt}\frac{X_{00}}{1+k_1} - \left(a_2\left[Ca^{2+}\right]_{cyt} + b_5\right)X_{10} \tag{D.2}$$

$$0 = (a_4k_1 + a_2)\left[Ca^{2+}\right]_{cyt}\frac{X_{00}}{1+k_1} + b_5X_{11} - \left(b_4k_3 + b_2 + a_5\left[Ca^{2+}\right]_{cyt}\right)\frac{X_{01}}{1+k_3} \tag{D.3}$$

$$X_{11} = 1 - X_{00} - X_{01} - X_{10} \tag{D.4}$$

For RyR,

$$0 = K_{r1}\left[Ca^{2+}\right]_{cyt}^2 R_{00} - \left(K_{-r1} + K_{r2}\left[Ca^{2+}\right]_{cyt}\right)R_{10} + K_{-r2}R_{11} \tag{D.5}$$

$$0 = K_{r2}\left[Ca^{2+}\right]_{cyt}R_{10} - (K_{-r1} + K_{-r2})R_{11} + K_{r1}\left[Ca^{2+}\right]_{cyt}^2 R_{01} \tag{D.6}$$

$$0 = K_{r2}\left[Ca^{2+}\right]_{cyt}R_{00} + K_{-r1}R_{11} - \left(K_{-r2} + K_{r1}\left[Ca^{2+}\right]_{cyt}^2\right)R_{01} \tag{D.7}$$

$$R_{00} = 1 - R_{01} - R_{10} - R_{11} \tag{D.8}$$

Resulting,

$R_{11} = 0.000002, \quad R_{10} = 0.002128, \quad R_{01} = 0.001004, \quad R_{00} = 0.996866,$

$X_{11} = 0.001861, \quad X_{10} = 0.002412, \quad X_{01} = 0.206240, \quad X_{00} = 0.789487$

The initial value of Vm is fixed to -54 mV based on the experimental observation of Harder and Sperelakis [62] in VSMCs of mesenteric artery.

$V_m = -54.03$ mV,

The initial variables of the rest of the state variables are simply the solution of steady state equations,

$$p_f = p_s = \frac{1}{1 + \mathrm{Exp}\left(-\frac{V_m - V_{0.5BK_{Ca}}}{18.25}\right)}$$

$$d_L = \frac{1}{1 + \mathrm{Exp}\left(\frac{V_m + 42}{9.1}\right)}$$

$$f_L = \frac{1}{1 + \mathrm{Exp}\left(-\frac{V_m}{8.3}\right)}$$

Appendix E

VSMC model: Parameters

In the VSMC model, five parameters are referred as model estimation, k_{NSC}, $k_{deg,DAG}$, and k_R.

Swaminathan [169] used 4625 s^{-1} for Q_{IP_3R} and 0.5 mM for intra-SR calcium concentration to obtain calcium puffs lifetimes and amplitudes consistent with the experiments. In our model, intra-SR calcium equals to 1.2 mM at the resting state. A value of 2000 s^{-1} is used for the Q_{IP_3R} in order to account the difference in intra-SR calcium compared with the Swaminathan et al. [170] study.

Kapela et al. [83] used a Michaelis constant of 170 nM whereas Jacobsen et al. [76] used a value of 200 nM. In Jacobsen et al. [76] study, the intracellular calcium at the resting state was 100 nM which is slightly higher than the corresponding value of 80 nM in our model. To account the difference in intracellular concentration compared with the Jacobsen et al. [76] study, Michaelis constant, k_{PMCA}, of 150 nM is used for PMCA. A low value for k_{PMCA} is used to satisfy the experimental observation of the high affinity to calcium and the value is within the range of k_{PMCA} values used in the previous models.

According to Helliwell and Large [63], Soboloff et al. [166], activation of NSC is obtained in micromolar concentrations of oleoyl-2-acetyl-sn-glycerol (OAG), a DAG analogue. Based on these experimental observations, k_{NSC} is fixed to 1 μM. The Kapela et al. [83] model used a DAG activation of the NSC channel. However, the k_{NSC} used in their model is 300 nM which appears small compared to the experiments.

In the case of k_R, Lemon et al. [101] used 5 μM and Kapela et al. [83] used 10 μM. As far as we know, there is no definite value for k_R. In our model, we have adjusted this value to 60 μM, so that calcium oscillations will be obtained at medium agonist concentrations as observed in the experimental studies of Lamboley et al. [95] and Schuster et al. [153].

Kapela et al. [83] used the degradation rate of DAG, $k_{deg,DAG}$, the same as the degradation rate of IP_3, k_{deg,IP_3R}. Kang and Othmer [82] used different degradation rate constants for

DAG and IP_3. In their model, $k_{deg,DAG}$ is smaller than k_{deg,IP_3R}. There is not enough data to choose a value of $k_{deg,DAG}$ independently. Similar to Kang and Othmer [82], we have chosen $k_{deg,DAG}$ to be 1 s^{-1}, smaller than the k_{deg,IP_3R} where a value of 1.25 s^{-1} is chosen.

Table E.1 Standard VSMC parameters

C_m	20 pF	Capacitance
T	293.0 K	Temperature
R	8341.0 mJ mol^{-1} K^{-1}	Universal gas constant
F	96487.0 C mol^{-1}	Faraday's constant
z_{Ca}	2	Calcium valency
z_{Na}	1	Sodium valency
z_K	1	Potassium valency
z_{Cl}	-1	Chloride valency
$\left[Ca^{2+}\right]_e$	2 mM	Extracellular calcium
$\left[Na^{+}\right]_e$	140 mM	Extracellular sodium
$\left[K^{+}\right]_e$	5 mM	Extracellular potassium
$\left[Cl^{-}\right]_e$	129 mM	Extracellular chloride
$\left[K^{+}\right]_{cyt}$	140 mM	Intracellular potassium
$\left[Cl^{-}\right]_{cyt}$	59.4 mM	Intracellular chloride
$\left[Na^{+}\right]_{cyt}$	8.4 mM	Cytosol sodium
Vol_{cyt}	0.7 pL	Cytosol volume [197]
Vol_{SMC}	1 pL	VSMC volume [197]
Vol_{SR}	0.05 pL	SR volume, 5% of the cell volume [194]

Table E.2 Calcium buffering parameters

k_{CM}	260 nM	Dissociation constant of calmodulin	Kapela et al. [83] and Yang et al. [197]
k_B	530 nM	Dissociation constant of other buffers	
B_{CM}	100 μM	Concentration of calmodulin	
$\bar{B}_F$	100 μM	Concentration of other buffers	

Table E.3 Parameters for SR channels and pumps

λ	12 nM s^{-1}	Maximum rate of calcium leak, obtained from intra-SR calcium balance at the resting condition.
k_{leak}	145×10^3 nM	Exponential growth factor, Zima et al. [202]
Q_{SERCA}	210×10^3 nM s^{-1}	Maximum rate of calcium efflux of SERCA, Balke et al. [9]
k_{SERCA}	500 nM	Michaelis constant of SERCA, Wimsatt et al. [191]
Q_{IP_3R}	2000 s^{-1}	Maximum rate, model estimation
Binding constants		Swaminathan et al. [170]
a_1	167.6×10^{-3} $nM^{-1}s^{-1}$	IP_3
a_2	3.81×10^{-3} $nM^{-1}s^{-1}$	Calcium inhibition
a_3	413.4×10^{-3} $nM^{-1}s^{-1}$	IP_3
a_4	0.3101×10^{-3} $nM^{-1}s^{-1}$	Calcium inhibition
a_5	53.9×10^{-3} $nM^{-1}s^{-1}$	Calcium activation
Dissociation constants		Swaminathan et al. [170]
b_1	228 s^{-1}	IP_3
b_2	0.409 s^{-1}	Calcium inhibition
b_3	188.5 s^{-1}	IP_3
b_4	0.096 s^{-1}	Calcium inhibition
b_5	4.52 s^{-1}	Calcium activation
Q_{RyR}	4000 s^{-1}	Maximum rate, model estimation and conductance of RyR is twice higher than that of IP_3R [49].
Binding constants		Yang et al. [197]
K_{r1}	2.5×10^{-6} $nM^{-2}s^{-1}$	Activation rate constant
K_{r2}	1.05×10^{-3} $nM^{-1}s^{-1}$	Inactivation rate constant
K_{-r1}	7.6 s^{-1}	Unbinding rate constant from activation
K_{-r2}	84 s^{-1}	Unbinding rate constant from inactivation

Table E.4 Parameters for alpha-adrenoceptor cascade and IP_3 formation

k_R	60 μM	Unphosphorylated receptor dissociation constant	Model estimation
GP_T	1×10^5	Total number of G-protein molecules	Bennett et al. [15]
k_{deg,IP_3}	1.25 s^{-1}	IP_3 degradation rate	
k_a	0.17 s^{-1}	G-protein activation rate	
k_d	1.5 s^{-1}	G-protein inactivation rate	
$PIP_{2,T}$	5×10^7	Total number of PIP2 molecules	
k_{PLC}	400 nM	Dissociation constant for calcium binding to PLC	
η	2.781×10^{-5} s^{-1}	Effective signal gain parameter	
N_{AV}	6.02252×10^{23} mol^{-1}	Avogadro's constant	
δ	1.235×10^{-3}	G-protein intrinsic activity parameter	Lemon et al. [101]
$k_{deg,DAG}$	1.0 s^{-1}	DAG degradation rate	Model estimation

Table E.5 Parameters for membrane channels, pumps and exchangers

G_{VOCC}	2.63 nS	Whole cell conductance of VOCC, calculated from the whole-cell voltage-current (V-I) relationship reported in Nikitina et al. [129]
$G_{BK_{Ca}}$	11.1 nS	Whole cell conductance of BK_{Ca} channel, obtained by balancing the membrane potential equation at resting condition
τ_{p_f}	0.84 ms	Fast activation time constant, Kapela et al. [83]
τ_{p_s}	35.9 ms	Slow activation time constant, Kapela et al. [83]
$\bar{I}_{NCX}$	0.25×10^{-3} pA	Scaling factor of NCX channel, obtained by adjusting it to get the intracellular calcium concentration within a physiological range of values upon agonist stimulation
k_{NCX}	125 nM	Dissociation constant for allosteric component, Weber et al. [186]
d_{NCX}	0.0003	Kapela et al. [83]
γ	0.45	Kapela et al. [83]
G_{CACC}	2.24 nS	Whole cell conductance of CACC, calculated from the whole cell V-I data published in Matchkov et al. [114]
k_{CACC}	587 nM	Dissociation constant of CACC, Ni et al. [127]
G_{NSC}	0.61 nS	Whole cell conductance of NSC channel, Helliwell and Large [63]
k_{NSC}	1000 nM	Dissociation constant of NSC channel, model estimation
E_{NSC}	9 mV	Reverse potential of NSC channel, Helliwell and Large [63]
Q_{PMCA}	9.993×10^3 nM s^{-1}	Maximum rate of calcium efflux of PMCA, estimated from $\left[Ca^{2+}\right]_{cyt}$ balance at the resting condition.
k_{PMCA}	150 nM	Michaelis constant of PMCA, model estimation

Appendix F

Definition of terms

F.1 Activation and relaxation phases of intracellular oscillations

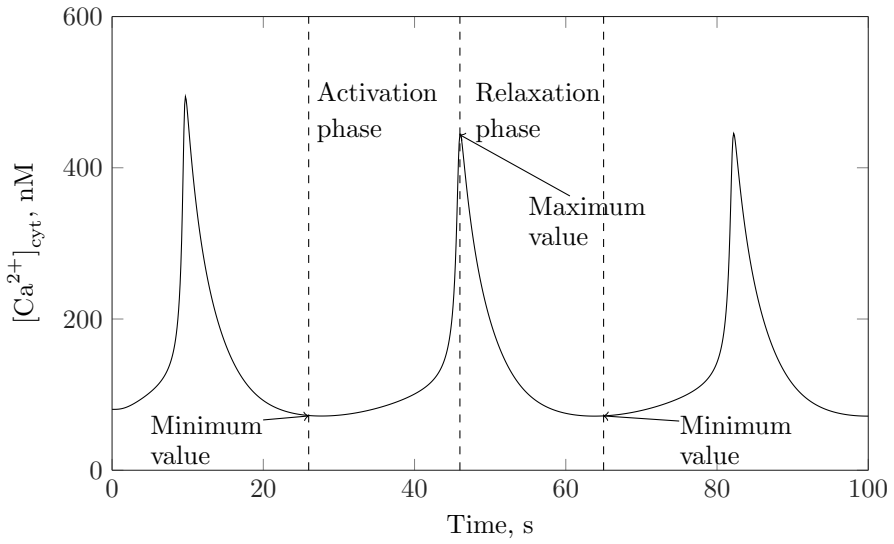

Fig. F.1 Activation and relaxation phases of intracellular calcium oscillations.

The activation phase is defined as the period of time during which the intracellular calcium concentration of the cell increases from the minimum value to the maximum value. Vice-versa, the relaxation phase is the period of time which from the minimum value to the maximum value of intracellular calcium.

F.2 Overall maximum and overall minimum

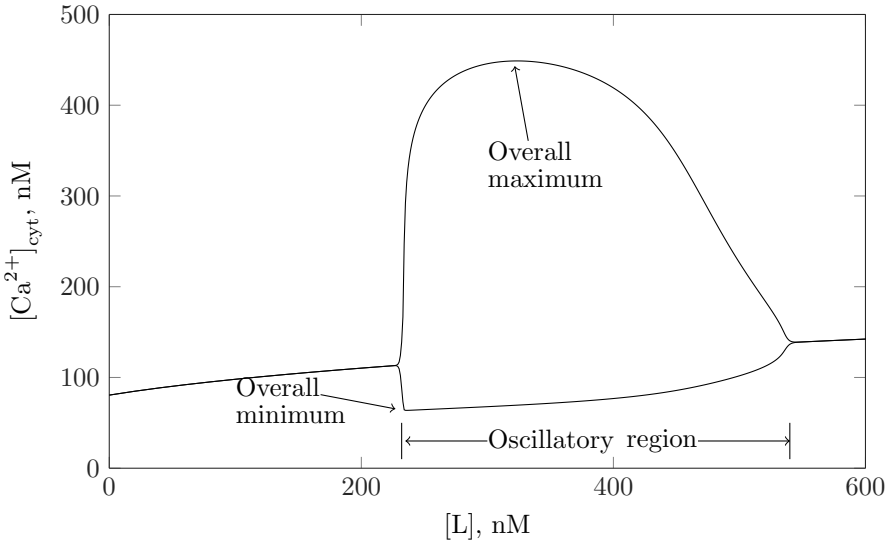

Fig. F.2 Overall calcium maximum and minimum

The overall maximum is defined as the maximum of the maximum values of intracellular calcium oscillations derived during the oscillatory region by varying a parameter. Similarly, overall minimum is the minimum of minimum values of intracellular calcium oscillations during the oscillatory region. The bifurcation points simply define the oscillatory region. In the given Figure F.2, the maximum and minimum values of intracellular calcium for varying agonist concentration are plotted. The oscillatory region, overall maximum and minimum values are shown in the figure.

F.3 Regenerative calcium rise

If the peak intracellular calcium concentration of a non-stimulated cell equals 75% of the calcium peak in the stimulated cell, we say that the cell attained regenerative calcium rise. If more than one cell is stimulated, then the maximum of peak intracellular calcium of all stimulated cells is used.

F.4 Regenerative propagation

Propagation of regenerative calcium rise is called regenerative propagation.

F.5 Penetration depth

Penetration depth, δ_{RP}, is defined as the number of cells that attain regenerative calcium rise. In another way, it is the length of regenerative calcium propagation.

F.6 Passive propagation

Passive propagation is the movement of a molecule from a region of higher concentration to a region of lower concentration, similar to Fickian transport. This movement is driven by the concentration gradient between the propagating regions and will be continued until the gradient vanishes. If stimulation raises the concentration of a molecule in the stimulated cell, a concentration gradient will be created with the non-stimulated neighbouring cell. This causes passive propagation of the molecule from the stimulated cell to the non-stimulated region. The maximum concentration of the molecule in the propagated cell might be lower than in the stimulated cell.

For example, when two VSMCs are connected and one cell is stimulated, the IP_3 concentration rise in the stimulated-cell creates a concentration gradient between it and the non-stimulated cell. The difference in concentration drives IP_3 to the non-stimulated cell causing a rise in IP_3 concentration. This is called passive propagation of IP_3.

F.7 Mediated propagation

In mediated propagation, propagation of a molecule is achieved without the physical movement of that molecule but by a mediating molecule. The mediating molecule propagates to the non-stimulated cell and activates an amplification mechanism that increases the concentration of another molecule, called mediated propagation of the latter one. The existence of mediated propagation entirely relies on the propagation of the mediating molecule. Mediated propagation of a molecule is important in situations where its passive propagation is restricted.

For example, if the passively propagated IP_3 activates IP_3R in the non-stimulated cell, the calcium release from IP_3R would increase the concentration of calcium in the non-stimulated cell. This is called IP_3 mediated calcium propagation, where IP_3 is the mediating molecule and calcium undergoes mediated propagation.